



**Australian Government**

**Geoscience Australia**

Geoscience Australia Survey 273 Post-cruise Report

# Biophysical Processes in the Torres Strait Marine Ecosystem II

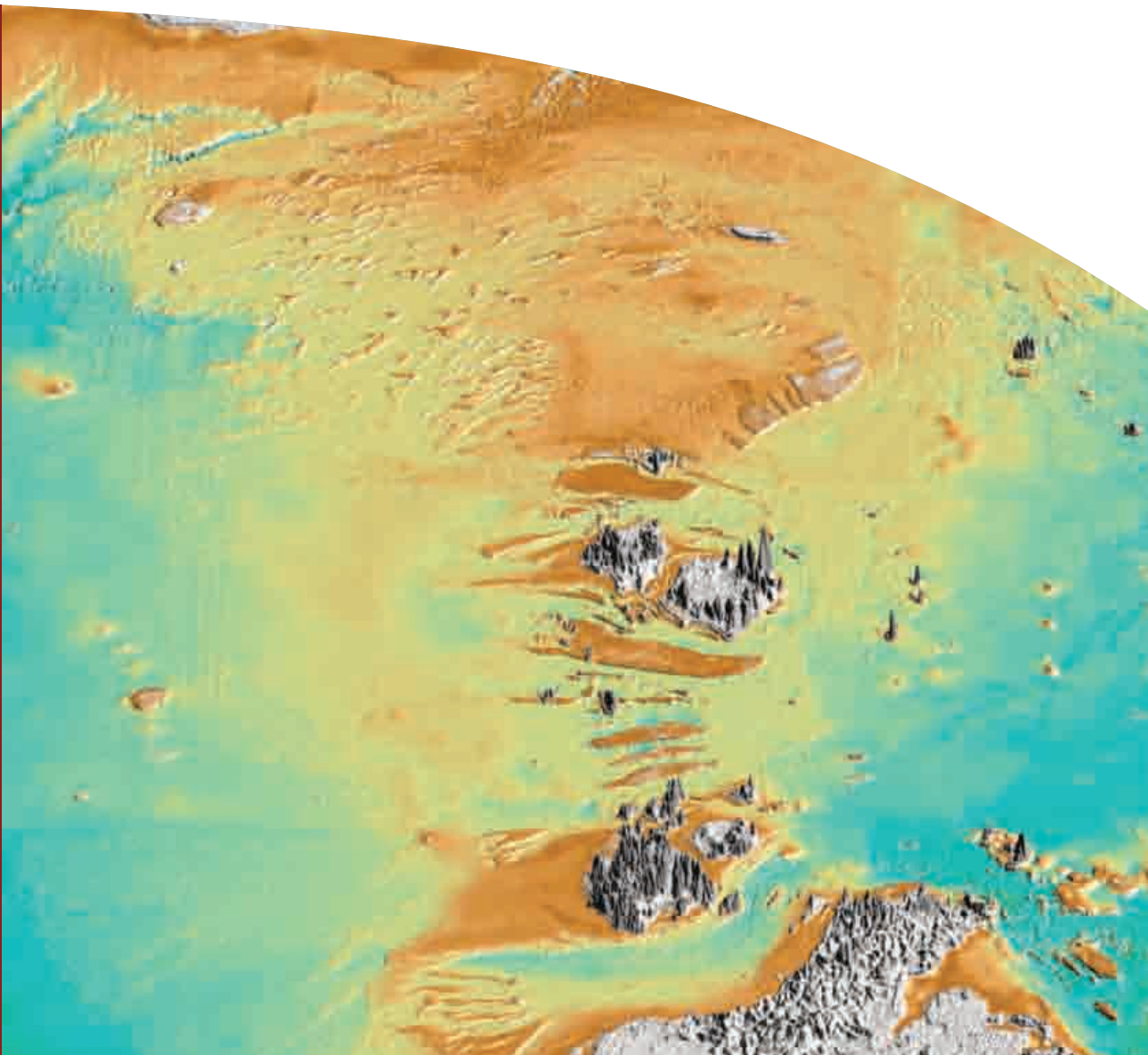
Survey results and review of activities in response to CRC objectives

RV *James Kirby* October 2004

James Daniell, Mark Hemer, Andrew Heap, Emma Mathews,  
Laura Sbaffi, Michael Hughes, & Peter Harris

Record

2006/10



**Geoscience Australia Survey 273**

**Post-cruise Report**

**Biophysical Processes in the Torres Strait  
Marine Ecosystem II**

**Survey results and review of activities in  
response to CRC objectives**

(Torres Strait CRC Task T2.2)

***RV James Kirby***

**October 2004**

James Daniell<sup>1</sup>, Mark Hemer<sup>1</sup>, Andrew Heap<sup>1</sup>, Emma Mathews<sup>1</sup>, Laura Sbaffi<sup>1</sup>,  
Michael Hughes<sup>2</sup>, & Peter Harris<sup>1</sup>

<sup>1</sup>. *Geoscience Australia, GPO Box 378, Canberra, ACT 2601*

<sup>2</sup>. *Sydney University, School of Geoscience, Sydney, NSW 2006*

# GEOSCIENCE AUSTRALIA

Chief Executive Officer: Neil Williams

## Department of Industry, Tourism & Resources

Minister for Industry, Tourism & Resources: Senator The Hon. Ian Macfarlane, MP

Parliamentary Secretary: The Hon. Bob Baldwin, MP

Secretary: Mark Paterson

© Commonwealth of Australia 2006

This work is copyright. Apart from any fair dealings for the purpose of study, research, criticism or review, as permitted under the *Copyright Act 1968*, no part may be reproduced by any process without written permission. Copyright is the responsibility of the Chief Executive Officer, Geoscience Australia. Requests and enquiries should be directed to the **Chief Executive Officer, Geoscience Australia, GPO Box 378 Canberra ACT 2601.**

ISSN: 1448-2177

ISBN: 1 920871 81 0

GeoCat No. 64198

Bibliographic reference: Daniell, J., Hemer, M., Heap, A., Mathews, E., Sbaffi, L., Hughes, M., & Harris, P. (2006). *Biophysical Processes in the Torres Strait Marine Ecosystem II. Survey Results and review of activities in response to CRC objectives*. Geoscience Australia, Record 2006/10, 210pp.

Correspondence for feedback:

**Andrew Heap**

Geoscience Australia

GPO Box 378

Canberra

ACT 2601

Andrew.Heap@ga.gov.au

Geoscience Australia has tried to make the information in this product as accurate as possible. However, it does not guarantee that the information is totally accurate or complete. **Therefore, you should not rely solely on this information when making a commercial decision.**

# Contents

	Page
<b>List of Figures .....</b>	<b>vi</b>
<b>List of Tables .....</b>	<b>ix</b>
<b>Executive Summary .....</b>	<b>xi</b>
<b>1. Introduction .....</b>	<b>1</b>
1.1. Background .....	1
1.1.1. <i>Regional Setting – Torres Strait</i> .....	2
1.1.2. <i>Study Area – Turnagain Island</i> .....	4
1.1.3. <i>Survey Objectives</i> .....	5
1.2. Cruise Participants .....	6
1.2.1. <i>Scientific Personnel</i> .....	6
1.2.2. <i>Ship’s Crew</i> .....	6
<b>2. Geophysics .....</b>	<b>7</b>
2.1. Data Acquisition .....	7
2.1.1. <i>Swath Sonar</i> .....	7
2.2. Data Processing and Analysis .....	8
2.2.1. <i>Swath Sonar</i> .....	8
2.3. Results .....	9
2.3.1. <i>Swath sonar survey</i> .....	9
2.3.2. <i>Sediment and sandwave crest movement</i> .....	10
2.3.3. <i>Comparison with monsoon survey – sandwave crests</i> .....	13
2.3.4. <i>Comparison with monsoon survey – bedform locations</i> .....	15
2.4. Landsat image processing .....	17
<b>3. Meteorology .....</b>	<b>19</b>
3.1. Synoptic observations .....	19
3.1.1. <i>Results for monsoon season survey</i> .....	20
3.1.2. <i>Results for trade wind season survey</i> .....	23
3.1.3. <i>Comparison between surveys</i> .....	26
3.1.4. <i>Wind observations from 1950-1993</i> .....	29

<b>4. Oceanography .....</b>	<b>31</b>
4.1. Hydrodynamic deployments.....	31
4.1.1. Station 01CM01.....	33
4.1.2. Station 02CM07.....	34
4.1.3. Station 03CM02.....	36
4.1.4. Station 04CM03.....	38
4.1.5. Station 05CM04.....	40
4.1.6. Station 06CM06.....	41
4.1.7. Station 07CM05.....	42
4.2. Data recovery .....	42
4.2.1. Station 01CM01.....	42
4.2.2. Station 02CM07.....	43
4.2.3. Station 03CM02.....	43
4.2.4. Station 04CM03.....	44
4.2.5. Station 05CM04.....	44
4.2.6. Station 06CM06.....	45
4.2.7. Station 07CM05.....	45
4.3. Data processing and analysis.....	46
4.3.1. Multi-sensor data.....	46
4.3.2. Suspended particle size analysis.....	47
4.3.3. Sea Level.....	48
4.3.4. Waves.....	49
4.3.5. Currents.....	49
4.3.6. Bedload transport estimates.....	51
4.3.7. Sandwave migration rates.....	53
4.4. Results .....	54
4.4.1. Multi-sensor data.....	54
4.4.2. Suspended particle size analysis.....	63
4.4.3. Sea Level.....	66
4.4.4. Waves.....	80
4.4.5. Currents.....	83
4.4.6. Bedload transport estimates.....	116
4.4.7. Sandwave migration rates.....	125
4.5. Seasonal differences between surveys 266 and 273.....	126
4.5.1. Salinity.....	126
4.5.2. Temperature.....	126
4.5.3. Turbidity.....	126
4.5.4. Sea Level.....	126
4.5.5. Waves.....	126
4.5.6. Currents.....	127
4.5.7. Bedload Transport and Sandwave migration rates.....	128

<b>5. Sedimentology .....</b>	<b>129</b>
5.1. Sample acquisition .....	129
5.1.1. <i>Water samples</i> .....	131
5.1.2. <i>Digital Video Footage</i> .....	131
5.1.3. <i>Surface sediment sampling</i> .....	131
5.1.4. <i>Subsurface sediment sampling</i> .....	132
5.2. Sample processing and analysis.....	132
5.2.1. <i>Water samples</i> .....	132
5.2.2. <i>Digital Video Footage</i> .....	136
5.2.3. <i>Surface sediment sampling</i> .....	136
5.2.4. <i>Subsurface sediment sampling</i> .....	137
5.3. Results.....	139
5.3.1. <i>Water samples</i> .....	139
5.3.2. <i>Digital Video Footage</i> .....	151
5.3.3. <i>Surface sediment sampling</i> .....	153
5.3.4. <i>Subsurface sediment sampling</i> .....	162
<b>6. Discussion and Summary .....</b>	<b>165</b>
6.1. Key comparisons and conclusions for surveys 266 and 273 .....	165
6.1.1. <i>Sandwave mobility</i> .....	165
6.1.2. <i>Wind regime</i> .....	167
6.1.3. <i>Turbidity</i> .....	167
6.1.4. <i>Wave activity</i> .....	168
6.1.5. <i>Current activity</i> .....	168
6.1.6. <i>Sedimentology</i> .....	168
<b>7. Statement addressing the scientific objectives of the Torres Strait CRC .....</b>	<b>170</b>
7.1. CRC Task objectives .....	170
<b>8. Acknowledgements.....</b>	<b>173</b>
<b>9. References .....</b>	<b>174</b>
<b>10. Appendices .....</b>	<b>177</b>
10.1. Appendix A – Survey Leaders Log .....	177
10.2. Appendix B – Digital Video Footage.....	182
10.3. Appendix C – Core Logs.....	183
10.4. Appendix D – Laser analysis of S273 Grab samples .....	195
10.5. Appendix E – S273 core samples .....	195
10.6. Appendix F – S273 water samples .....	197
10.7. Appendix G – S273 Grab Sample Lab Results .....	201
10.8. Appendix H – Results from 24 hour stations.....	203

# List of Figures

	Page
<b>1. Introduction .....</b>	<b>1</b>
Figure 1.1. Regional Map of Torres Strait. ....	3
Figure 1.2. Satellite image of sandwaves in Torres Strait .....	4
Figure 1.3. Map showing regions of significant seagrass dieback.....	5
<b>2. Geophysics .....</b>	<b>7</b>
Figure 2.1. Map showing migration vectors for sandwaves in Area A. ....	11
Figure 2.2. Map showing migration vectors for sandwaves in Area B.....	12
Figure 2.3. Scattergram of crest migration vectors for Area A.....	13
Figure 2.4. Scattergram of crest migration vectors for Area B .....	14
Figure 2.5. Map showing changes in location of sandwaves in Area A.....	15
Figure 2.6. Map showing changes in location of sandbank in Area B.....	16
Figure 2.7. Displacement of sand bank apex's .....	18
<b>3. Meteorology .....</b>	<b>19</b>
Figure 3.1. Monsoon season meteorological data at Horn Island .....	21
Figure 3.2. Monsoon season meteorological data at Coconut Island.....	22
Figure 3.3. Trade wind season meteorological data at Horn Island .....	24
Figure 3.4. Trade wind season meteorological data at Coconut Island.....	25
Figure 3.5. Progressive vector diagram of wind data - monsoon season .....	27
Figure 3.6. Progressive vector diagram of wind data - trade wind season.....	27
Figure 3.7. Progressive vector diagram of hourly wind data 2003-2004 .....	28
Figure 3.8. Progressive vector diagram of yearly wind data 1950-1993 .....	29
Figure 3.9. Scattergram plot of seasonal wind displacements 1950-1993.....	30
<b>4. Oceanography .....</b>	<b>31</b>
Figure 4.1. Locations of Moorings deployed during survey 273. ....	32
Figure 4.2. Mooring 01CM01 .....	34
Figure 4.3. RD Instruments Workhorse Sentinel 600kHz ADCP .....	35
Figure 4.4. Mooring 03CM02 (BRUCE mooring) .....	37
Figure 4.5. Benthos Optical backscatter Sensor.....	38
Figure 4.6. Mooring 04CM03.....	40
Figure 4.7. 01CM01 SBE-19 time series plots .....	55
Figure 4.8. 01CM01 SBE-19 low pass filtered time series plots.....	56
Figure 4.9. 02CM07 SBE-19 time series plots .....	57
Figure 4.10. 02CM07 SBE-19 low pass filtered time series plots.....	58
Figure 4.11. 06CM06 SBE-19 time series plots .....	59

Figure 4.12. 06CM06 SBE-19 low pass filtered time series plot.....	60
Figure 4.13. 03CM02 LISST time series plots .....	64
Figure 4.14. 03CM02 LISST time series plots .....	65
Figure 4.15. 01CM01 results of harmonic analysis of pressure data.....	67
Figure 4.16. 02CM07 results of harmonic analysis of sea level record .....	70
Figure 4.17. 03CM02 results of harmonic analysis of sea level record .....	72
Figure 4.18. 04CM03 results of harmonic analysis of sea level record .....	74
Figure 4.19. 05CM04 results of harmonic analysis of sea level record .....	76
Figure 4.20. 06CM06 results of harmonic analysis of sea level record .....	79
Figure 4.21. 03CM02 time series wave statistics .....	81
Figure 4.22. 04CM03 time series wave statistics .....	82
Figure 4.23. 02CM07 current meter progressive vector plot.....	84
Figure 4.24. 02CM07 current meter time series for Bin 1 .....	86
Figure 4.25. 02CM07 current meter time series for Bin 9 .....	87
Figure 4.26. 02CM07 Low pass filtered current meter data for Bin 1 .....	88
Figure 4.27. 02CM07 Low pass filtered current meter data for Bin 9 .....	89
Figure 4.28. 02CM07 scatter plots with ellipses.....	90
Figure 4.29. 02CM07 Tidal ellipse parameters.....	91
Figure 4.30. 04CM03 current meter time series for Bin 1 .....	93
Figure 4.31. 04CM03 current meter time series for Bin 1 .....	94
Figure 4.32. 04CM03 current meter time series for Bin 10 .....	95
Figure 4.33. 04CM03 Low pass filtered current meter data for Bin 1 .....	96
Figure 4.34. 04CM03 Low pass filtered current meter data for Bin 9 .....	97
Figure 4.35. 04CM03 scatter plots with ellipses.....	98
Figure 4.36. 04CM03 Tidal ellipse parameters.....	100
Figure 4.37. 06CM06 current meter progressive vector plot .....	102
Figure 4.38. 06CM06 current meter time series for bin 1.....	103
Figure 4.39. 06CM06 current meter time series for bin 27.....	104
Figure 4.40. 06CM06 Low pass filtered current meter data for Bin 1 .....	105
Figure 4.41. 06CM06 Low pass filtered current meter data for bin 27 .....	106
Figure 4.42. 06CM06 Scatter plots with ellipses.....	107
Figure 4.43. 06CM06 Tidal ellipse parameters .....	108
Figure 4.44. 07CM05 current meter progressive vector plots.....	110
Figure 4.45. 07CM05 current meter time series.....	111
Figure 4.46. 07CM05 Low pass filtered current meter series.....	112
Figure 4.47. 07CM05 Scatter plot with ellipses .....	113
Figure 4.48. 07CM05 tidal ellipse parameters .....	114
Figure 4.49. 02CM07 vector stick plots of bedload transport .....	117
Figure 4.50. 04CM03 vector stick plots of bedload transport .....	119
Figure 4.51. 06CM06 vector stick plots of bedload transport .....	121
Figure 4.52. 07CM05 vector stick plots of bedload transport .....	123
Figure 4.53. Comparison of average bedload transport calculations .....	124

<b>5. Sedimentology.....</b>	<b>129</b>
Figure 5.1. Sample stations for survey 273.....	130
Figure 5.2. Suspended sediment concentrations from Neap 24Hr station....	139
Figure 5.3. Suspended sediment concentrations from Springs 24Hr station	140
Figure 5.4. EDX analysis for station 25 .....	143
Figure 5.5. EDX analysis for station 26 .....	144
Figure 5.6. EDX analysis of grab samples and filter papers Si/Ca.....	146
Figure 5.7. EDX analysis of grab samples and filter papers Ca/Al.....	147
Figure 5.8. SXAM-XRF images of grab sample mud fractions.....	149
Figure 5.9. SXAM-XRF images of grab sample sand fractions .....	150
Figure 5.10. Video footage from 24 hour stations .....	152
Figure 5.11. Grab sample locations for Area A .....	153
Figure 5.12. Area A sediment sample comparison .....	154
Figure 5.13. Grab sample locations for Area B .....	155
Figure 5.14. Area B sediment sample comparison.....	156
Figure 5.15. Grab sample location for Turnagain/Saibai transect.....	157
Figure 5.16. Grab sample locations for Saibai Island.....	158
Figure 5.17. Saibai Island sediment sample comparisons .....	160
Figure 5.18. Mud fraction comparison .....	161
Figure 5.19. Grab sample location for northern Turnagain Island.....	162
 <b>10. Appendices.....</b>	 <b>177</b>
Figure 10.1. Core log for 27VC01.....	184
Figure 10.2. Core log for 27VC02.....	185
Figure 10.3. Core log for 28VC04.....	186
Figure 10.4. Core log for 28VC05.....	187
Figure 10.5. Core log for 29VC06.....	188
Figure 10.6. Core log for 30VC07.....	189
Figure 10.7. Core log for 32VC01.....	190
Figure 10.8. Core log for 33VC02.....	191
Figure 10.9. Core log for 34VC03.....	192
Figure 10.10. Core log for 35VC09.....	193
Figure 10.11. Core log for 36VC10.....	194

# List of Tables

	Page
<b>2. Geophysics.....</b>	<b>7</b>
Table 2.1. Details of swath sonar surveys.....	10
<b>3. Meteorology.....</b>	<b>19</b>
Table 3.1. Raw meteorological statistics for survey 266 .....	23
Table 3.2. Raw meteorological statistics for survey 273 .....	26
<b>4. Oceanography .....</b>	<b>31</b>
Table 4.1. Summary of deployed sensors. ....	31
Table 4.2. 01CM01 SBE-19 statistics.....	54
Table 4.3. 02CM07 SBE-19 statistics.....	54
Table 4.4. 06CM06 SBE-19 statistics.....	54
Table 4.5. 03CM02 LISST statistics.....	64
Table 4.6. 01CM01 harmonic analysis of sea level record from SBE-19 .....	66
Table 4.7. Regression Statistics for CSIRO Mooring 2 .....	68
Table 4.8. 02CM07 harmonic analysis of sea level record from SBE-19 .....	68
Table 4.9. 02CM07 harmonic analysis of sea level record from ADCP .....	68
Table 4.10. 03CM02 harmonic analysis of sea level record from Nortek.....	71
Table 4.11. 04CM03 harmonic analysis of sea level record from ADCP .....	73
Table 4.12. 05CM04 harmonic analysis of sea level record from ADCP .....	75
Table 4.13. 06CM06 regression statistics for tidal records.....	77
Table 4.14. 06CM06 harmonic analysis of sea level record from RBR.....	77
Table 4.15. 06CM06 harmonic analysis of sea level record from SBE-19 .....	78
Table 4.16. 06CM06 harmonic analysis of sea level record from ADCP .....	78
Table 4.17. 03CM02 wave statistics from Nortek pressure sensor .....	81
Table 4.18. 04CM03 wave statistics from Nortek pressure sensor .....	82
Table 4.19. 02CM07 raw current meter statistics .....	85
Table 4.20. 02CM07 principal axes of currents.....	90
Table 4.21. 02CM07 tidal ellipse parameters.....	92
Table 4.22. 04CM03 raw current meter statistics .....	93
Table 4.23. 04CM03 principal axes of currents.....	99
Table 4.24. 04CM03 Tidal ellipse parameters.....	100
Table 4.25. 06CM06 raw current meter statistics .....	102
Table 4.26. 06CM06 principal axes of currents.....	108
Table 4.27. 06CM06 Tidal ellipse parameters.....	109
Table 4.28. 07CM05 Raw current meter statistics .....	110
Table 4.29. 07CM05 principal axes of currents.....	113
Table 4.30. 07CM05 current ellipse parameters .....	114

Table 4.31. 02CM07 bedload transport .....	116
Table 4.32. 04CM03 bedload transport .....	118
Table 4.33. 06CM06 bedload transport .....	120
Table 4.34. 07CM05 bedload transport .....	122
Table 4.35. 02CM07 predicted average migration rate.....	125
<b>5. Sedimentology .....</b>	<b>129</b>
Table 5.1. Summary of station operations.....	133
Table 5.2. Water samples used for EDX analysis .....	135
Table 5.3. Summary of 24 hour stations .....	139
Table 5.4. Average suspended sediment concentration for Area A.....	141
Table 5.5. Average suspended sediment concentration for Area B.....	141
Table 5.6. EDX analysis of S273 grab samples.....	145
Table 5.7. Compositions of co-located grabs and filter papers .....	147
Table 5.8. Results from Area A sediment sample analyses .....	154
Table 5.9. Results from Area B sediment sample analyses.....	156
Table 5.10. Results from Turnagain/Saibai transect sediment samples.....	158
Table 5.11. Results from Saibai Island sediment sample analyses .....	159
Table 5.12. Results from miscellaneous sediment samples .....	162
Table 5.13. Results from vibro-core recovery .....	163
Table 5.14. Multi-sensor core logger statistics.....	163
<b>10. Appendices.....</b>	<b>177</b>
Table 10.1. Sediment samples taken from S273 cores.....	195
Table 10.2. Weights of S273 filter papers.....	197
Table 10.3. Textural analysis of S273 grab samples .....	201
Table 10.4. Station 25 log sheet .....	203
Table 10.5. Station 26 log sheet .....	205
Table 10.6. Station 37 log sheet .....	207
Table 10.7. Station 36 log sheet .....	209

# Executive Summary

This report contains the preliminary results of Geoscience Australia survey 273 to northwest Torres Strait. This survey was undertaken as part of a research program within the Torres Strait CRC aimed at understanding marine biophysical processes in Torres Strait and their effect on seagrass habitats. Two Geoscience Australia surveys were undertaken as part of this program, survey 266 measured monsoon season conditions (Heap et al., 2005), and survey 273 measured trade wind conditions. [Section 6](#) compares and contrasts the survey results acquired for both surveys. [Section 7](#) addresses the results of the survey program in light of the objectives of the CRC proposal.

Survey 273 acquired numerous different data types to assist with characterising the mobile sediments and hydrodynamic nature of the region. Multibeam sonar, current meters, grab samples, vibro-cores, underwater video, meteorological data (from the Bureau of Meteorology), Landsat imagery, were all used to characterise the seabed hydrodynamics of Torres Strait.

Repeat multibeam sonar surveys were carried out over two study areas SW and SE of Turnagain Island (the same two study areas as survey 266). This allowed for measurement of dune crest migration to be made in both the monsoon and trade wind seasons. Contrasting styles of dune crest migration were evident between the two surveys. During survey 266 a typically strong westward migration of >10m was observed over a 14 day period. By comparison survey 273 had reduced rates of crest migration, less than 4 m in both east and west directions. All multibeam surveys in Area B (south east Turnagain Island) showed distinct regions of east facing and west facing sandwaves. The size and shape of these regions changed due to seasonal variations in the current regime. This result demonstrated that the sandwave orientation is not necessarily aligned to wind driven current but instead sediment appears to circulate around the sandwaves due to the activity of mutually evasive ebb and flood currents.

The main result from the oceanographic data was that the currents during both survey 266 and 273 were very similar. This result was in contrast to what was observed in the multibeam survey data. It would be expected that under similar oceanographic conditions that similar rates of crest migration would be observed, this was not the case. The different rates of bedform migration are explained by the seasonal reversal of bedforms. Low frequency, wind driven, currents in Torres Strait reverse with the changes in the seasons, from south easterly during the trades to north westerly during the monsoon, these currents have a direct relationship to the orientation of sandwaves in Torres Strait. Survey 266 sampled trade wind conditions at the very end of the monsoon season, hence all bedforms were aligned to monsoon conditions but were being acted upon by trade wind conditions. The bedforms had changed from being hydrodynamically stable to unstable with the change in the wind (and therefore current) regime, hence the increased rates of erosion and

migration observed during survey 266. The crest migration observed during survey 273 is assumed to be typical for trade wind season conditions. The increased rate of bedform migration at the end of the monsoon season indicates that the sandwaves reverse their orientations rapidly to suit the seasonal changes in flow regime. However these results also indicated that sandwaves monitored in this study are unlikely to impact upon seagrasses, except on a local scale.

The principal result from the sampling program was that the turbid sediment found around Turnagain Island was sourced locally and not from the rivers on the southern coast of Papua New Guinea. Energy Dispersive X-ray analysis (EDX) of sediment samples and filter paper samples showed a strong contrast in the composition of seabed sediments between the fine, mobile sediments in the Turnagain Island region and the Saibai Island region. Sediment samples and filter papers from Turnagain Island had a low terrigenous component and high carbonate content, indicative of open marine conditions with little to no terrigenous influence. The similarity in the compositions of the sediment samples and filter papers from around Turnagain Island indicates that the fine, mobile sediment is locally derived. By contrast the sediments from Saibai Island contained a high terrigenous component. It is inferred that the influx of sediments from rivers in close proximity to Saibai Island provide a source for most of this terrigenous material.

Data acquired over both surveys was used to investigate the activity of bedforms in the survey region and the composition of sediments. The activity of bedforms and turbidity were two possible mechanisms for initiating seagrass dieback. It has been shown that the large sandbanks in Torres Strait are unlikely to affect seagrass communities on a regional scale. Whether this also holds true for smaller, individual sandwave remains unclear. It has also been shown that turbidity from rivers on the south coast of Papua New Guinea is also unlikely to reach the Turnagain Island region, however, the mechanisms for initiating turbid plumes from the seabed is a subject of further research, and an aspect to be incorporated into a hydrodynamic model for the Torres Strait region.

All data acquired from surveys 266 and 273 have been made available to ground truth and calibrate the hydrodynamic model for Torres Strait, as per the objectives of the CRC. Details of the hydrodynamic modelling in Torres Strait will be detailed in a report submitted to the CRC.

# 1. Introduction

This record contains the results of Geoscience Australia marine survey 273. The survey was conducted from 7 October to 29 October 2004 in north-western Torres Strait, near Turnagain Island using James Cook University's research vessel *James Kirby*. The survey included scientists from Geoscience Australia, University of Sydney and CSIRO.

Geoscience Australia is a partner in the Torres Strait CRC which is a 3-year supplementary program of the Reef CRC based in Townsville. The Torres Strait Cooperative Research Centre was set up to identify and quantify the physical and biological processes operating within Torres Strait. Geoscience Australia's research focus is to investigate the key physical processes associated with the distribution, dieback and recovery of seagrass. This includes documentation of seabed sediments and associated habitats, sediment transport pathways and fluxes, seabed stability and Late Quaternary history in the region.

Part of Geoscience Australia's commitment to the Torres Strait CRC involved conducting two marine surveys in the vicinity of Turnagain Island. The purpose of the marine surveys was to characterise the habitats and oceanographic processes during both the trade wind and monsoon seasons. Survey 273 was undertaken at the end of the trade wind season and results were to be compared against data acquired during Geoscience Australia survey 266 which was conducted at the end of the monsoon season (Heap et al., 2005).

This report contains the comparisons made between key datasets acquired for both the monsoon and trade wind surveys. For both surveys repeat multibeam sonar surveys were used to detect changes in location of sandwave crests, oceanographic moorings were also deployed to measure current strength, waves, turbidity (as well as other variables), and to estimate rates of bedload transport. Synoptic observations from the Bureau of Meteorology were used to compare the wind regime experienced during each season. Sediment samples, cores, and filter papers were used to characterise both sediments on the seabed and in suspension. The oceanographic, geophysical, and sediment sample data collected from both surveys assisted in identifying benthic habitats, and provided crucial information on the hydrodynamic processes that mobilise sediments in Torres Strait.

## 1.1. BACKGROUND

As recently as 1999 and 2001, significant dieback events were recorded in central Torres Strait by local fishers and CSIRO scientists (Long et al., 1997). The Torres Strait Island community is concerned that the dieback events are triggering a reduction in the populations of dugong and sea turtles, which they have traditionally hunted for food. It has been suggested that increased sediment load from the Fly River (Papua New Guinea) produced by the Ok Tedi gold mine has significantly raised turbidity

levels in Torres Strait to a point where the reduction in light to the seabed has resulted in seagrass dieback. However, hydrodynamic modelling of the ocean currents indicates that very little water or sediment probably enters Torres Strait from the Gulf of Papua (Hemer et al., 2004). The Torres Strait CRC is investigating numerous hypotheses for the seagrass dieback, including the smothering of seagrasses by mobile sandwaves, elevated turbidity, and changing oceanographic conditions in the region (due to rising sea levels, climate change, El Nino, or other climatic events).

During March-April 2004 Geoscience Australia survey 266 acquired geophysical, oceanographic and sediment data to characterise the hydrodynamic and sedimentary processes operating in the Torres Strait at the end of the monsoon season (Heap et al., 2005).

Principal observations made during survey 266 (from Heap et al., 2005) were:

- 1) The seabed next to Turnagain Island was complex and comprised of hard-grounds, reefal platforms, and mobile sandwaves;
- 2) The sandwaves were in the process of changing their orientation from east-facing to west-facing. This observation was consistent with the seasonal reversal of bedform orientation that has been noted in other areas in Torres Strait (Harris 1991);
- 3) The migration patterns of sandwaves within the sandbanks were complex, with the larger sandwaves moving greater distances than the smaller sandwaves. The crests of the largest sandwaves migrated by up to 16 meters over 14 days;
- 4) The tides near Turnagain Island have a strong, mixed, semi-diurnal signature, with ebb and flood near-bed currents of up to  $75 \text{ cm s}^{-1}$ , coupled with a relatively strong wind driven residual flow to the west-south-west;
- 5) The seabed sediments samples were poorly-sorted calcareous sands and gravels. Fine grained sediment was in low concentrations in the samples due to the strong tidal currents in the region winnowing out all but the coarsest sediment.
- 6) Peak levels of turbidity are linked to period of highest current strength (typically during the spring tides).

### 1.1.1. Regional Setting – Torres Strait

Torres Strait is located at the northern end of the Cape York Peninsula and separates Australia from Papua New Guinea (Fig. 1.1). Water depths in Torres Strait are typically 15-25 m and the seabed forms a low-relief plain that was a land bridge connecting Australia with Papua New Guinea throughout most of the Late

Quaternary (Harris, 1988). The topography of the strait is complex with numerous scattered islands, reefs and sandbanks.

Surface sediments in Torres Strait are mostly a mixture of locally-derived carbonate and siliciclastic material. Sands and gravels dominate the carbonate fraction and reflect the high energy conditions. The surface sediments are regularly mobilised by strong tide and wave currents. Tides are mixed with one high-high water (HHW) and low-high water (LHW) per day (Harris, 1989). The numerous reefs and islands form a barrier to tides and greatly attenuate the tidal ranges. Tidal currents are directed east-west and attain  $2.5 \text{ m s}^{-1}$  due to the constricted coastal geometry. Superimposed on this energetic tidal regime are wave-induced currents, wind-driven circulation, ocean currents and storm surges. A review of Torres Strait's geology, geography, oceanography, has been undertaken by Heap et al. (2004).

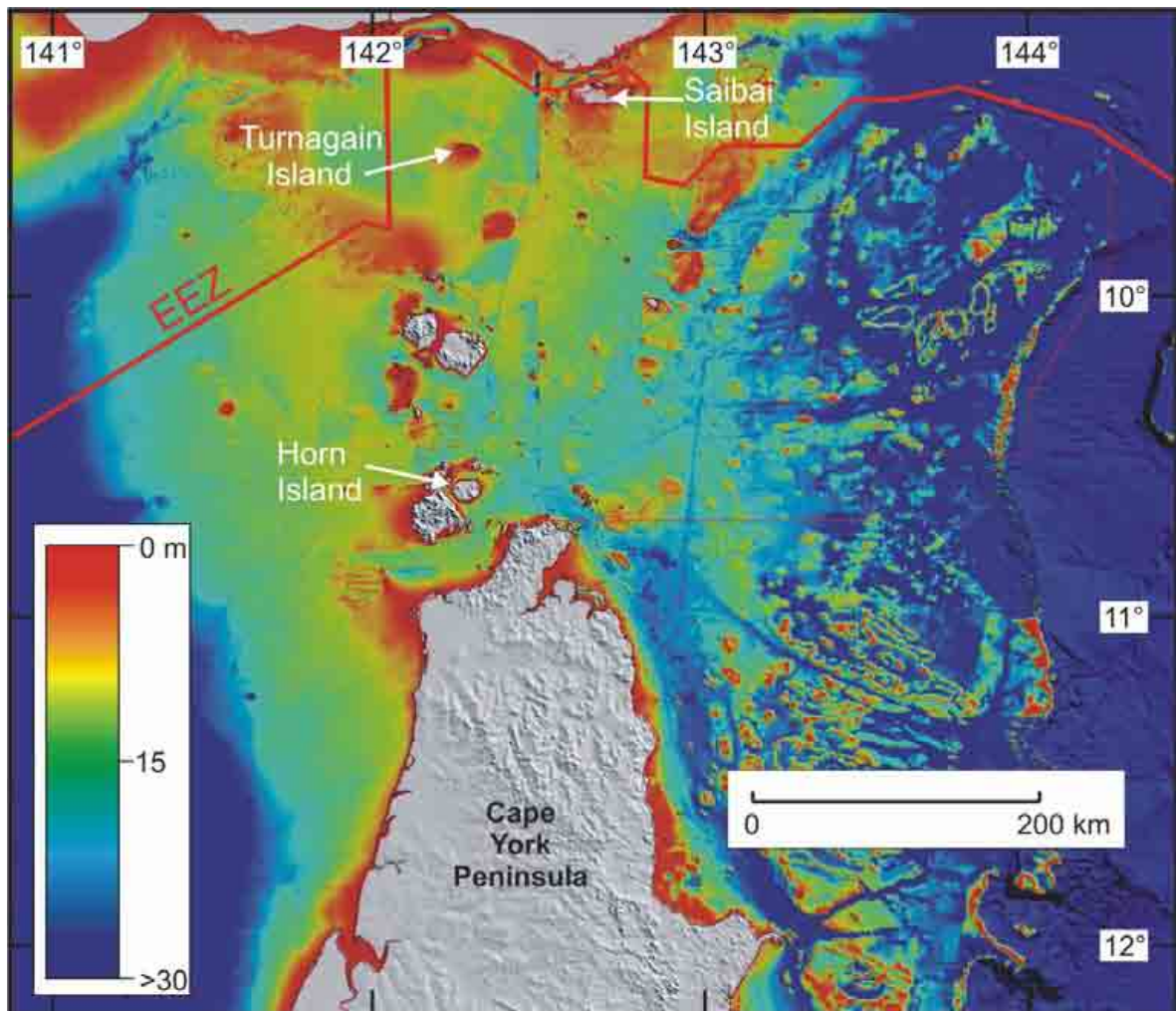


Figure 1.1. Region map of Torres Strait. Torres Strait is a shallow (<15m) seaway separating Australia in the south from Papua New Guinea in the north.

### 1.1.2. Study Area – Turnagain Island

Widespread areas of the seabed in Torres Strait are covered with mobile sandbanks (Fig. 1.2). These sandbanks are numerous, are principally located in the north west and exhibit a variety of forms that are related to the availability of bed sediment and tidal current velocities. In the vicinity of Turnagain Island, the sandbanks are also located in regions of significant seagrass dieback (Fig. 1.3). These sandbanks have a wavelength of 100's of meters and often reach heights of up to 5 meters (Heap et al., 2005). The sandbanks typically have smaller sandwaves superimposed upon them. During the monsoon survey the sandwaves were observed to reverse their orientation from east-facing to west-facing (Heap et al., 2005) due to the reversal of wind driven currents from NW to SE with the onset of the trade wind season. This observation is consistent with previous research in the Torres Strait area. Harris (1991) observed that sandwaves in the Adolphus Channel may display opposite migration directions in monsoon and trade wind seasons under the forcing of the prevailing wind directions (Harris, 1991). Interspersed between the sandwaves are hard-grounds and seagrass and algal reef habitats. The transition between these habitats occurs over only a few metres.

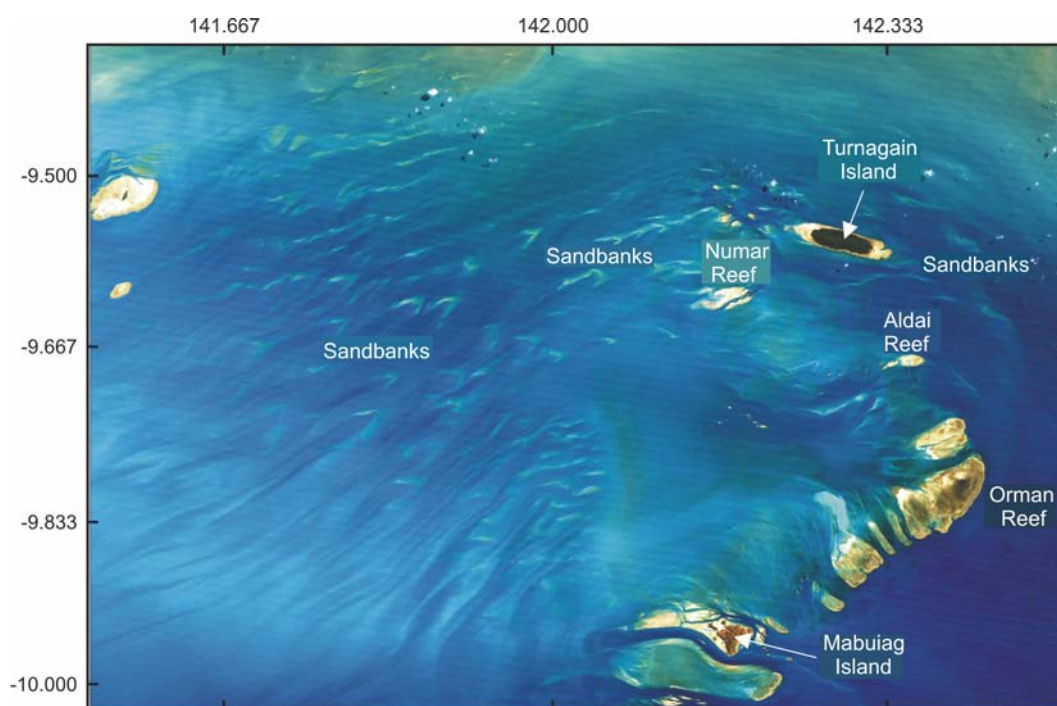


Figure 1.2. Satellite image of the sandbanks in central and western Torres Strait. The extensive sandbank fields are formed by strong tidal currents and have smaller sandwaves superimposed on them.

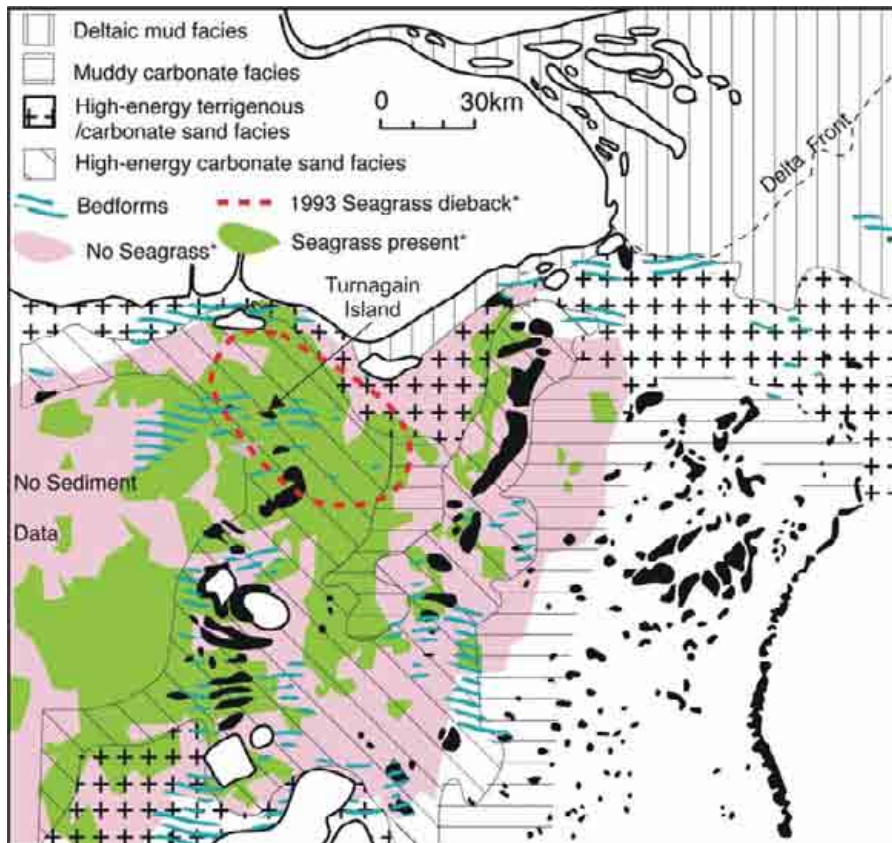


Figure 1.3. Map showing regions of significant seagrass dieback. Areas where seagrass dieback has been documented occur in the vicinity of Turnagain Island. Regions southwest and southeast of Turnagain Island are the focus of this study.

### 1.1.3. Survey Objectives

The survey objectives were designed to complement those for the monsoon survey (survey 266) and provide data for the end of the trade wind season. The objectives were:

- Conduct repeat multibeam sonar surveys mobile of sandwaves SW and SE of Turnagain Island, using the same areas as survey 266, to compare seasonal variations in sandwave migration;
- Deploy oceanographic moorings to acquire data on tides, waves, currents, turbidity, and temperature to characterise oceanographic processes during the survey;
- Conduct '24 hour stations' to estimate onset of bedload transport and acquire water samples to estimate turbidity over a 24 hour period for both spring and neap tides;
- Acquire sediment samples and underwater video data to characterise seabed environments in the region; and
- Acquire shallow cores to understand the temporal variations in the bedform composition.

The trade wind survey (survey 273) had an additional objective which was to collect surface samples in a transect to, and in the vicinity of, Saibai Island (northern Torres Strait) to compare their composition against samples collected in the Turnagain Island region.

## **1.2. CRUISE PARTICIPANTS**

The vessel used for the survey was James Cook University's research vessel *James Kirby*. The RV *James Kirby* is a 20 m converted trawler, with accommodation for 8 participants (including 2 crew), and contains a central winch and A-frame for deployments of up to 1 ton. A quick conversion and the A-frame and winch can be used to conduct vibrocoreing operations. The multi-disciplinary nature of the research required the efforts of a group of people with a wide variety of complimentary skills to make it successful. The survey personnel with their substantive expertise are listed below.

### **1.2.1. Scientific Personnel**

Dr Peter Harris (GA) – co-cruise leader 18/10/04 – 28/10/04;  
Dr Andrew Heap (GA) – co-cruise leader 08/10/04 – 18/10/04;  
Dr Mark Hemer (GA) – oceanographer 18/10/04 – 28/10/04;  
Dr Fredrick Saint-Cast (GA/CSIRO) – oceanographer 08/10/04 – 18/10/04;  
Dr Michael Hughes (USYD) – physical sedimentologist 08/10/04 – 18/10/04;  
Mr James Daniell (GA) – swath sonar 08/10/04 – 18/10/04;  
Mr Franz Villagran (GA) – marine technician 08/10/04 – 18/10/04;  
Mr Mike Sexton (GA) - swath sonar 18/10/04 – 28/10/04;  
Mr Jack Pittar (GA) – marine technician 18/10/04 – 28/10/04;

### **1.2.2. Ship's Crew**

Mr Don Battersby (JCU) – skipper  
Mr Kevin Hooper (JCU) – deck-hand/electronic technician/swath mapping

## 2. Geophysics

The trade wind survey (survey 273) resurveyed the area investigated at the end of the monsoon (survey 266). Repeat multibeam sonar surveys were again used to estimate rates of sandwave migration. Satellite imagery was used to monitor changes in the position of sandbank in Torres Strait over a 15 year period to supplement the results from the multibeam sonar work. The regions investigated have been denoted Area A (SW Turnagain Island) and Area B (SE Turnagain Island). Both Areas A and B were surveyed twice, approximately 14 days apart, using a high resolution swath sonar system.

### 2.1. DATA ACQUISITION

#### 2.1.1. Swath Sonar

A Reson<sup>TM</sup> 240 kHz swath sonar system (model no. 8101) was hired from the School of Earth Sciences at James Cook University for the purposes of gathering high-resolution bathymetry. The swath transducer head was fixed to a pole attached to the starboard side of the vessel's hull. This configuration ensured that the transducer head projected approximately 0.5 m below the hull. The 8101 transducer emits 101 acoustic beams of  $1.5^\circ \times 1.5^\circ$  to produce a  $150^\circ$  wide swath. Typically, this gives a swath width of approximately 7 times the water depth. The TSS DMS motion sensor was mounted on the ship's centre line and given reference coordinates of  $x = 0$  m,  $y = 0$  m, and  $z = 0$  m, where  $x$  is starboard positive,  $y$  is bow positive, and  $z$  is elevation positive. Relative to the motion sensor, the transducer head was at co-ordinates of  $x = 2.9$  m,  $y = 1.8$  m, and  $z = -3.0$  m, and the DGPS antenna at co-ordinates of  $x = -0.9$  m,  $y = -0.7$  m, and  $z = 9.1$  m. As the survey plan included repeat seabed surveys to monitor changes in topography a high degree of positional accuracy was needed. An Ashtech G12 DGPS was considered adequate for our survey needs with a quoted accuracy of 0.4 m in the X and Y plane. The swath sonar system was operated at  $9\text{--}11\text{ km hr}^{-1}$  (5-6 knots) in smooth to moderate seas. The data from all the peripheral sensors was recorded using the Reson 6042 Ver. 7.2 format software.

Swath mapping of the study sites was conducted in water depths of 3-12 m, allowing for a maximum allowable ping rate of 20 times per second. To ensure 100% coverage, each site was swathed with a constant line spacing of between 20 and 25 m depending on water depth (closer spacing for shallower water). Due to significant, and often rapid, changes in the shallow bathymetry, this line spacing did not always provide 100% coverage and additional lines were inserted to fill the gaps. Each study site was mapped twice; once at the start of the survey and then again at the end of the survey. There was approximately 14 days between the subsequent surveys to ensure that a full spring/neap tide cycle was recorded. Time constraints prevented

the entire areas surveyed during survey 266 to be remapped. Surveying was generally limited to areas with known mobile bedforms.

## **2.2. DATA PROCESSING AND ANALYSIS**

Processing of the multibeam sonar data during the survey was a priority because it was necessary for monitoring the swath width and to assist in improving the survey design.

### **2.2.1. Swath Sonar**

The swath sonar data were initially acquired in the proprietary Reson™ \*.db format. Each line consisted of a separate file to keep the file sizes manageable. The data for each line were converted to Extended Triton-Elics (XTF) format using the *ExportXTF* module supplied with the Reson™ 6024v7 software. This conversion allowed the data to be imported into the Caris™ HIPS/SIPS processing software. All of the post-processing of the swath sonar data, including data editing, tide corrections and sound velocity profile corrections were undertaken using Caris™ HIPS/SIPS.

#### *General Processing Procedure:—*

The acoustic signals were corrected for temperature and salinity of the seawater using an Applied Microsystems Ltd SV PLUS™ acoustic velocity profiler. As expected, the sound velocity profiles showed very little variation through the water column, which is well mixed. The acoustic velocity of seawater was measured at  $1539 \pm 1 \text{ m s}^{-1}$  and was consistent through the water column and between the survey areas. High quality tide models were generated from pressure sensors that were co-located with the current meters. Once the current meters were recovered after the survey these pressure models were used to correct the bathymetry changes for changes in tide height over the survey period. Bathymetry soundings were visually inspected and bad data were removed to create a level and clean dataset relative to mean-sea level.

*Data Analysis and Presentation:—*

The bathymetry data was gridded with a 1 m cell size, this was considered appropriate considering the size of the survey areas, the data quality, and data density. Attempts at gridding the data at higher resolutions such as 0.5 m cell size did not improve the quality of the grid as it often highlighted small errors in the data such as the swath head vibrating. Smaller grid sizes also showed data gaps between pings at the outermost extents of each swath.

*Data Quality and Errors:—*

The shallow water depths in the study area allowed for a ping rate of 20 times per second and produced accurate bathymetric soundings over the entire 150° of the swath (i.e., the quality of the soundings was relatively consistent across all 101 beams). Data quality varied during the survey, although the overall quality was adequate for the purpose of the study. The quality of the data was degraded to variable degrees by waves, and strong tidal currents.

During ideal conditions, the swath sonar survey was able to delineate small sandwaves (0.2 m high). However, these subtle features were not discernible when waves up to 1.5 m were present.

*Extraction of sandwave migration vectors*

Methods for the processing of multibeam sonar data to extract sandwave migration vectors are described in Heap et al. (2005).

## **2.3. RESULTS**

### **2.3.1. Swath Sonar survey**

In total, including the transit lines, the swath mapping survey comprised 460 lines which amounted to 438 line-km of data. Data were acquired over 12 days with a total volume of 21 gigabytes.

Due to a good knowledge of the survey area it was possible to limit the repeat surveys to areas with sandwaves (see Table 2.1). The swath surveys revealed water depths within the study areas to be between 3 m to 12 m.

Table 2.1. Details of swath sonar surveys.

Site	Survey	Max Length (km)	Max Width (km)	Area (km <sup>2</sup> )	Number of Lines	Total Line-km
Area A	Survey 1	1.4	1.6	2.0	87	102
	Survey 2	1.5	1.3	1.6	133	83
Area B	Survey 1	2.2	1.3	2.2	104	108
	Survey 2	2.2	1.3	2.9	136	145

### 2.3.2. Sediment and sandwave crest movement

The repeat swath surveys present an opportunity to measure sandwave crest movement in Areas A and B over the survey period. Comparing the bathymetry at the beginning of the survey with that at the end of the survey shows changes in the seabed morphology. Due to the very high resolution swath data (gridded at 1 m x 1 m), very small changes in the position and form of the seabed can be determined. This extends to measuring the movement of the entire form of a seabed feature rather than inferring the movement from a single measurement location (e.g., from an oceanographic mooring).

As the sediment mobility in both Areas A and B are considered to be quite complex, especially as the bedforms are known to reverse their orientation over short time periods, a distinction has to be made between crest migration and bedform migration. Changes in sandwave crest morphology are good indicators of current activity but are not necessarily good indicators of bedform migration since bedform migration infers that the centre of gravity of the bedform has moved. If bedforms are reversing their orientation then the position of the crest will change much more rapidly than the centre of gravity. If the bedforms are not reversing then changes in crest position and centre of gravity are assumed to be similar.

### 2.3.2.1. Sandwave Crest Migration in Area A

There were two distinct areas of crest migration for Area A during the survey period (Fig 2.1). The sandwaves in the northern section of the survey area migrated to the west at an average of 2.5 m over the survey period. In the south, the sand waves moved in a southeast direction at an average of 2.5 m over the survey period. The sandwaves to the south are in deeper water than the sandwaves in the north (approximately 7 m compared to 4), and the difference in migration directions is inferred to be a result of the influence of wind driven currents in shallow water and local steering of the tidal currents.

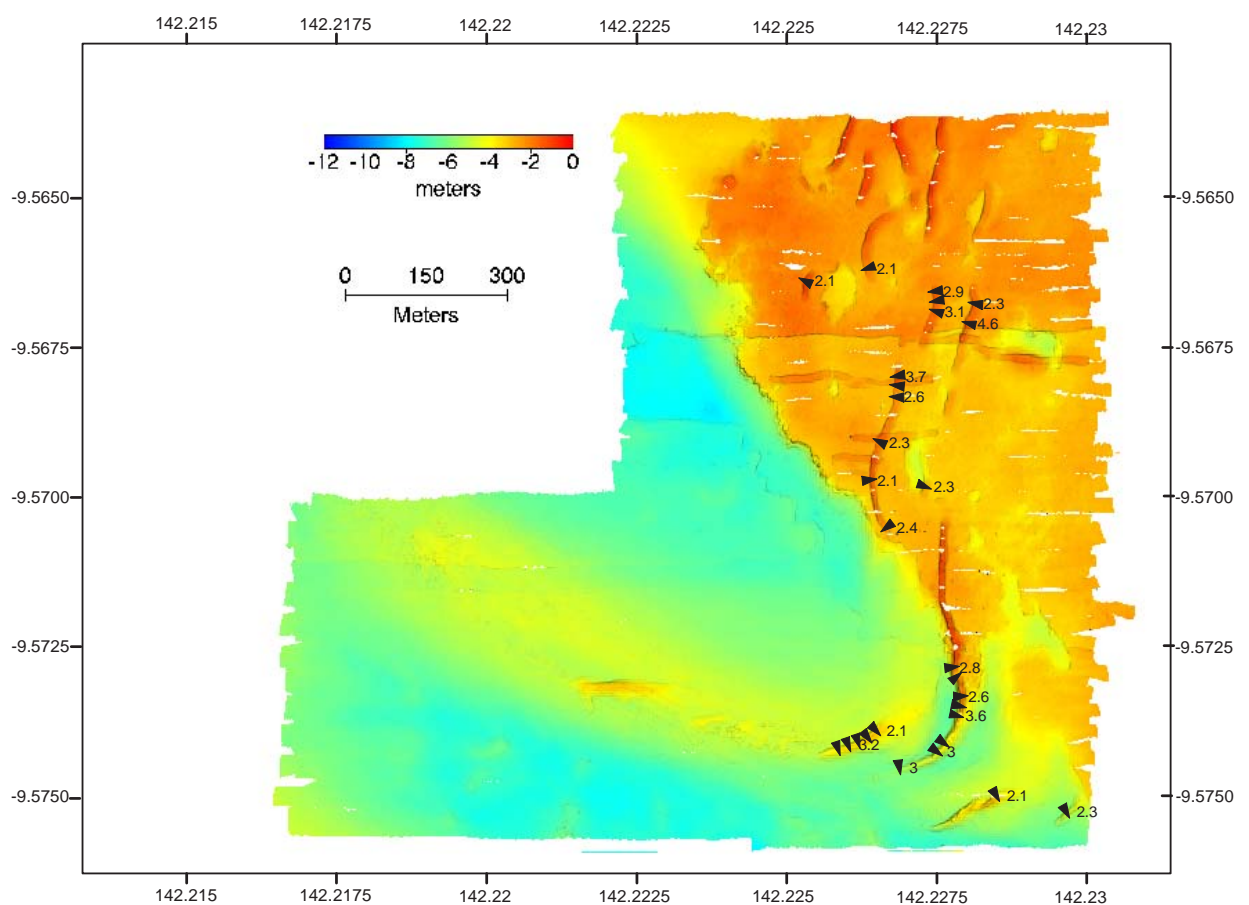


Figure 2.1. Sandwave crest migration as determined from repeat multibeam sonar surveys of Area A. Arrows show the direction of sandwave crest migration over a 14 day period. Values associated with each arrow indicate the distance (in meters) each crest moved during that time.

### 2.3.2.2. Sandwave Crest migration in Area B

Area B also showed regions with different directions of sandwave crest migration (Fig. 2.2). The western and central portions of Area B show a dominantly eastward migration direction, at an average of 3 m over the survey period. The eastern portion of the sandbank shows a complex arrangement of transport vectors with some areas of westward migration.

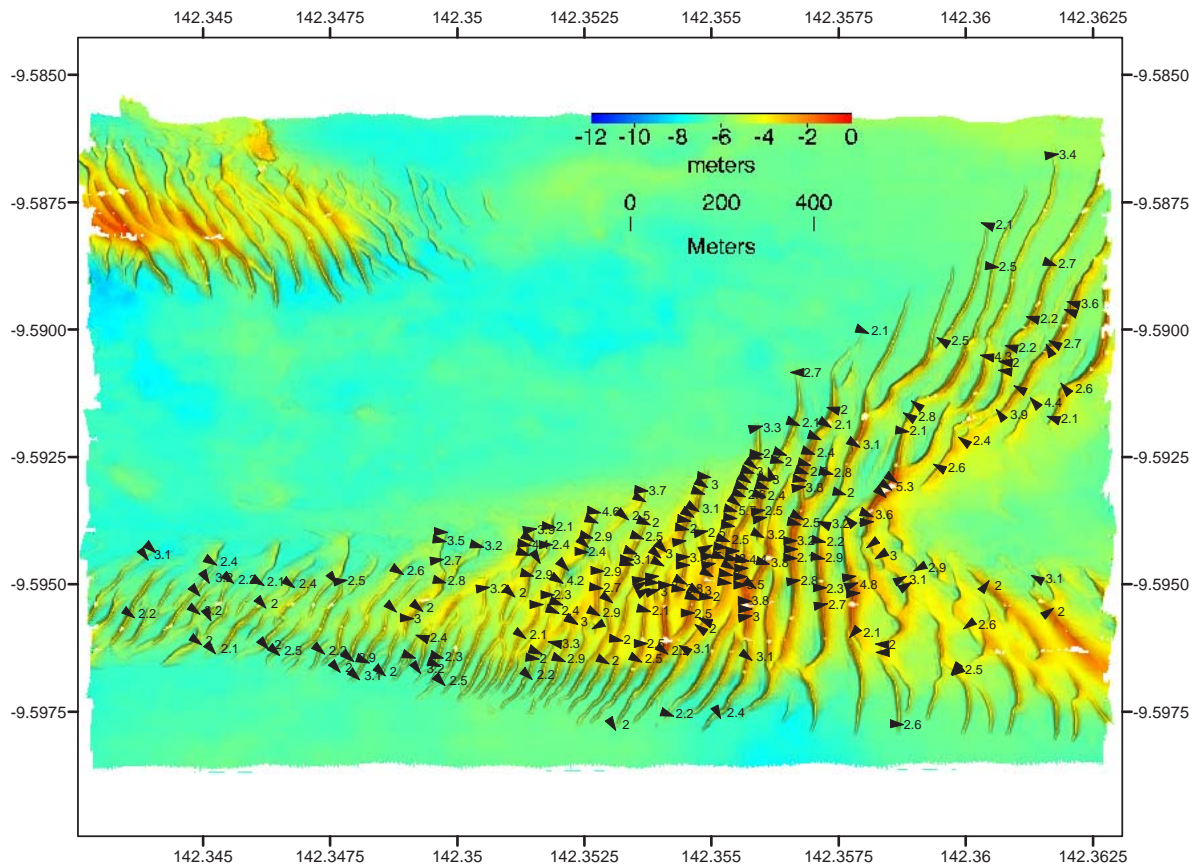


Figure 2.2. Sandwave crest migration as determined from repeat multibeam sonar surveys of Area B. Arrows show the direction of sandwave crest migration over a 14 day period. Values associated with each arrow indicate the distance (in meters) each crest moved during that time.

### 2.3.3. Comparison with monsoon survey – sandwave crests

In order to estimate how the sandwave crest migration changed between the two survey seasons scatterplots of the migration vectors were created (Fig. 2.3 & 2.4). For both Areas A and B vectors smaller than 2 meters were not considered due to the degree of error involved in calculating the migration rates.

#### 2.3.3.1. Area A

Different patterns of crest migration were observed at the end of the monsoon and trade wind seasons (surveys 266 and 273 respectively). During the monsoon season, Area A was characterised by crest migration to the east, often at greater than 10 m over the 14 day study period (Fig. 2.3). During the trade wind season, the overall magnitude of the sand wave movement was less than 4 m and the direction of the migration was either to the west or south east (Fig. 2.3).

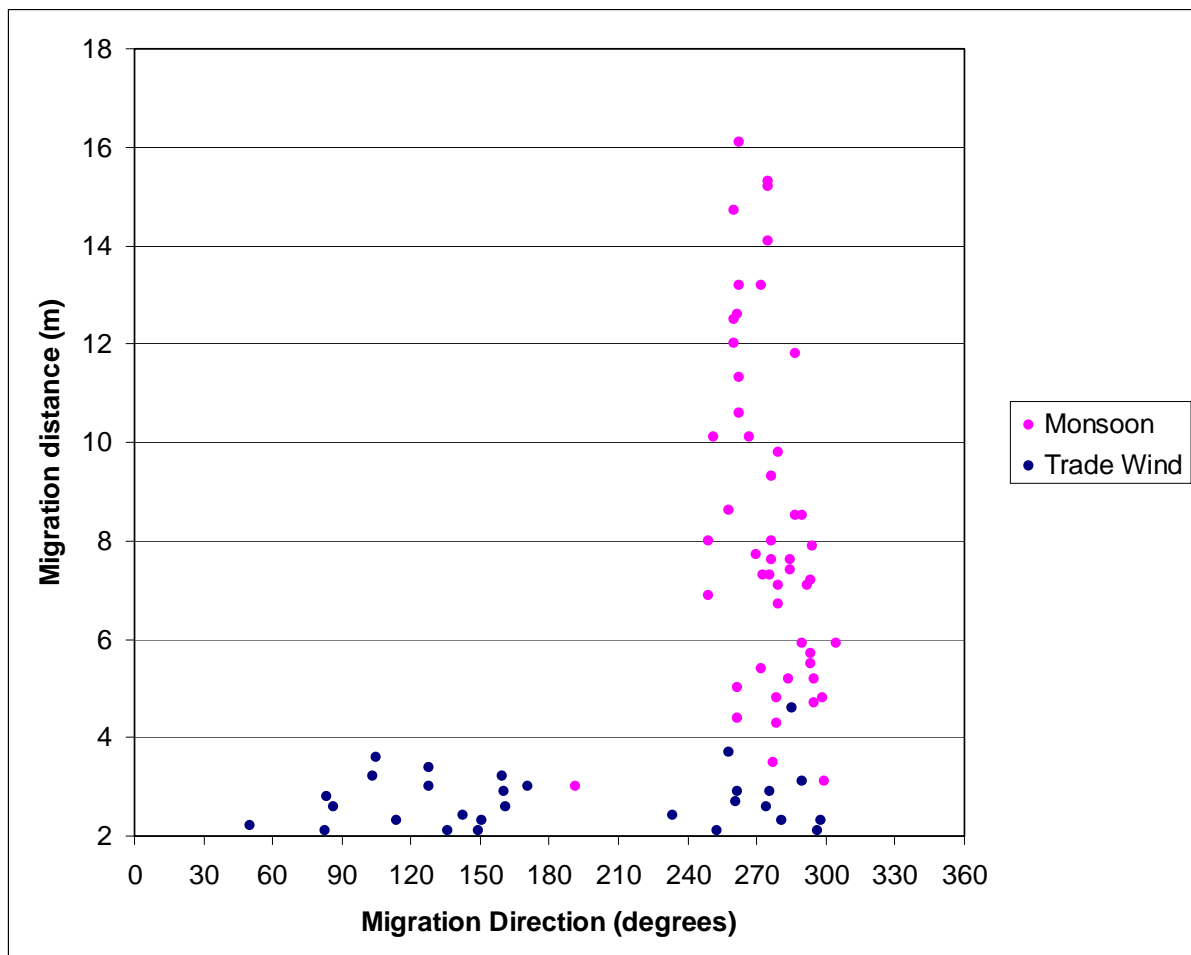


Figure 2.3 Scattergram of crest migration vectors for Area A using data from both the monsoon and trade wind surveys. Strong, westward migration is shown for the monsoon season survey while a more variable result was obtained for the trade wind season.

### 2.3.3.2. Area B

Sandwaves in Area B also showed different patterns of crest migration between the two surveys (Fig. 2.4). During the monsoon season (survey 266) the crests moved to the east and northeast similar to the crests in Area A. The maximum crest migration reached approximately 11 m. By comparison, during the trade wind season (survey 273) migration was directed generally towards the east, with some crests migrating to the west. The magnitude of the crest migration reached 4 m.

Both the monsoon and trade wind surveys recorded a bimodal pattern of crest migration. The monsoon season, despite having a dominant westwards migration pattern, maintained a region of weak, eastward, crest migration along its northwest margin. During the trade wind survey, this bimodal pattern is opposite with eastward migration dominating over the bank and weak westward migration present on the western side of the bank.

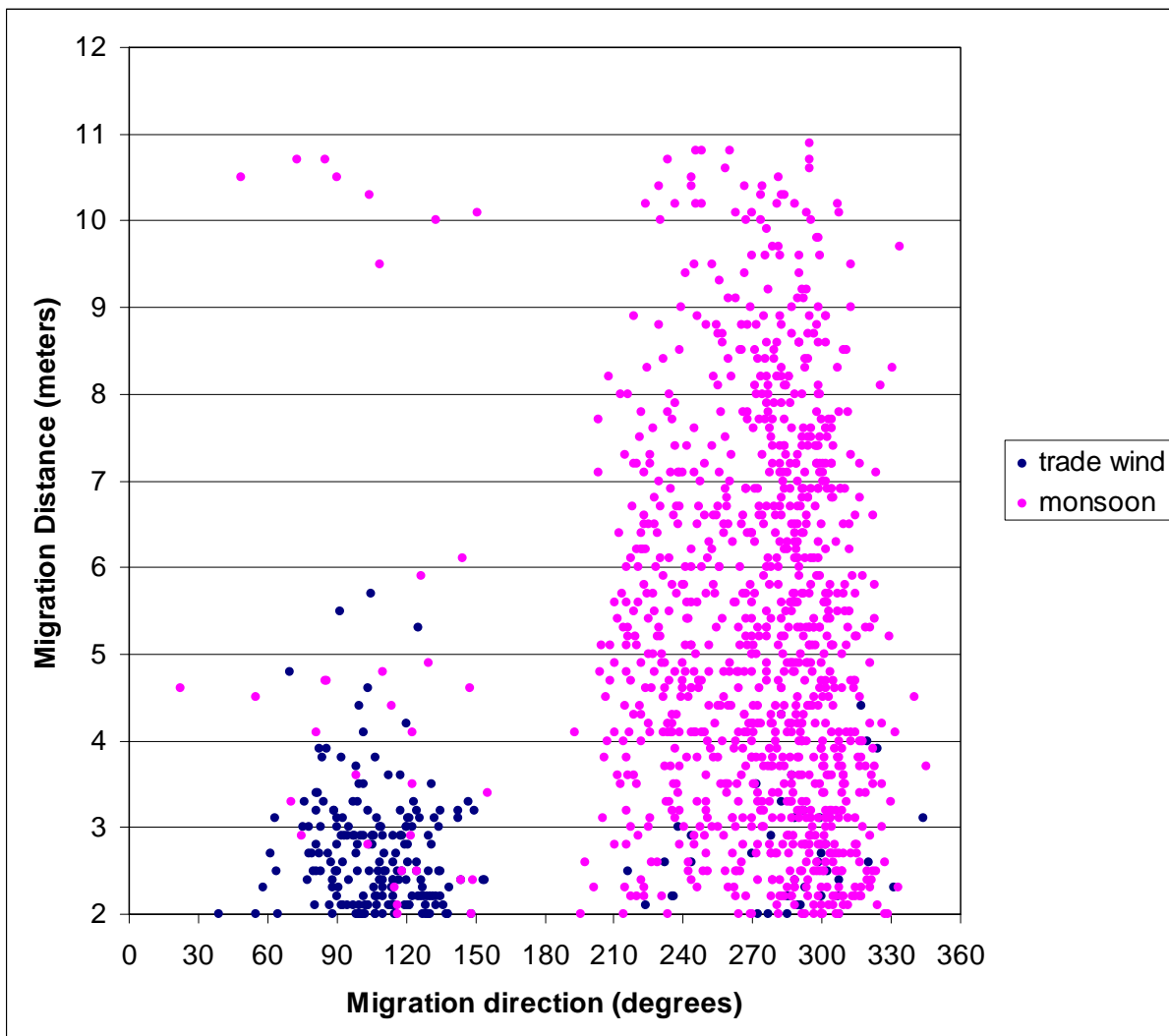


Figure 2.4. Scattergram of crest migration vectors for Area B. Strong, westward migration is shown for the monsoon season survey while a typically eastwards result was obtained for the trade wind season.

### 2.3.4. Comparison with monsoon survey – bedform locations

#### 2.3.4.1. Area A

The overall migration of the sandbank in Area A was observed by tracing the areas covered by the sandwaves and comparing their extents between the two surveys. Between the monsoon and trade wind surveys the sandwaves in Area A migrated to the west by up to 60 m from their original position. In the north the direction was roughly perpendicular to their crests. In the south the sandbanks migrated obliquely to their crests.

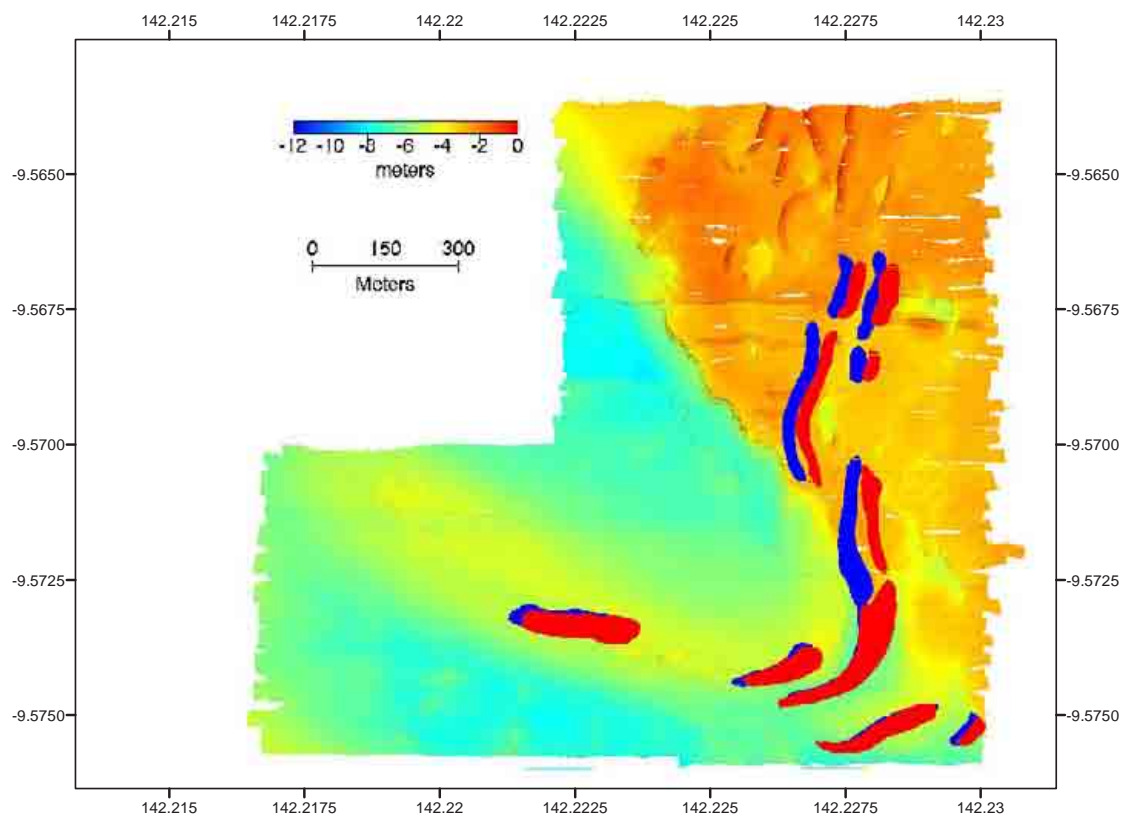


Figure 2.5. Map showing changes in locations of sandwaves in Area A. Areas in red indicate the outlines of sandwaves during the monsoon season survey (266) whilst the blue areas indicate the outlines of the sandwaves during the trade wind season survey (273).

### 2.3.4.2. Area B

In Area B the overall migration of the sandbanks was estimated by tracing the area covered by the banks and comparing their extents between the two surveys. Very little movement (close to zero) was observed in the over all extents of the sandbank between the two survey seasons. The only part of the sandbank that appeared to move any significant distance over the 6 months was the western edge of the north eastern arm of the sandbank which migrated approximately 15 m to the west.

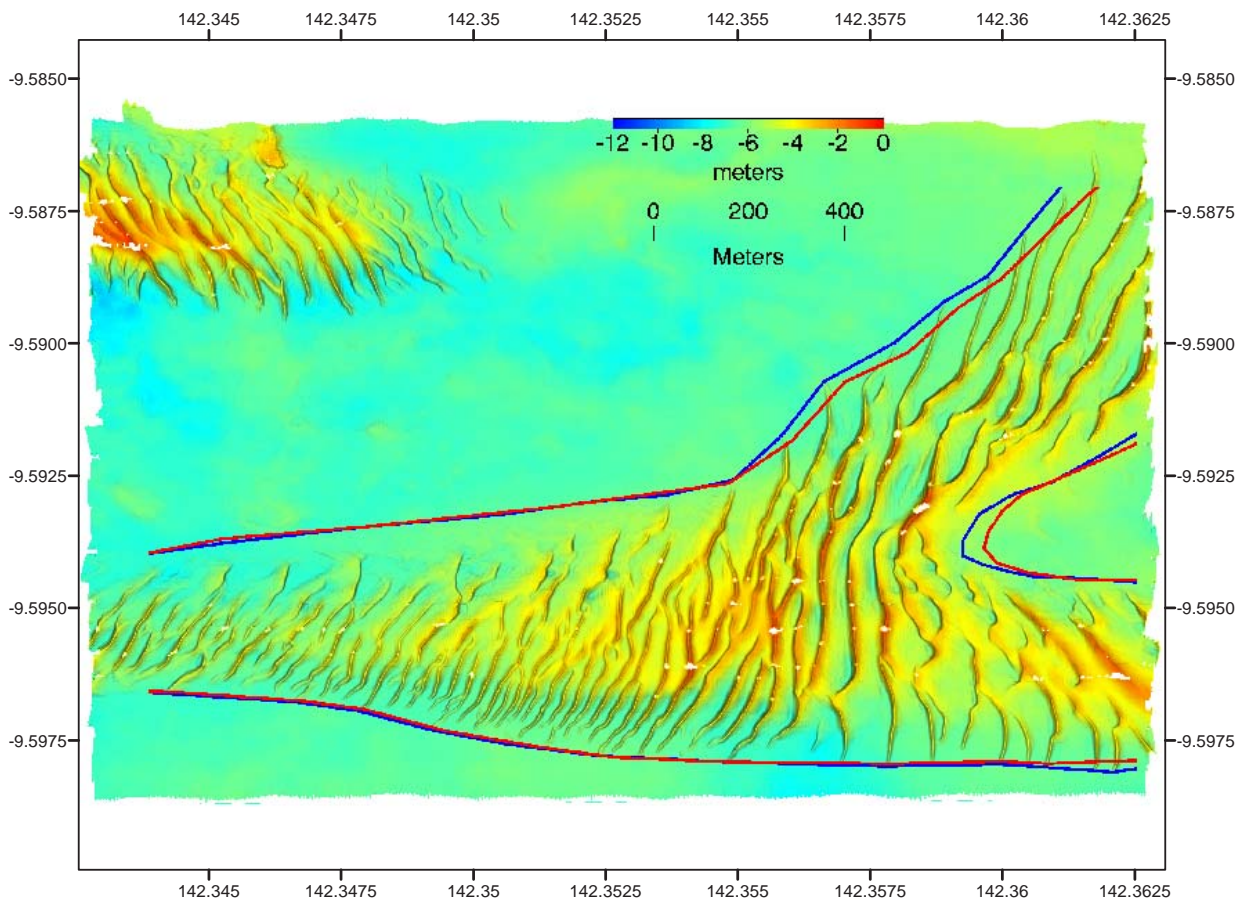


Figure 2.6. Map showing changes in location of sandbanks in Area B. The area outlined in yellow mark the extents of the sandbank during the monsoon season survey (266). The area outlines in red mark the extents of the sandbank during the trade wind season survey (273).

## 2.4. Landsat Image Processing

Two Landsat scenes were used to estimate the rates at which the large sandbanks in western Torres Strait migrated over a 15 year period. Two scenes, one from 1987 and one from 2003, were used in the study. The measurements were made by digitising the apex of each sandbank for both scenes and then measuring the displacement. The sandbanks in northwest Torres Strait typically have a barchan 'form' and the apex is defined as the location where their two horns meet on the 'lee' side of the sandbank to form a chevron-shaped slip face. This apex can be located year to year and hence can be used for long term monitoring of sand bank movement.

The overall displacement was highly variable. A maximum displacement of 540 m was recorded for one bank, however- the average was approximately 200 m over the 15 years or approximately 13 m per year (Fig. 2.7). As the pixel resolution of the scenes is 30 m, analysing yearly or season migration rates was not feasible. The average yearly migration is measured from the Landsat imagery is comparable with migration rate measured in Area B using multibeam sonar (Fig. 2.6).

These results suggest that the large (typically barchan or linear) sandbanks in Torres Strait are mobile but unlikely to significantly impact on seagrasses in Torres Strait on a regional scale. Smaller sandwaves, such as those seen in Area A (Fig. 2.5), are more mobile than the large sandbanks and hence may pose a threat to the adjacent seagrass habitats. Small sandwaves are not always visible in Satellite imagery and hence a historic record of their movement is not available.

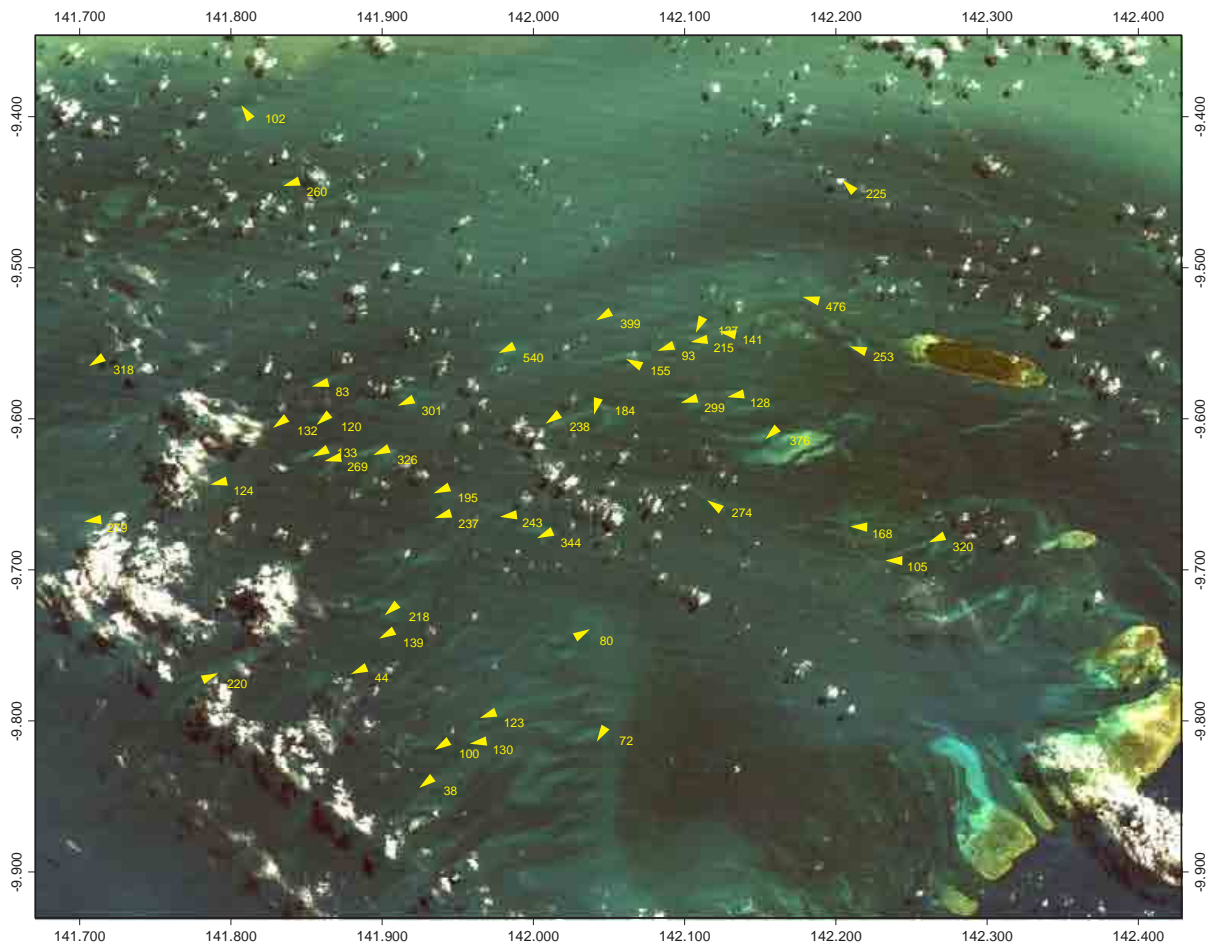


Figure 2.7. Displacement of sandbanks over a 15 year period (1988-2003). Arrows define the direction that each bank has moved over a 15 year period. The values associated with the arrows indicate the displacement in meters, of the banks over the 15 year period.

## 3. Meteorology

### 3.1. Synoptic Observations

Post-survey, meteorological data were obtained from the Bureau of Meteorology Climate and Consultancy Office for the two nearest sites to Turnagain Island in Torres Strait:

- Horn Island ( $-10^{\circ}35'S$ ,  $142^{\circ}13'E$ ), and
- Coconut Island ( $-10^{\circ}03'S$ ,  $143^{\circ}04'E$ ).

As meteorological data was not available at the time of the publishing of the monsoon survey report (Heap et al., 2005) it has been included here for comparison to the trade wind season. For the monsoon season pre-processed meteorological data were acquired for the period 13-March-2004 to 19-April-2004 inclusive, to cover both the two-week period before the survey, and the survey period itself (27-Mar-2004 to 18-April-2004). For trade wind season pre-processed meteorological data were acquired for the period 27-September-2004 to 29-October-2004 inclusive, to cover both the two-week period before the survey, and the survey period itself (7 October to 29 October 2004). A wind record for Horn Island dating back to 1950 was also obtained to investigate seasonal differences in wind strength.

At the Horn Island site, meteorological data are recorded at 4 m above sea level. The following variables are recorded hourly:

- Date/Time (EST)
- Wind Direction ( $^{\circ}N$ )
- Wind Speed (kph)
- Gust Speed (kph)
- Dry-bulb Temperature ( $^{\circ}C$ )
- Wet-bulb Temperature ( $^{\circ}C$ )
- Dew-point Temperature ( $^{\circ}C$ )
- Relative Humidity (%)
- Atmospheric Pressure (hPa)
- Rain since 9am (mm)

At the Coconut Island site, meteorological data are recorded at 3.5 m above sea level. The following variables are recorded every 3-hours:

- Date/Time (EST)
- Wind Direction (°N)
- Wind Speed (kph)
- Dry-bulb Temperature (°C)
- Atmospheric Pressure (hPa)
- Rain since last observation (mm)

Although these sites are located approximately 110 km (Horn Island) and 50 km (Coconut Island) distance from Turnagain Island, they are expected to be similar to the conditions at the field areas.

### 3.1.1. Monsoon Season (Survey 266: 13/03/04 – 19/04/04)

The meteorological conditions experienced at Horn Island and Coconut Island are shown in [Figs. 3.1 & 3.2](#) respectively. Some data are missing from the meteorological record at the Horn Island site ([Fig. 3.1](#)). The longest period for which data are absent occurs between 0500, 26-March 2004 GMT – 0400 28-March-2004 GMT which coincides with the commencement of the survey. Recorded winds from Coconut Island indicate that winds were light during this period ([Fig. 3.2](#)).

The meteorological data from both Horn Island and Coconut Island indicate that the two-week period before the survey were characterised by strong north-westerly winds, particularly between Julian Days (JD) 75 and 80. Wind speed gusts at Horn Island during this period reached a maximum of  $15.3 \text{ m s}^{-1}$ , and mean wind speeds reached a maximum of  $9.2 \text{ m s}^{-1}$ . This period was associated with the passage of a monsoonal low (atmospheric pressure of  $<1000 \text{ hPa}$  at both locations) passing across northern Australia, and high rainfall (64 mm of rain recorded at Horn Island on JD 75).

At the commencement of the survey (JD 85), the wind direction changed from the northwest to the southeast. Winds remained from the southeast for the entire survey. Wind speeds were light ( $\sim 5 \text{ m s}^{-1}$ ) for the first week of survey (to JD 93). For the period of JD 95 – 105, wind speeds strengthened to record mean wind speeds of approximately  $10 \text{ m s}^{-1}$ , gusting to approximately  $15 \text{ m s}^{-1}$ , at Horn Island. For the period JD 105-108, wind speeds reduced to approximately  $5 \text{ m s}^{-1}$  at Horn Island.

Atmospheric pressure remained above 1000 hPa throughout the entire survey. Small amounts of rain (typically <20 mm per day), were recorded at Coconut Island.

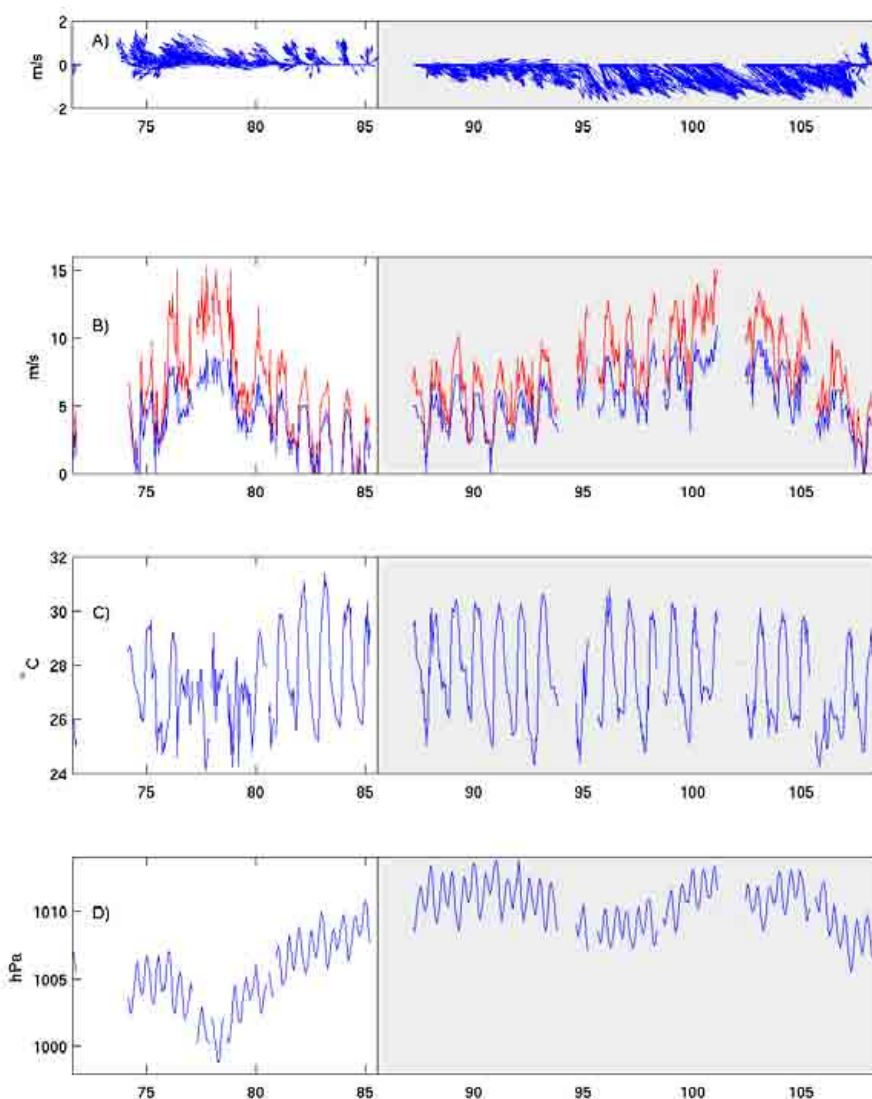


Figure 3.1. Time-series of raw meteorological data at Horn Island. a) Vector plot of mean wind speed. Direction indicates direction from which wind is coming. b) Wind speed. The lower line is the mean wind speed, and the upper line is the maximum gust experienced during the hour, c) Dry-bulb (air) temperature, d) Air Pressure. The shaded region corresponds to the period of the monsoon survey.

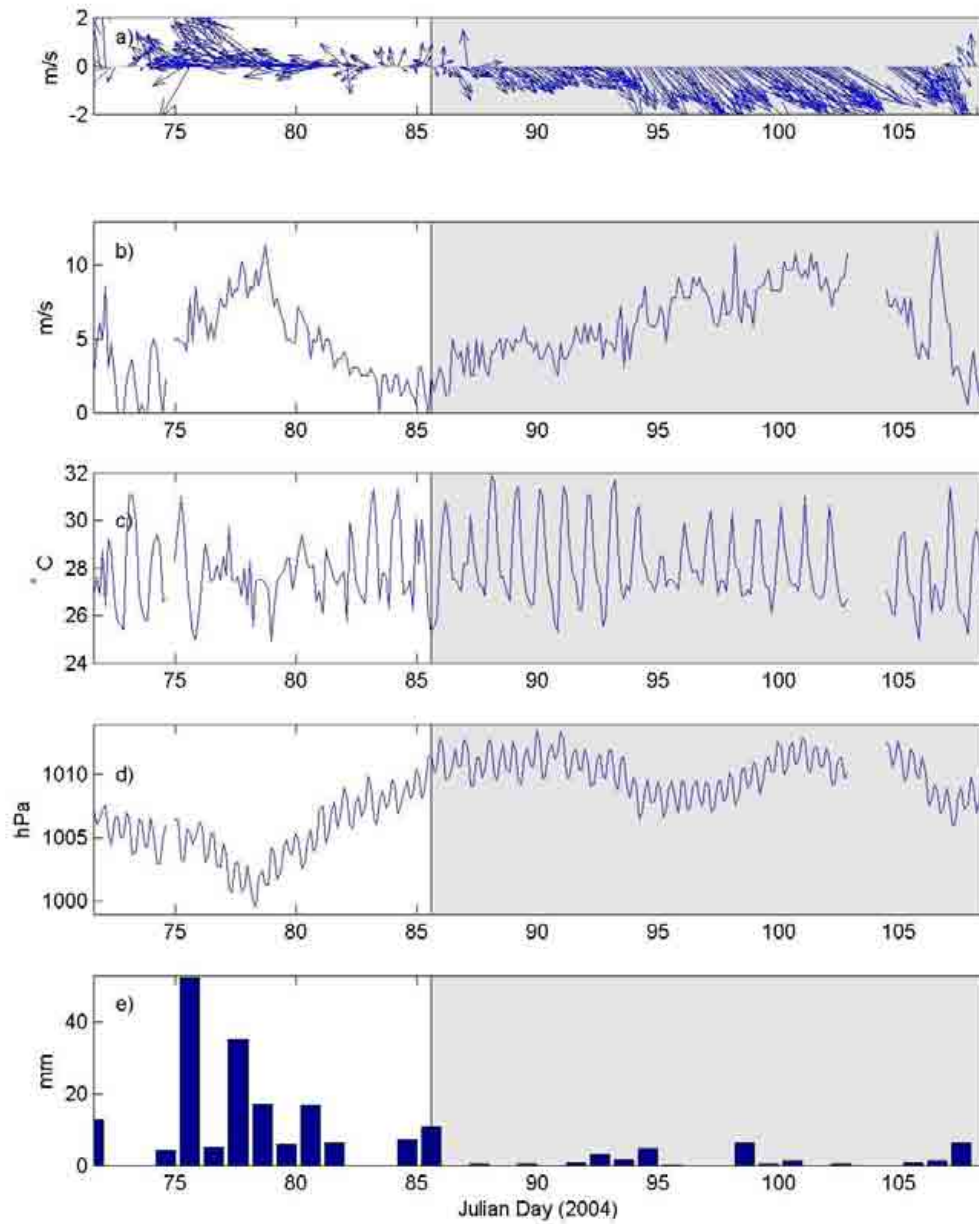


Figure 3.2. Time-series of raw meteorological data at Coconut Island. a) Vector plot of mean wind speed, b) mean wind speed, c) Dry-bulb (air) temperature, d) Air Pressure, and e) Daily rainfall. The shaded region corresponds to the period of the monsoon survey.

Table 3.1. Meteorological statistics from data obtained from Bureau of Meteorology for the Monsoon survey.

Location	Latitude Longitude	First Record EST (2004)	Last Record EST (2004)	Sampling Interval	Wind Spd Mean Wind Spd Std Wind Spd Max	Gust Mean Gust Std Gust Max	Temp Min Temp Mean Temp Max	Pres Min Pres Mean Pres Max
Horn Island	10°34.8'S 142°17.4'E	00:00 13 March	00:00 19 April	Hourly	4.85 m/s 2.43 10.83	7.40 m/s 3.20 15.28	24.1°C 27.42 31.40	998.8 hPa 1008.4 1013.7
Coconut Island	10°3.0'S 142°4.2'E	00:00 13 March	00:00 19 April	3-Hourly	5.45 m/s 2.74 12.22	- - -	24.9°C 27.95 31.90	999.6 hPa 1008.3 1013.5

### 3.1.2. Trade Wind Season (Survey 273: 08/10/04 - 28/10/04)

The meteorological conditions experienced at Horn Island and Coconut Island are shown in [Figs. 3.3 & 3.4](#) respectively

For the period leading up to the survey, and the entire survey period itself, winds were relatively strong (mean  $\sim 6 \text{ m s}^{-1}$ ) from the south-east, typical of the trade wind season. Two periods of decreased wind speeds were observed during the survey period: JD 282-284, and JD 288-290. Strongest winds (mean wind speed peaked at  $10.83 \text{ m s}^{-1}$  at Horn Island, and  $9.81 \text{ m s}^{-1}$  at Coconut Island on JD 299) were experienced during the two periods of JD 284-287, and JD 298-301. Temperature at both stations are observed to have a strong diurnal variation, varying between  $\sim 24^\circ\text{C}$  during night hours to a peak of  $\sim 31^\circ\text{C}$  during the afternoon. Atmospheric pressure shows a strong semi-diurnal signal at both stations. At lower frequencies, the region experienced higher pressure of  $\sim 1014 \text{ hPa}$  during the first week of the survey, before falling to  $\sim 1010 \text{ hPa}$  on JD 288, and remaining relatively steady for the remaining time. No rainfall was recorded at either sampling location throughout the period of the survey.

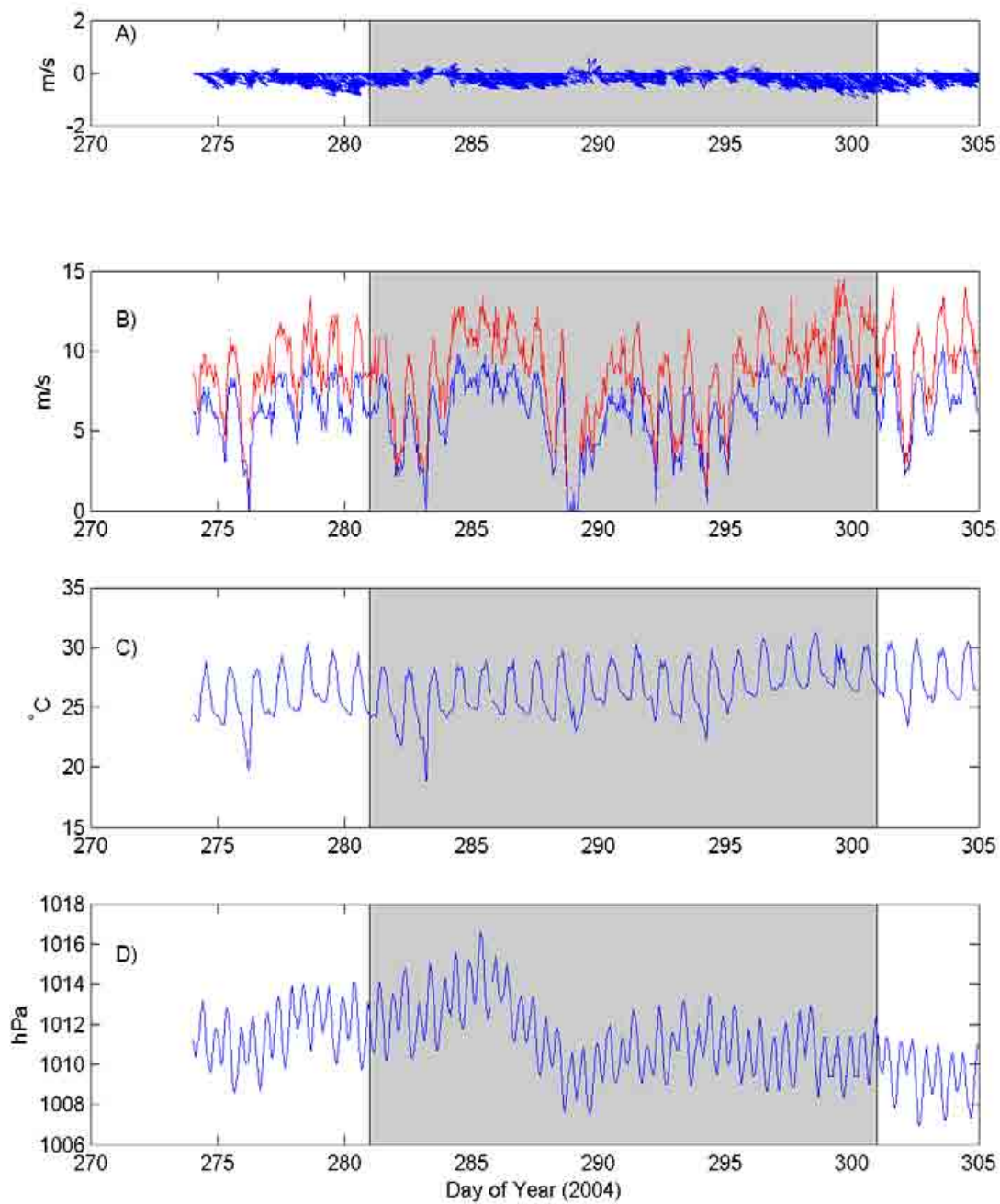


Figure 3.3. Time-series of raw meteorological data at Horn Island for the month of October 2004. a) Vector plot of mean wind speed. Direction indicates direction from which wind is coming. b) wind speed. The lower line is the mean wind speed, and the upper line is the maximum gust experienced during the hour, c) Dry-bulb (air) temperature, and d) Air Pressure. The shaded region corresponds to the period of the survey.

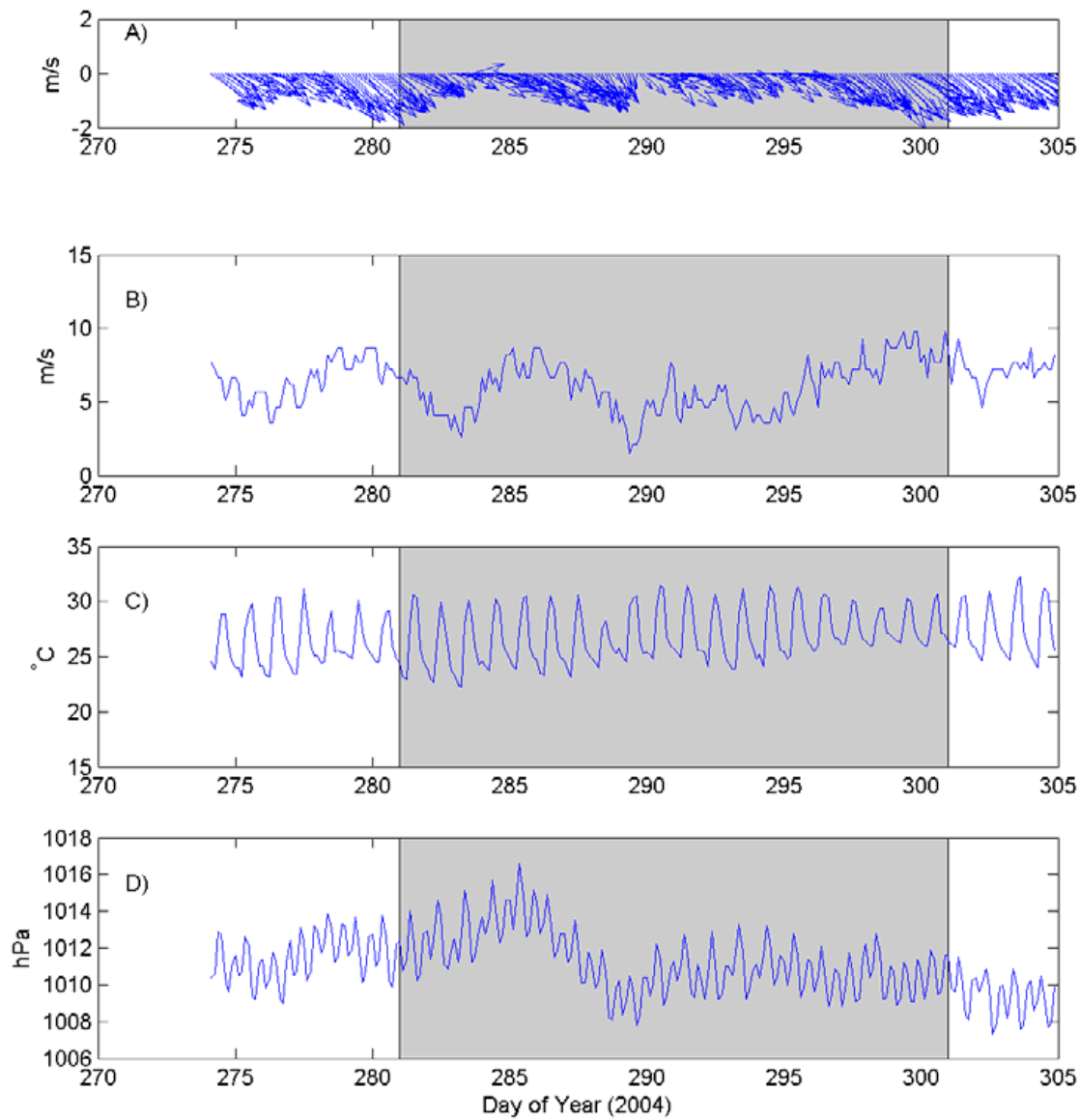


Figure 3.4. Time-series of raw meteorological data at Coconut Island for the month of October 2004. a) Vector plot of mean wind speed, b) mean wind speed, c) Dry-bulb (air) temperature, d) Air Pressure. The shaded region corresponds to the period of the survey.

Table 3.2. Meteorological statistics from data obtained from Bureau of Meteorology for the trade wind survey.

Location	Latitude Longitude	First Record EST (2004)	Last Record EST (2004)	Sampling Interval	Wind Spd Mean Wind Spd Std Wind Spd Max	Gust Mean Gust Std Gust Max	Temp Min Temp Mean Temp Max	Pres Min Pres Mean Pres Max
Horn Island	10°34.8'S 142°17.4'E	00:00 8 October	00:00 28 October	Hourly	6.19 m/s 2.19 10.84	8.71 m/s 2.78 14.44	18.90°C 26.63 31.30	1007.5 hPa 1011.3 1016.6
Coconut Island	10°3.0'S 142°4.2'E	00:00 8 October	00:00 28 October	3-Hourly	5.96 m/s 1.81 9.81	- - -	22.3°C 26.91 31.40	1007.8 hPa 1011.3 1016.6

### 3.1.3. Comparisons between Monsoon and Trade Wind seasons

Of all the meteorological data acquired, the wind data gave an indication of two different modes of activity between the two seasons.

There is a strong contrast between wind speed and direction in the two weeks preceding the monsoon and the wind during the survey (Figs. 3.1a, 3.2a, 3.5). Before the survey, the wind was dominantly (but highly variable) from the northwest. During the survey the wind changed direction from the northwest to a strong and persistent southeast direction. During these four weeks both typically monsoon conditions (variable north westerlies) and trade wind conditions (persistent south easterlies) were observed. During the trade wind survey strong south easterlies were observed (Figures 3.3a, 3.4a, 3.6). These are typical conditions for the trade wind season for this region.

The wind record for Horn Island from early 2003 to late 2004 shows that monsoon survey coincided with the rapid change from monsoon (north westerly winds) to trade wind condition (strong and consistent south easterlies) (see figure 3.7).

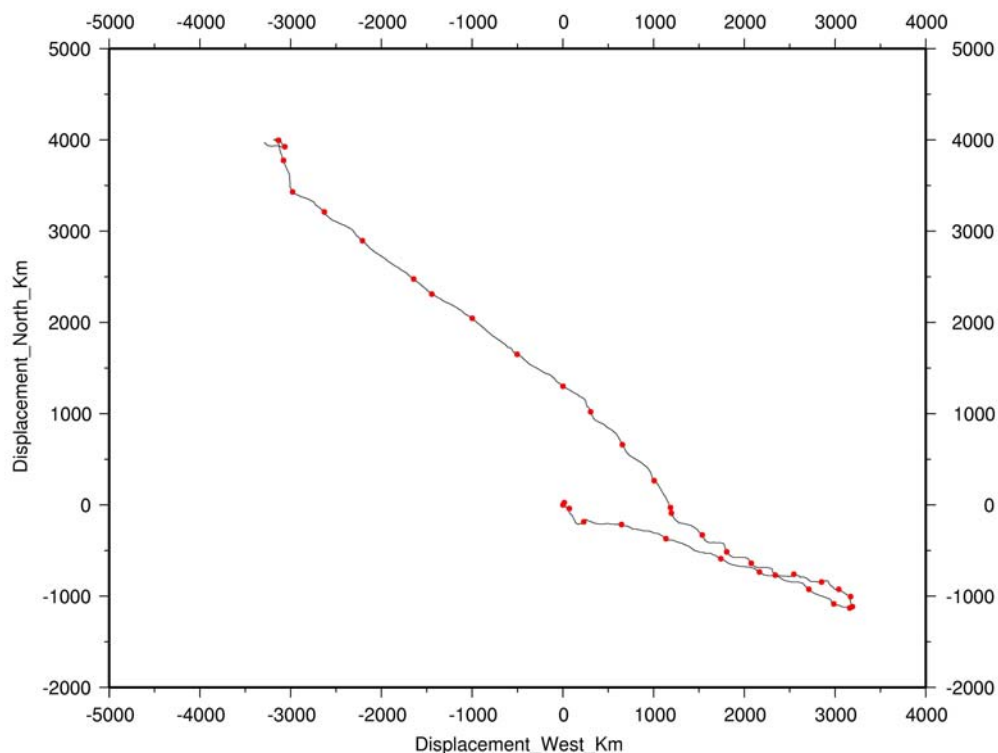


Figure 3.5. Progressive Vector Diagram of wind vectors in km from Horn Island during survey 266 and the two weeks preceding (13-March-2004 to 19-April-2004). Red dots indicate the start of each day.

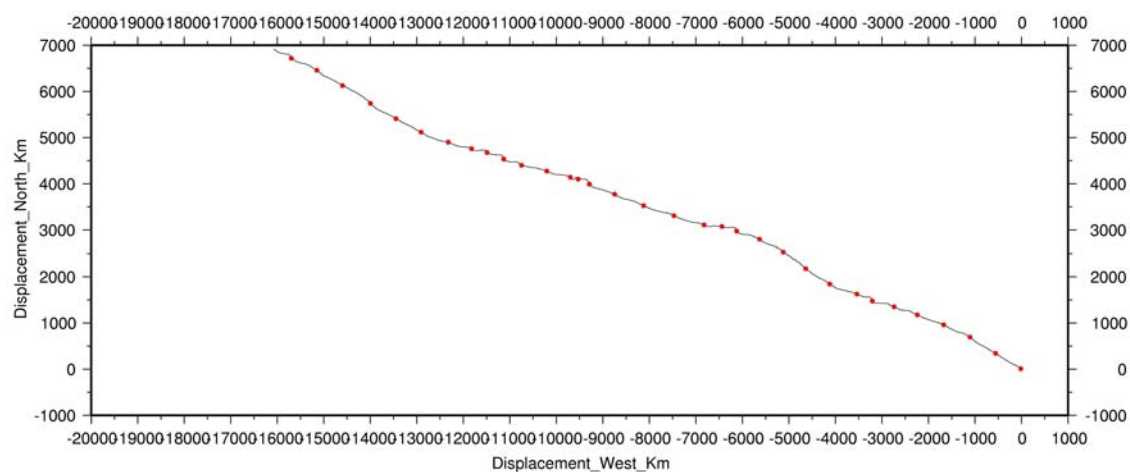


Figure 3.6. Progressive Vector Diagram of wind vectors in km from Horn Island during survey 273 and the two weeks preceding (27-September-2004 to 29-October-2004). Red dots indicate the start of each day.

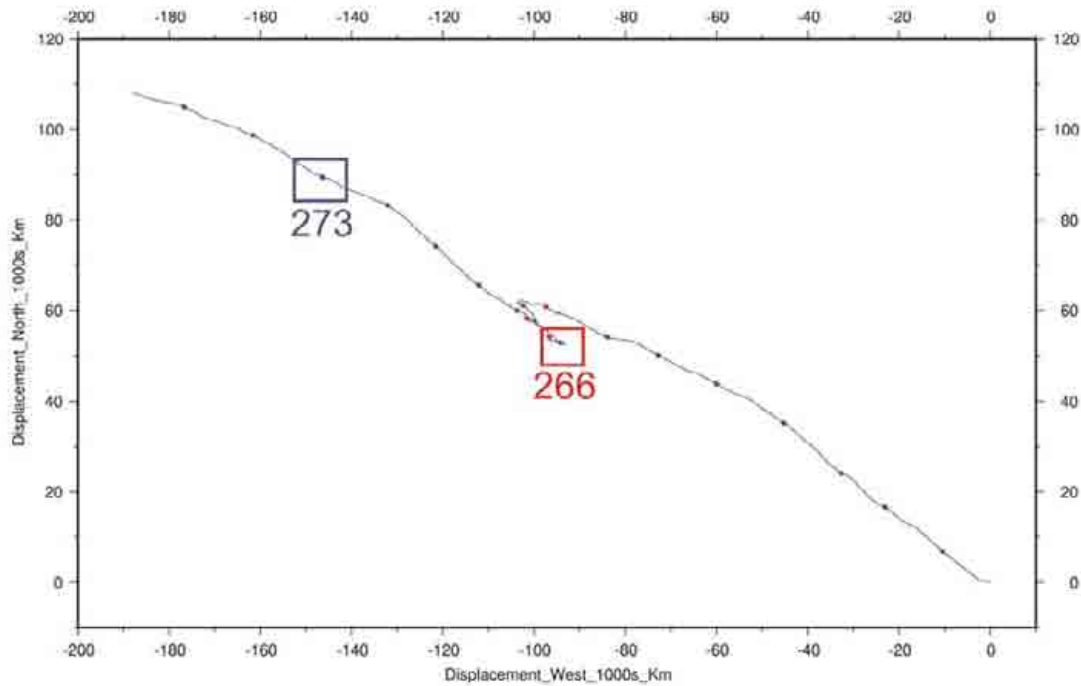


Figure 3.7. Progressive vector diagram of wind data recorded at Horn Island from early 2003 to late 2004. Blue dots indicate the start of each month of the Trade Wind season (April-November), Red dots indicate the start of each month of the monsoon months (December-March). The blue and Red boxes indicate approximate times at survey 266 (monsoon) and 273 (trade wind) were undertaken.

The multibeam bathymetry acquired during the monsoon survey indicated that the sandwaves were facing the east at the beginning of the survey period (Heap et al., 2005). This is consistent with the wind directions observed before the survey and considered representative of the monsoon season (Figs. 3.5, 3.7). Heap et al. (2005) concluded that the westward migration of the sandwave crests during the survey may have been enhanced by the change to the south easterly wind. Harris (1991) demonstrated that in the Adolphus Channel (SE Torres Strait) that similar scale bedforms do reverse their orientation with the season change in wind directions. Data acquired during the monsoon season survey supports this conclusion.

The overall rate of sandwave migration during trade wind survey was much less than during the monsoon season (compare Heap et al., (2005) and [section 2](#) this volume), hence the consistent south easterly wind experienced during the trade wind survey did not translate into strong, westward migration of the bedforms (Figs. 2.3, 2.4). These results indicate that during the transition from the monsoon season to the trade wind season the sandwaves adjust quickly to the new hydrodynamic regime resulting in rapid reworking and migration of the sandwave crests. The comparatively weak crest migration observed during the trade wind season suggests that once the sandwaves have re-equilibrated themselves to the hydrodynamics of the trade wind season there is then a minimal amount of crest migration.

### 3.1.4. Wind observations from 1950-1993

Wind observations from Horn Island for the period 1950-1993 were compiled for inter annual comparisons (Fig. 3.8). A net displacement to the northwest is observed for every year in the record.

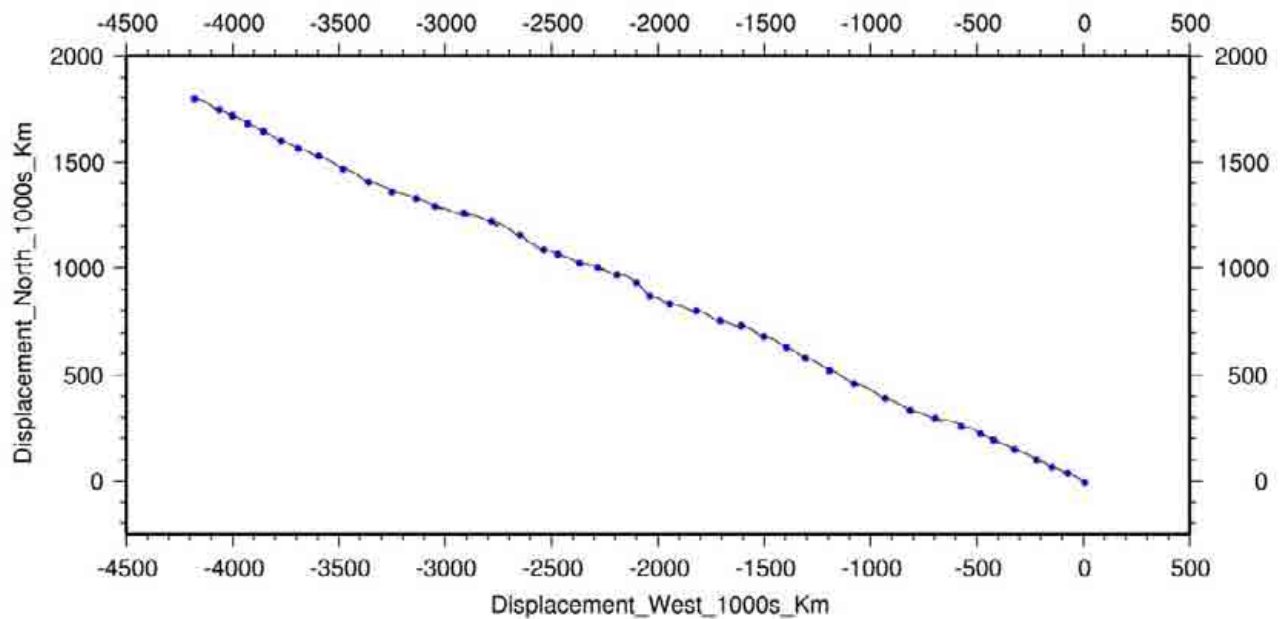


Figure 3.8. Progressive vector diagram of the wind data acquired at Horn Island, the data is acquired hourly and no filtering is applied. The record shows that there is a consistent south easterly trend in the data over the 42 year period. Blue dots indicate on beginning of each year.

There is a change in wind conditions expected between the trade wind season which is characterised by strong southeasterly winds and the monsoon season which is characterised by weak and variable winds (Fig. 3.9). The strong and consistent nature of the trade winds is shown by a displacement to the northwest whilst the monsoon winds are more variable (Fig. 3.9). Although all the points that are plotted as monsoon season are well grouped, they occur around the origin (0,0). This indicates that the seasonal vectors for the monsoon winds cannot be characterised by a single azimuth as the trade winds can. This has implications for sandwave mobility as a weak monsoon season may prevent sandwaves from reversing at the end of the monsoon season and create a situation where continuous cycles of westward transport of sandwaves could occur. This scenario could have significant implications of seagrass communities and warrants further investigation.

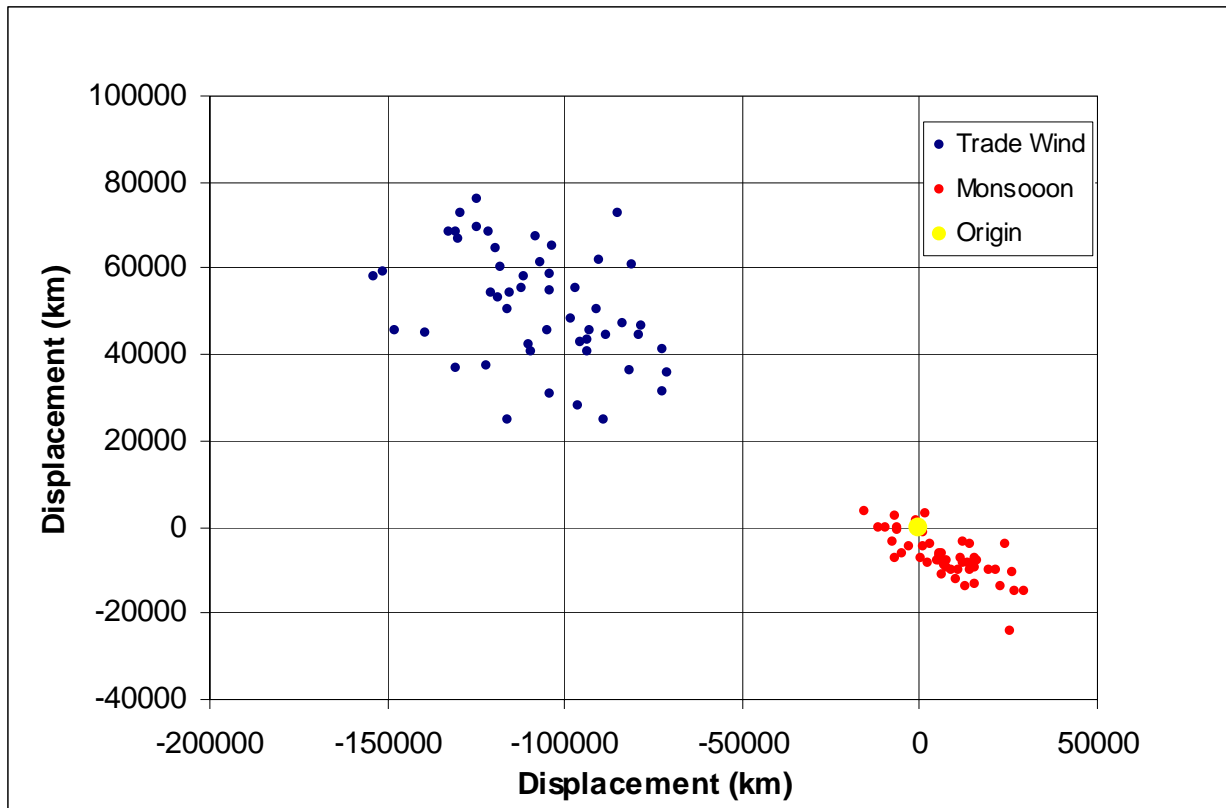


Figure 3.9. Scattergram plot of seasonal wind displacements 1950-1993. Blue dots indicate displacement vectors for each trade wind season from 1950-1993. Red dots indicate displacement vectors for each monsoon season from 1950-1993. The origin (0,0) is indicated in yellow and indicates zero net displacement.

## 4. Oceanography

### 4.1. Hydrodynamic Deployments

The hydrodynamic conditions were recorded with an array of instruments designed to measure currents, temperature, salinity, and turbidity. Moorings were deployed at seven locations (Fig. 4.1). One mooring was located to the east of the Orman Reefs (01CM01), One mooring was located in Area A (02CM07), and five moorings were located in Area B (03CM02 (BRUCE), 04CM03, 05CM04, 06CM06, 07CM05). Table 4.1 summarises the sensors located on each mooring. Descriptions of the seven moorings are given in sections 4.1.1-4.1.7.

Table 4.1. Summary of deployed sensors.

Mooring	ADCP	Current Meter	Depth	Salinity	Pressure	Conductivity	Fluorescence	Turbidity	Temperature	Dissolved Oxygen	Light (PAR)	Chlorophyll (Fluorometer)	Laser In-situ Scattering Transmissometer	Optical Backscatter Sensor (OBS)
01CM01				+	+	+	+	+	+	+	+	+		
02CM07	+			+	+	+	+	+	+	+	+	+		
03CM02		+	+		+	+			+				+	+
04CM03	+													
05CM04	+													
06CM06	+			+	+	+	+	+	+	+	+	+		
07CM07		+												

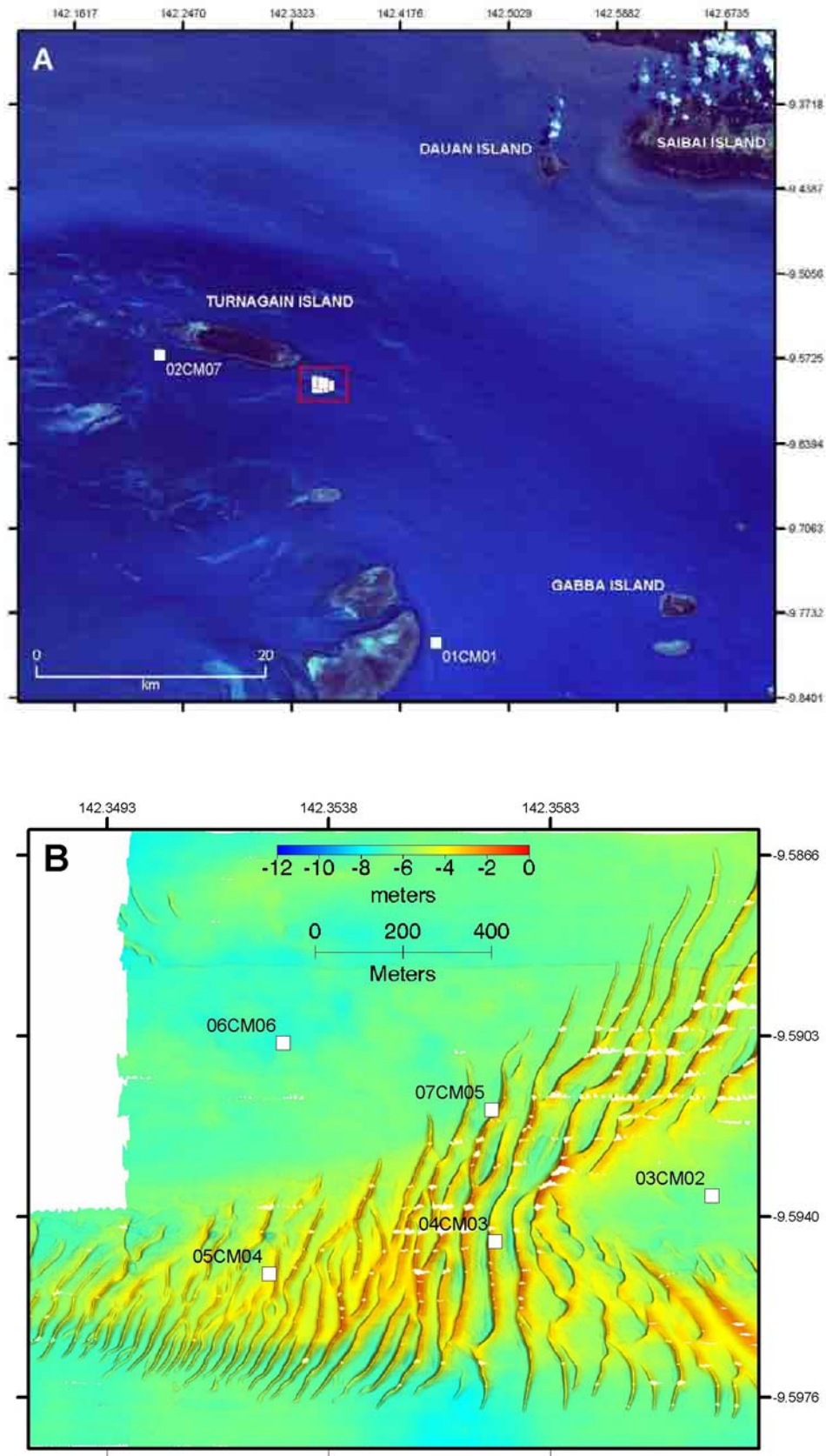


Fig. 4.1a. Locations of hydrodynamic deployments over the Torres Strait region. The area enclosed by the red box (Area B) is shown in detail in Fig. 4.1b.

#### 4.1.1. Station 01CM01

01CM01 contained instrumentation supplied by CSIRO Marine and Atmospheric Research. The mooring was deployed to the east of the Orman Reefs at location -9° 47.794' S, 142° 26.764' E in 10.5 m water depth. Bottom sediment at the site was composed of poorly-sorted calcareous muddy, fine sand with a mean grain size of 0.219 mm (273/01GRVV01). The mooring was deployed at 07:38 8/10/2004 GMT and recovered at 20:22 26/10/2004 GMT, resulting in a total deployment length of 18.5 days.

Due to the problems with the instrument frame planned to be used for mooring 04CM03, the frames for 04CM03 and 01CM01 were swapped. This had no influence on the instrumentation, however the mooring design was altered from that of other CSIRO moorings to that used for GA moorings. Geoscience Australia Acoustic Release Unit 117 was deployed with this mooring. The aim of the deployment was to determine the hydrography of water near to a site of high seagrass abundance during the well established trade-wind season.

Mooring 01CM01 contained a Seabird Electronics (SBE™) 19 Multi-sensor (#19P34180-4537) with fluorometer (#097) attached (see Fig. 4.2). The SBE-19 contains a suite of instrumentation which sample for conductivity, temperature, dissolved oxygen, light (PAR), and chlorophyll (fluorometer). The instrument was programmed to pump water through the dissolved oxygen sensor for 20 seconds for each sample, and each variable was sampled every 10 minutes for the period of deployment.

On deployment, a water sample to obtain suspended sediment concentration (273/01WS01), a sediment grab (273/01GR01), and video footage (273/01CAM01) of the seabed were collected.

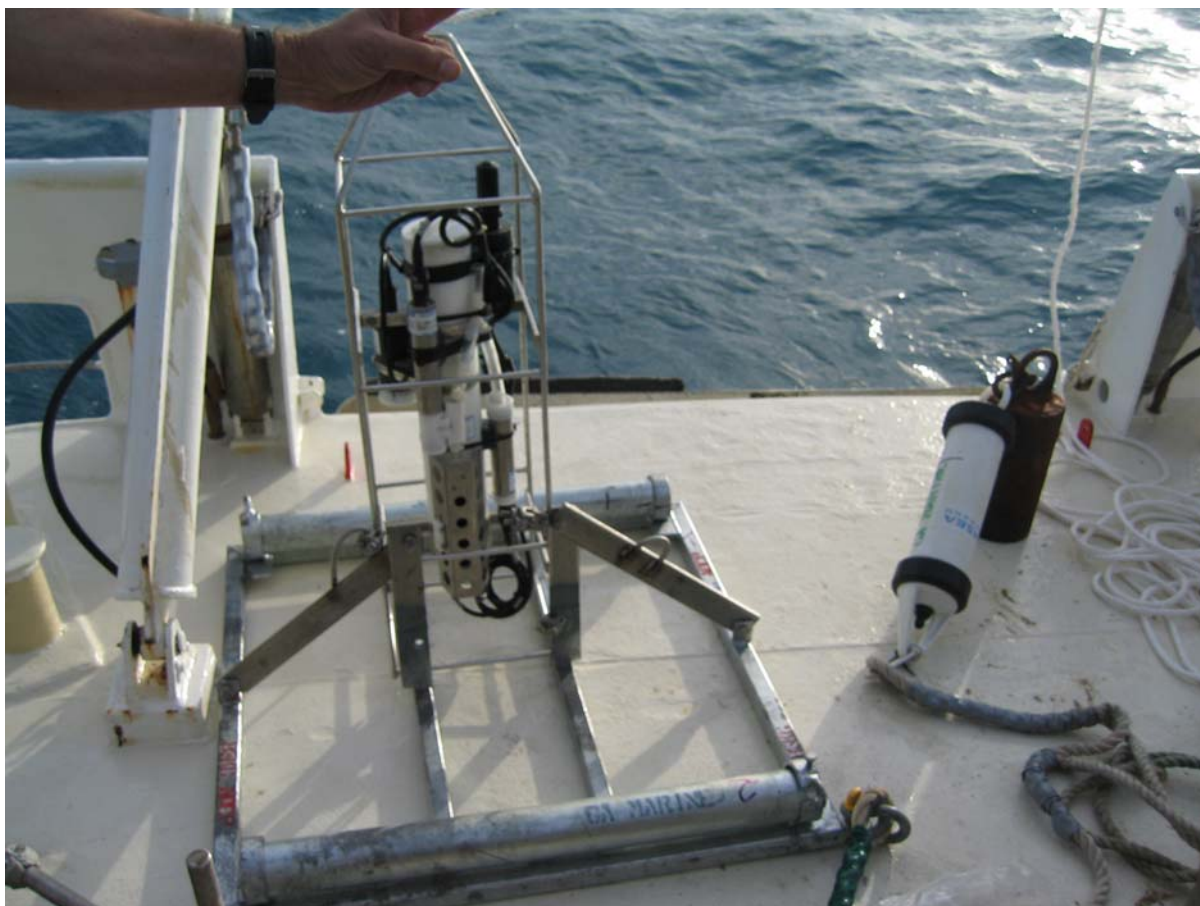


Figure 4.2. Mooring 01CM01 with Seabird-19 multi-sensor attached frame (left) and acoustic release unit to the right.

#### 4.1.2. Station 02CM07

Mooring 02CM07 was supplied by CSIRO Marine and Atmospheric Research. The mooring was deployed to the south-west of Turnagain Island on the reef platform in Area A at location  $-9^{\circ} 34.186' \text{ S}$ ,  $142^{\circ} 13.753' \text{ E}$  in 3.8 m water depth. Bottom sediment at the site was composed of poorly-sorted calcareous muddy, gravelly, medium sand with a mean grain size of 0.274 mm (273/02GRVV02). Instrumentation commenced logging at 00:00 8/10/2004 GMT. The mooring was deployed at 22:07 8/10/2004 GMT. The instrument was recovered at 06:22 26/10/2004 GMT. All sensors became fouled to some degree during the deployment.

The aims of the deployment were to determine the hydrography and ocean currents in a region of seagrass cover during the well-established trade-wind season, and determine sediment transport rates.

Mooring 02CM07 contained:

1. A Seabird Electronics (SBE™) 19 Multi-sensor (# 19P34180-4535) with fluorometer (# 098) attached. The SBE-19 contains a suite of instrumentation which sample for conductivity, temperature, dissolved oxygen, light (PAR), and chlorophyll (Fluorometer). The instrument was programmed to pump water through the dissolved oxygen sensor for 20 seconds for each sample, and each variable was sampled every 10 minutes for the period of deployment.
2. An RD Instruments Workhorse Sentinel 600kHz ADCP (# 2424) (Fig. 4.3). The instrument measures currents from the doppler shift of sound reflected from the water column from two pairs of orthogonal acoustic beams (Gordon, 1996). This instrument was programmed to sample in “High Resolution Mode 8” to obtain profiles of currents from about 1.2 m above the seabed to near the water surface with measurements spaced 0.25 m apart through the water column. The instrument averaged the currents over 10 minutes, and recorded these internally for download on recovery. ADCP data were recorded in AEST (GMT+1000).

On deployment, a water sample to obtain suspended sediment concentration (273/02WS02), a sediment grab (273/02GRVV02), and video footage (273/02CAM02) of the seabed were also collected.



Figure 4.3. RD Instruments Workhorse Sentinel 600kHz ADCP

#### 4.1.3. Station 03CM02

Mooring 03CM02 consisted of the Geoscience Australia instrument frame, BRUCE (Benthic Research frame for Underwater sediment Concentration Experiments, Fig. 4.4). BRUCE was deployed in Area B, south east of Turnagain Island at location  $-9^{\circ} 35.612' \text{ S}$ ,  $142^{\circ} 21.699' \text{ E}$  in 8.0 m water depth. Bottom sediment at the site was composed of poorly-sorted calcareous coarse sand with a mean grain size of 0.614 mm (273/03GRVV03). Calibration of the optical instruments were carried out between 00:38 9/10/2004 GMT and 01:10 9/10/2004 GMT. The mooring was deployed at 01:45 9/10/2004 GMT, and recovered at 02:30 24/10/2004 GMT, resulting in a total deployment length of 15.1 days. The aim of the deployment was to quantify sediment transport rates as a result of waves and currents in Area B, in an area unaffected by the sandbank. Turbulence effects as a result of the sandbank are expected during eastward (ebb) currents.

BRUCE comprises a 300 kg weighted steel frame equipped with:

1. A Nortek™ Vector Acoustic Doppler Velocimeter (ADV #N4103) (Fig. 4.4). This instrument was positioned to sample at 100 cm above the seabed. The vector uses acoustic sampling techniques to measure flow in a remote sampling volume (Nortek, 2000). The instrument was programmed to burst sample every hour for 8 minutes at 8 Hz to record at turbulent time scales. This instrument logs vector components of velocity (east, north and up), pressure and temperature internally to be downloaded on recovery. The Nortek vector (ADV #N4103) contains 82 MB of internal memory ( $\sim 2 \times 10^6$  samples).
2. A type-B Sequoia™ Laser In-Situ Scattering and Transmissiometry – 100 (LISST-100) transmissometer laser particle sizer (LISST #104579) (Fig. 4.4). This instrument was positioned to sample at 0.3m above the seabed. The LISST measures the scatter of a laser light source to infer the size distribution of suspended matter (Agrawal & Pottsmith, 2000). The LISST was programmed to burst sample for 8 mins at 0.125 Hz at the commencement of the ADV burst (i.e. every hour). The instrument internally logs the scattering at 32 angles; size distribution as concentration ( $\mu\text{l l}^{-1}$ ) in 32 log-spaced size bins ranging from 1.25-250  $\mu\text{m}$ ; optical transmission; water depth and temperature, to be downloaded on recovery. The LISST (#104579) contains 2 megabytes of internal memory. The LISST-100 requires calibration before each deployment. For the calibration, a bucket sample was taken from the side of the vessel, and the LISST placed in the bucket vertically to sample during one burst before mooring deployment (1 hour). After the LISST was removed from the sample, a 1 litre sub-sample (273/03WS03) of the bucket was filtered, and the filter paper weighed on return to the lab to establish the

suspended sediment concentration of the bucket sample for calibration of the LISST recorded value.

3. Two D&A Instruments™ optical backscatter sensors (Fig. 4.5), positioned to sample at 1 m (OBS #897) and 0.3 cm (OBS #2167) above the seabed. The OBS instruments measure suspended sediment concentration in the water column. These instruments were powered by, sampled at the same rate as, and logged to, the Nortek Vector as “analog inputs” on the Advanced Tab of the Deployment Planning dialog box. The OBS instruments also require calibration before each deployment. The calibration was carried out using the same procedure as that specified for the LISST-100.
4. A Seabird Electronics (SBE™) CTD (CTD #1620) (Fig. 4.4) positioned to sample at 0.3 m above the seabed. The CTD was programmed to be powered by and sample at the same rate as the LISST-100. Temperature and conductivity were logged to the LISST internal memory to be downloaded on recovery.

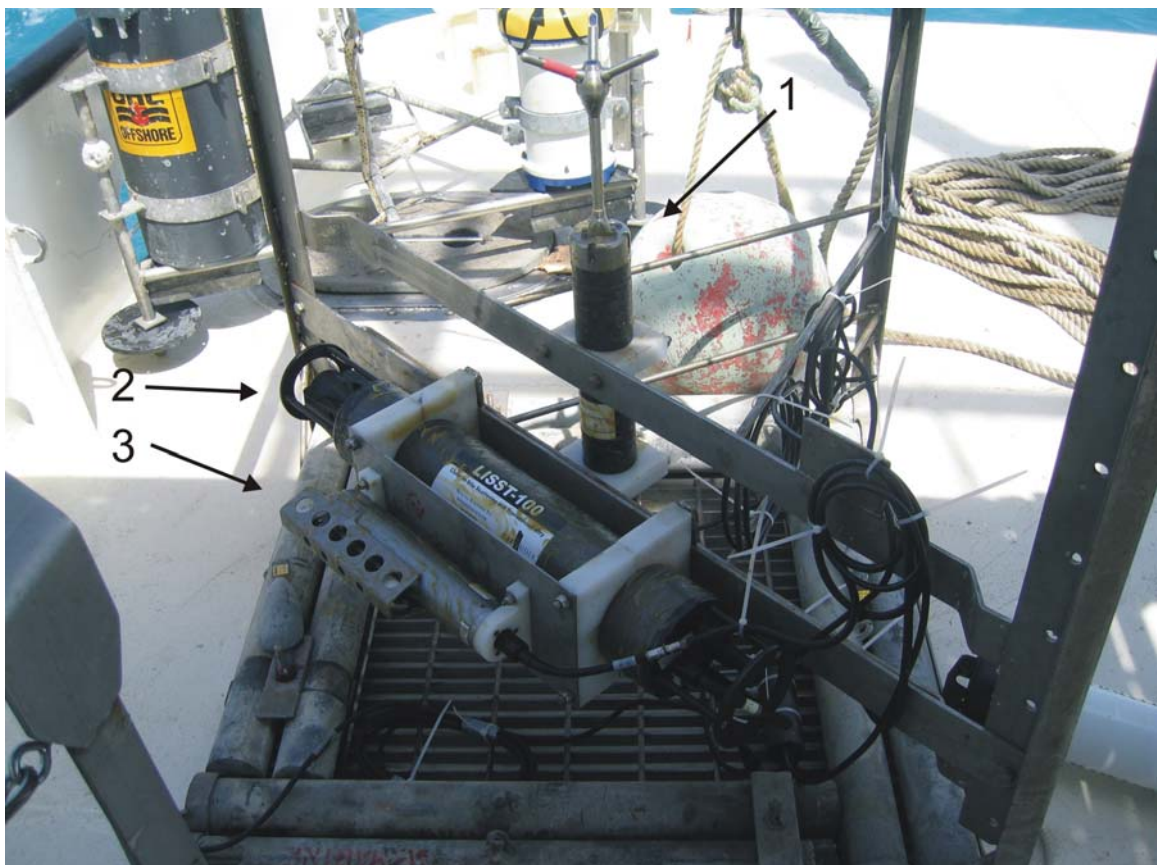


Figure 4.4. BRUCE (Benthic Research frame for Underwater sediment Concentration Experiments) mooring. Sensors shown: 1. Nortek™ Vector Acoustic Doppler Velocimeter; 2. Type-B Sequoia™ Laser In-Situ Scattering and Transmissiometry – 100 (LISST-100); 3. Seabird Electronics (SBE™) CTD (CTD #1620)



Figure 4.5. D&A Instruments™ Optical backscatter sensor (OBS)

On deployment, a water sample to obtain suspended sediment concentration (273/03WS04), a sediment grab (273/03GRVV03), and video footage of the seabed (273/03CAM03) were also collected.

Acoustic release unit 154 was used on the BRUCE Mooring. On recovery, the buoyancy of the floats to which the acoustic release was attached was insufficient to raise the acoustic release to the surface due to the strong currents. Consequently, the buoys did not appear at the surface when the release was triggered, and the mooring was recovered using a grappling hook. Some damage to instruments was experienced during this operation. The mooring dropped from some height on recovery. Consequently, the optics in the LISST are likely to require re-alignment, and electronic pins were bent on the Seabird CT. The instrument frame itself also buckled.

#### 4.1.4. Station 04CM03

Mooring 04CM03 consisted of the Geoscience Australia Acoustic Doppler Current Profiler. The mooring was deployed to the south-east of Turnagain Island in Area B in the centre of the southern sandbank at location -9° 35.668' S, 142° 21.433' E in 6.3 m water depth. Bottom sediment at the site was composed of calcareous, gravelly, coarse sand containing coral rubble and carbonate nodules with a mean grain size of 0.513 mm (273/4GRVV4). Instrumentation commenced logging at 00:00 9/10/2004 GMT. The mooring was deployed at 02:10 9/10/2004 GMT and recovered at 21:45 24/10/2004 GMT, resulting in a total deployment time of 15.8 days.

The instrument frame used for this mooring was constructed of stainless steel. Before the survey, the instrument was tested to determine whether the frame affected the instrument compass. Compass errors in excess of  $30^\circ$  were recorded. Consequently, the CSIRO instrument frame planned for CM01 was adjusted to hold the ADCP, and the instrumentation frames for CM03 and CM01 were swapped. Instrumentation on CM01 contained no compass to be affected by the steel frame. Acoustic release unit #30447 was deployed with this mooring. The aims of the deployment were to determine the currents and waves on top of the sandbank in Area B, and determine the sediment transport rates.

The 04CM03 mooring contained an RD Instruments Workhorse Sentinel 600kHz ADCP (# 5581) (Fig. 4.6). The instrument measures currents from the doppler shift of sound reflected from the water column from two pairs of orthogonal acoustic beams (Gordon, 1996). ADCP #5581 contains the following feature upgrades: Mode 5, 8, and 11 high resolution modes; high ping rate mode 12; and waves array upgrade. The instrument contains internal memory of 144 MB. This instrument was programmed to sample in “High Ping-rate Mode 12” to obtain profiles of currents from about 1.2 m above the seabed to near the water surface with measurements spaced 0.25 m apart. Mode 12 allows a higher ping rate, allowing more data to be collected, thus improving ensemble average accuracy. The RDI software estimates a standard deviation of velocity estimates of  $2.1 \text{ cm s}^{-1}$ . The instrument averaged the currents over 10 minutes, and recorded these internally for download on recovery. This ADCP is also capable of measuring for waves and was set-up to simultaneously burst sample for waves at 2 Hz, for 10 minutes every hour.

On deployment, a water sample to obtain suspended sediment concentration (273/04WS05), a sediment grab (273/04GRVV04), and video footage of the seabed (273/04CAM04) were also collected.



Figure 4.6. Mooring 04CM03 showing acoustic release system (front of image), and ADCP (rear and to the right).

#### 4.1.5. Station 05CM04

Mooring 05CM04 consisted of a ADCP supplied by the University of Sydney. The mooring was deployed to the southeast of Turnagain Island in Area B at the westward end of the southern sandbank at location  $-9^{\circ} 35.708' \text{ S}$ ,  $142^{\circ} 21.156' \text{ E}$  in 6.3 m water depth. Bottom sediment at the site was composed of calcareous gravelly, coarse sand containing mollusc fragments and coral with a mean grain size of 0.722 mm (273/05GRVV05). Instrumentation commenced logging at 01:30 9/10/2004 GMT. The mooring was deployed at 03:30 9/10/2004 GMT and recovered at 07:30 24/10/2004 GMT, resulting in a total deployment period of 15.25 days. The aims of the deployment were to determine the currents and sediment transport on top of the sandbank in Area B and determine whether the sandwaves are capable of steering currents.

The 04CM03 mooring contained an RD Instruments Workhorse Sentinel 1200kHz ADCP (# 1323). The instrument measures currents from the doppler shift of sound

reflected from the water column from two pairs of orthogonal acoustic beams (Gordon, 1996). This instrument was programmed to obtain profiles of currents from about 1.2 m above the seabed to near the water surface with measurements spaced 0.25 m. The RDI software estimates a standard deviation of velocity estimates of 2.1 cm s<sup>-1</sup>. The instrument averaged the currents over 10 minutes, and recorded these internally for download on recovery.

On deployment, a water sample to obtain suspended sediment concentration (273/05WS06). A sediment grab (273/05GRVV05), and video footage of the seabed (273/05CAM05) were also collected.

#### 4.1.6. Station 06CM06

Mooring 06CM06 was provided by CSIRO Marine and Atmospheric Research. The mooring was deployed to the south-east of Turnagain Islandon Area B in the flat area between the two sandbanks at location -9° 35.425' S, 142° 21.173' E in 9.8 m water depth. Bottom sediment at the site was composed of poorly-sorted calcareous muddy, medium sand and gravel with a mean grain size of 0.328 mm (273/06GRVV06). Instrumentation commenced logging at 00:00 8/10/2004 GMT. The mooring was deployed at 04:26 9/10/2004 GMT and recovered at 21:15 24/10/2004 GMT, resulting in a total deployment period of 15.7 days. Acoustic release unit #30446 was deployed with this mooring. The aims of the deployment were to determine the hydrography and ocean currents and sediment transport rates in a region of no seagrass cover and no sandwaves.

The 06CM06 mooring contained:

1. A Seabird Electronics (SBE™) 19 Multi-sensor (# 19P34180-4533) with fluorometer attached. The SBE-19 contains a suite of instrumentation which sample for conductivity, temperature, dissolved oxygen, light (PAR), and chlorophyll (Fluorometer). The instrument was programmed to pump water through the dissolved oxygen sensor for 20 seconds for each sample, and each variable was sampled every 10 minutes for the period of deployment.
2. An RD Instruments Workhorse Sentinel 600kHz ADCP (# 2388). The instrument measures currents from the doppler shift of sound reflected from the water column from two pairs of orthogonal acoustic beams (Gordon, 1996). This instrument was programmed to sample in “High Resolution Mode 8” to obtain profiles of currents from about 1.2 m above the seabed to near the water surface with measurements spaced 0.25 m apart in the vertical. The instrument averaged the currents over 10 minutes, and recorded these internally for download on recovery.
3. An RBR XR-240-TG Pressure Sensor (#010096). The pressure sensor was programmed to sample pressure every 5 minutes.

On deployment, a water sample to obtain suspended sediment concentration (273/06WS07), a sediment grab (273/06GRVV06), and video footage of the seabed (273/06CAM06) were also collected.

#### **4.1.7. Station 07CM05**

Mooring 07CM05 consisted of the Falmouth Scientific Inc. (FSI) 3D ACM current meter (# 1352A) from the University of Sydney. The FSI current meter uses Phase-Shift technology to provide high-accuracy velocity measurement with excellent low-velocity resolution (Falmouth, 2004). The instrument averaged the currents over 10 minutes, and recorded these internally for download on recovery. The mooring was deployed to the south-east of Turnagain Island in Area B on the north side of the southern sandbank in Area B at location  $-9^{\circ} 35.507' \text{ S}$ ,  $142^{\circ} 21.429' \text{ E}$  in 7.8 m water depth. Bottom sediment at the site was composed of calcareous, gravelly, coarse sand containing mollusc fragments and coral with a mean grain size of 0.566 mm (273/07GRVV07). Instrumentation commenced logging at 01:00 9/10/2004 GMT. The mooring was deployed at 00:54 10/10/2004 GMT and recovered at 20:50 24/10/2004 GMT, resulting in a total deployment period of 14.8 days. The aims of the deployment were to determine the currents and sediment transport on top of the sandbank and determine whether the sandwaves are capable of steering currents.

On deployment, a water sample to obtain suspended sediment concentration (273/07WS08), a sediment grab (273/07GRVV07), and video footage of the seabed (273/07CAM07) were also collected.

## **4.2. DATA RECOVERY**

### **4.2.1. Station 01CM01 – Multi-sensor only**

Mooring 01CM01 commenced logging data at 00:00 08/10/2004 GMT (Julian Day 281.00). The first reading of the instrument after the mooring was complete occurs at 07:40 08/10/2004 (Julian Day 281.32). The first 8 hours of the records have been deleted while the mooring was out of the water. The last reading to occur before the mooring was recovered occurred at 20:20 26/10/2004 (JD 299.85). All recordings after this time have also been deleted. The total record length is 18.5 days. Geoscience Australia staff did not have software to communicate with SBE-19 instrumentation, and consequently data were not downloaded from these instruments until they were returned to CSIRO Marine and Atmospheric Research in Hobart. ASCII SBE-19 data as downloaded directly from the instruments were transferred to Geoscience Australia via FTP on 20/01/05.

#### 4.2.2. Station 02CM07 – Multi-sensor and ADCP

Mooring 02CM07 commenced logging data at 00:00 08/10/2004 GMT (Julian Day 281.00). The first reading of the instrument after the mooring was completed occurs at 22:10 08/10/2004 (Julian Day 281.92). The first 22 hours of the records have been deleted while the mooring was out of the water. The last reading to occur before the mooring was recovered occurred at 06:20 26/10/2004 (JD 299.26). All recordings after this time have also been deleted. The total record length is 17.34 days. Binary ADCP data were downloaded directly from the instruments whilst on survey. Geoscience Australia staff did not have software to communicate with SBE-19 instrumentation, and consequently data were not downloaded from these instruments until they were returned to CSIRO Marine Research in Hobart. ASCII SBE-19 data were downloaded directly from the instruments were transferred to Geoscience Australia via FTP on 20/01/05.

#### 4.2.3. Station 03CM02 – BRUCE mooring

Mooring 03CM02 commenced logging data on the Nortek Vector at 00:00 09/10/2004 GMT (Julian Day 282.00), and on the Sequoia LISST one hour later. The first reading of the instrument after the mooring was completed occurs at 02:00 09/10/2004 (JD 282.08). The first 2 hours of the records have been deleted while the mooring was out of the water. The last reading to occur before the mooring was recovered occurred at 02:00 24/10/2004 (JD 297.08). All recordings after this time have also been deleted. The total record length is 15.00 days. Binary data were downloaded directly from the instruments (Nortek Vector, and Sequoia LISST) whilst on survey. On return to Canberra, these data were converted to a readable ASCII format. At this point, it was found that the Nortek Vector data appeared extraordinarily noisy. Maximum velocities were no greater than approximately  $0.35 \text{ m s}^{-1}$ , in strong contrast to nearby current meters which indicated velocities of approximately  $1.00 \text{ m s}^{-1}$ . The deployment configuration was revisited where it was found that the 'nominal velocity' range was set to  $0.10 \text{ m s}^{-1}$  instead of  $1.00 \text{ m s}^{-1}$ . This error results in the current data (u,v, and w components of velocity) being unusable from the BRUCE mooring. Pressure data from the Nortek and auxiliary 'OBS' channels are unaffected. LISST data was also available for the period of deployment. However, it should be noted that the clock on the LISST is 1 day ahead.

#### 4.2.4. Station 04CM03 – ADCP only

Mooring 04CM03 commenced logging data at 00:00 09/10/2004 GMT (Julian Day 282.00). The first reading of the instrument after the mooring was complete occurs at 02:20 09/10/2004 (Julian Day 282.09). The first 2 hours of the records have been deleted while the mooring was out of the water. The last reading to occur before the mooring was recovered occurred at 21:40 24/10/2004 (JD 297.90). All recordings after this time have also been deleted. The total record length is 15.81 days. Binary ADCP data were downloaded directly from the instruments whilst on survey. On return to Canberra, RDI proprietary software 'Wavesmon' was used to extract wave and current data from the binary dataset using an autoseup configuration. The 'Wavesmon' software recorded no valid bursts in the WVS file whilst processing the data. Errors which resulted in no valid bursts were logged in the file 'wmerrlog.txt'. The reasons were: 1) Percent good data were lower than 90% which was the minimum %good threshold, and 2) many bin 2 screenings. Bin 2 is the upper bin in the array. RDI engineers state that 'many bin 2 screenings indicates that bin 2 is too close to the surface. This commonly results when the ADCP is tilted more than 1 or 2 degrees. The tilt recorded on the ADCP on 04CM3 indicates that the ADCP was tilted by as much as 15 degrees at the beginning of the deployment. The above problems has the effect of making wave measurements unusable, however the current and sea-level measurements are unaffected.

#### 4.2.5. Station 05CM04 – ADCP only

Mooring 05CM4 commenced logging data at 01:30 09/10/2004 GMT (Julian Day 282.06). The first 2 hours of the records have been deleted while the mooring was out of the water. The first reading of the instrument after the mooring was complete occurs at 03:30 09/10/2004 (Julian Day 282.15). The last reading to occur before the mooring was recovered occurred at 07:30 24/10/2004 (JD 297.31). All recordings after this time have also been deleted. The total record length is 15.17 days. Binary ADCP data were downloaded directly from the instruments whilst on survey. On return to Canberra, the data were converted to a readable format using RDI proprietary software 'WinADCP'. At this stage, it was observed that the ADCP data were extraordinarily noisy with the percent of good data recorded at less than 50%. On closer inspection of the data, it was observed that the recorded 'pitch' and 'roll' of the instrument both contained a strong semi-diurnal 'tidal' signature where the instrument changed its tilt from -5° to +5° in response to the tides. This change in instrument tilt is expected to be responsible for the observed instrument error. In summary, the current data (u, v, and w) components retrieved from the ADCP are unusable, however the pressure record is unaffected.

#### 4.2.6. Station 06CM06 – Multi-sensor, ADCP, and RBR pressure sensor

Mooring 06CM06 commenced logging data at 00:00 08/10/2004 GMT (Julian Day 281.00). The first reading of the instrument after the mooring was complete occurs at 04:30 09/10/2004 (Julian Day 282.19). The first 28 hours of the records have been deleted while the mooring was out of the water. The last reading to occur before the mooring was recovered occurred at 21:10 24/10/2004 (JD 297.88). All recordings after this time have also been deleted. The total record length is 15.69 days. Binary ADCP data were downloaded directly from the instruments whilst on survey. Geoscience Australia staff did not have software to communicate with SBE-19 instrumentation, and consequently data were not downloaded from these instruments until they were returned to CSIRO Marine and Atmospheric Research in Hobart. ASCII SBE-19 data as downloaded directly from the instruments were transferred to Geoscience Australia via FTP on 20/01/05. Pressure on the RBR pressure sensor is recorded in absolute decibars. Hence, a surface value of 10.2 db was subtracted from the measured value to obtain a depth beneath the seasurface.

#### 4.2.7. Station 07CM05 – FSI current meter

Mooring 07CM05 commenced logging data at 01:00 09/10/2004 GMT (Julian Day 282.04). The first reading of the instrument after the mooring was completed occurs at 01:00 10/10/2004 (Julian Day 283.04). The first 24 hours of the records have been deleted while the mooring was out of the water. The last reading to occur before the mooring was recovered occurred at 21:00 24/10/2004 (JD 297.88). All recordings after this time have also been deleted. The total record length is 14.83 days. Geoscience Australia staff did not have software to communicate with FSI instrumentation, and consequently data were not downloaded from these instruments until they were returned to the University of Sydney. ASCII data were transferred to Geoscience Australia from University of Sydney via email on 7/02/05.

## 4.3. DATA PROCESSING AND ANALYSIS

### 4.3.1. Multi-sensor data

The following parameters are recorded by the SBE-19:

- Time (Hours since first reading)
- Temperature ( $^{\circ}\text{C}$ )
- Salinity (PSU)
- Conductivity ( $\text{mS cm}^{-1}$ )
- Dissolved Oxygen ( $\text{mg l}^{-1}$ )
- Pressure (db)
- PAR (Photosynthetically Active Radiation) ( $\text{Wm}^{-2}$ )
- Fluorescence ( $\text{mg m}^{-3}$ )
- Turbidity (FTU)

SBE-19 data is stored internally. After recovery, SEASOFT programs (Sea-Bird Electronics, Inc. [www.seabird.com](http://www.seabird.com)) were used to read the data into a file on a personal computer, convert to calibrated oceanographic units, and write the data to ASCII files. The data were edited, truncated, and filtered using the computer software program Matlab. Time-series of all variables recorded by the multi-sensors (at 10 minute intervals), and low-pass filtered data, for each mooring are presented to obtain an overview of the data collected at each site.

Outliers were identified in the data using the following thresholds:

1. PAR – outliers removed if over  $800 \text{ uE m}^{-2} \text{ s}^{-1}$
2. Fluorescence – outliers removed if over  $2 \text{ mg m}^{-3}$
3. Turbidity – outliers removed if over 6 ftu

#### 4.3.2. Suspended particle size analysis (LISST Data) and Sediment Concentrations

The LISST-100 particle sizer data were used to derive a number of particle size distribution parameters to provide an easily accessible summary of the data. No attempts were made to correct the data for potential instrument-specific or sampling-specific bias in the particle size distribution.

The following steps were applied to the data:

1. Data were burst averaged. Each burst consisted of 8 minutes sampling at 0.125 Hz (58 samples), and these bursts occurred hourly.
2. Burst averaged pressure, temperature and beam attenuation were obtained.
3. Burst-averaged particle volume concentrations  $V_i$  were obtained for each of the 32 size classes (as represented by its median grain size).
4. Burst-averaged total particle volumes  $V_t$  were obtained by summing particle volume for each size class.
5. Burst-averaged frequency distribution by Volume  $F_i$  were calculated;

$$F_i = V_i * 100 / V_t \quad (1)$$

6. Burst-averaged particle size mode was determined as the centre of the size class with the greatest percentage frequency.
7. Burst averaged mean grain size  $S$  was determined via two methods: 1) using the method of moments, and 2) using the formulae:

$$S = F_i * S_i / 100 \quad (2)$$

Where  $S_i$  is the centre of each size class and  $F_i$  is its associated percentage frequency by number.

8. Burst-averaged arithmetic standard deviation of the distribution was determined using two methods: 1) using the method of moments, and 2) using the formulae:

$$S_{dev} = \sqrt{(F_i * (S_i - S)^2) / 100} \quad (3)$$

9. Burst-averaged skewness and kurtosis were calculated using the method of moments.
10. Burst averaged particle size median was determined by the linear interpolation between the two frequencies closest to 50 percent.

Burst-averaged 95<sup>th</sup> and 75<sup>th</sup> percentiles were extracted from the cumulative frequency distribution with the size classes sorted in order of increasing particle sizes (fine to coarse). They represent the centre of the size class for which the cumulated frequency was lower than 95 and 75% respectively.

#### 4.3.3. Sea Level

A pressure record is recorded by each of the instruments listed here:

1. The SBE-19 on which pressure is recorded in decibars below the sea-surface. This reading has been converted to a measurement of water-depth with respect to the seabed by adding 0.5 m to the measured reading, representing the height of the SBE-19 sensors above the seabed.
2. The RD Instruments ADCP on which 'depth' is recorded in meters. This reading has also been converted to a measurement of waterdepth with respect to the seabed by adding 0.5 m to the measured reading, representing the height of the ADCP sensors above the seabed.
3. The RBR pressure sensor present on 04CM03. The RBR pressure sensor records pressure in absolute decibars. This reading has been converted to a measurement of water depth with respect to the seabed by subtracting the surface atmospheric pressure (10.2 db) and adding 0.8 m being the height of the RBR pressure sensor above the seabed.
4. The Nortek Vector ADCP. Sea-level is recorded in meters above the instrument.
5. The Sequoia LISST, which records pressure in meter from the seabird CT.

Where two or more of these instruments are deployed on the same mooring, correlation statistics between pressure records at a mooring site have been determined. Where an offset in timing occurs between pressure records, one record (time-series 2) has been linearly interpolated in time to match that of the other time series (time-series 1).

A classical harmonic tidal analysis has been carried out on the sea-level record obtained from each instrument of a mooring using the T\_TIDE package in MATLAB (Pawlowicz et al., 2002). The results of the analysis for the four largest constituents (M2, S2, K1, O1) are presented in the following sections.

To determine the nature of the tides at each mooring location, the 'form ratio',  $F = (K1+O1)/(M2+S2)$ , a measure of the signature based on the relative magnitudes of their main diurnal and semi-diurnal constituents (Pond & Pickard, 2000), has been calculated.

$F = 0$  to  $0.25$ : semi-diurnal tides.

$F = 0.25$  to  $1.5$ : mixed, mainly semi-diurnal tides.

$F = 1.5$  to  $3.0$ : mixed, mainly diurnal tides.

$F > 3.0$ : Diurnal tides.

#### 4.3.4. Waves

Wave data was acquired by the Nortek pressures sensors on deployments 03CM02 and 04CM03. Each 8 minute burst, obtained hourly, on the pressure sensor has been used to compute the standard (non-directional) wave parameters of significant wave height and peak wave period (Tucker and Pitt, 2001).

#### 4.3.5. Currents

The Acoustic Doppler Current Profiler's (ADCP) were configured to record data in Earth coordinates (latitude and longitude). Upon recovery, the ADCP data were transferred to a personal computer using the RD Instruments ([www.rdinstruments.com](http://www.rdinstruments.com)) software. Using the RDI™ ADCP software WinADCP, recorded variables East, North, Up, Error and Depth were exported to MATLAB format for times that the Mooring was in the water. Matlab routines were used to check for data quality, flag bad values, and discard bins that were always beyond the water surface. Data were then eliminated where correlation (SNR) was  $<90\%$ . Additional bad data were eliminated using the following criteria:

- Error  $> 10$  cm s, u, v, w were removed.
- If mid bin depth was higher than the recorded water level (depth), u, v, w were removed.

Some near-surface bins were not discarded. At times of low tide, the side-beam reflection renders this data invalid, so near-surface ADCP data must be interpreted with care. On occasion, the ADCP skips an ensemble record because the data are poor.

Because our interest is in sea-bed processes, processing and analysis of current meter data is focussed on data obtained from the first bin. The ADCP's were configured such that the centre of first bin was 1.14 m above the sensors. This corresponds to approximately 1.6 m above the seabed. To provide an indication of the vertical current profile at each site, data from the nearest bin below lowest tide (i.e., the highest bin with a continuous record), has also been processed. Comparing both the bottom and the top of the water column should also provide an estimate of the degree of internal shear within the water column

At each current meter mooring, the following analyses have been carried out on bottom and 'surface' currents:

1. Progressive vector plots, and determination of the mean residual current during the deployment;
2. Time series plots, to provide an overview of the observations and to determine the mean absolute current speeds during the deployment;
3. Principal axes for both the basic 10-min processed data and the low-passed currents were computed for the entire record and by month. Major and minor axes, orientation, and ellipticity were computed from the east (u) and north (v) current components as:

$$\text{major axis} = [0.5 (UU + VV) + R] / n^{(1/2)} \quad (4)$$

$$\text{minor axis} = [0.5 (UU + VV) - R] / n^{(1/2)} \quad (5)$$

$$\text{orientation} = 90^\circ - 0.5 \tan^{-1} [2 UV / (UU - VV)] \quad (6)$$

$$\text{ellipticity} = 1 - (\text{minor axis} / \text{major axis})$$

Where

$$UV = \sum (u \cdot v) - n \cdot \bar{U} \cdot \bar{V} \quad (8)$$

$$UU = \sum (u \cdot u) - n \cdot \bar{U} \cdot \bar{U} \quad (9)$$

$$VV = \sum (v \cdot v) - n \cdot \bar{V} \cdot \bar{V} \quad (10)$$

$$R = [ (0.5 (UU - VV))^2 + (UV)^2 ]^{(1/2)} \quad (11)$$

U and V are the means of the east and north velocity components, respectively. Sum means sum over the entire data set of n values. The orientation is measured clockwise from true north. 0° is true north, and 90° is east; and

4. Scatter plots of the basic 10-min processed data and the low-passed currents (subsampling to be 6-hourly) to visually show the distribution of the current speed and direction. Superimposed on the scatter plots are the mean vector current over the entire deployment, and the principal axes of the currents, shown as an ellipse.

As well as these analyses, a tidal analysis was undertaken on the current data to determine the tidal ellipses. First, the mean values for the horizontal velocity time series (u, v) were removed from the time series of these components and then the amplitude and phase of each tidal constituent was computed for the u and v components separately using the T\_TIDE software in MATLAB® (Pawlowicz et al., 2000). For each tidal constituent, the fit amplitudes were then used to compute the tidal ellipse parameters using the 'Tidal\_Ellipse' software in MATLAB® (Xu, 2002).

This analysis provides estimates of: 1) the semi-major axis (or maximum current velocity); 2) the ellipse eccentricity (i.e., the ratio of semi-minor to semi-major axis) where a negative value indicates that the ellipse is traversed in a clockwise direction; 3) the ellipse inclination, or the angle between east (x-) and the semi-major axis; and 4) the phase, or the angle that the oppositely rotating circular components must traverse from their initial positions for them to meet.

#### 4.3.6. Bedload Transport Estimates

Current meters deployed at moorings 2 and 3 are not capable of sampling for wave statistics. Consequently, estimates of bed shear stresses, and hence bedload transport, are based on the assumption of a steady flow. Five methods have been used to estimate bedload transport at the site. These include:

- a) Bagnold's bedload equation, modified by Gadd et al. (1978)

$$q = (\beta/\rho_s)(u_{100}-u_{cr})^3 \quad (12)$$

where  $q$  is the volume rate of sediment transport per unit width of bed [ $m^2 s^{-1}$ ],  $\beta$  has a value of 1.73, as used in the SEDTRANS96 model, outlined in Li and Amos. (2001). The critical velocity for the initiation of bedload transport  $u_{cr}$  is obtained from  $\tau_{cr} = 0.5\rho f_{cs}u_{cr}^2$ , and  $u_{100}$  is the current speed measured 100 cm above the bed.

- b) The Engelund-Hansen (1967) total load equation. For continental shelf conditions, this equation is modified to (Li and Amos, 2001):

$$q = 0.05u_{100}^2\rho^2 u^{*3}/D(\Delta\rho g)^2 \quad (13)$$

where  $\Delta\rho = \rho_s - \rho$ , and  $\rho_s$  is the density of the sediment (For quartz  $2650 \text{ kg m}^{-3}$ ), and  $\rho$  is the density of seawater;  $u^*$  is the skin-friction shear velocity.

- c) The Einstein-Brown bedload equation (Brown, 1950). This equation can be written in the form (Li and Amos., 2001)

$$q = 40W_s D(\rho/\Delta\rho g D)^3 u^{*5} |u^*| \quad (14)$$

where  $W_s$  is the settling velocity.

d) Yalin bedload equation (Yalin, 1963).

$$q = 0.635 D u^* [(\tau^* - (1/a) \ln(1 + a \tau^*))] \quad (15)$$

where  $\tau^* = (\tau_b - \tau_{cr})/\tau_{cr}$  is the normalised shear stress and  $a$  is equal to  $2.45(\rho/\rho_s)^{0.4}(\tau_{cr}/\Delta\rho g D)^{0.5}$ .

e) Bagnold's bedload equation as modified by Hardisty (1983)

$$q = k_1 (u_{100}^2 - u_{cr}^2) u_{100} \quad (16)$$

$u_{cr}$  is the critical threshold velocity defined in this instance as

$$u_{cr} = 1.226 (100D)^{1.29} \quad (17)$$

as outlined by Miller et al. (1977).  $k_1$  is a function of sediment grain size ( $D$ ) such that:

$$k_1 = (1/6.6 (1000D)^{1.23} \text{ kg m}^{-4} \text{ s}^2) \quad (18)$$

It is this bedload transport equation which has been used in all previous Geoscience Australia cruise reports, so is included here for completeness.

For consistency with previous cruise reports, the above estimates of  $q$  in units  $[\text{m}^2 \text{ s}^{-1}]$  must be multiplied by  $1/(10\rho_s)$  to express bedload transport in units  $\text{g cm}^{-1} \text{ s}^{-1}$ . Grain-size data at each site was unavailable at the time of writing, so a mean grain size of 0.0005 m (0.5 mm) has been assumed. Vector Stick plots of bedload transport estimates are presented to enable an overview of the main stage of tide at which bedload is important.

#### 4.3.7. Sandwave Migration Rates

The movement of sandwaves in each area has been detailed in [Section 2](#), and indicates that the sandwaves moved by approximately 3 m and 4 m in Areas A and B, respectively, during the survey, equating to approximately 0.21 m day<sup>-1</sup> and 0.28 m day<sup>-1</sup>.

The volume of sand transported by a moving sandwave of height H can be estimated as the product of the sandwave's cross sectional area (A) and its celerity (C), divided by the wavelength (crest spacing; L). Assuming the sandwaves are triangular in cross-section ( $A=0.5 LH$ ), then:

$$q_c = 0.5 HC \quad (18)$$

Where the subscript c denotes that the voids between sediment grains are included in the volume transport rate. In terms of the dry weight of sediment grains:

$$q=0.5d(1-p)HC \quad (19)$$

Where p is the porosity of the sediment (assume value of 0.45), and d is the grain density (2.72 g cm<sup>-3</sup> for calcite). Sandwave celerity may thus be estimated solving the above equation for C, and using the predicted total transport vector q derived above and the observed sandwave height (2.0 m). A range of values have been computed based on the five different bedload estimates.

The predicted average migration rate, C, for all moorings, is given in [Table 4.35](#) for each bedload transport estimate. All measures of sandwave migration rates are in m day<sup>-1</sup> (or celerity C).

## 4.4. Results

### 4.4.1. SBE-19 multi-sensor data (01CM01, 02CM07, and 06CM06)

The SBE-19 multi-sensor data provided hydrological information at each of the moorings (01CM01, 02CM07, and 06CM06) and allowed insights into the oceanographic conditions during the survey. The time series plots of each parameter acquired by the SBE-19 at 01CM01, 02CM07, and 06CM06 are displayed in [Figs. 4.7, 4.9, and 4.11](#), respectively. Low pass filtered plots displayed in [Figs. 4.8, 4.10, and 4.12](#) and are used to indicate low frequency variations in each dataset. Statistics for each of the parameters recorded by the SBE-19 for each mooring are displayed in [Tables 4.2-4.4](#).

Table 4.2. Statistics for 01CM01 SBE-19 deployment.

	Min	Mean	Max	StDev
Temp (°C)	26.03	27.03	28.11	0.55
PAR ( $\mu\text{E m}^{-2} \text{s}^{-1}$ )	4.03	189.15	799.88	193.15
Pressure (db)	8.11	9.72	11.35	0.81
Salinity (PSU)	31.74	33.05	35.44	1.15
Oxygen ( $\text{mg l}^{-1}$ )	5.92	6.38	7.24	0.18
Fluorescence ( $\text{mg m}^{-3}$ )	0.04	0.25	0.99	0.10
Turbidity (FTU)	0.29	1.25	3.29	0.37

Table 4.3. Statistics for 02CM07 SBE-19 deployment.

	Min	Mean	Max	StDev
Temp (°C)	26.00	27.20	28.56	0.66
PAR ( $\mu\text{E m}^{-2} \text{s}^{-1}$ )	0.71	48.16	340.37	69.81
Pressure (db)	3.51	5.17	6.70	0.64
Salinity (PSU)	31.81	33.95	35.22	0.70
Oxygen ( $\text{mg l}^{-1}$ )	5.04	5.50	6.44	0.25
Fluorescence ( $\text{mg m}^{-3}$ )	0.0	0.23	1.73	0.24
Turbidity (FTU)	1.08	2.63	5.99	0.86

Table 4.4. Statistics for 06CM06 SBE-19 deployment.

	Min	Mean	Max	StDev
Temp (°C)	26.12	27.07	28.23	0.56
PAR ( $\mu\text{E m}^{-2} \text{s}^{-1}$ )	0.50	25.45	164.27	35.28
Pressure (db)	8.65	10.22	11.71	0.70
Salinity (PSU)	32.24	33.78	35.28	0.76
Oxygen ( $\text{mg l}^{-1}$ )	5.44	6.24	6.75	0.16
Fluorescence ( $\text{mg m}^{-3}$ )	0.0	0.21	1.91	0.20
Turbidity (FTU)	0.0	2.29	5.99	1.23

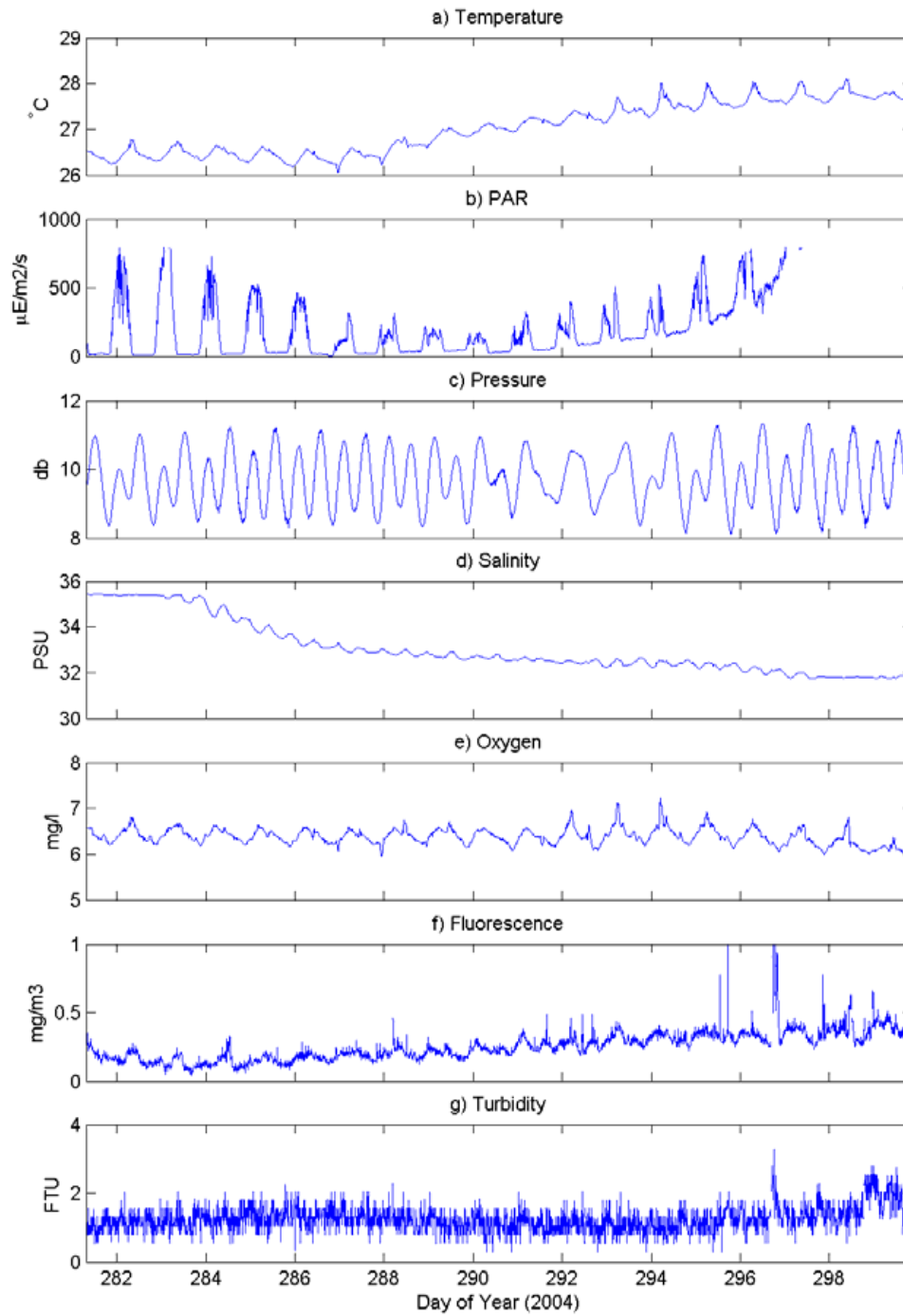


Fig. 4.7. Time-series plots of processed 10-minute data for each variable recorded by the SBE-19 at 01CM01.

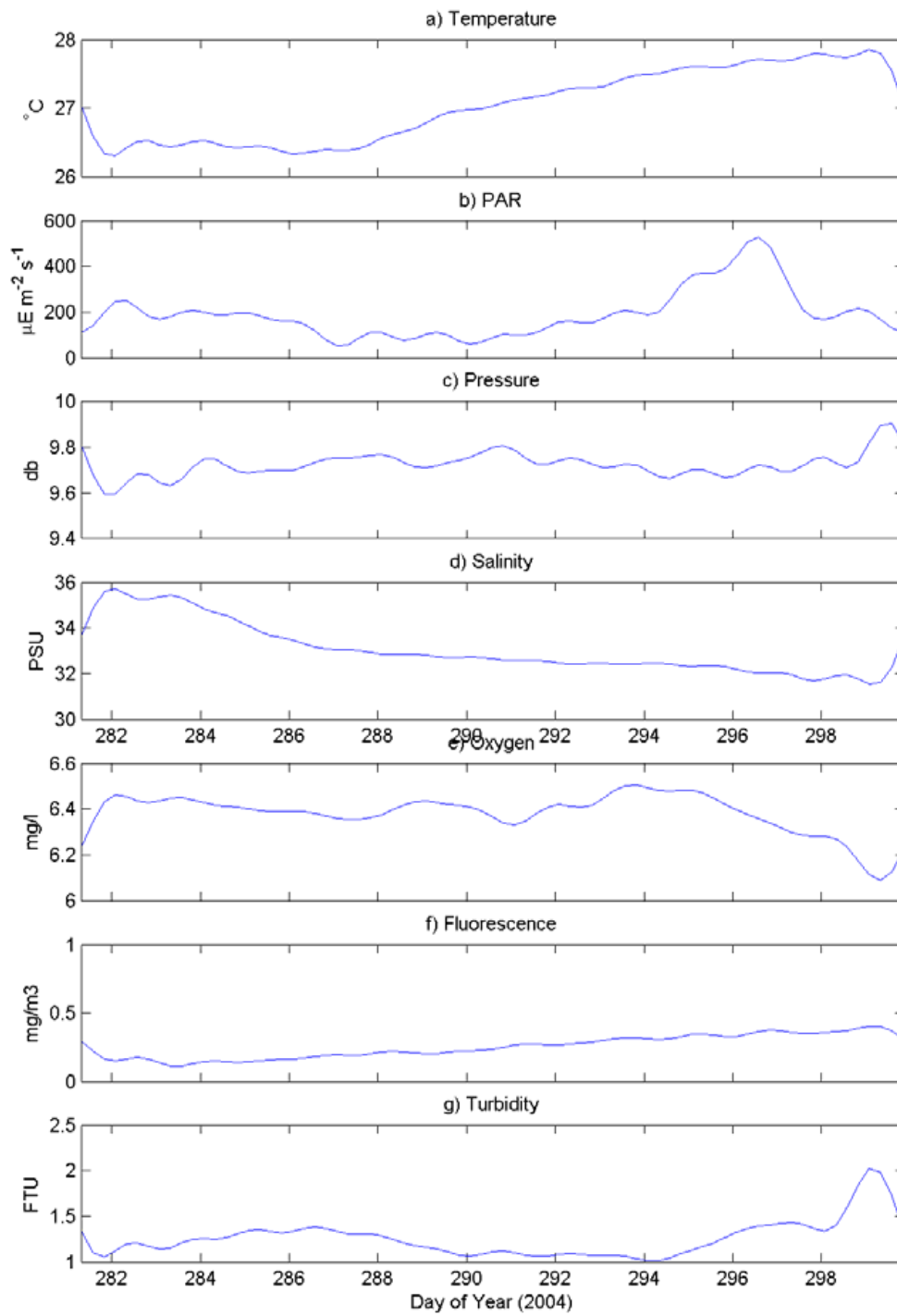


Fig. 4.8. Time-series plots of processed low-pass filtered data for each variable recorded by the SBE-19 at 01CM01.

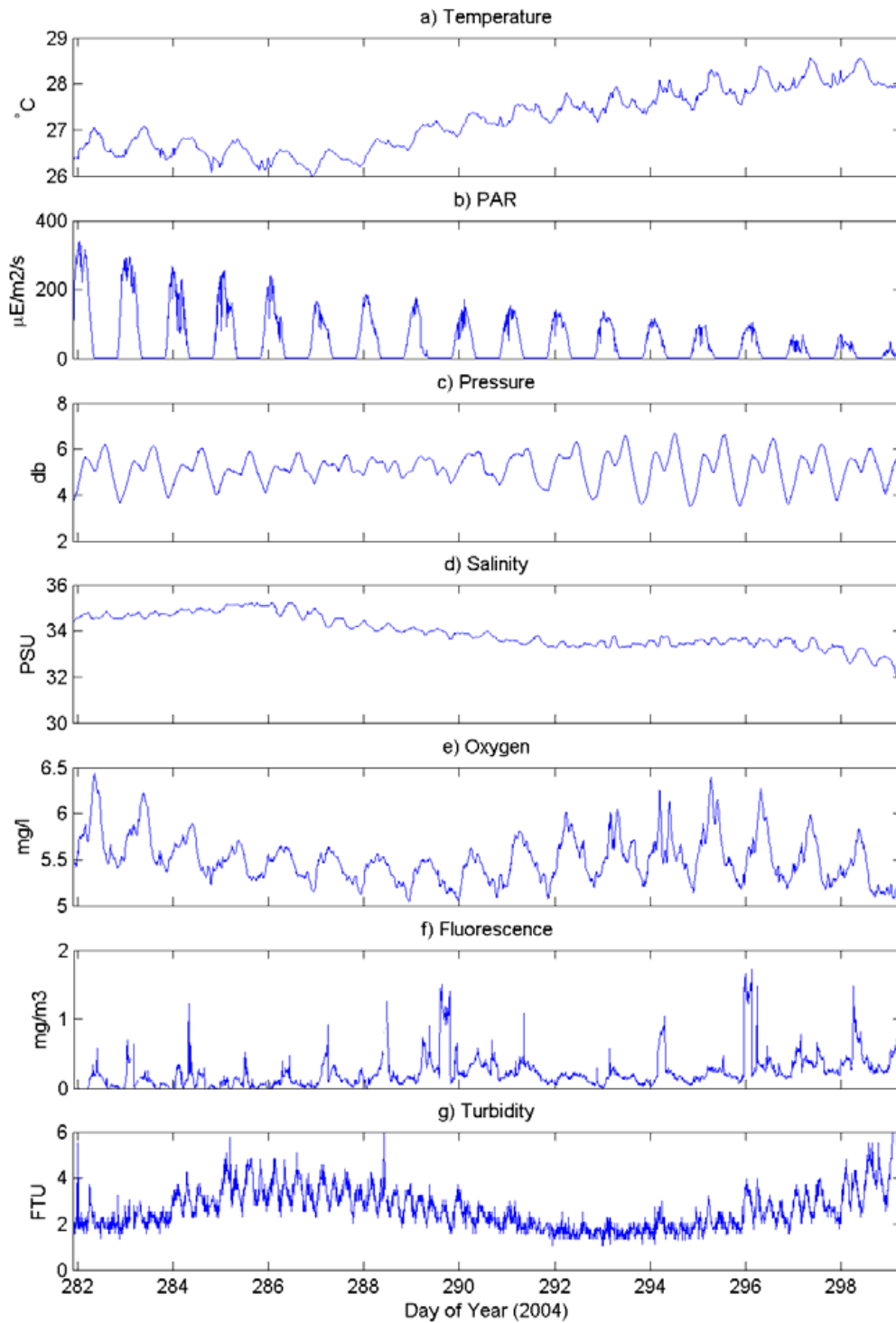


Fig. 4.9. Time-series plots of processed 10-minute data for each variable recorded by the SBE-19 at 02CM07.

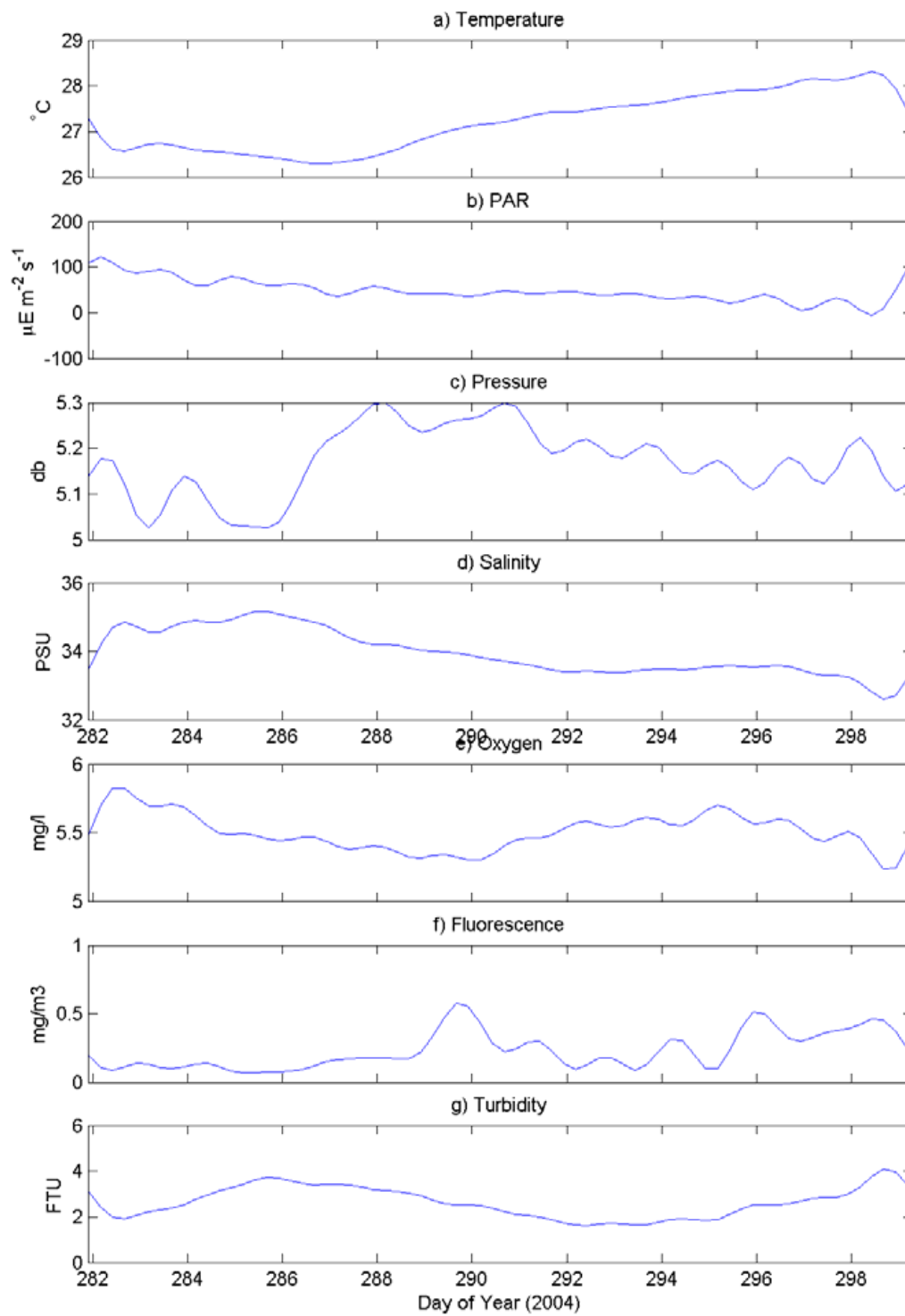


Fig. 4.10. Time-series plots of processed low-pass filtered data for each variable recorded by the SBE-19 at 02CM07.

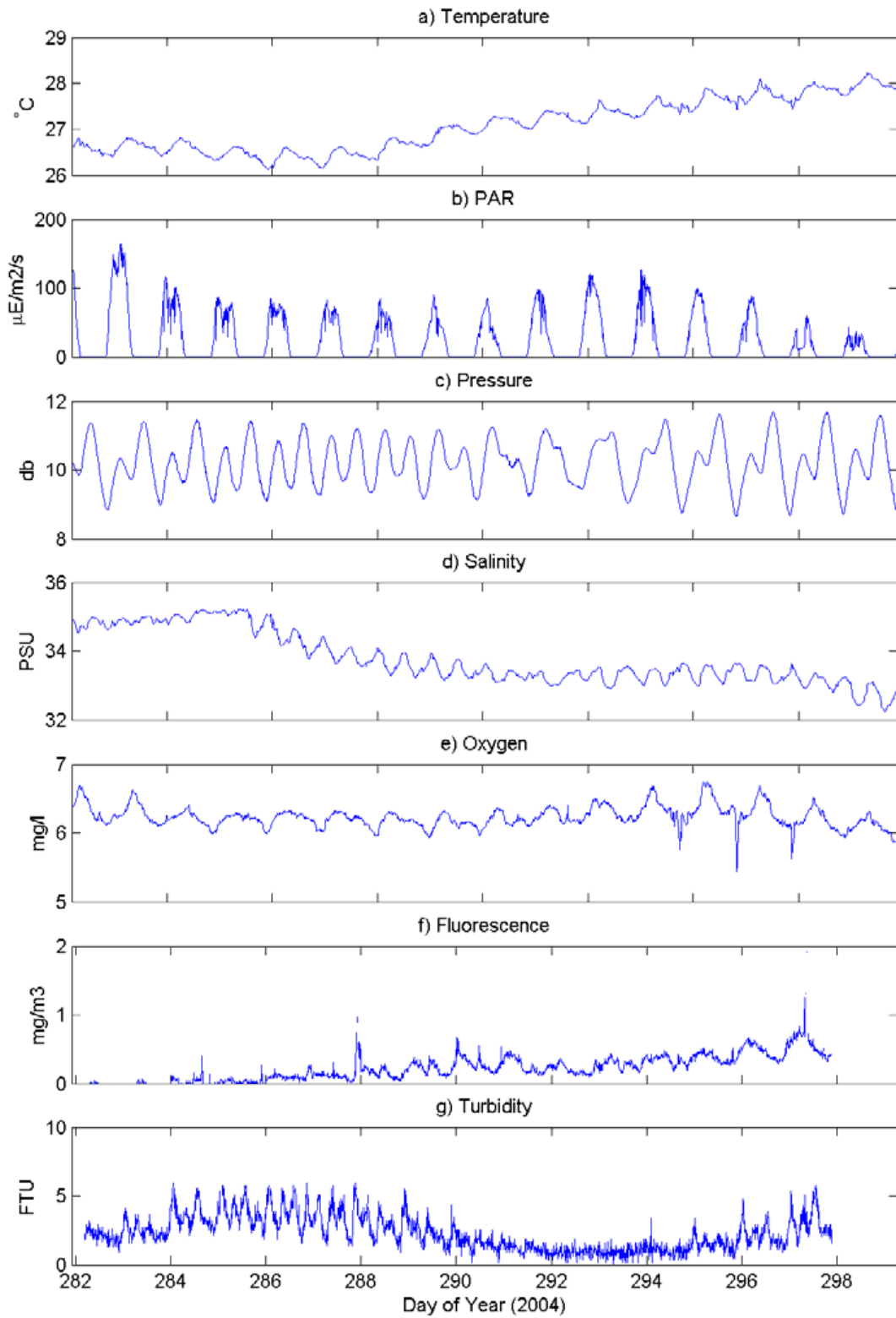


Fig. 4.11. Time-series plots of processed 10-minute data for each variable recorded by the SBE-19 at 06CM06.

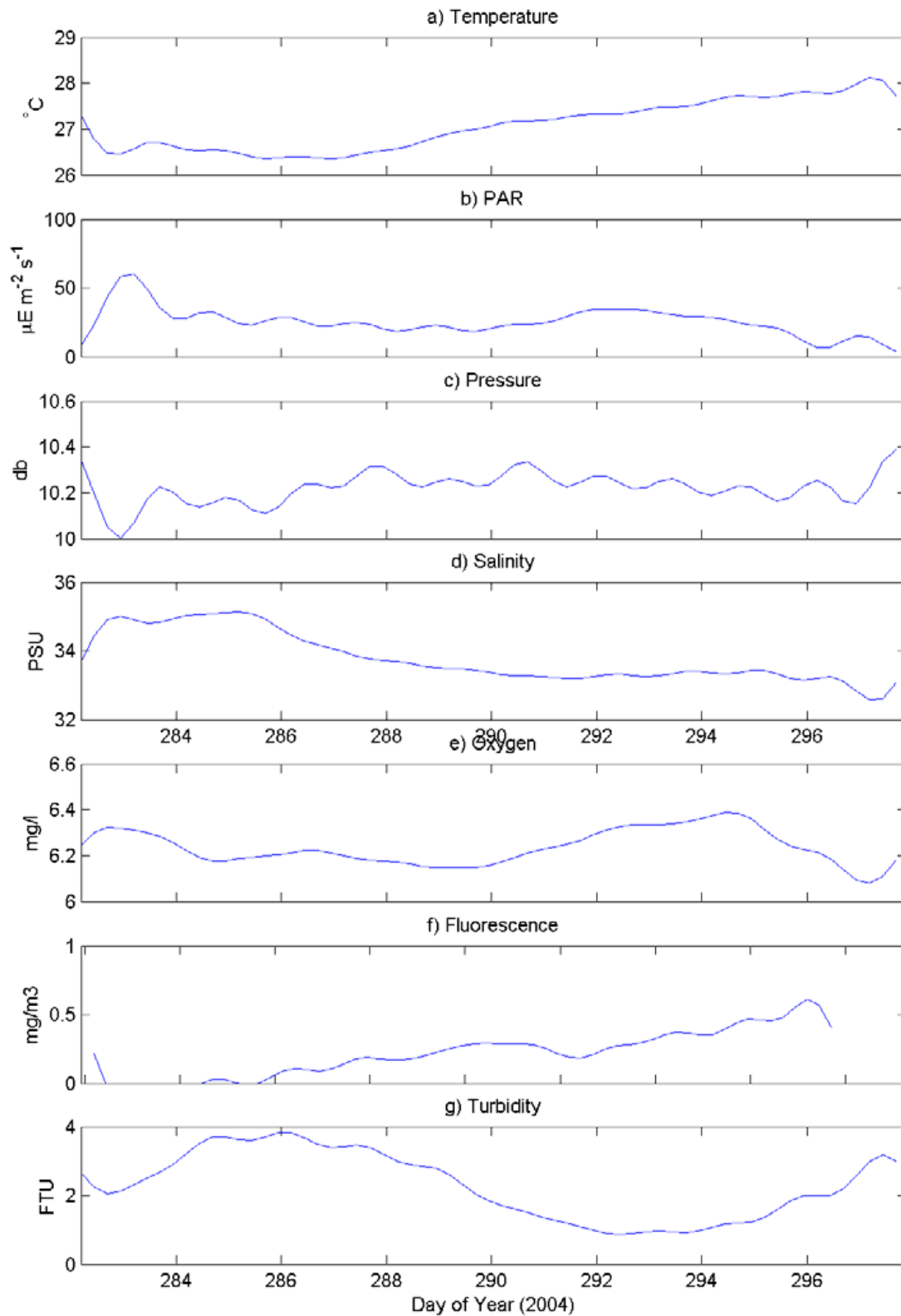


Fig. 4.12. Time-series plots of processed low-pass filtered data for each variable recorded by the SBE-19 at 06CM06.

The temperature records for 01CM01, 02CM07, and 06CM06 show a weak diurnal signal with the night time water temperature often reaching  $0.5^{\circ}\text{C}$  higher than day time temperatures (Figs. 4.7a, 4.9a, 4.10a). The diurnal signal in the temperature is at its weakest during the middle of the survey (JD289-293) and that time appears to be correlated with the neap tides. During the deployments the temperature at all three stations increased by  $\sim 1.5^{\circ}\text{C}$  over 11 days (JD288-299) (Figs. 4.8a, 4.10a, 4.12a). The temperature statistics in Tables 4.2-4.4 indicate that there is little difference in the temperature records at any of the 3 stations. There is a  $0.45^{\circ}\text{C}$  difference between the maximum temperatures at 01CM01 and 02CM02, all other statistics vary by less than  $0.2^{\circ}\text{C}$ . The tidal signatures evident in the temperature records indicate that tidal processes appear to be exchanging cooler and warmer waters past the temperature sensors at both diurnal and spring/neap frequencies. The increasing temperature measured at the sensors over time show that warmer water from the east are being transported to the west over time as a result of tidal and wind driven currents (easterly at that time of year) active at the time.

Photosynthetically Active Radiation (PAR) provides an estimate of the amount of visible light available for photosynthesis. The PAR records show a strong diurnal signature in all the datasets though the overall levels of PAR reaching each sensor are significantly different (Fig. 4.7b, 4.9b, 4.11b). Of the SBE-19 deployments, 02CM07 (Area A) is the shallowest of the 3 moorings, with mean pressure of 5.17 db. Despite this, light levels (PAR) are greater at the deeper (mean pressure of 9.72 db) 01CM01 Orman Reefs mooring with mean PAR of  $189.15\ \mu\text{E m}^{-2}\text{s}^{-1}$  and  $48.164\ \mu\text{E m}^{-2}\text{s}^{-1}$  at 01CM01 and 02CM07; respectively (Tables 4.2-4.4). The different levels of PAR at the three stations may be linked to different levels of turbid sediment. Station 06 is in close proximity to an active sand bank, whilst station 02 is also in close proximity to active sand dunes and hence there is evidence for strong currents and mobile sediments in those areas. Station 01 by contrast is located in a region without sandwaves and with notably finer sediments. The mean grain size values (50<sup>th</sup> percentile) for stations 01, 02, and 06 are 0.219 mm, 0.274 mm, 0.382 mm and the 20<sup>th</sup> percentiles are 0.024 mm, 0.066 mm 0.133 mm (see Appendix D for detailed lab results). The results indicate that the sediments from Station 01 are finer and hence not reworked (and advected) by currents and waves to the same degree as the other two stations. There is a low frequency rise in the light record over the course of the survey at 01CM01 (Fig 4.7b), this is assumed to be a result of fouling of the light sensor.

A detailed treatment of the pressure sensor data for 01CM01, 02CM07, and 06CM06 are located in section 4.4.3.1, 4.4.3.2, and 4.4.3.6 respectively.

The salinity records, show a weak, apparently tidally driven (semi-diurnal) signature superimposed on a low frequency component. Over the course of the survey the salinity drops from ~35 to ~32 PSU at each station (Figs 4.8d, 4.10d, 4.12d). The low-frequency component of the salinity record is similar to a mirror-image of the temperature record, suggesting that a relatively warm, less saline water mass is advected past the stations over the deployment period. The semi-diurnal component in the salinity record is slightly out of phase with the pressure record, but is probably phase-locked to the current record, and indicates tidal oscillation of the water mass superimposed on its quasi-steady advection (Fig. 4.7c-d, 4.9c-d, 4.11c-d).

The dissolved oxygen record shows a strong diurnal signature with data rarely exceeding the 5-7 mg l<sup>-1</sup> range (Fig. 4.7e, 4.9e, 4.11e). 02CM02 (Area A) has a lower average oxygen concentration of 5.5 mg l<sup>-1</sup>, compared to the other two datasets, 6.38 mg l<sup>-1</sup> and 6.24 mg l<sup>-1</sup> for 01CM01 and 06CM06. The cause of this difference in the average oxygen concentrations is unclear. There is no obvious low frequency trend within these dataset (Fig. 4.8e, 4.10e, 4.12e).

Fluorescence is a measure of primary productivity. Although noisy, the fluorescence records show weak diurnal signatures (Fig. 4.7f, 4.9f, 4.11f). In all three datasets the primary productivity increases consistently over the course of the survey (Figs. 4.8f, 4.10f, 4.12f). In addition to temperature and salinity, the fluorescence record also shows the advection of a water body past the stations. The low frequency increase in primary productivity over time (Figs. 4.8f, 4.10f, 4.12f), matches a similar rise in temperature and drop in salinity.

Station 01CM01 at the Orman Reef shows relatively low levels of turbidity compared to the stations further north (02CM02 and 06CM06) supporting the idea that turbidity is influencing the level of light (PAR) reaching the seabed. Average values for the survey period are 1.25, 2.63, and 2.29 FTU respectively (Tables 4.2-4.4). Stations 02MC02 and 06CM06 show strong semi-diurnal and spring-neap tidal variations, (Figs. 4.9g & 4.11g), but any tidal signal at station 01CM01 is too weak to rise above the instrument noise level (Fig. 4.7g).

#### 4.4.2. Suspended sediment concentration (Station 03CM02)

The time series plots of each variable recorded and calculated from the LISST-100 at 03CM02 are displayed in figures 4.13 and 4.14. The low-frequency increase towards the end of the dataset is suspected to be a result of biofouling. Statistics for data collected by the LISST-100 during the entire deployment are listed in Table 4.5.

A detailed treatment of the pressure sensor data for 06CM06 (Fig. 4.13a) is located in section 4.4.3.6.

The temperature record shows a weak diurnal signal with the daytime water temperature often reaching 0.4° C higher than night time temperatures (Fig. 4.13a). During the deployment the temperature increased by ~1.5° C over 11 days (JD288-299) (Fig. 4.13b) similar to the other temperature sensors (01CM01 – Fig. 4.8a, 02CM07 – Fig. 4.10a, 06CM06 – Fig. 4.12a).

The beam attenuation is constant from the start of the deployment until JD 290. After JD 290 the beam attenuation increases over time as a result of biofouling (Fig. 4.13c), the onset of biofouling appears to be linked with the neap tides starting at about that time (Fig. 4.13a).

A coherent record of particle volumes was collected over the first 7 days of the deployment, biofouling decreases the clarity of observations made after this time. From JD 283-285 the suspended sediment is concentrated between 100 and 250  $\mu\text{m}$  (average of ~100  $\mu\text{m}$ ) with very few grains between 0 and 100  $\mu\text{m}$ . Between JD 285 and 290 the mean grain size fell to ~50  $\mu\text{m}$  and increases to ~100  $\mu\text{m}$ , with a corresponding drop and gradual increase in concentrations of sediments >100  $\mu\text{m}$ . After JD 290 the average particle volume data lacks sufficient clarity to determine how the volumes changed over this time though it is likely that there was a decrease in particle volumes due to the weaker currents experienced during neap tides. The burst averaged mean grainsize was consistent throughout the deployment and showed an average grainsize of 83.68  $\mu\text{m}$  with a standard deviation of 23.41 (Table 4.5). The Burst averaged particle volumes show weak cyclicity at times which is tide related. Particle sizes between 100 and 250  $\mu\text{m}$  are commonly suspended during spring tides though there is no comparable data for the neap tides due to biofouling. It is likely that sediments coarser than 250  $\mu\text{m}$  are being transport as bedload transport rather than as suspended load and hence are not represented in this dataset.

Table 4.5. Statistics from time-series analysis of LISST data

	Min	Mean	Max	StDev
Pressure (m)	11.25	12.19	13.15	0.43
Temp (°C)	26.15	27.03	28.09	0.53
Beam Attenuation ( $\text{m}^{-1}$ )	0	9.58	25.11	5.92
MGS ( $\mu\text{m}$ )	20.79	83.68	207.61	23.41
Vt ( $\mu\text{l l}^{-1}$ )	0	13.02	59.12	15.03

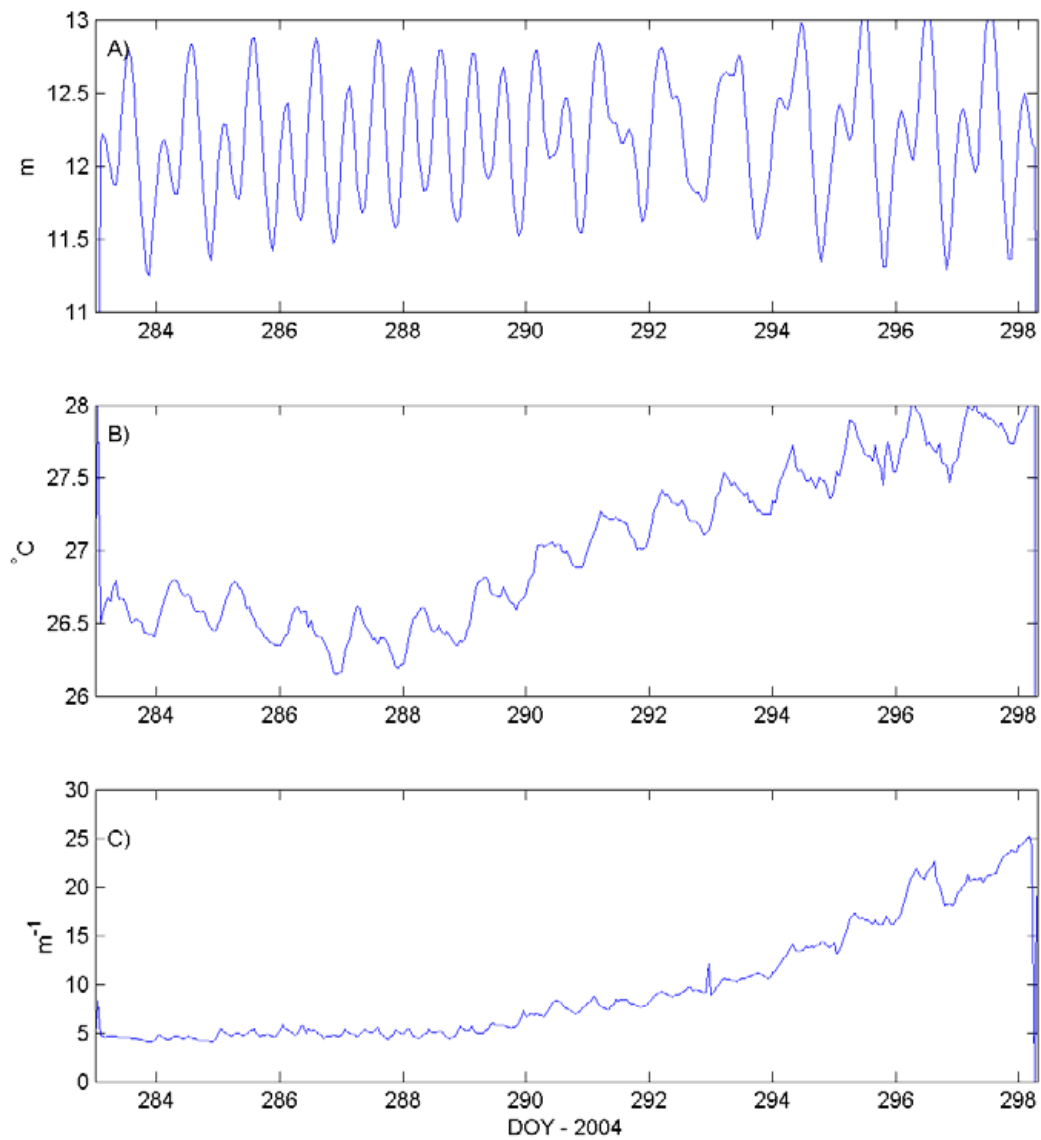


Fig. 4.13. a) Burst-averaged pressure time-series measured on the SBE-37 at 03CM02; b) Burst-averaged temperature time-series measured on the SBE-37 at 03CM02; c) Burst-averaged beam-attenuation measured by the LISST at 03CM02.

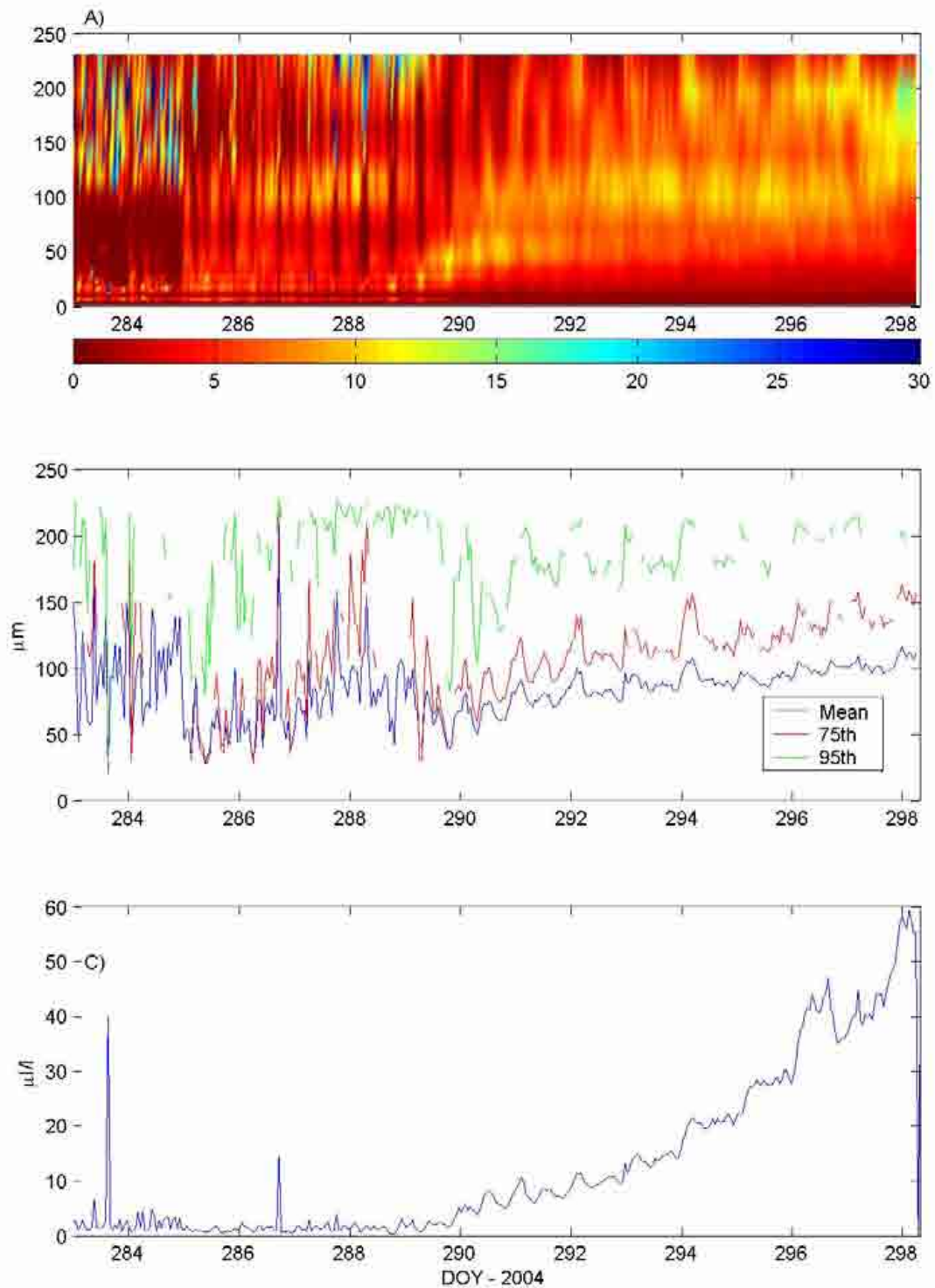


Fig. 4.14. a) Time-series of the burst-averaged particle volume concentrations  $V_i$  for each of the 32 size classes recorded by the LISST at 03CM02; b) Burst-averaged mean grain-size, with the 75<sup>th</sup> and 95<sup>th</sup> percentiles also shown; c) Burst-averaged median grain-size.

### 4.4.3. Sea-level

The original survey design had 5 current meters located within Area B to determine changes in flow and wave characteristics over the sandbank. However, with two of these current meters not recording any data, this could not be achieved. Although the data are reliable, and allow some assessment of localised variation in flow, this report will concentrate only on comparing three areas: Orman Reefs (01CM01), Area A (02CM07), and Area B (04CM03 and 06CM06).

#### 4.4.3.1. Station 01CM01

At 01CM01, pressure is recorded by the SBE-19 only. A time-series plot of sea-level recorded by the SBE-19 is presented in the previous section (Fig. 4.7c). Table 4.6 presents the results of the tidal analysis of the sea-level record for the four largest constituents (M2, S2, O1, K1).

Table 4.6. Results from the classical harmonic analysis. Record Length 18.53 days. Start time is 8/10/04 07:50:19. Mean water depth from record is 10.2 m. Phase is with respect to Greenwich Mean Time.

Tide	Frequency (cph)	Amplitude (m)	Amp. Error (m)	Phase (degrees)	Ph. Error (degrees)
O1	0.0387307	0.2653	0.073	19.90	13.78
K1	0.0417807	0.4272	0.074	61.17	9.54
M2	0.0805114	0.5998	0.174	87.69	18.19
S2	0.0833333	0.6900	0.152	44.94	15.18

The form ratio,  $F$ , calculated at 01CM01 is equal to 0.57, indicating that tides are mixed & semi-diurnal at the site.

Significant constituents calculated within the tidal analysis, where amplitude of a tidal constituent is greater than the calculated error in amplitude for that constituent, are predominantly in the diurnal and semi-diurnal bands (~0.04 and ~0.08 cycles per hour respectively) (Fig. 4.15). Some higher frequency constituents are also significant. Tidal phase (Fig. 4.15c) shows that the significant constituents generally have small phase errors. The residual time-series after removal of the tidal signal has low amplitudes, indicating that the sea surface signal is almost entirely driven by tidal effects.

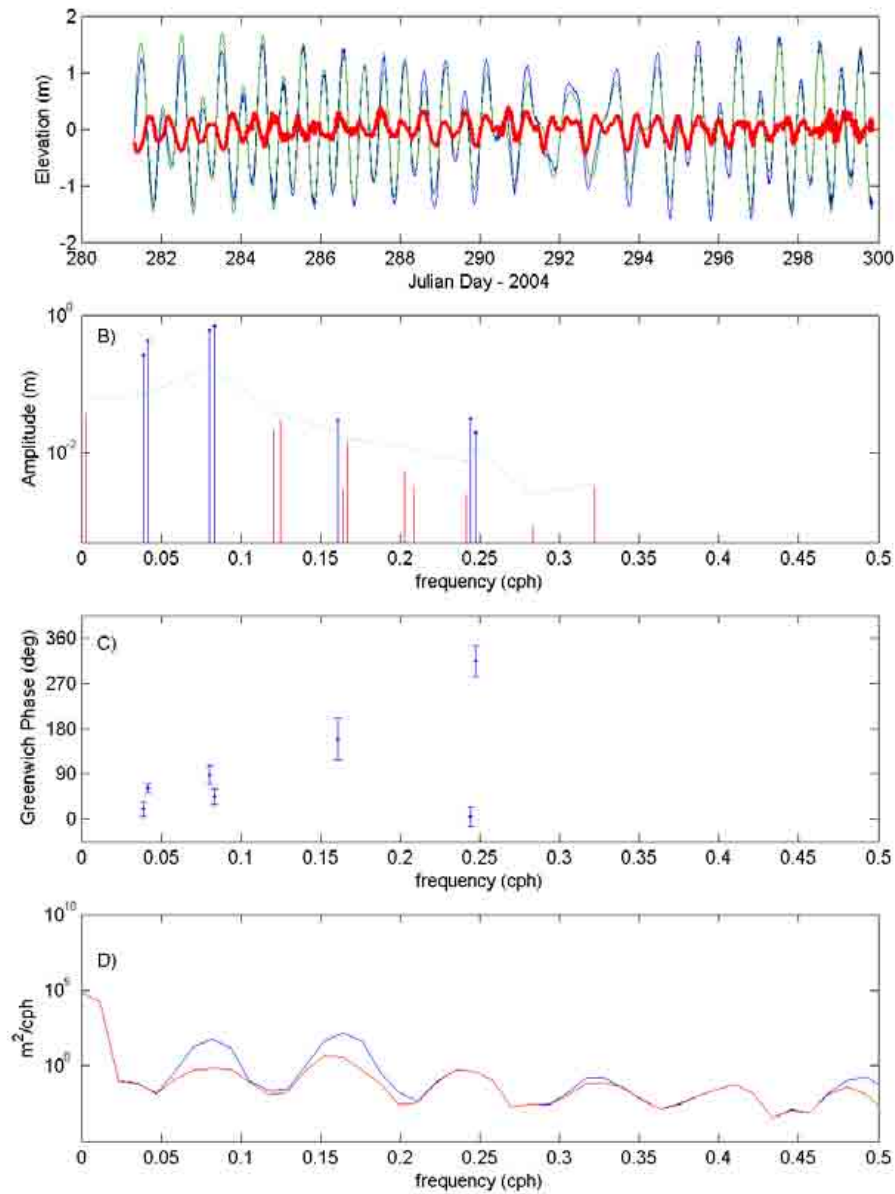


Fig. 4.15. Results of classical harmonic analysis of sea-level record obtained from the SBE-19 at 01CM01. a) Blue line is raw time series referenced to the mean level in the record, Green line is tidal prediction from analysis referenced to the mean, Red line is residual time series after removal of the tidal signal; b) Amplitude of all analysed components with 95% significance level (green dashed line). Significant constituents ( $amp > amp\_err$ ) are marked with a solid circle; c) Phase of significant constituents with 95% confidence interval; d) Spectral estimates before and after removal of tidal energy. Blue-line is energy of original time-series, red-line is non-tidal energy.

#### 4.4.3.2. Station 02CM07

A sea-level record is available from both the SBE-19 and the ADCP at 02CM07. A time series plot of the pressure record from the SBE-19 was displayed in the previous section (Fig. 4.9c). A time series plot of the pressure record from the ADCP is shown in Fig. 4.16. Tables 4.8 and 4.9 present the results of the tidal analysis of the sea-level records for both the SBE-19 and the ADCP displaying the four largest constituents (M2, S2, O1, K1).

A linear regression analysis has been carried out between the ADCP sea-level time-series and the SBE-19 sea-level time-series. Regression statistics are displayed in table 4.7. A slope of <1 indicates that Time-series 2 overestimates time-series 1. If slope is close to 1, but R<sup>2</sup> indicates lower correlation, this is generally a result of a slight phase shift between the two records.

Table 4.7. Regression statistics between pressure records at CSIRO Mooring 2.

Time-series 1 (Y)	Time-series 2 (X)	R <sup>2</sup>	Slope
SBE-19	ADCP	0.9981	1.0443

Table 4.8. Results from the classical harmonic analysis of the sea-level record obtained from the SBE-19 at 02CM07. Record length 17.35 days. Start time is 8/10/04 22:10:19. Mean water depth from record is 5.68 m. Phase is with respect to Greenwich Mean Time.

Tide	Frequency (cph)	Amplitude (m)	Amp. Error (m)	Phase (degrees)	Ph. Error (degrees)
O1	0.0387307	0.3397	0.046	14.48	7.62
K1	0.0417807	0.5285	0.050	69.31	4.89
M2	0.0805114	0.3408	0.148	199.15	20.89
S2	0.0833333	0.3606	0.143	77.55	20.12

Table 4.9. Results from the classical harmonic analysis of the sea-level record obtained from the ADCP at 02CM07. Record length 17.35 days. Start time is 08/10/04 08:10:00. Mean water depth from record is 5.35 m. Phase is with respect to Greenwich Mean Time.

Tide	Frequency (cph)	Amplitude (m)	Amp. Error (m)	Phase (degrees)	Ph. Error (degrees)
O1	0.0387307	0.4613	0.065	70.36	7.79
K1	0.0417807	0.6279	0.060	73.63	5.55
M2	0.0805114	0.3034	0.122	239.23	23.78
S2	0.0833333	0.3469	0.138	75.64	22.89

The form ratio,  $F$ , is calculated as 1.26 using the results of the SBE-19 sea-level analysis and 1.67 using the results of the ADCP sea-level analysis. The SBE-19 data indicate that tides are mixed and semi-diurnal at the site and the ADCP sea-level record indicates that tides are mixed and diurnal at the site.

Both analyses indicate that the significant constituents are predominantly in the diurnal and semi-diurnal bands ( $\sim 0.04$  and  $\sim 0.08$  cycles per hour respectively) (Fig. 4.16). Some higher frequency constituents are also significant, which can lead to tidal distortion. Tidal phase, presented in Fig. 4.16C show that the significant constituents generally have small phase errors. The residual time-series after removal of the tidal signal has low amplitudes, indicating that the sea surface signal is almost entirely driven by tidal effects.

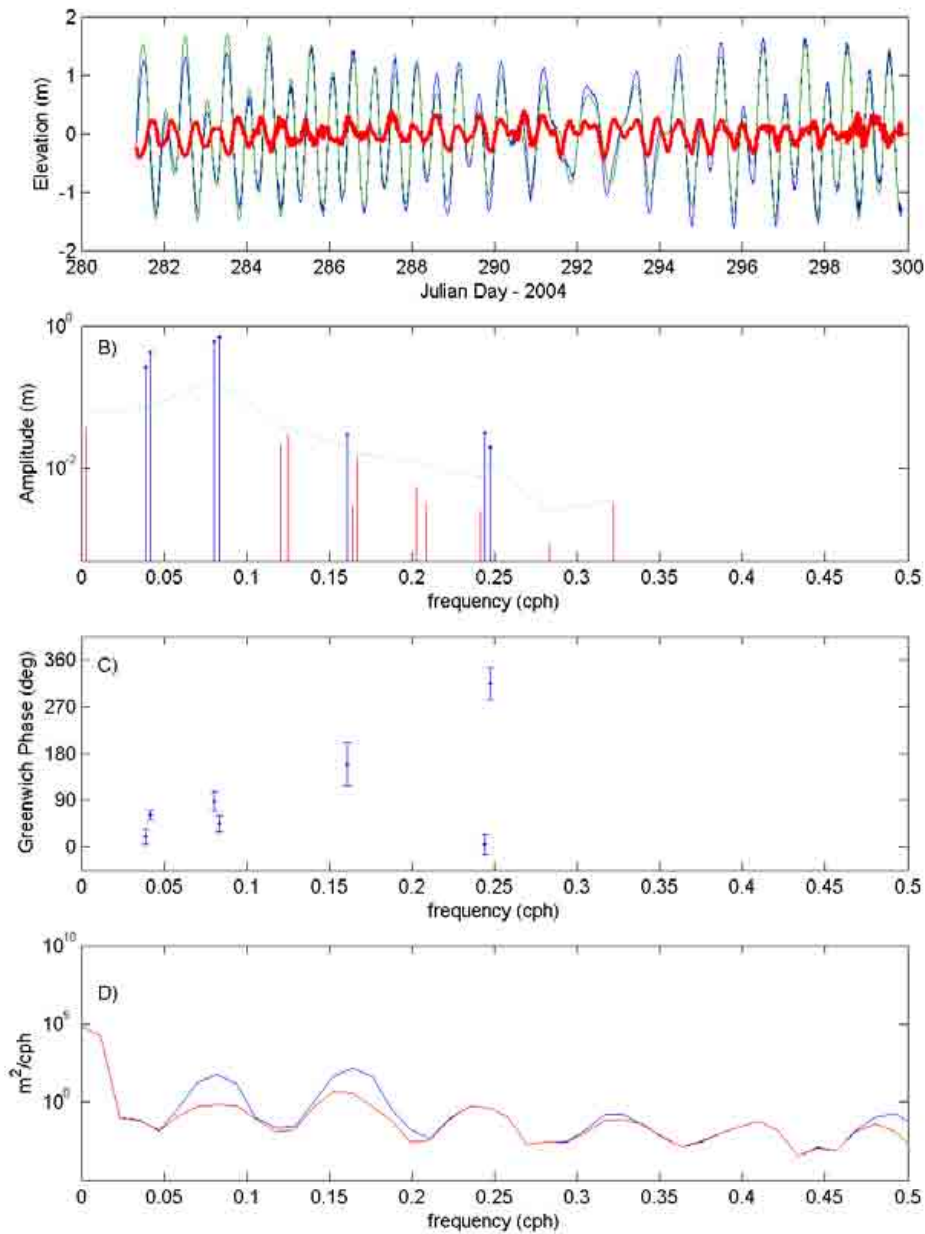


Fig. 4.16. Results of classical harmonic analysis of sea-level record obtained from the SBE-19 at 02CM07. a) Blue line is raw time series referenced to the mean level in the record, Green line is Tidal prediction from analysis referenced to the mean, Red line is residual time series after removal of the tidal signal; b) Amplitude of all analysed components with 95% significance level (green dashed line). Note frequency dependence. Significant constituents (amp > amp\_err) are marked with a solid circle; c) Phase of significant constituents with 95% confidence interval; d) Spectral estimates before and after removal of tidal energy. Blue-line is energy of original time-series, red-line is non-tidal energy.

#### 4.4.3.3. Station 03CM02

Although currents are unavailable from 03CM02, a sea-level record is available from the Nortek sensor attached to the BRUCE mooring. Each burst has been averaged to obtain a time series plot of the tidal pressure record from the Nortek is shown in [Fig. 4.17](#). Table 4.10 presents the results of the tidal analysis of the sea-level record for the four largest constituents (M2, S2, O1, K1).

Table 4.10. Results from the classical harmonic analysis of the sea-level record obtained from the Nortek at 03CM2. Record length 15.1 days. Start time is 09/10/04 02:00.00. Mean water depth from record is 8.89 m. Phase is with respect to Greenwich Mean Time.

Tide	Frequency (cph)	Amplitude (m)	Amp. Error (m)	Phase (degrees)	Ph. Error (degrees)
O1	0.0387307	0.3063	0.066	21.89	12.45
K1	0.0417807	0.4802	0.079	70.57	7.94
M2	0.0805114	0.3962	0.160	117.83	23.40
S2	0.0833333	0.6049	0.154	64.16	15.94

The form ratio,  $F$ , is calculated as 0.7856 using the results of the Nortek sea-level analysis. The Nortek sea-level record indicates that tides are mixed, mainly semi-diurnal at the site.

Both analyses indicate that the significant constituents are predominantly in the diurnal and semi-diurnal bands ( $\sim 0.04$  and  $\sim 0.08$  cycles per hour respectively) ([Fig. 4.17](#)). Some higher frequency constituents are also significant, which can lead to tidal distortion. Tidal phase, presented in [Fig. 4.17C](#) show that the significant constituents generally have small phase errors. The residual time series after removal of the tidal signal has low amplitudes, indicating that the sea surface signal is almost entirely driven by tidal effects.

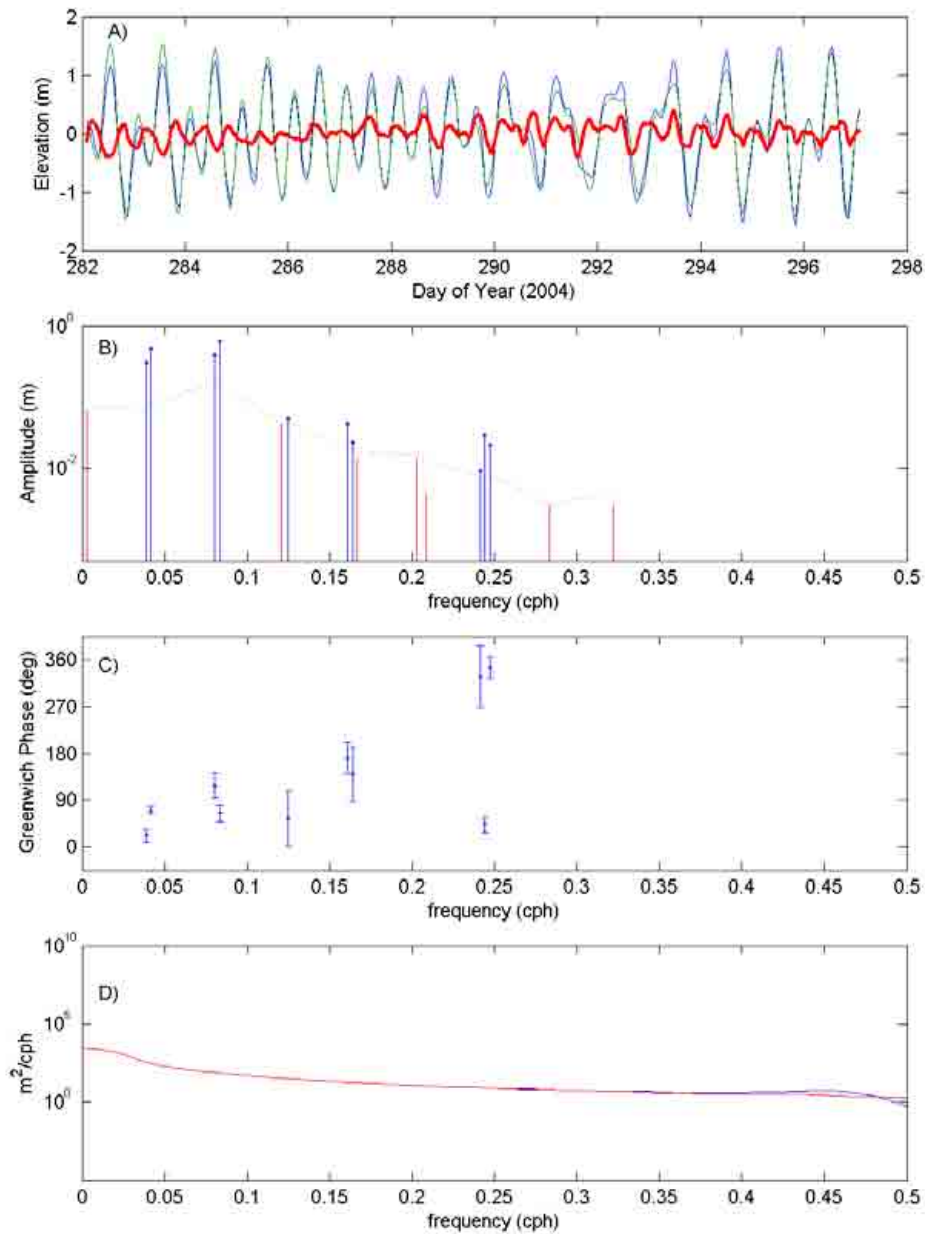


Fig. 4.17. Results of classical harmonic analysis of sea-level record obtained from the Nortek at 03CM02. a) Blue line is raw time series referenced to the mean level in the record, Green line is tidal prediction from analysis referenced to the mean, Red line is residual time series after removal of the tidal signal; b) Amplitude of all analysed components with 95% significance level (green dashed line). Note frequency dependence. Significant constituents (amp>amp\_err) are marked with a solid circle; c) Phase of significant constituents with 95% confidence interval; d) Spectral estimates before and after removal of tidal energy. Blue-line is energy of original time-series, red-line is non-tidal energy.

#### 4.4.3.4. Station 04CM03

A sea-level record is available from the ADCP. Table 4.11 presents the results of the tidal analysis of the sea-level record for the four largest constituents (M2, S2, O1, K1). A time series plot of the pressure record from the ADCP is shown in [Fig. 4.18](#).

Table 4.11. Results from the classical harmonic analysis of the sea-level record obtained from the ADCP at 04CM3. Record length 15.81 days. Start time is 08/10/04 08:10.00. Mean water depth from record is 5.88 m. Phase is with respect to Greenwich Mean Time.

Tide	Frequency (cph)	Amplitude (m)	Amp. Error (m)	Phase (degrees)	Ph. Error (degrees)
O1	0.0387307	0.4169	0.101	78.66	13.36
K1	0.0417807	0.5711	0.094	75.58	10.31
M2	0.0805114	0.3446	0.162	184.52	23.64
S2	0.0833333	0.5748	0.161	62.80	19.24

The form ratio,  $F$ , is 1.0746 using the results of the ADCP sea-level analysis. The ADCP sea-level record indicates that tides are mixed and mainly semi-diurnal at the site.

Both analyses indicate that the significant constituents are predominantly in the diurnal and semi-diurnal bands ( $\sim 0.04$  and  $\sim 0.08$  cycles per hour respectively) ([Fig. 4.18](#)). Some higher frequency constituents are also significant, which can lead to tidal distortion, which can lead to tidal distortion. Tidal phase, presented in [Fig. 4.18C](#)) show that the significant constituents generally have small phase errors. The residual time-series after removal of the tidal signal has low amplitudes, indicating that the sea surface signal is almost entirely driven by tidal effects.

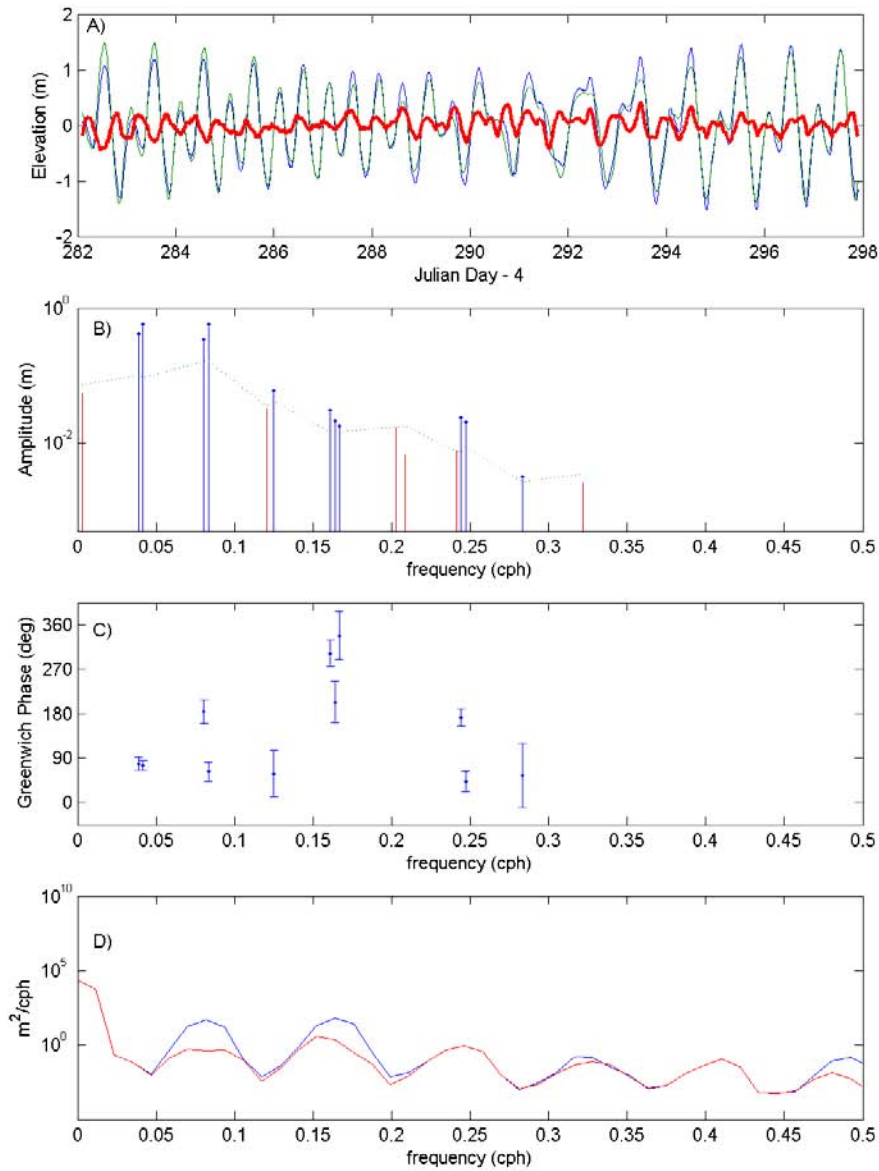


Fig. 4.18. Results of classical harmonic analysis of sea-level record obtained from the ADCP at 04CM03. a) Blue line is raw time series referenced to the mean level in the record, Green line is tidal prediction from analysis referenced to the mean, Red line is residual time series after removal of the tidal signal; b) Amplitude of all analysed components with 95% significance level (green dashed line). Note frequency dependence. Significant constituents (amp>amp\_err) are marked with a solid circle; c) Phase of significant constituents with 95% confidence interval; d) Spectral estimates before and after removal of tidal energy. Blue-line is energy of original time-series, red-line is non-tidal energy.

#### 4.4.3.5. Station 05CM04

A sea-level record is available from the ADCP at 05CM04. Table 4.12 presents the results of the tidal analysis of the sea-level record for the four largest constituents (M2, S2, O1, K1). A time series plot of the pressure record from the ADCP is shown in [Fig. 4.19](#).

Table 4.12. Results from the classical harmonic analysis of the sea-level record obtained from the ADCP at 04CM03. Record length 15.17 days. Start time is 08/10/04 08:10.00. Mean water depth from record is 7.09 m. Phase is with respect to Greenwich Mean Time.

Tide	Frequency (cph)	Amplitude (m)	Amp. Error (m)	Phase (degrees)	Ph. Error (degrees)
O1	0.0387307	0.2930	0.075	21.56	13.11
K1	0.0417807	0.4615	0.085	68.24	8.34
M2	0.0805114	0.3633	0.149	116.69	22.27
S2	0.0833333	0.5674	0.139	61.80	13.06

The form ratio,  $F$ , is 0.81 using the results of the ADCP sea-level analysis. The ADCP sea-level record indicates that tides are mixed and mainly semi-diurnal at the site.

Both analyses indicate that the significant constituents are predominantly in the diurnal and semi-diurnal bands ( $\sim 0.04$  and  $\sim 0.08$  cycles per hour respectively) ([Fig. 4.19](#)). Some higher frequency constituents are also significant, which can lead to tidal distortion. Tidal phase, presented in [Fig. 4.19C](#)) show that the significant constituents generally have small phase errors. The residual time-series after removal of the tidal signal has low amplitudes, indicating that the sea surface signal is almost entirely driven by tidal effects.

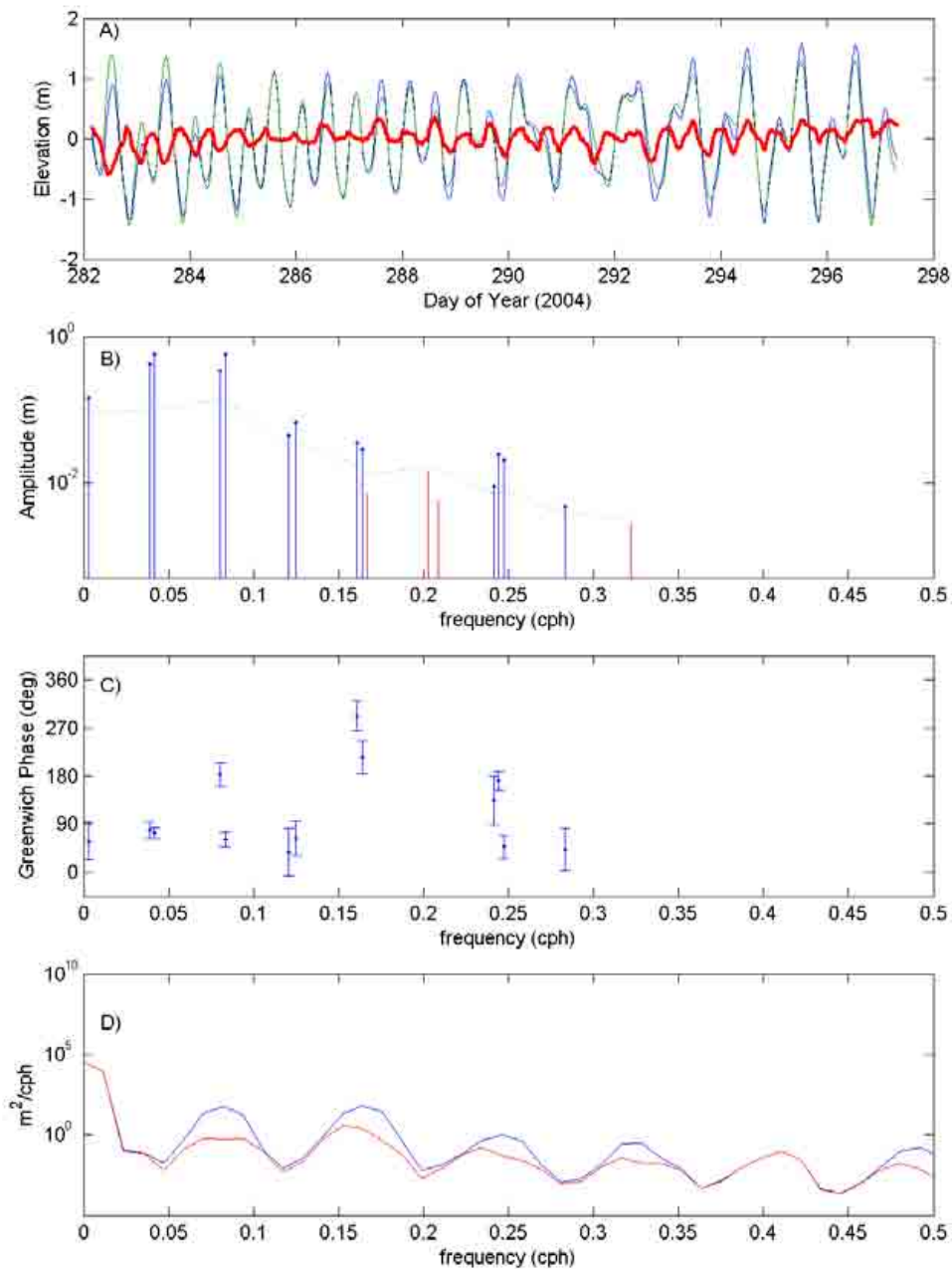


Fig. 4.19. Results of classical harmonic analysis of sea-level record obtained from the ADCP at 05CM4. a) Blue line is raw time series referenced to the mean level in the record, Green line is tidal prediction from analysis referenced to the mean, Red line is residual time series after removal of the tidal signal; b) Amplitude of all analysed components with 95% significance level (green dashed line). Note frequency dependence. Significant constituents (amp>amp\_err) are marked with a solid circle; c) Phase of significant constituents with 95% confidence interval; d) Spectral estimates before and after removal of tidal energy. Blue-line is energy of original time-series, red-line is non-tidal energy.

#### 4.4.3.6. Station 06CM06

A sea-level record is available from the RBR pressure sensor, the SBE-19 and the ADCP at 06CM06. A time series plot of the pressure record from the SBE-19 was displayed in the previous section (Fig. 4.13c). A time series plot of the pressure record from the RBR sensor is shown in Fig. 4.20. Tables 4.14, 4.15 and 4.16 present the results of the tidal analysis of the sea-level records for both the RBR sensor, SBE-19 and the ADCP displaying the four largest constituents (M2, S2, O1, K1).

A linear regression analysis has been carried out between the RBR time-series and the ADCP time-series, and the RBR time-series and the SBE-19 time-series (Table 4.13). A slope less than 1 indicates that time-series 2 overestimates time-series 1.

Table 4.13. Regression statistics between pressure records at 06CM06.

Time-series 1 (Y)	Time-series 2 (X)	R <sup>2</sup>	Slope
RBR	ADCP	0.9928	1.0121
RBR	SBE-19	0.9943	1.0012

Table 4.14. Results from the classical harmonic analysis of the sea-level record obtained from the RBR pressure sensor. Record length 15.71 days. Start time is 09/10/04 04:20:00. Mean water depth from record is 10.8 m. Phase is with respect to Greenwich Mean Time.

Tide	Frequency (cph)	Amplitude (m)	Amp. Error (m)	Phase (degrees)	Ph. Error (degrees)
O1	0.0387307	0.3062	0.072	19.16	13.75
K1	0.0417807	0.4753	0.078	67.63	9.24
M2	0.0805114	0.3723	0.126	208.48	26.54
S2	0.0833333	0.5879	0.132	59.14	13.92

Table 4.15. Results from the classical harmonic analysis of the sea-level record obtained from the SBE-19. Record length 15.71 days. Start time is 9/10/04 04:30:00. Mean water depth from record is 10.7 m. Phase is with respect to Greenwich Mean Time.

Tide	Frequency (cph)	Amplitude (m)	Amp. Error (m)	Phase (degrees)	Ph. Error (degrees)
O1	0.0387307	0.3052	0.076	21.41	14.15
K1	0.0417807	0.4738	0.076	69.91	8.13
M2	0.0805114	0.3710	0.132	119.71	22.54
S2	0.0833333	0.5860	0.127	63.75	12.83

Table 4.16. Results from the classical harmonic analysis of the sea-level record obtained from the ADCP. Record length 15.74 days. Start time is 08/10/2004 04:30 GMT. Mean water depth from record is 10.8 m. Phase is with respect to Greenwich Mean Time.

Tide	Frequency (cph)	Amplitude (m)	Amp. Error (m)	Phase (degrees)	Ph. Error (degrees)
O1	0.0387307	0.4188	0.074	88.12	12.16
K1	0.0417807	0.5839	0.084	83.53	8.02
M2	0.0805114	0.2972	0.139	195.16	28.36
S2	0.0833333	0.5978	0.153	77.84	14.67

The form ratio,  $F$ , is calculated as 0.81 using the results of the RBR sea-level analysis, 0.81 using the results of SBE-19 sea-level analysis and 1.12 using the results of the ADCP sea-level analysis. Despite the ADCP sea-level analysis suggesting diurnal tidal constituents are much more dominant than observed by the other records, all datasets indicate that tides are mixed and semi-diurnal at the site.

All three analyses indicate that the significant constituents are predominantly in the diurnal and semi-diurnal bands ( $\sim 0.04$  and  $\sim 0.08$  cycles per hour respectively) (Fig. 4.20). Some higher frequency constituents are also significant, which can lead to tidal distortion. Tidal phase, presented in Fig. 4.20C) shows that the significant constituents generally have small phase errors. The residual time-series after removal of the tidal signal has low amplitudes, indicating that the sea surface signal is almost entirely driven by tidal effects.

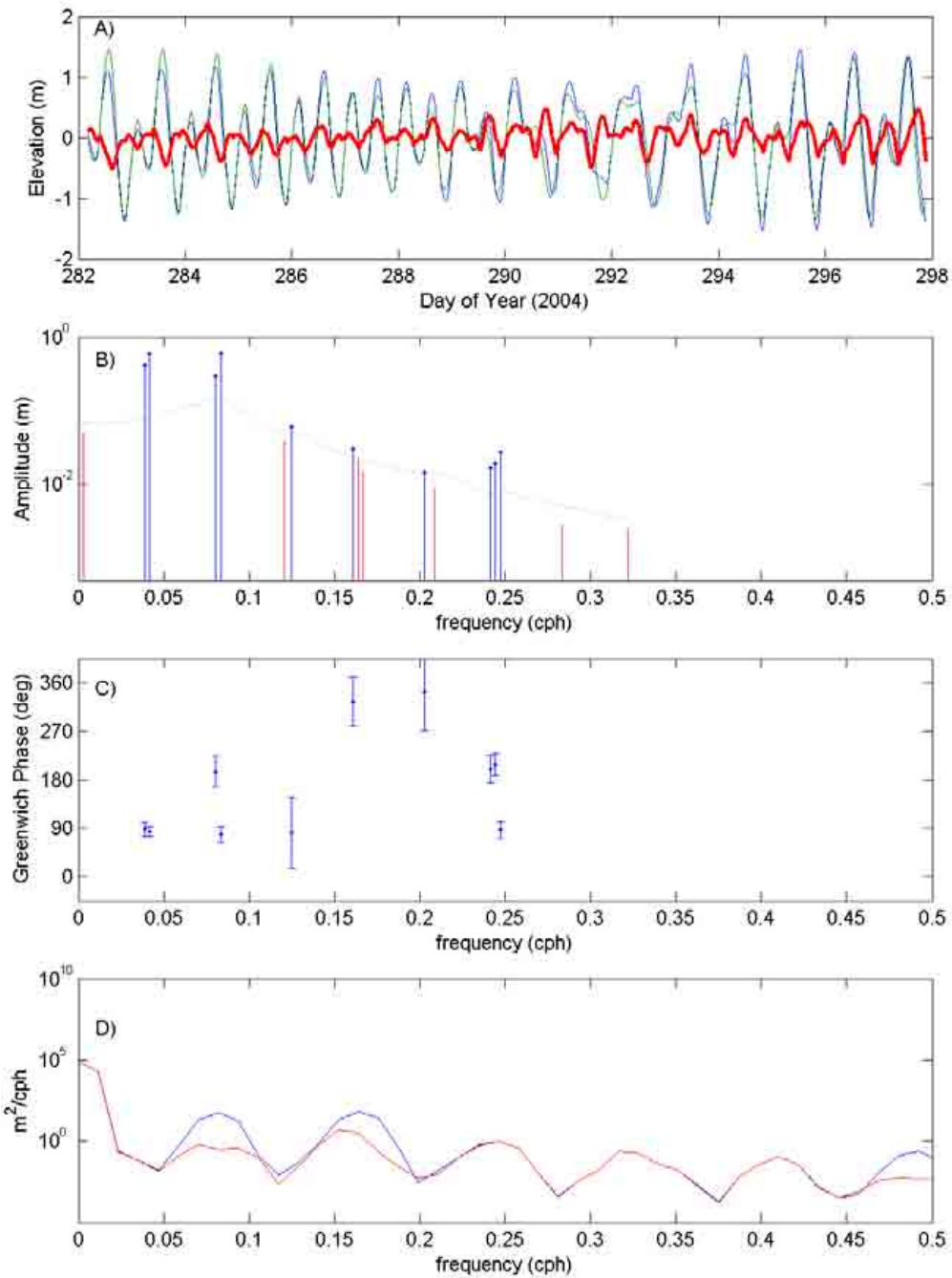


Fig. 4.20. Results of classical harmonic analysis of pressure data from 06CM06 (RBR pressure record). a) Blue line is raw time series, Green line is tidal prediction from analysis, Red line is residual time series after removal of the tidal signal; b) Amplitude of all analysed components with 95% significance level (green dashed line). Note frequency dependence. Significant constituents ( $\text{amp} > \text{amp\_err}$ ) are marked with a solid circle; c) Phase of significant constituents with 95% confidence interval; d) Spectral estimates before and after removal of tidal energy. Blue-line is energy of original time-series, red-line is non-tidal energy.

#### 4.4.3.7. Station 07CM05

Although a pressure sensor is present on the FSI current meter, the U-shaped mooring used for this current meter means that the current meter may have moved vertically in the water column. Consequently, there is no reliable sea-level record at this site.

#### 4.4.3.8. Review of tidal analysis

Results from the harmonic analysis of sea-level records from the 3 areas indicate high tidal variability within the Torres Strait. In agreement with the results from the monsoon survey (Heap et al., 2005), the form ratio  $F$  confirms that tides are mixed & semi-diurnal at all locations. The length of record for this survey (approximately 18 days), is significantly less than from the monsoon survey (approximately 31 days). Consequently, results of the harmonic analysis from the monsoon survey will more accurately describe tidal conditions than the present survey and is reflected by the listed errors in the tables.

Low frequency sea-level variation within the ~18 day record is less than 0.15 m in each of the sea-level records (Figs. 4.8C, 4.10C, 4.12C). With current meters deployed at different locations with different water depths for each survey, no seasonal variability of sea-level can be determined from the pressure data.

#### 4.4.4. Waves

The directional wave spectra were not recorded. The wave direction is assumed to be in the same direction as the wind, (i.e., wave direction = wind direction+180°).

##### 4.4.4.1. Station 03CM02

The calculated significant wave height ( $H_s$ ) and the peak wave period ( $T_p$ ) for the period of deployment are shown in Fig. 4.21. Statistics of the waves recorded at 03CM02 are displayed in Table 4.17. Periods with the highest intensity of wave activity occur from JD 284-288, 291, 295-296. The maximum wave height experienced during the course of the survey was 2.49 m on Julian Day 285.00. This peak wave height ( $H_{max}$ ), is significantly greater than the average wave height recorded during the same 8 minute burst (1.21 m). The peak wave period during this period was 4 s.

The wave statistics are indicative of locally generated wind-waves (i.e., sea). Generally, slight sea conditions ( $H \approx 0.5$  m) were punctuated by times of moderate seas ( $H = 1.0$ - $1.2$  m) coinciding with increased wind strengths and wave period (Section 3.1.2).

Table 4.17 Wave statistics from 03CM02

	Minimum	Mean	Maximum	Std Deviation
Hs (m)	0.43	0.61	1.21	0.14
Hmax (m)	0.74	1.14	2.49	0.27
Tp (s)	2.79	3.90	5.00	0.45
Tmean (s)	1.02	1.43	2.56	0.30

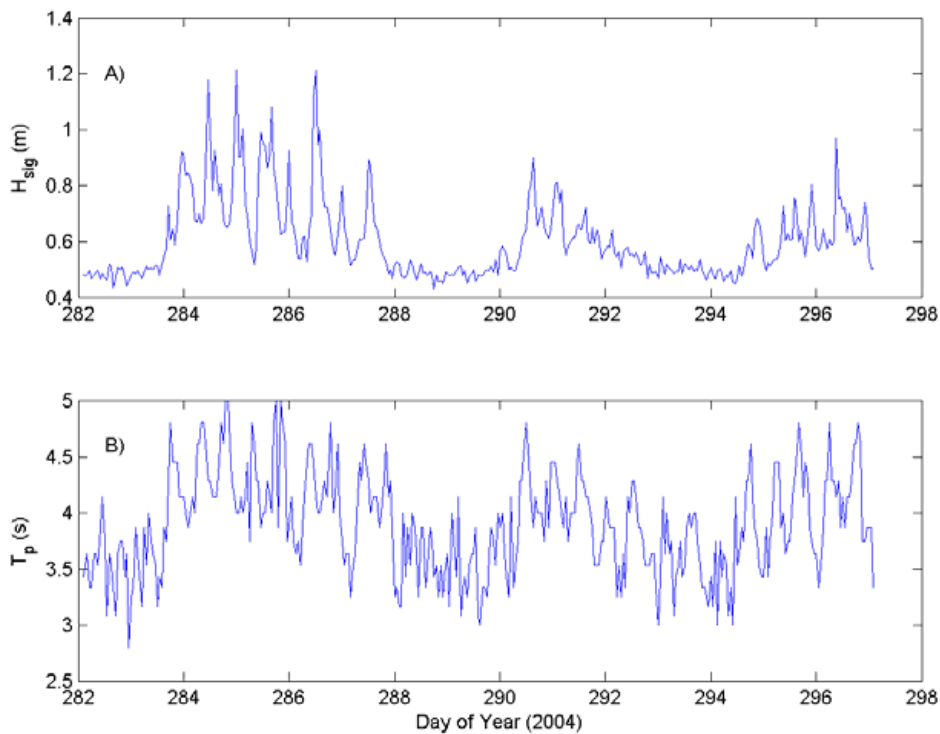


Fig. 4.21. Time series of wave statistics recorded at 03CM02. a) significant wave height, and b) peak wave period. Velocities were not available, and consequently wave direction data were not able to be computed.

#### 4.4.4.2. Station 04CM03

The calculated significant wave height ( $H_s$ ) and the peak wave period ( $T_p$ ) for the period of deployment are shown in Fig. 4.22. Statistics of the waves recorded at 04CM03 are displayed in Table 4.18. Periods with the highest intensity of wave activity occur from JD 284-288, 291, 295-298. The maximum wave height experienced during the course of the survey was 3.43 m on Julian Day 284.96. This peak wave height ( $H_{max}$ ), is significantly greater than the average wave height recorded during the same 8 minute burst (2.13 m). The peak wave period during this period was 4.2 s

This station is more exposed than Station 03CM02. Nevertheless, the wave statistics are again indicative of locally generated wind-waves (i.e., sea). Generally, slight sea conditions ( $H \approx 0.5\text{--}0.6$  m) were punctuated by times of moderate seas ( $H > 1.2$  m) coinciding with increased wind strengths and wave period ([Section 3.1.2](#)).

Table 4.18 Wave statistics recorded at 04CM03

	Minimum	Mean	Maximum	Std Deviation
Hs (m)	0.55	1.03	2.13	0.36
Hmax (m)	0.77	1.62	3.43	0.61
Tp (s)	3.10	4.04	5.77	0.53
Tmean (s)	3.52	4.05	4.80	0.23

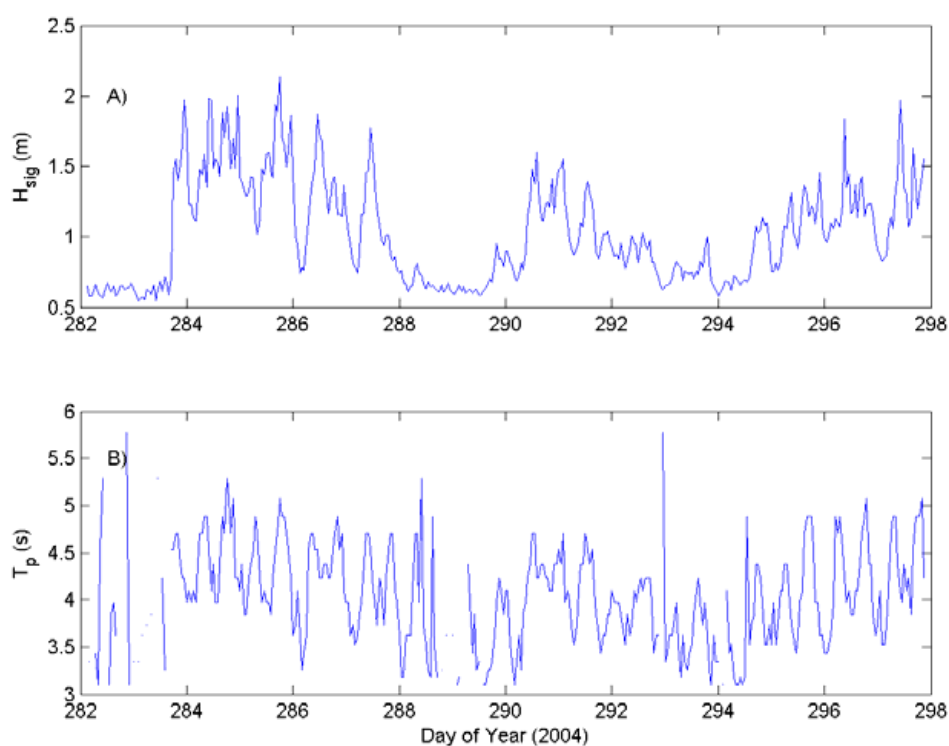


Fig. 4.22. Time series of wave statistics recorded at 04CM03. a) significant wave height, and b) peak wave period. Velocities were not available, and consequently wave direction data were not able to be computed.

#### 4.4.4.3. Comparison between 03CM02 and 04CM03

The pressure sensor at 03CM02 was stationed off the sandbank on the eastern side and 04CM03 was on a sandwave in the centre of the sandbank (see Fig. 5.1b). The two moorings are approximately 500 m apart. The sensor on top of the sandbank (04CM03) consistently recorded higher wave heights than the sensor off the bank (see Tables 4.17 and 4.18). This is a result of the shallower water on top of the bank causing the waves to become slower and taller, and eventually to break on the bank.

#### 4.4.5. Currents

##### 4.4.5.1 Station 01CM01

No current meter was deployed with 01CM01.

##### 4.4.5.2. Station 02CM07

02CM07 was stationed in Area A to the east of the sandwaves on top of the carbonate platform. Progressive vector plots for each of the bed currents (Bin 1 = 1.6 m), and at the top of the water column (Bin 9 = 3.6 m), are shown in Figs 4.23. The overall displacement for bin 1 was 151.1 km at  $-96.8^\circ$  indicating a net westward flow past the ADCP during the deployment at the seabed. The displacement for bin 9 was 87.2 km at  $-118.0^\circ$ . This displacement is notably less than the displacement for Bin 1 and is directed an extra  $20^\circ$  to the south.

Statistics for each of the currents recorded by the ADCP at 02CM07 are displayed in Table 4.19. The average currents east and north for bins 1 ( $-8.37 \text{ cm s}^{-1}$  and  $-2.4 \text{ cm s}^{-1}$ , respectively) and 9 ( $-8.17 \text{ cm s}^{-1}$  and  $-4.62 \text{ cm s}^{-1}$ , respectively). Although the easterly displacements are similar the difference is nearly a factor of two for the northerly displacements. The fastest currents at the bed attained  $77.5 \text{ cm s}^{-1}$ , at the surface they attained  $107.42 \text{ cm s}^{-1}$ .

Displacement is not constant over the deployment because of the transition from spring to neap to spring tides over the course of the deployment. Neap tides occur near the middle of the deployment and the displacement between the top and the bottom of the water column is in opposite directions during this time. The currents at the surface have a net displacement to the west while the seabed currents have a net displacement to the south east. This result indicates that there is a significant amount of shear within the water column, and the shear is at its strongest during the neap tides. It is unlikely that the shear was created by flow separation as the ADCP is located over 100 m from the nearest sandwave, hence wind shear is the likely mechanism. The winds during the survey were dominantly from the southeast

(Figs. 3.3, 3.4) and appears to have assisted the strong westward displacement in Fig. 4.23a. The currents at the seabed at 02CM07 appear to be more tidally driven and hence respond strongly to the ebb and flood currents. This is best demonstrated in the first 8 days of the deployment when the surface currents move strongly to the west (Fig. 4.23a) whilst the seabed currents have strong displacements to the east and west (Fig. 4.23b).

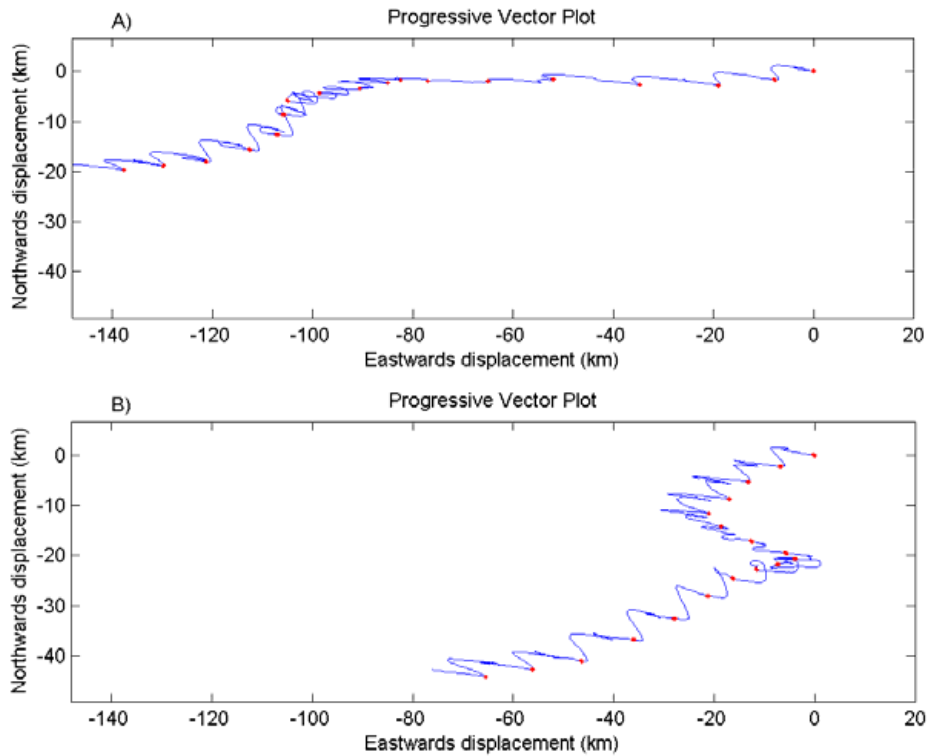


Fig. 4.23. 02CM07 current meter progressive vector plot obtained from data recorded in: a) bin 9 (3.6 m above seabed); b) bin 1 (1.6 m above seabed). The origin of the plot corresponds to the location of the 02CM07 mooring. Dots indicate the beginning of each 24 hour period. Note that missing data does not contribute to calculated displacement (the degree of missing data is shown in Figs. 4.24 and 4.25).

Table 4.19. Raw current meter statistics for 02CM07 at the bed (Bin 1: 1.6 m above seabed) and 'surface' below lowest tide (Bin 9: 3.55 m above bed) All statistics are in  $\text{cm s}^{-1}$ .

Bin	East min	East mean	East max	East Std Dev.	North min	North mean	North max	N Std Dev.	Speed min	Speed mean	Speed max
1	-76.70	-8.37	65.20	34.53	-40.00	-2.41	50.60	11.06	15.87	33.74	77.50
9	-95.30	-8.17	105.90	44.47	-63.00	-4.62	32.90	15.18	18.35	44.26	107.42

A time series of current meter data for the sea-bed and surface are shown in Figs. 4.24 and 4.25, respectively. Missing data in Figures 4.24 and 4.25 indicate times where data has been considered erroneous and removed from the ADCP record. Time series of low-pass filtered current meter data from bins 1 and 9 at 02CM07 are show in Figs. 4.26 and 4.27, respectively.

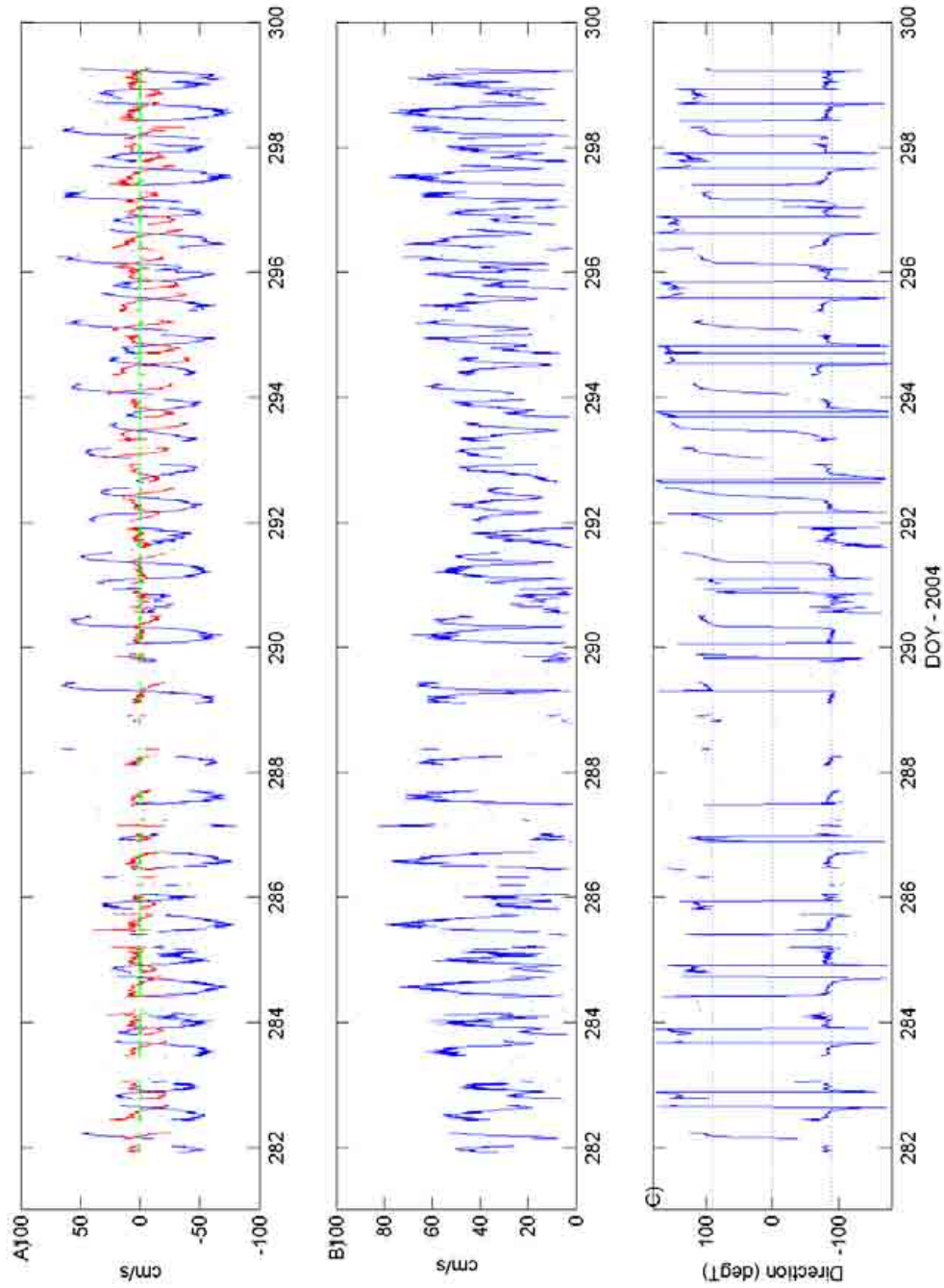


Fig. 4.24. 02CM07 current meter time-series obtained from data recorded in bin 1 (1.6 m above seabed). a) Time series of East (Blue), North (Red), and Up (Green) velocity components; b) Time series of absolute current speed; c) Time series of current direction.

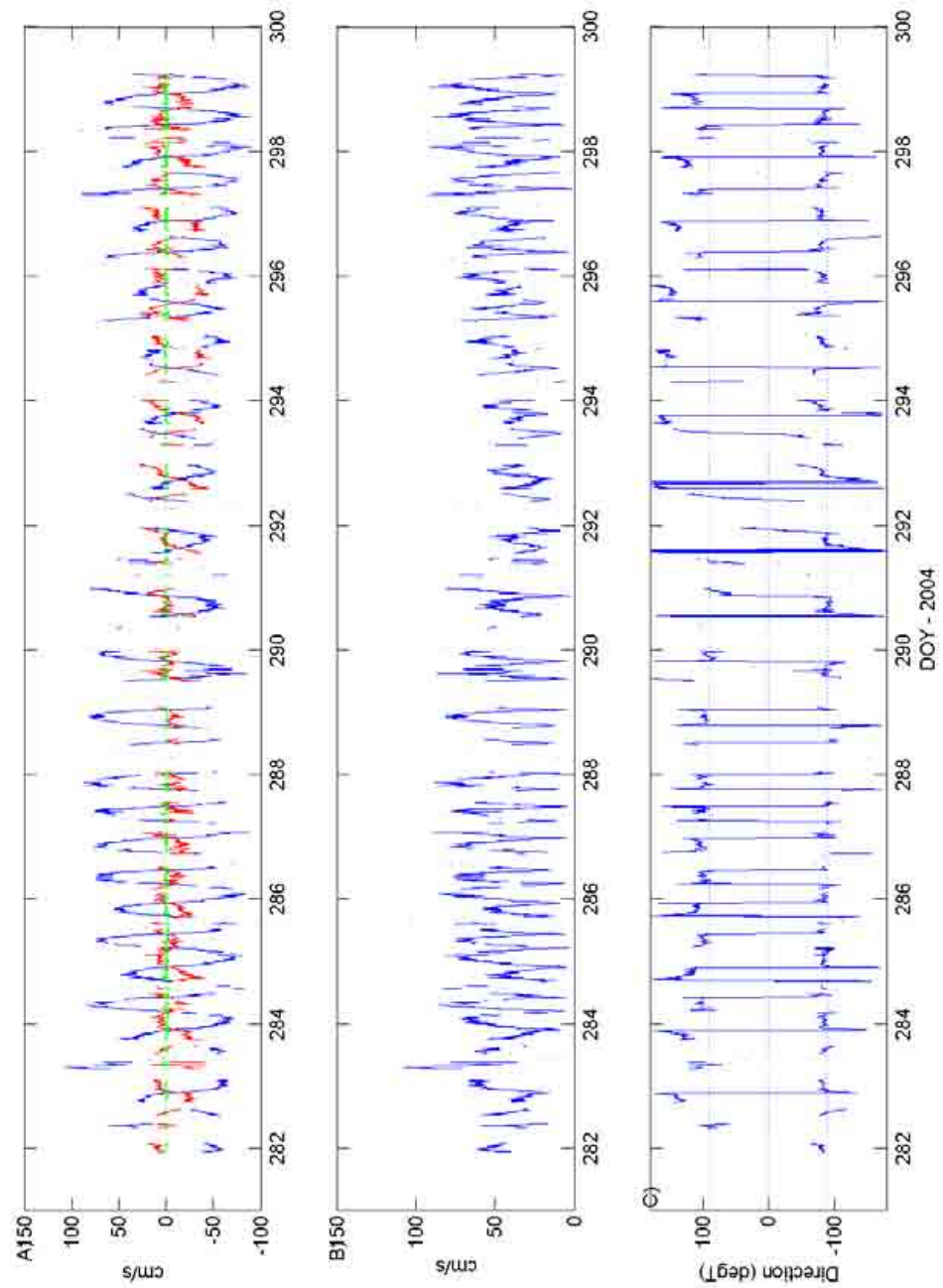


Fig. 4.25. 02CM07 current meter time-series obtained from data recorded in bin 9 (3.6 m above seabed). a) Time series of East (Blue), North (Red), and Up (Green) velocity components; b) Time series of absolute current speed; c) Time series of current direction.

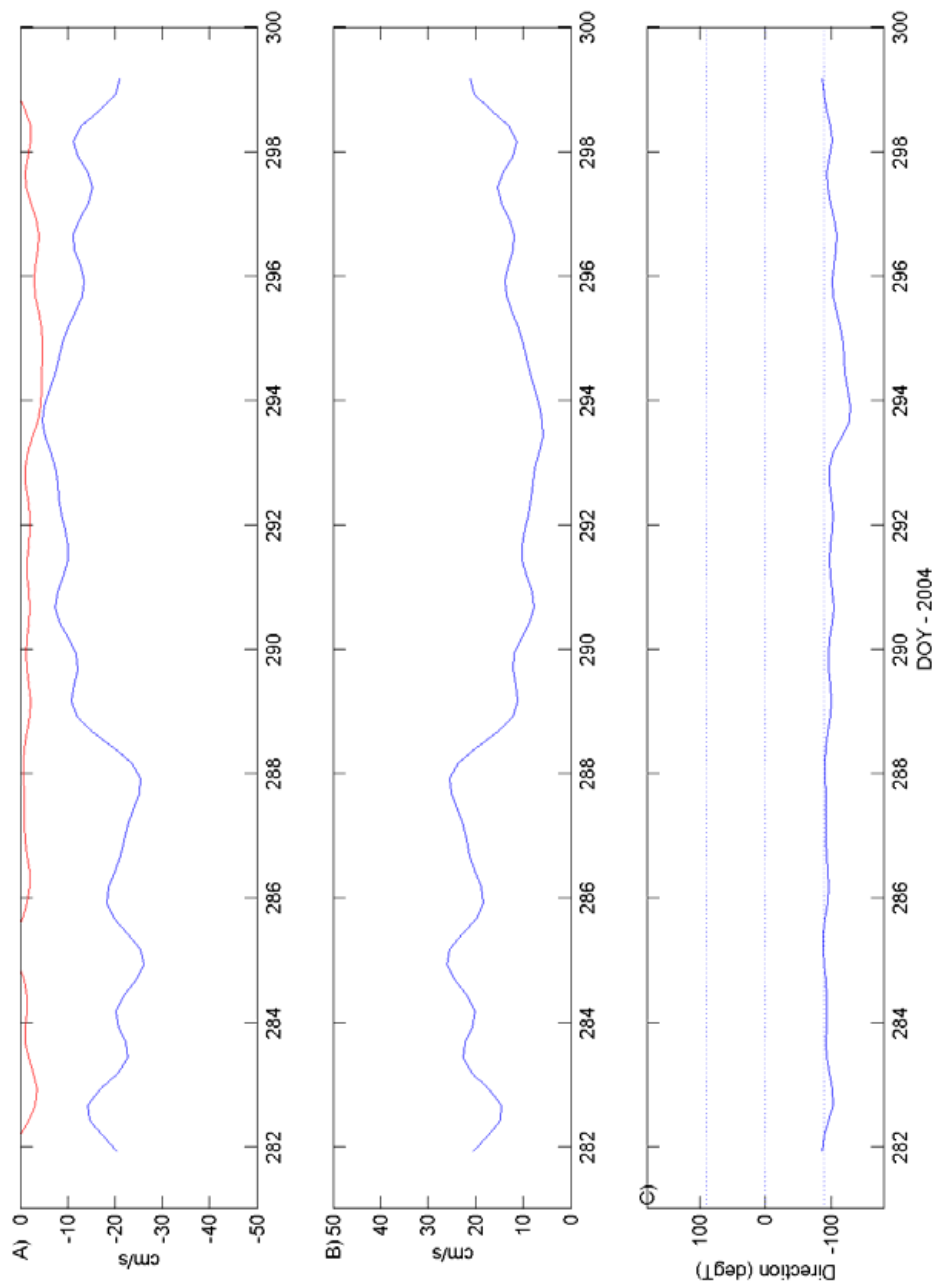


Fig. 4.26. 02CM07 Low-Pass Filtered current meter time-series obtained from data recorded in bin 1 (1.6 m above seabed). a) Time series of East (Blue), North (Red), and Up (Green) velocity components; b) Time series of absolute current speed; c) Time series of current direction.

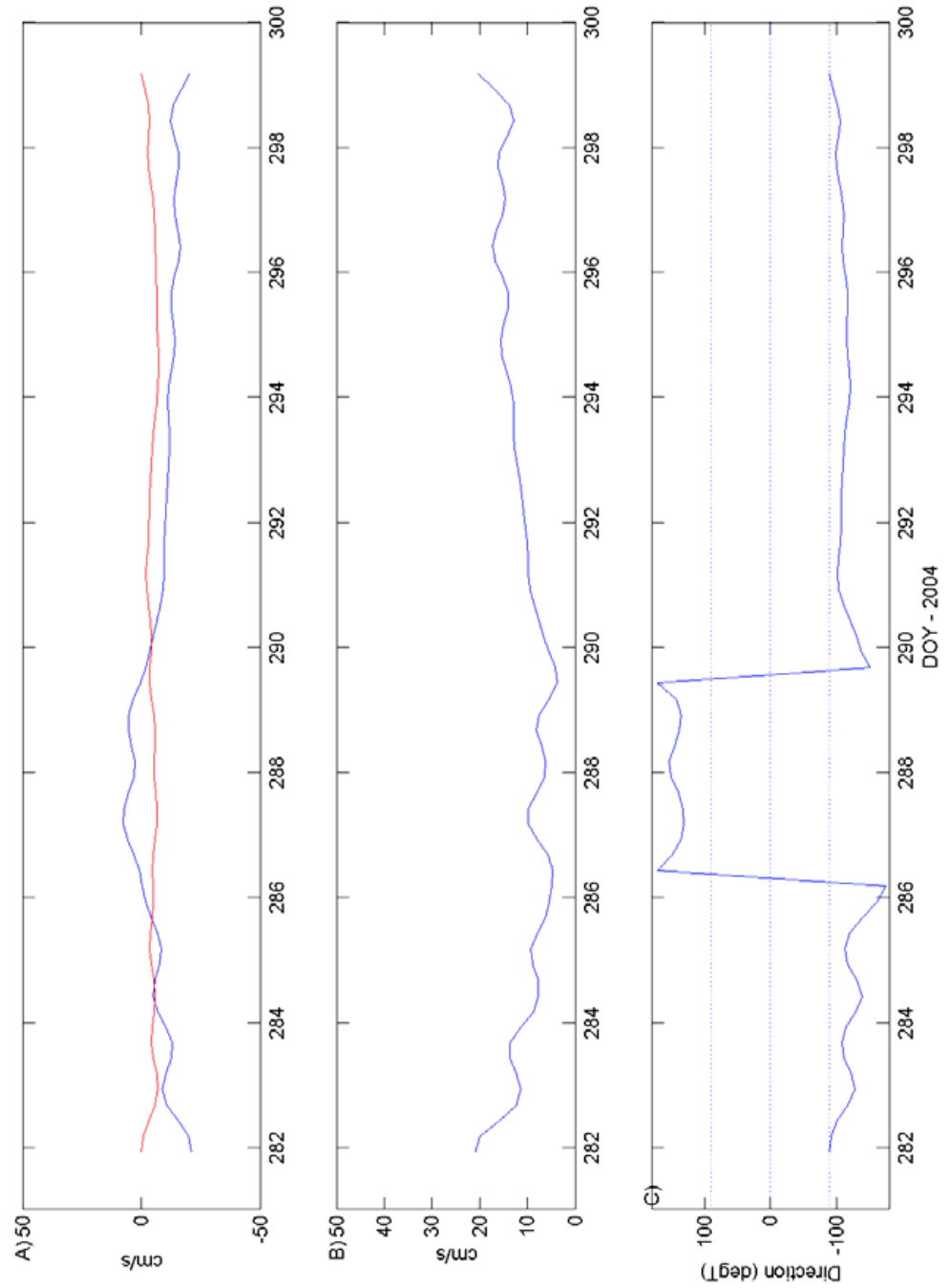


Fig. 4.27. 02CM07 Low-Pass Filtered current meter time-series obtained from data recorded in bin 9 (3.6 m above seabed). a) Time series of East (Blue), North (Red), and Up (Green) velocity components; b) Time series of absolute current speed; c) Time series of current direction.

Scatter plots of the current vectors for both 10 minute data and the low-pass filtered data are plotted in Fig. 4.28. Derived from these scatter plots are the mean current vectors and ellipse for the principal current. Table 4.20 shows the principal axes for both the processed data and the low-passed currents for currents recorded in bin 1 (1.6 m above the bed), and bin 9 (3.6 mab).

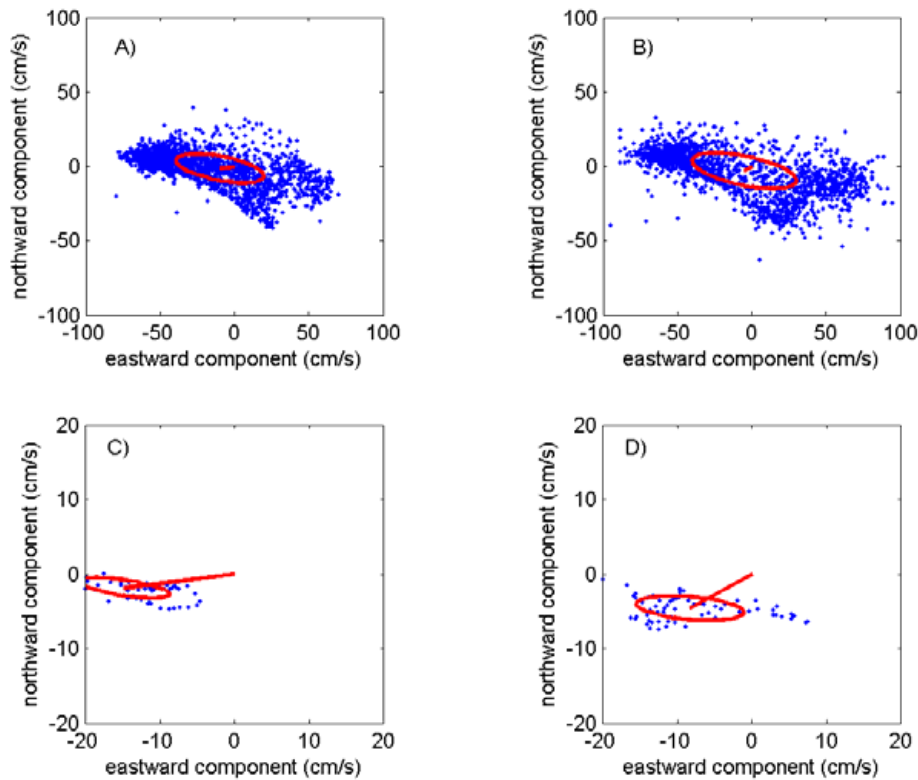


Fig. 4.28. 02CM07 scatter plots with the mean current vector (origin zero), and the ellipse of the principal axes of currents superimposed. The ellipse is centred upon the mean current vector: A) displays scatter plots of the basic 10-min processed current data from bin 1 (1.6 mab); B) displays scatter plots of the basic 10-min processed current data from bin 9 (3.6 mab); C) displays scatter plots of the low-pass filtered current data from bin 1 (1.6 mab); D) displays scatter plots of the low-pass filtered current data from bin 9 (3.6 mab).

Table 4.20. Principal axes of currents at sea-bed and sea 'surface' at 02CM07. LP, indicates from Low Pass filtered record.

	Bin 1 (1.6 m)	Bin 9 (3.6 m) surface
Major ( $\text{cm s}^{-1}$ ) 10 min avg.	32.50	35.86
Minor ( $\text{cm s}^{-1}$ ) 10 min avg.	8.28	9.99
Orient. ( $^{\circ}\text{N}$ ) 10 min avg.	-79.02	-68.44
Ellip. 10 min avg.	0.7451	0.7213
Major ( $\text{cm s}^{-1}$ ) low pass	5.47	7.28
Minor ( $\text{cm s}^{-1}$ ) low pass	0.97	1.57
Orient ( $^{\circ}\text{N}$ ) 10 low pass	-169.82	-175.29
Ellip. low pass	0.8236	0.7845

Tidal ellipses are plotted for the four major constituents (M2, S2, K1, O1) in Fig. 4.29. Red indicates that the ellipses are travelled clockwise, dashed lines indicate surface (bin 9) ellipses. [Table 4.21](#) shows the tidal ellipse parameters for the four major tidal constituents.

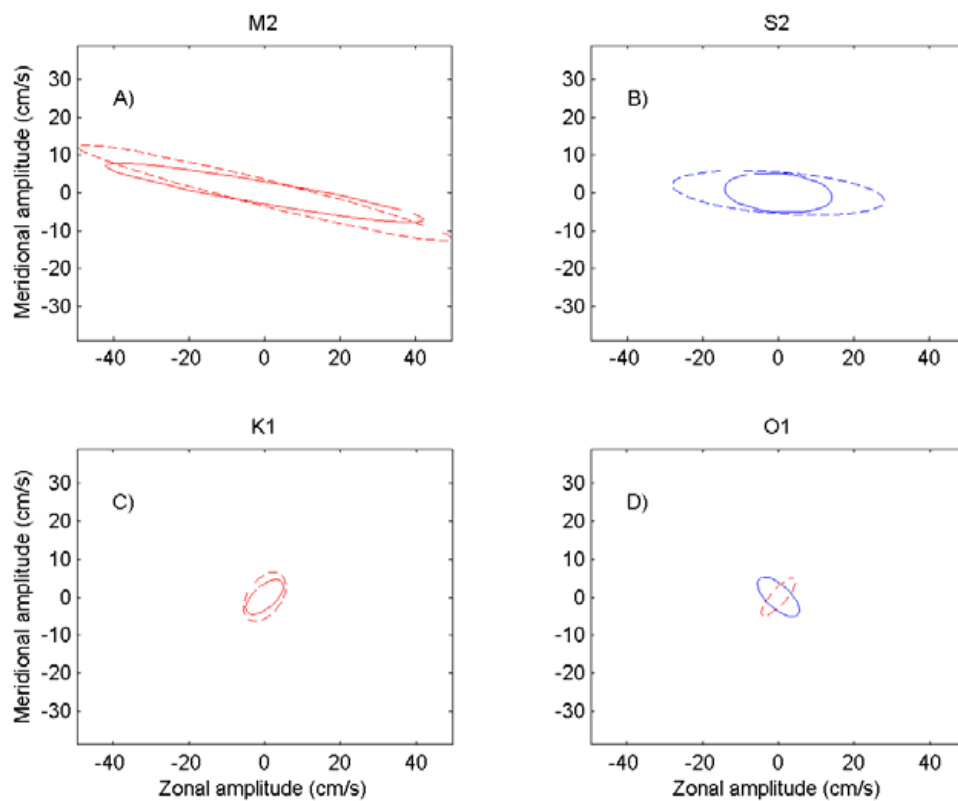


Fig. 4.29 02CM07 tidal ellipses plotted for the four major constituents: a) M2; b) S2; c) K1; and d) O1. Red indicates that the ellipses are travelled clockwise, blue indicates that the ellipses are travelled anti-clockwise. Dashed lines indicate 'surface' (bin 9, 3.6 mab) ellipses, solid lines indicate 'bed' ellipses (bin1, 1.6 mab)

Table 4.21. 02CM07. Tidal Ellipse parameters of bed and surface currents from Mooring 02CM07.

Bin	Constituent	Semi-major Axis (cm s)	Eccentricity	Inclination (degrees)	Phase (degrees)
1	M2	39.74	-0.0884	168.7	204.97
	S2	14.92	0.356	171.9	48.86
	K1	5.91	-0.5121	41.93	83.47
	O1	5.04	0.5579	116.59	346.90
9	M2	51.00	-0.0666	166.07	202.92
	S2	28.20	0.196	175.64	58.35
	K1	7.34	-0.61	54.31	86.07
	O1	6.36	-0.313	48.58	355.72

#### 4.4.5.3. Station 03CM02

Current meter data obtained from the Nortek Vector current meter deployed on Mooring 03CM02 is un-usable as a result of an erroneous nominal velocity having been defined. No data analysis has been carried out on the current meter data from this site.

#### 4.4.5.4. Station 04CM03

04CM03 was stationed on top of the sandbank in Area B. Progressive vector plots for each of the bed currents (Bin1 = 1.8 m), and at the top of the water column (Bin10 = 4.1 m), are shown in [Figs 4.30](#). The overall displacement for bins 1 and 9 were 86.0 km at  $-107.6^\circ$  and 86.2 km at  $-111.8^\circ$  indicating very similar displacements for each bin.

Statistics for each of the currents recorded by the ADCP at 04CM03 during the entire deployment are displayed in [Table 4.22](#). The average currents east and north for bins 1 ( $-6.17 \text{ cm s}^{-1}$  and  $-2.01 \text{ cm s}^{-1}$  respectively) and 10 ( $-6.41 \text{ cm s}^{-1}$  and  $-2.61 \text{ cm s}^{-1}$ ). The fastest currents measured were  $93.37 \text{ cm s}^{-1}$  at the bed and  $101.76 \text{ cm s}^{-1}$  at the surface.

Unlike 02CM07 the vector plots for 04CM03 show very little internal shear. This is demonstrated by the similar displacements of the current vectors through the deployment.

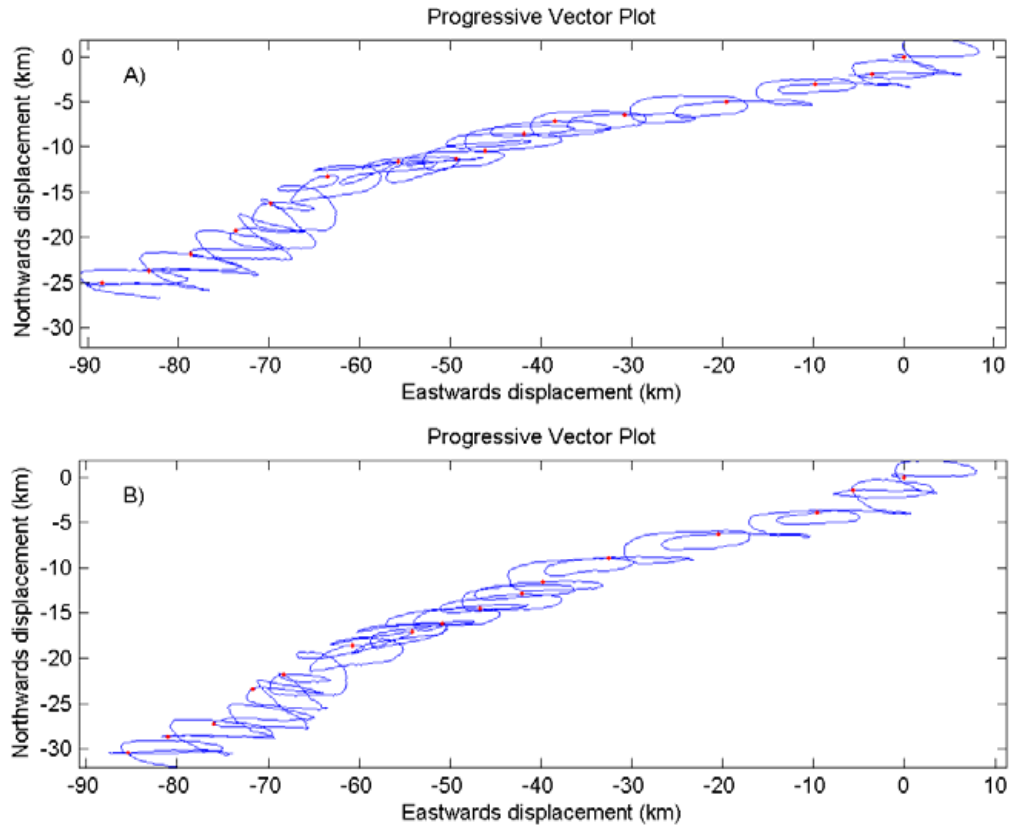


Fig. 4.30. 04CM03 current meter progressive vector plot obtained from data recorded in a) bin 10 (4.1 m above seabed), b) bin 1 (1.8 m above seabed). The origin of the plot corresponds to the location of the 04CM03 mooring. Dots indicate the beginning of each 24 hour period. Note that missing data does not contribute to calculated displacement.

Table 4.22 Current Meter Statistics

Bin	East min	East mean	East max	East Std Dev.	North min	North mean	North max	N Std Dev.	Speed min	Speed mean	Speed max
1	-93.30	-6.17	84.00	48.46	-43.30	-2.01	47.70	13.01	18.18	47.21	93.37
10	-98.80	-6.41	101.60	53.80	-50.50	-2.61	50.00	14.03	19.83	52.39	101.76

A time series of current meter data for the seabed and surface are shown in [Figs. 4.31](#) and [4.32](#), respectively. Missing data in [Figures 4.31](#) and [4.32](#) indicate times where data has been considered erroneous and removed from the ADCP record, though by comparison to the data recorded at 02CM07 and 06CM06 the data records for

04CM03 are relatively complete. Time series of low-pass filtered current meter data from bins 1 and 10 at 04CM03 are show in Fig. 4.33 and 4.34; respectively.

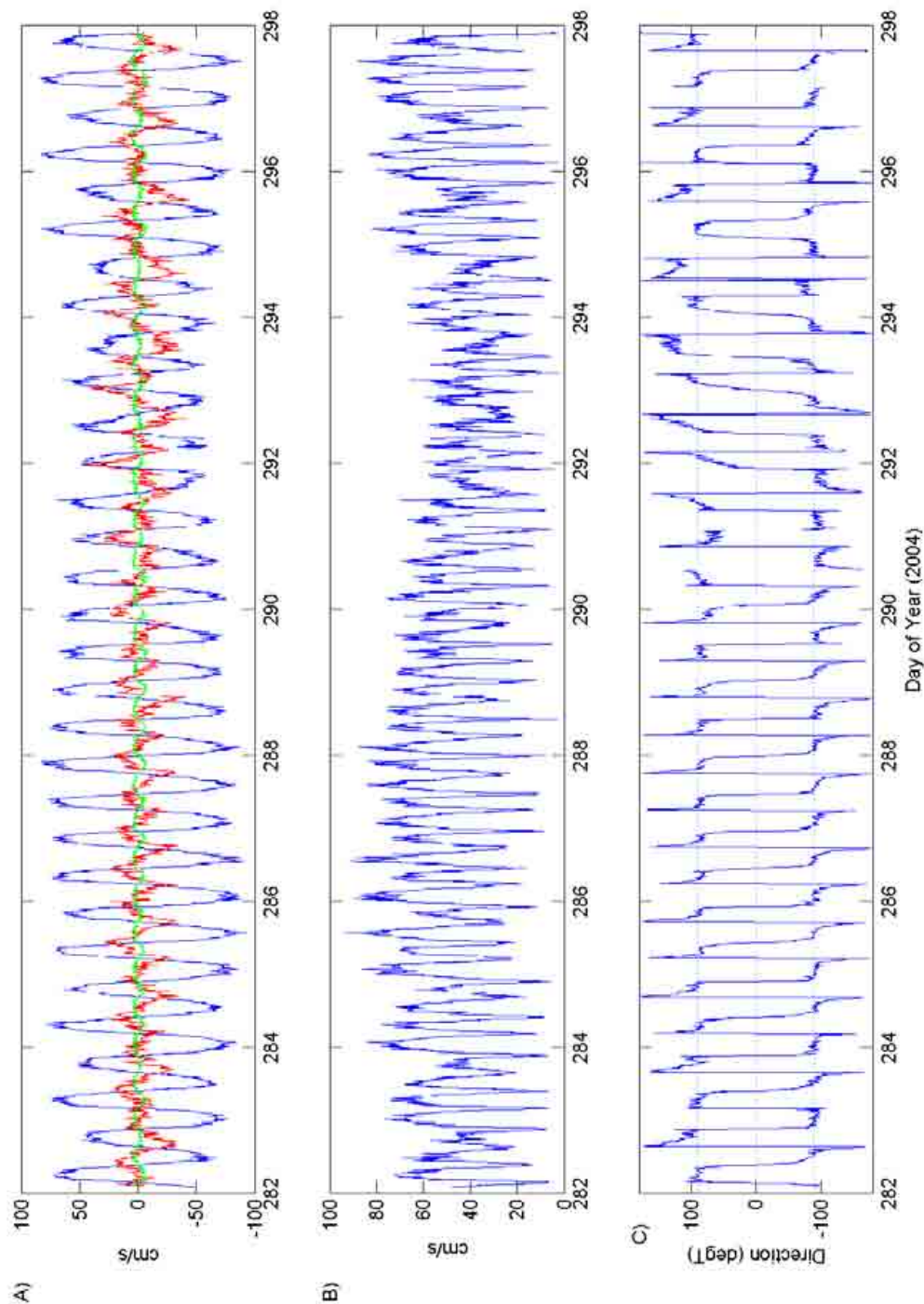


Fig. 4.31. 04CM03 current meter time-series obtained from data recorded in bin 1 (1.8 m above seabed). a) Time series of East (Blue), North (Red), and Up (Green) velocity components; b) Time series of absolute current speed; c) Time series of current direction.

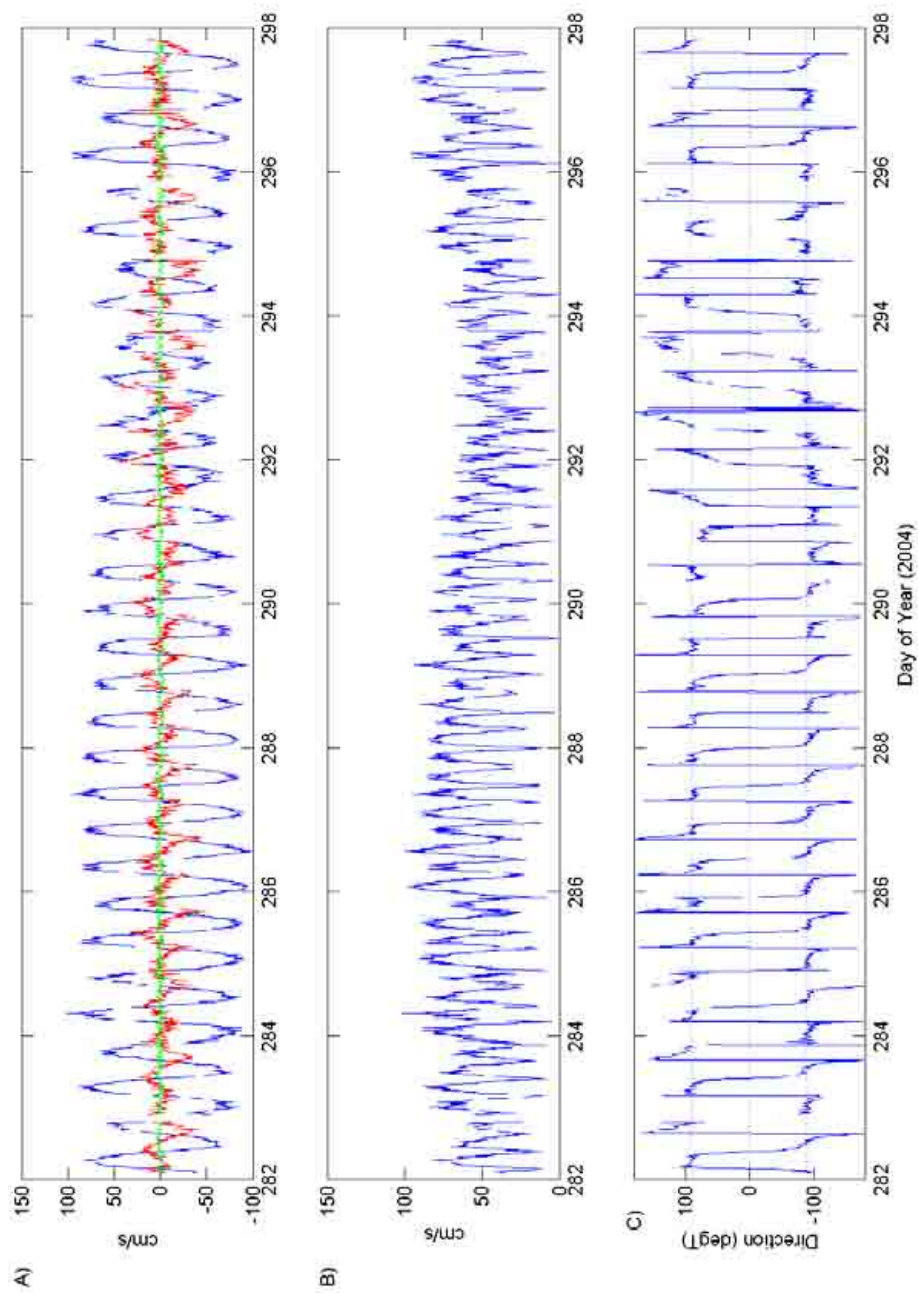


Fig. 4.32. 04CM03 current meter time-series obtained from data recorded in bin 10 (4.1 m above seabed). a) Time series of East (Blue), North (Red), and Up (Green) velocity components; b) Time series of absolute current speed; c) Time series of current direction.

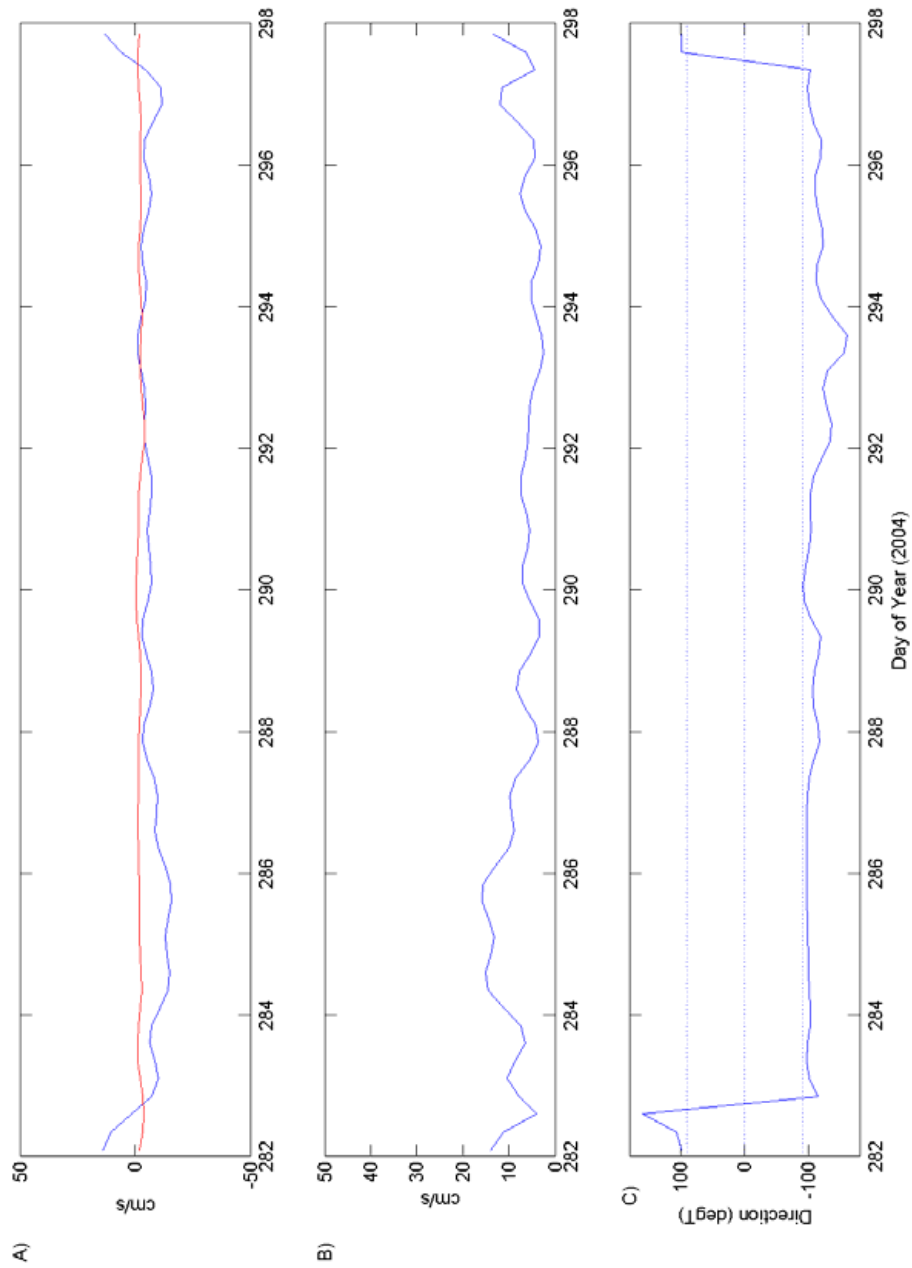


Fig. 4.33. 04CM03 Low-Pass Filtered current meter time-series obtained from data recorded in bin 1 (1.6 m above seabed). a) Time series of East (Blue), North (Red), and Up (Green) velocity components; b) Time series of absolute current speed; c) Time series of current direction.

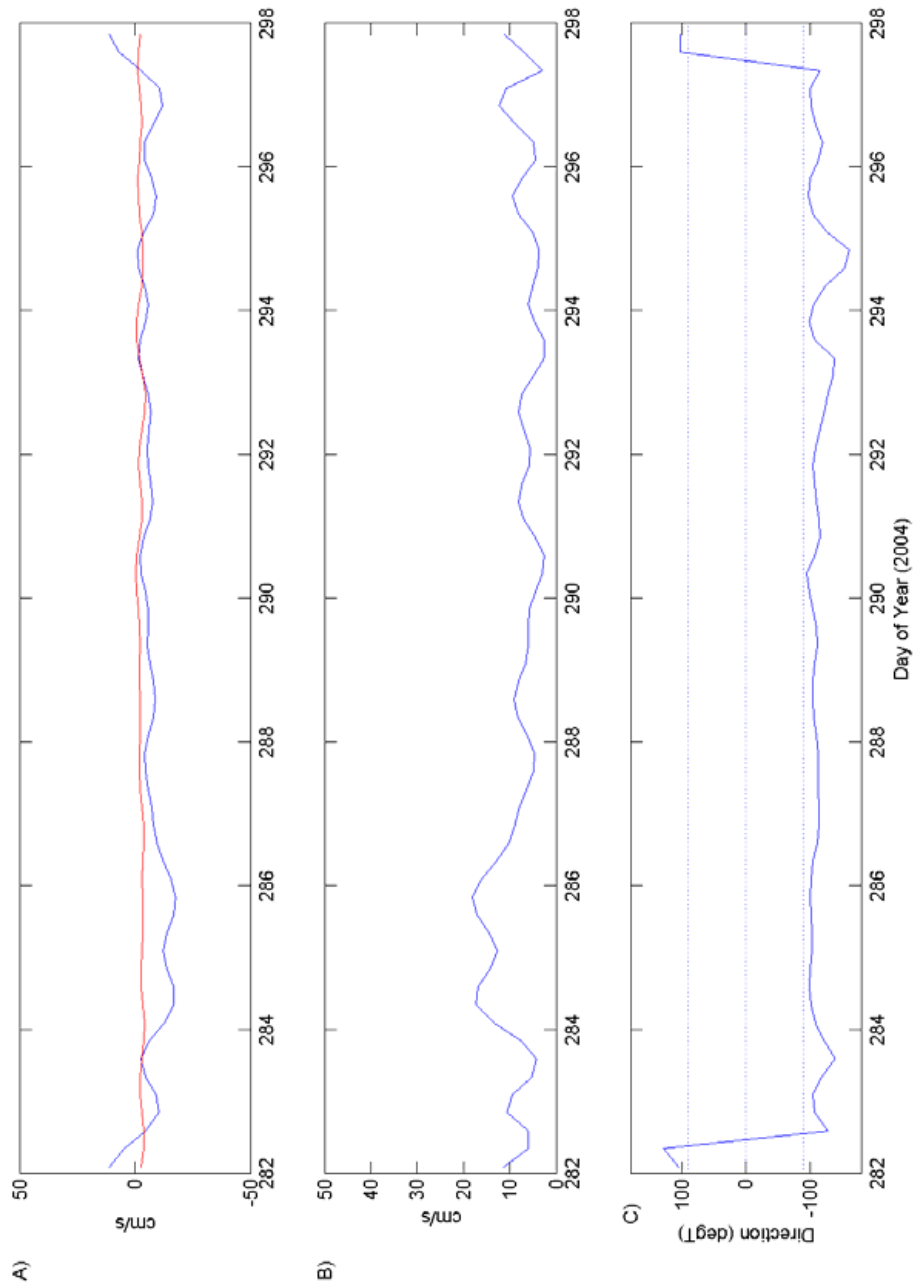


Fig. 4.34. 04CM03 Low-Pass Filtered current meter time-series obtained from data recorded in bin 9 (3.6 m above seabed). a) Time series of East (Blue), North (Red), and Up (Green) velocity components; b) Time series of absolute current speed; c) Time series of current direction.

Scatter plots of the current vectors for both 10 minute data and the low-pass filtered data are plotted in Fig. 4.35. Derived from these scatter plots are the mean current vectors and ellipse for the principal current. Table 4.23 shows the principal axes for both the processed data and the low-passed currents for currents recorded in bin 1 (1.8 m above the bed), and bin 10 (4.1 mab).

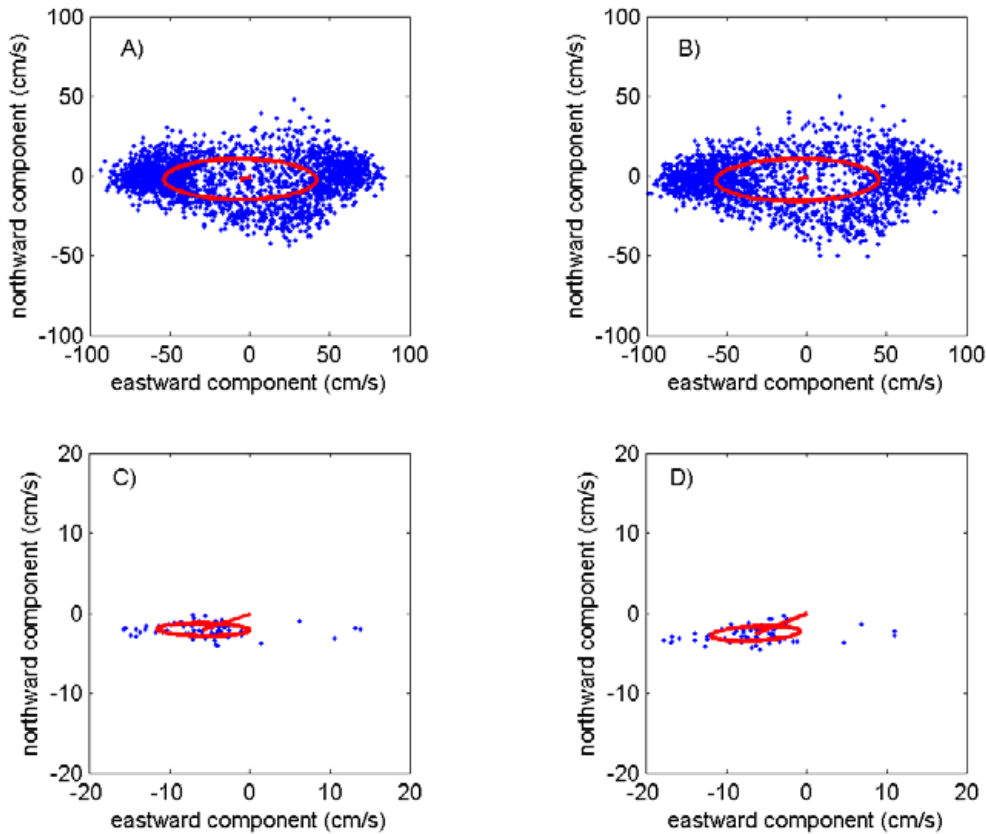


Fig. 4.35. 04CM03 scatter plots with the mean current vector (origin zero), and the ellipse of the principal axes of currents superimposed. The ellipse is centred upon the mean current vector: a) displays scatter plots of the basic 10-min processed current data from bin 1 (1.6 mab); b) displays scatter plots of the basic 10-min processed current data from bin 10 (4.1 mab); c) displays scatter plots of the low-pass filtered current data from bin 1 (1.6 mab); d) displays scatter plots of the low-pass filtered current data from bin 10 (4.1 mab).

Table 4.23. 04CM3. Principal axes of currents for currents at sea-bed and sea 'surface'. LP, indicates from Low Pass filtered record.

	Bin 1 (1.8 m)	Bin 10 (4.1 m) surface
Major ( $\text{cm s}^{-1}$ ) 10 min avg.	47.80	51.07
Minor ( $\text{cm s}^{-1}$ ) 10 min avg.	12.83	13.33
Orient. ( $^{\circ}\text{N}$ ) 10 min avg.	-89.75	-90.55
Ellip. 10 min avg.	0.7315	0.7391
Major ( $\text{cm s}^{-1}$ ) low pass	5.81	5.62
Minor ( $\text{cm s}^{-1}$ ) low pass	0.82	0.93
Orient ( $^{\circ}\text{N}$ ) 10 low pass	-89.34	-92.81
Ellip. low pass	0.8587	0.8342

Tidal ellipse parameters for the four major constituents (M2, S2, K1, O1) are listed in [Table 4.24](#) for the 04CM03 Mooring for each of the bed currents (bin 1), and from the 'surface' currents (bin 10). The ellipses are plotted for the four major constituents (M2, S2, K1, O1) in [Fig. 4.32](#). Red indicates that the ellipses travelled clockwise, dashed lines indicate surface (bin 10) ellipses. The major M2 component is largely rectilinear and aligned roughly parallel to the axis of the sand bank.

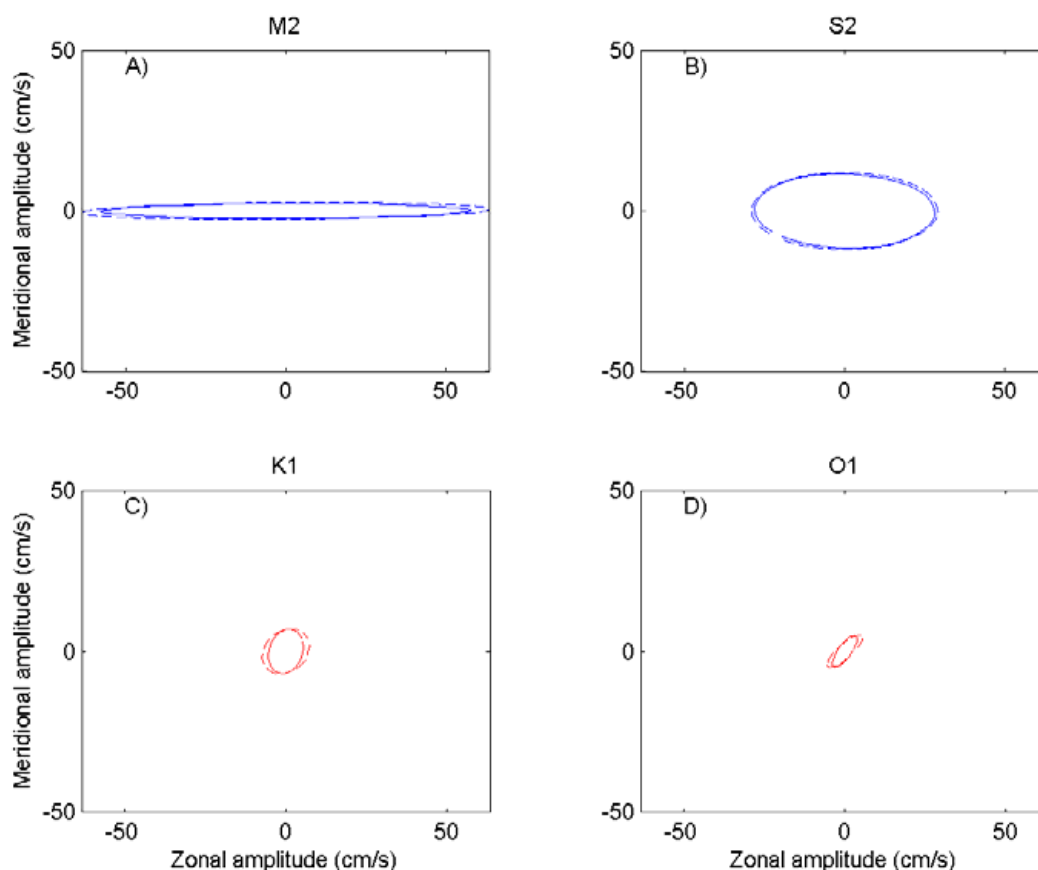


Fig. 4.36. 04CM03 tidal ellipses plotted for the four major constituents: a) M2; b) S2; c) K1; and d) O1. Red indicates that the ellipses are travelled clockwise, blue indicates that the ellipses are travelled anti-clockwise. Dashed lines indicate 'surface' (bin 10, 4.1 mab) ellipses, solid lines indicate 'bed' ellipses (bin 1, 1.6 mab)

Table 4.24. 04CM03. Tidal Ellipse parameters of bed and surface currents from Mooring 04CM03.

Bin	Constituent	Semi-major Axis (cm s <sup>-1</sup> )	Eccentricity	Inclination (degrees)	Phase (degrees)
1	M2	57.98	0.0392	0.1715	175.08
	S2	28.15	0.4116	178.96	313.10
	K1	7.01	-0.7447	70.41	310.63
	O1	5.93	0.3436	53.61	284.58
10	M2	63.64	0.0402	0.4545	173.80
	S2	29.16	0.4161	179.87	313.95
	K1	8.04	-0.7735	40.45	337.32
	O1	7.07	-0.3254	41.86	285.38

#### 4.4.5.5. Station 05CM04

Current meter data obtained from the ADCP deployed on Mooring 05CM04 is unusable as a result of the changing tilt of the current meter in the gimble. No data analysis has been carried out on the current meter data from this site.

#### 4.4.5.6. Station 06CM06

Progressive vector plots for each of the bed currents (Bin1 = 1.8 m), and at the top of the water column (Bin27 = 8.5 m), are shown in [Figs 4.37](#). The overall displacement for bins 1 and 9 were 17.5 km at  $-113.6^\circ$  and 118.0 km at  $-89.5^\circ$ . Statistics for each of the currents recorded by the ADCP at 06CM06 during the entire deployment are displayed in [Table 4.25](#). The average currents east and north for bins 1 ( $-0.16 \text{ cm s}^{-1}$  and  $-0.43 \text{ cm s}^{-1}$  respectively) and 10 ( $-10.15 \text{ cm s}^{-1}$  and  $-0.21 \text{ cm s}^{-1}$ ) are similar and do not identify the divergence between the currents at the two depths. Currents at the bed attain  $88.41 \text{ cm s}^{-1}$ . Currents at the surface attain  $134.21 \text{ cm s}^{-1}$ .

A time series of current meter data for the seabed and surface are shown in [Figs. 4.38](#) and [4.39](#), respectively. The missing data in [Figs. 4.38](#) and [4.39](#) indicate times where data has been considered erroneous and removed from the ADCP record and there is a strong contrast in the levels of bad data between the two bins. [Fig. 4.38](#) shows a near complete record for bin 1 whilst [Fig. 4.39](#) shows a record with significant data gaps especially at times of peak currents. It is concluded that the progressive vector diagram for the sea surface current ([Fig. 4.37a](#)) is misleading (though the raw statistics in [Table 4.25](#) are probably still accurate). The seabed current ([Fig. 4.37b](#)) comes from a near complete data record. Time series of low-pass filtered current meter data from bins 1 and 10 at 04CM03 are shown in [Fig. 4.40](#) and [4.41](#), respectively.

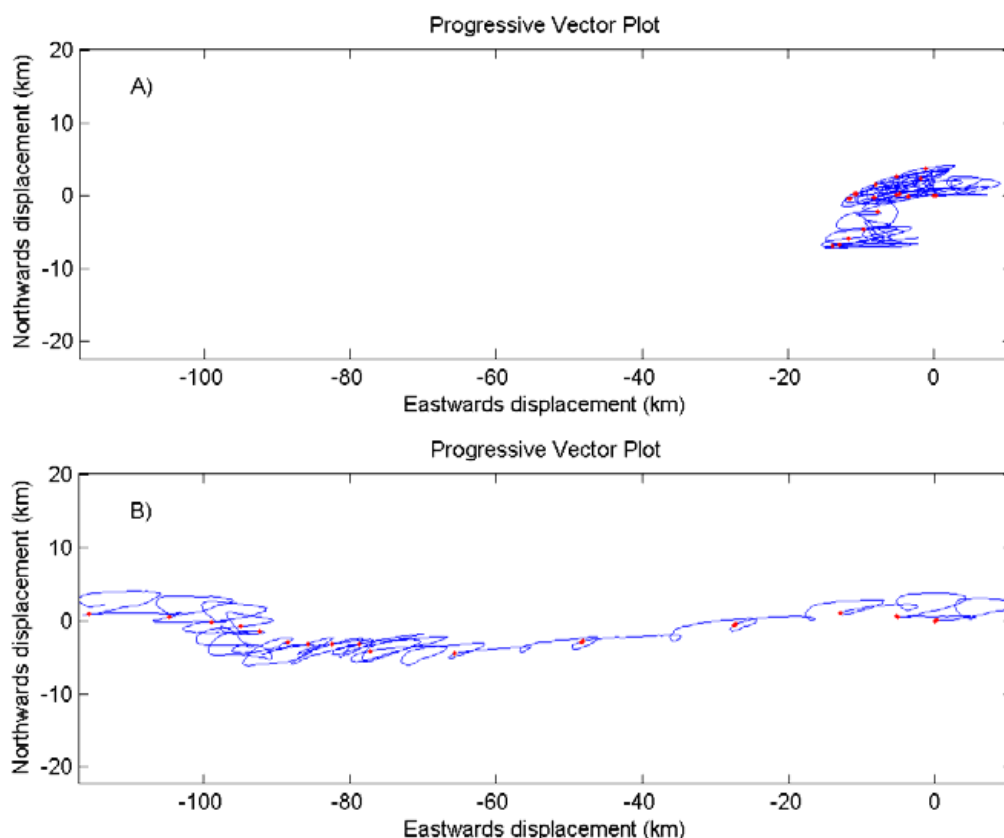


Fig. 4.37. 06CM06 current meter progressive vector plot obtained from data recorded in: a) bin 27 (8.5 m above seabed); b) bin 1 (1.8 m above seabed). The origin of the plot corresponds to the location of the 06CM06 mooring. Dots indicate the beginning of each 24 hour period. Note that missing data does not contribute to calculated displacement.

Table 4.25. Raw current meter statistics for 06CM06 at the bed (Bin 1: 1.6 m above seabed) and 'surface' below lowest tide (Bin 27: 8.52m above bed) All statistics are in  $\text{cm s}^{-1}$ .

Bin	East min	East mean	East max	East Std Dev.	North min	North mean	North max	North Std Dev.	Speed min	Speed mean	Speed max
1	-74.60	-0.16	85.50	42.02	-27.90	-0.43	31.70	11.57	18.01	39.68	88.41
27	-101.30	-10.15	110.00	49.77	-35.30	0.21	76.90	14.86	20.44	48.80	134.21

A time series of current meter data for the seabed and surface are shown in Figs. 4.38 and 4.39 respectively. Missing data in Figures 4.38 and 4.39 indicate times where data has been considered erroneous and removed from the ADCP record. Time series of low-pass filtered current meter data from bins 1 and 27 at 06CM06 are shown in Fig. 4.40 and 4.41; respectively.

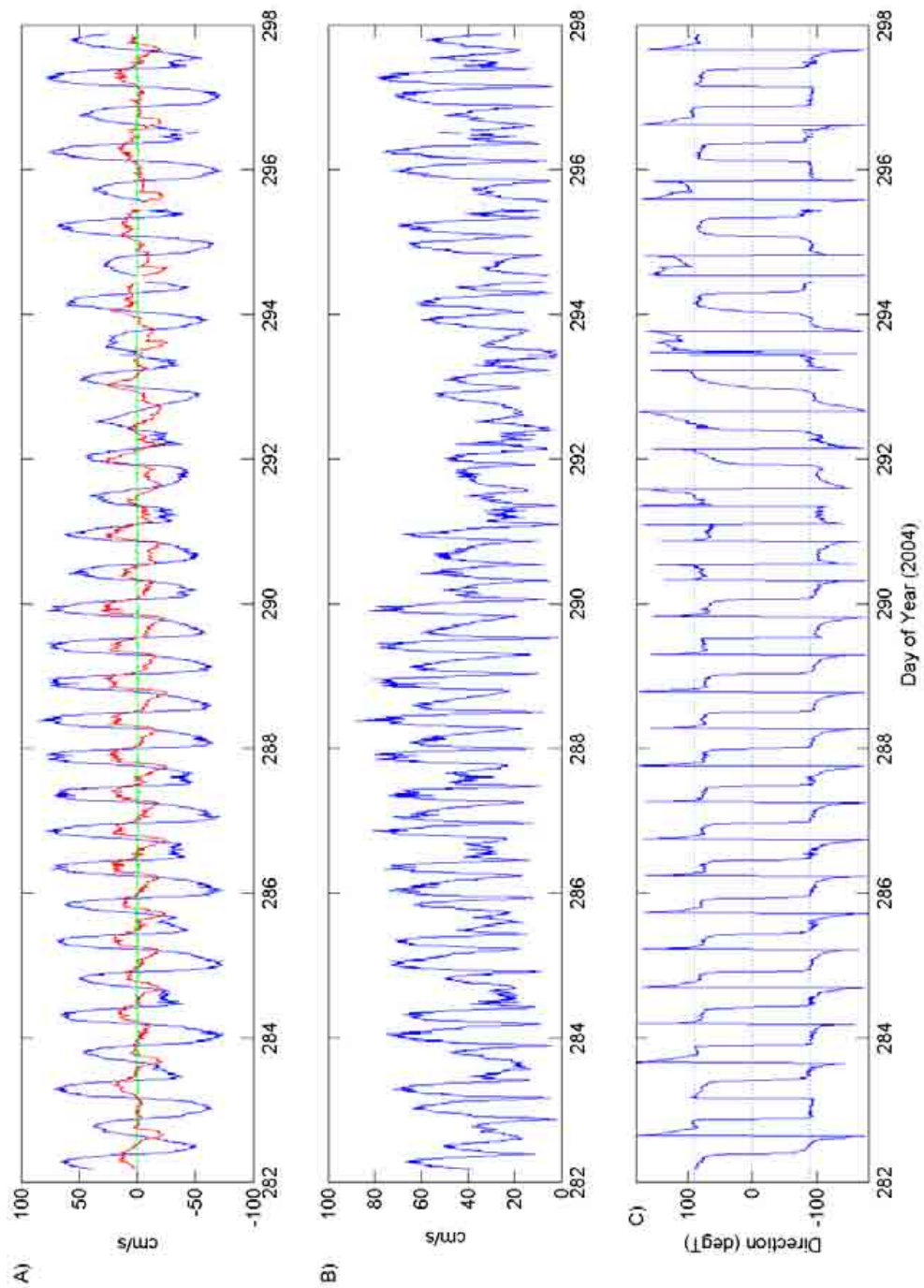


Fig. 4.38. 06CM06 current meter time-series obtained from data recorded in bin 1 (1.8 m above seabed). a) Time series of East (Blue), North (Red), and Up (Green) velocity components; b) Time series of absolute current speed; c) Time series of current direction.

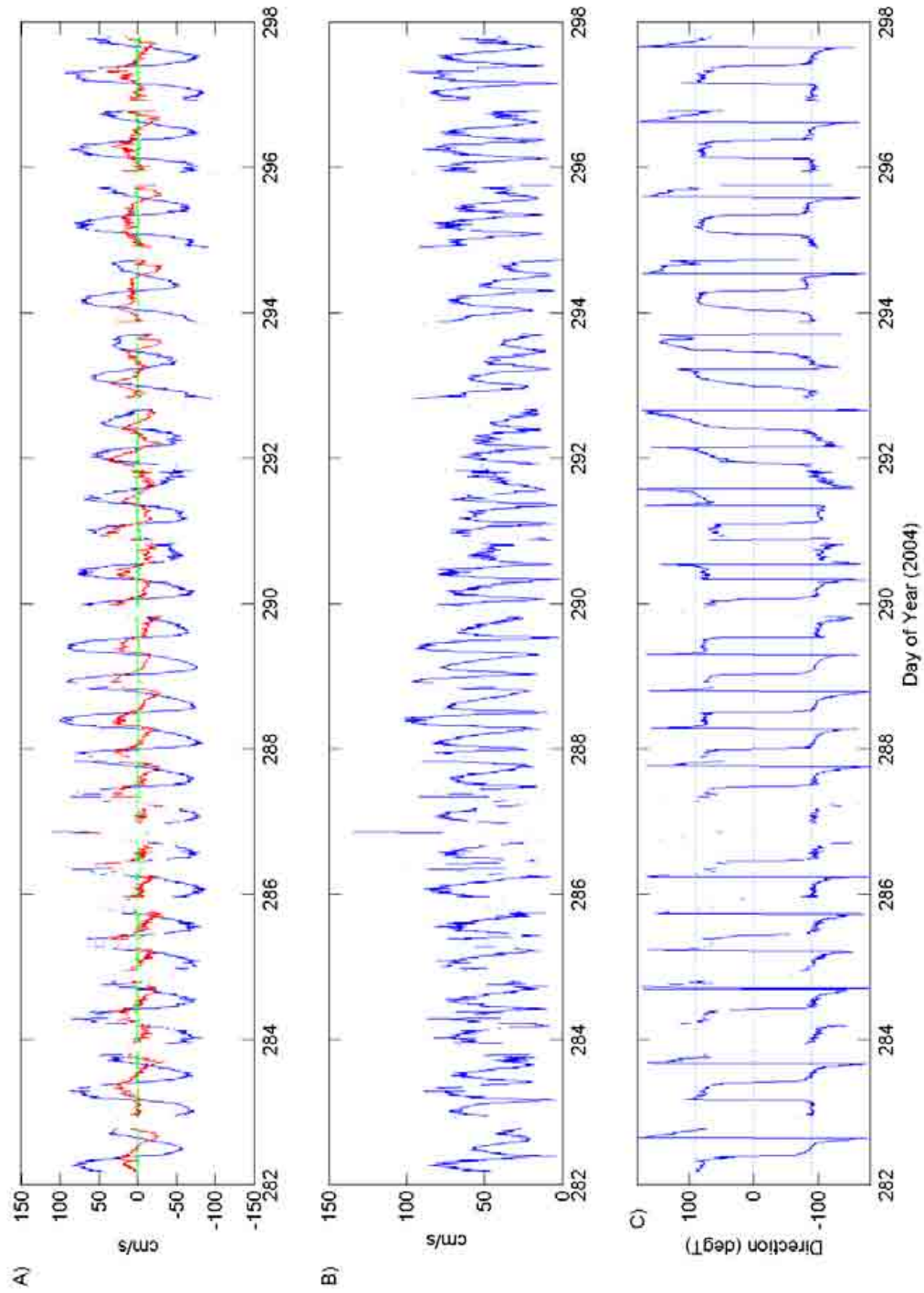


Fig. 4.39. 06CM06 current meter time-series obtained from data recorded in bin 27 (8.5 m above seabed). a) Time series of East (Blue), North (Red), and Up (Green) velocity components; b) Time series of absolute current speed; c) Time series of current direction.

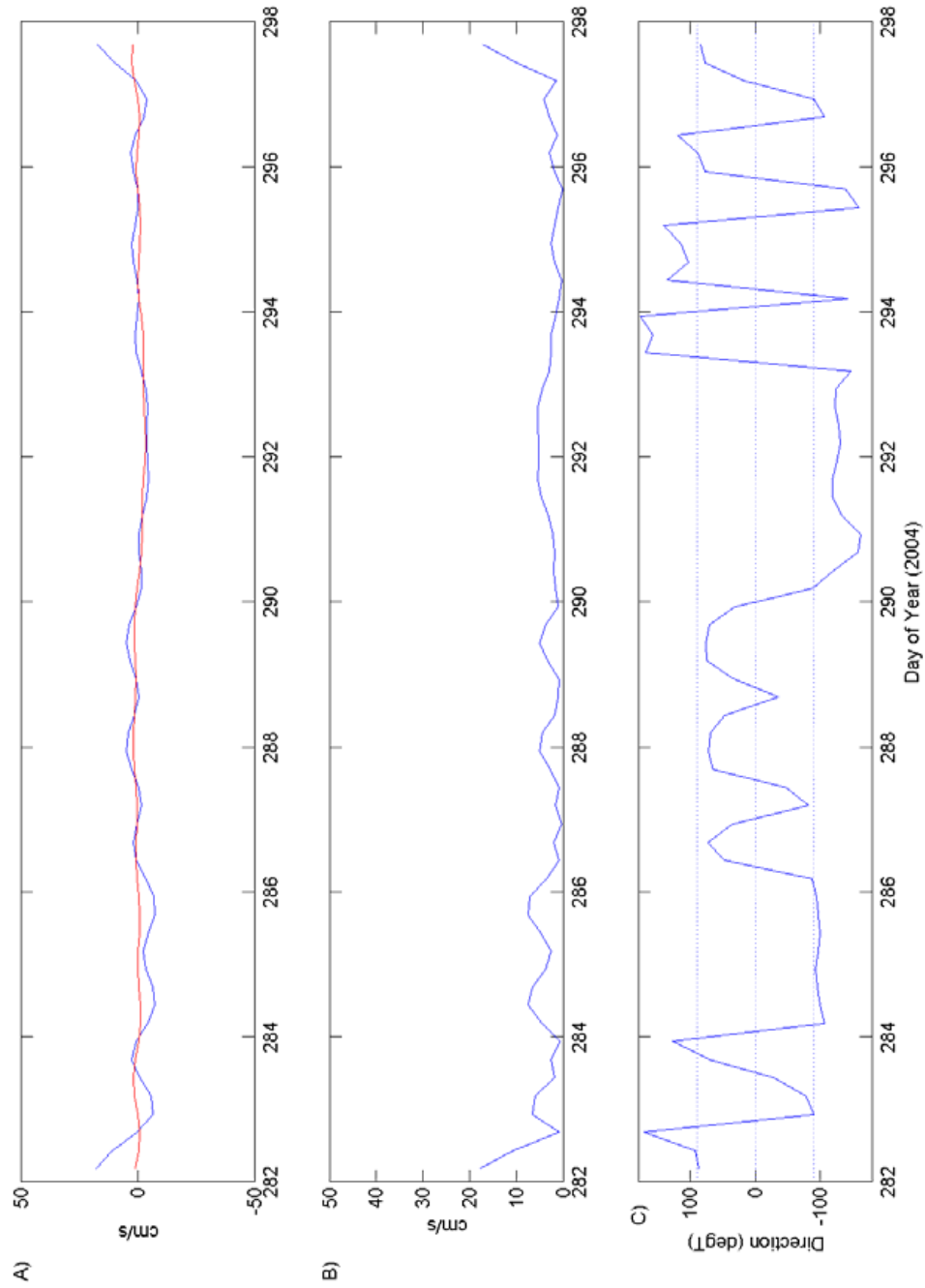


Fig. 4.40. 06CM06 Low-Pass Filtered current meter time-series obtained from data recorded in bin 1 (1.6 m above seabed). a) Time series of East (Blue), North (Red), and Up (Green) velocity components; b) Time series of absolute current speed; c) Time series of current direction.

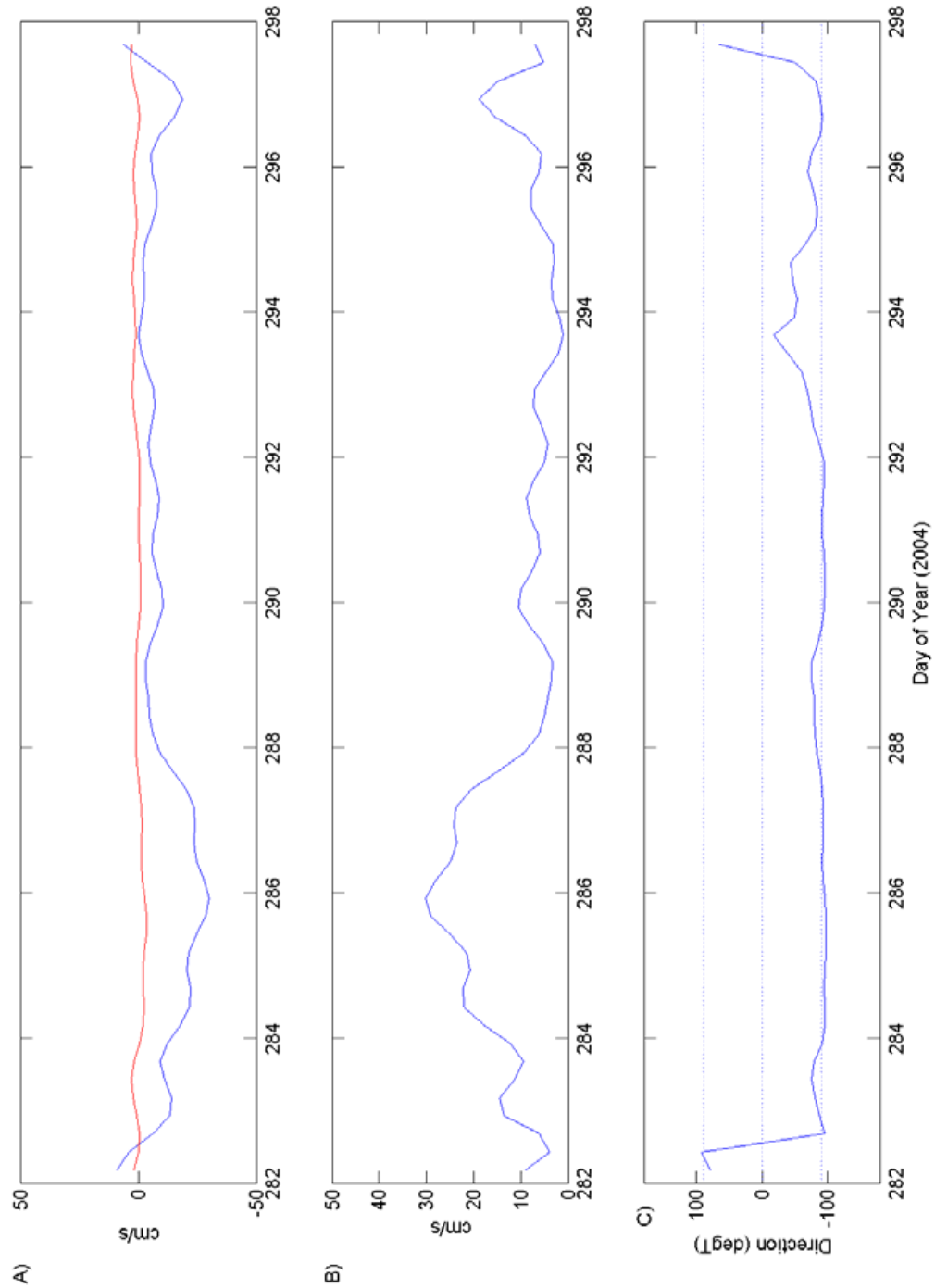


Fig. 4.41. 06CM06 Low-Pass Filtered current meter time-series obtained from data recorded in bin 27 (8.5 m above seabed). a) Time series of East (Blue), North (Red), and Up (Green) velocity components; b) Time series of absolute current speed; c) Time series of current direction.

Scatter plots of the current vectors for both 10 minute data and the low-pass filtered data are plotted in Fig. 4.42. Derived from these scatter plots are the mean current vectors and ellipse for the principal current. Table 4.26 shows the principal axes for both the processed data and the low-passed currents for currents recorded in bin 1 (1.6 m above the bed), and bin 27 (8.5 mab).

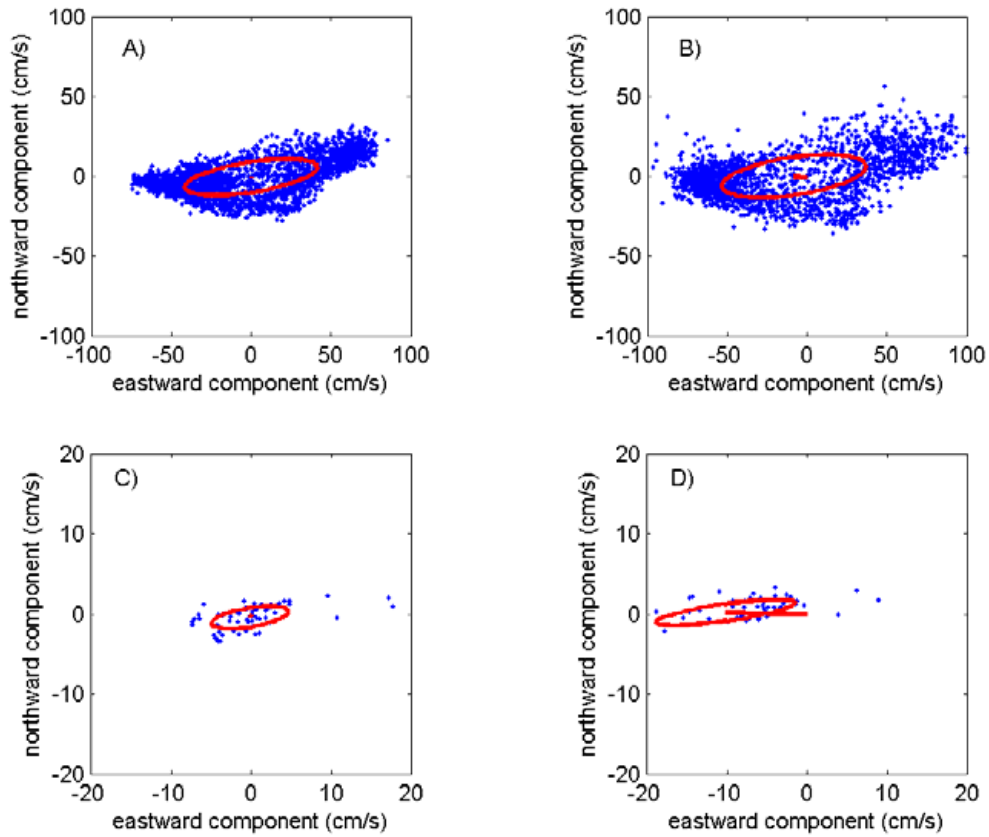


Fig. 4.42. 06CM06 scatter plots with the mean current vector (origin zero), and the ellipse of the principal axes of currents superimposed. The ellipse is centred upon the mean current vector: a) displays scatter plots of the basic 10-min processed current data from bin 1 (1.6 mab); b) displays scatter plots of the basic 10-min processed current data from bin 27 (8.5 mab); c) displays scatter plots of the low-pass filtered current data from bin 1 (1.6 mab); d) displays scatter plots of the low-pass filtered current data from bin 27 (8.5 mab).

Table 4.26. 06CM06. Principal axes of currents for currents at sea-bed and sea 'surface'. LP, indicates from Low Pass filtered record.

	Bin 1 (1.6 m)	Bin 27 (8.5 m) surface
Major ( $\text{cm s}^{-1}$ ) 10 min avg.	42.15	45.78
Minor ( $\text{cm s}^{-1}$ ) 10 min avg.	9.59	11.92
Orient. ( $^{\circ}\text{N}$ ) 10 min avg.	-98.83	-98.19
Ellip. 10 min avg.	0.7724	0.7395
Major ( $\text{cm s}^{-1}$ ) low pass	4.90	8.83
Minor ( $\text{cm s}^{-1}$ ) low pass	1.22	1.08
Orient ( $^{\circ}\text{N}$ ) 10 low pass	-99.20	-98.02
Ellip. low pass	0.7508	0.8773

Tidal ellipse parameters for the four major constituents (M2, S2, K1, O1) are listed in [Table 4.27](#) for the 06CM06 Mooring for each of the bed currents (bin 1), and from the 'surface' currents (bin 10). The ellipses are plotted for the four major constituents (M2, S2, K1, O1) in [Fig. 4.39](#). Red indicates that the ellipses clockwise, dashed lines indicate surface (bin 27) ellipses. The major axis of the M2 constituent is oriented at a similar direction to the sandbank in Area B (similar to 04CM03).

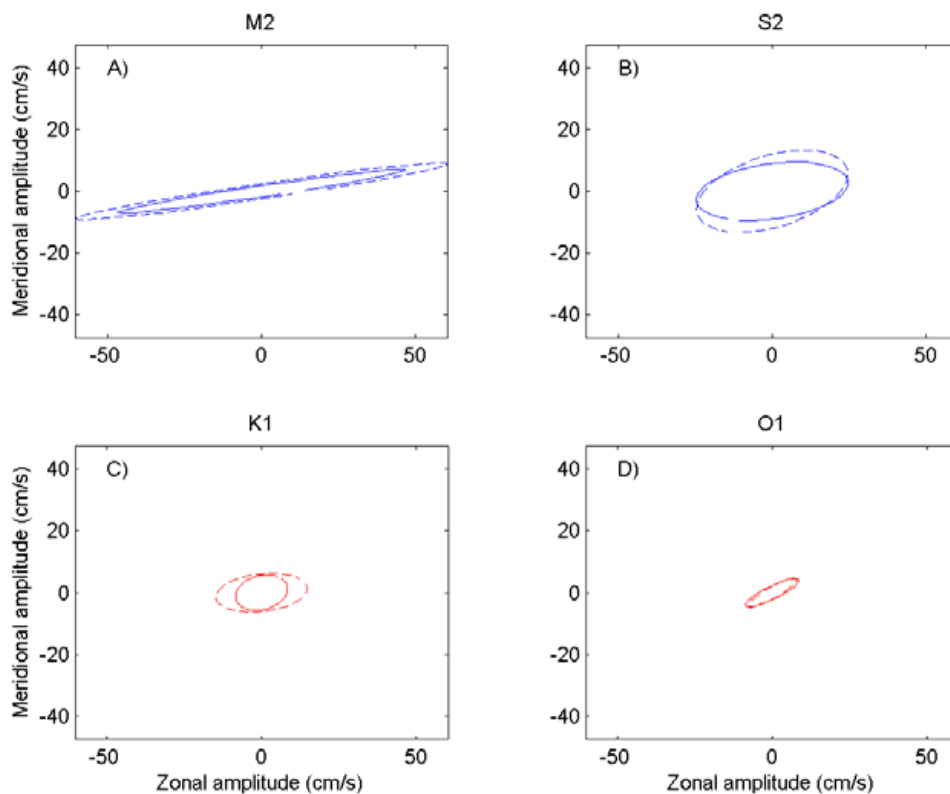


Fig. 4.43. 06CM06 tidal ellipses plotted for the four major constituents: a) M2; b) S2; c) K1; and d) O1. Red indicates that the ellipses are clockwise, blue indicates that the ellipses are anti-clockwise. Dashed lines indicate 'surface' (bin 27, 8.5 mab) ellipses, solid lines indicate 'bed' ellipses (bin1, 1.6 mab)

Table 4.27. Tidal Ellipse parameters of bed and surface currents from Mooring 06CM06.

Bin	Constituent	Semi-major Axis (cm s <sup>-1</sup> )	Eccentricity	Inclination (degrees)	Phase (degrees)
1	M2	47.23	0.0369	8.51	72.65
	S2	24.82	0.3639	7.38	118.52
	K1	8.55	-0.6536	13.92	32.16
	O1	9.63	-0.2136	25.72	171.63
10	M2	60.97	0.0294	8.43	70.85
	S2	25.40	0.4596	16.81	123.88
	K1	14.84	-0.4102	6.81	20.47
	O1	8.99	-0.2116	29.52	165.56

#### 4.4.5.7. Station 07CM05

A progressive vector plot for the currents recorded by the FSI current meter is shown in Fig 4.44. The overall displacement for the deployment was 140.5 km at -130.9°. Statistics for each of the currents recorded by the FSI at 07CM05 during the entire deployment are displayed in Table 4.28. The average currents east and north 1 were -8.17 cm s<sup>-1</sup> and -7.33 cm s<sup>-1</sup> respectively. The fastest current measured at the bed was 70.99 cm s<sup>-1</sup>.

Displacement is not constant over the course of the deployment because of the transition from spring to neap to spring tides. Neap tides occur near the middle of the deployment. The wind direction is consistently from the southeast over the duration of the survey. The wind speeds range from 4 – 10 m s<sup>-1</sup> (Figs. 3.3 and 3.4), with peak wind speeds occurring during JD 285-286 and 298-300 (i.e., near the start and end of the deployment).

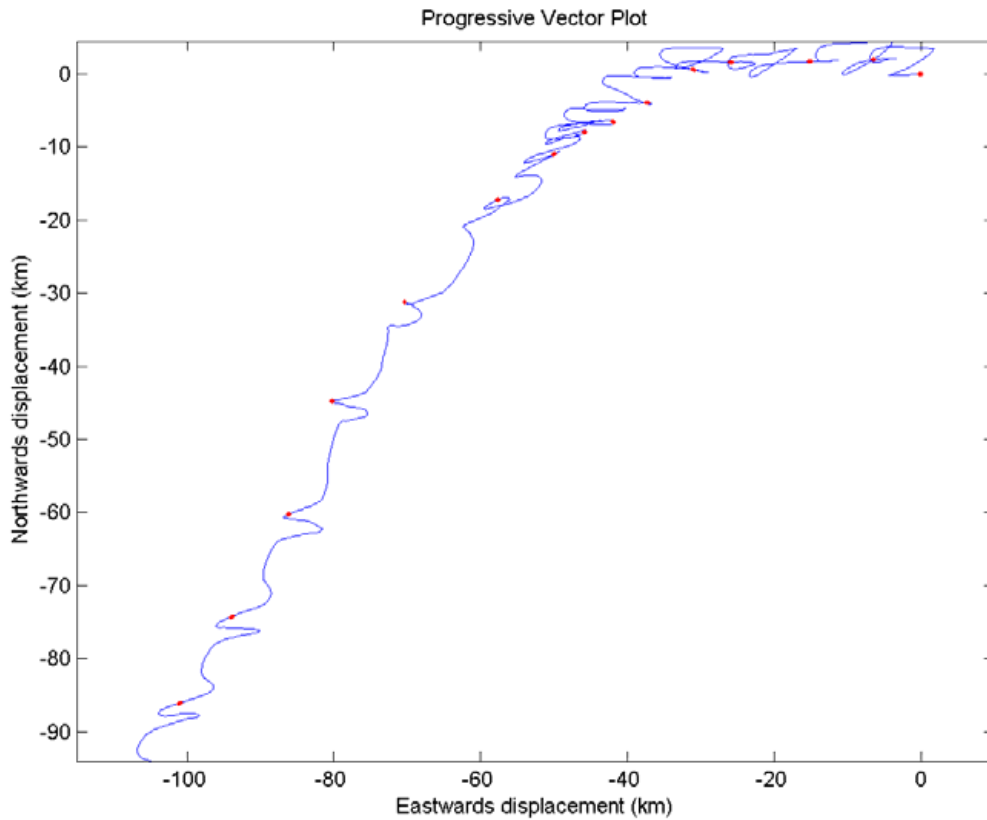


Fig. 4.44. 07CM05 current meter progressive vector plot obtained from the FSI current meter data. The origin of the plot corresponds to the location of the 07CM05 mooring. Dots indicate the beginning of each 24 hour period. Note that missing data does not contribute to calculated displacement.

Table 4.28. Raw current meter statistics for 07CM05. All statistics are in  $\text{cm s}^{-1}$

depth	East min	East mean	East max	East Std Dev.	North min	North mean	North max	N Std Dev.	Speed min	Speed mean	Speed max
	-66.18	-8.17	62.04	30.35	-57.69	-7.33	36.41	13.66	12.70	32.65	70.99

A time series of current meter data for the seabed is shown in [Fig. 4.45](#). Missing data in [Fig. 4.45](#) indicate times where data has been considered erroneous and removed from the currentmeter. Time series of low-pass filtered current meter data for the seabed at 07CM05 is shown in [Fig. 4.46](#).

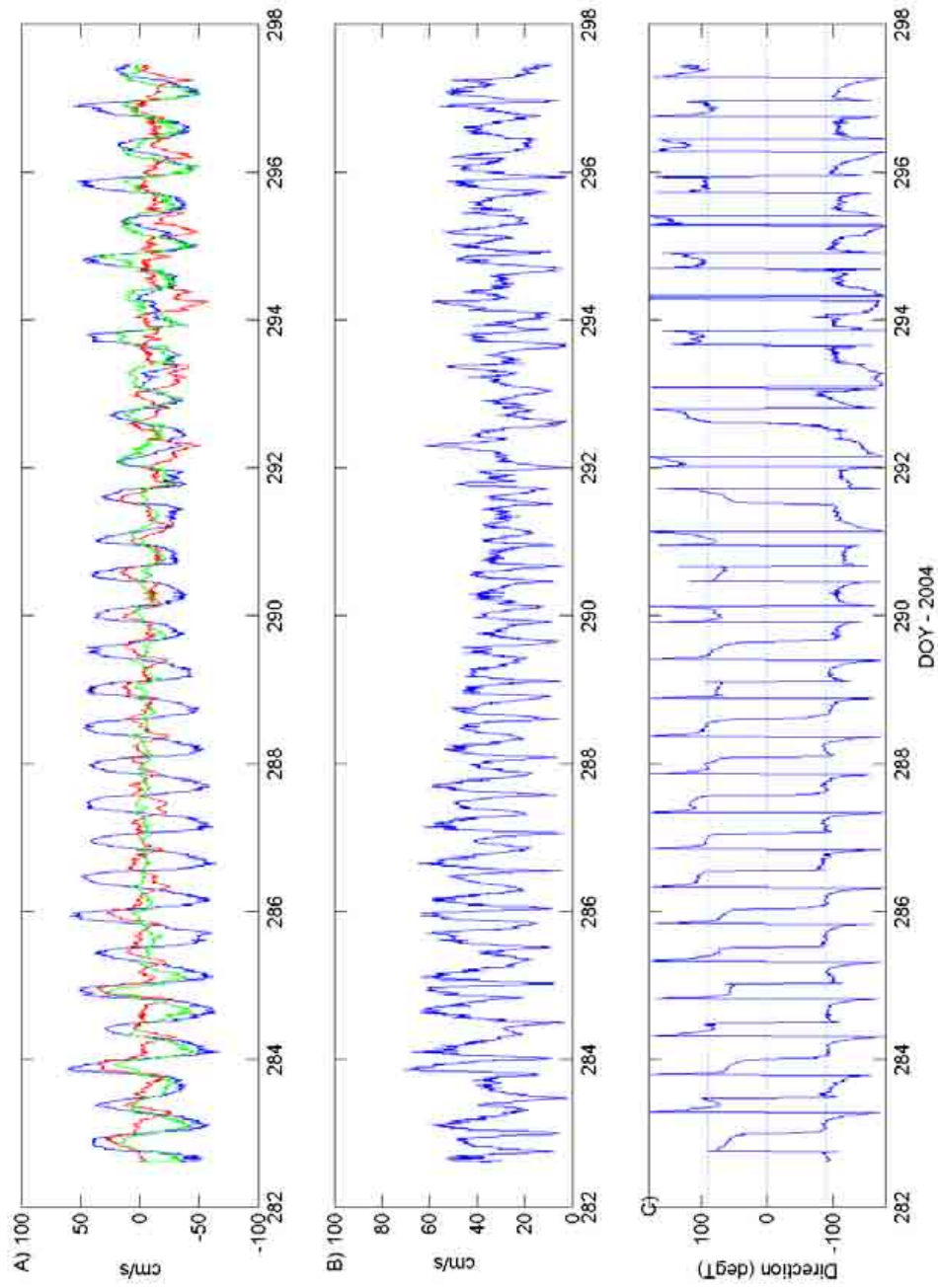


Fig. 4.45. 07CM05 current meter time-series: a) Time series of East (Blue), North (Red), and Up (Green) velocity components; b) Time series of absolute current speed; c) Time series of current direction.

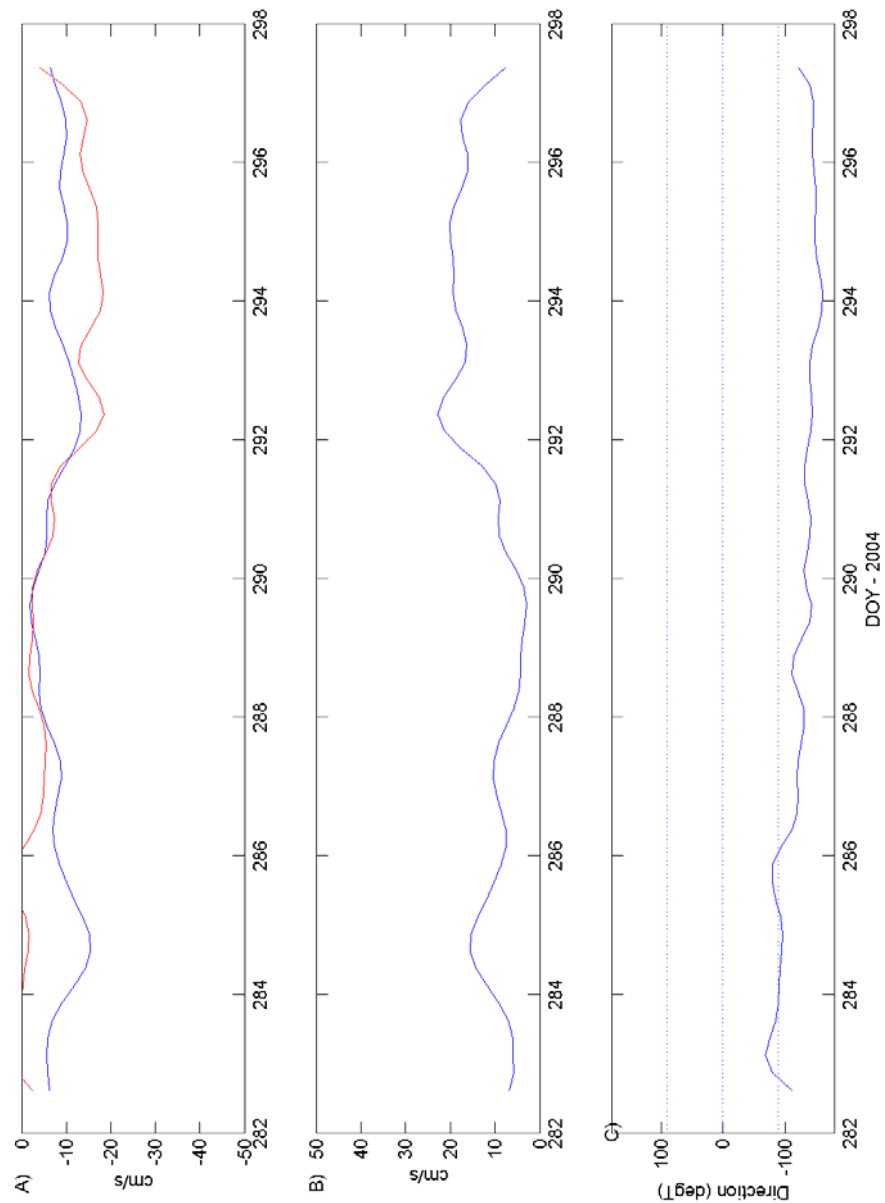


Fig. 4.46. 07CM05 Low-Pass Filtered current meter time-series. a) Time series of East (Blue), North (Red), and Up (Green) velocity components; b) Time series of absolute current speed; c) Time series of current direction.

Scatter plots of the current vectors for both 10 minute data and the low-pass filtered data are plotted in Fig. 4.47. Derived from these scatter plots are the mean current vectors and ellipse for the principal current. Table 4.29 shows the principal axes for both the processed data and the low-passed currents.

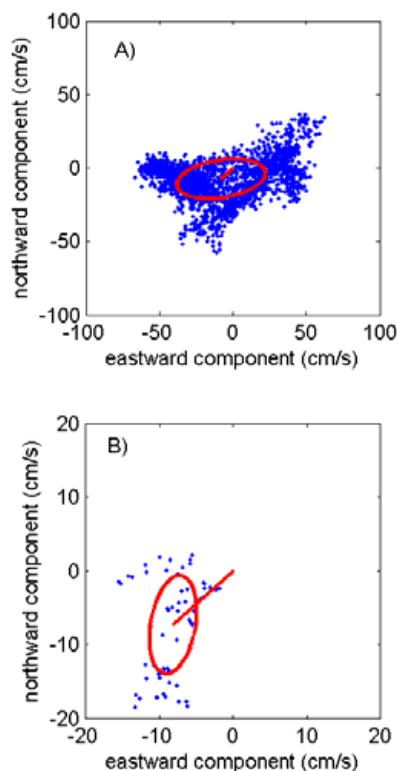


Fig. 4.47. 07CM05 scatter plots with the mean current vector (origin zero), and the ellipse of the principal axes of currents superimposed. The ellipse is centred upon the mean current vector: a) displays scatter plots of the basic 10-min processed current data; b) displays scatter plots of the low-pass filtered current data.

Table 4.29. Principal axes of currents for 07CM05.

	cm s <sup>-1</sup>
Major (cm s <sup>-1</sup> ) 10 min avg.	30.65
Minor (cm s <sup>-1</sup> ) 10 min avg.	12.97
Orient. (°N) 10 min avg.	-98.86
Ellip. 10 min avg.	0.5769
Major (cm s <sup>-1</sup> ) low pass	6.78
Minor (cm s <sup>-1</sup> ) low pass	3.08
Orient (°N) 10 low pass	9.72
Ellip. low pass	0.55

Tidal ellipse parameters for the four major constituents (M2, S2, K1, O1) are listed in Table 4.30 for the 07CM05 Mooring. The ellipses are plotted for the four major constituents (M2, S2, K1, O1) in Fig. 4.48. Red indicates that the ellipses are travelled clockwise. Similar to 04CM03 and 06CM06 the M2 constituent is aligned roughly parallel to the axis of the sandbank in Area B.

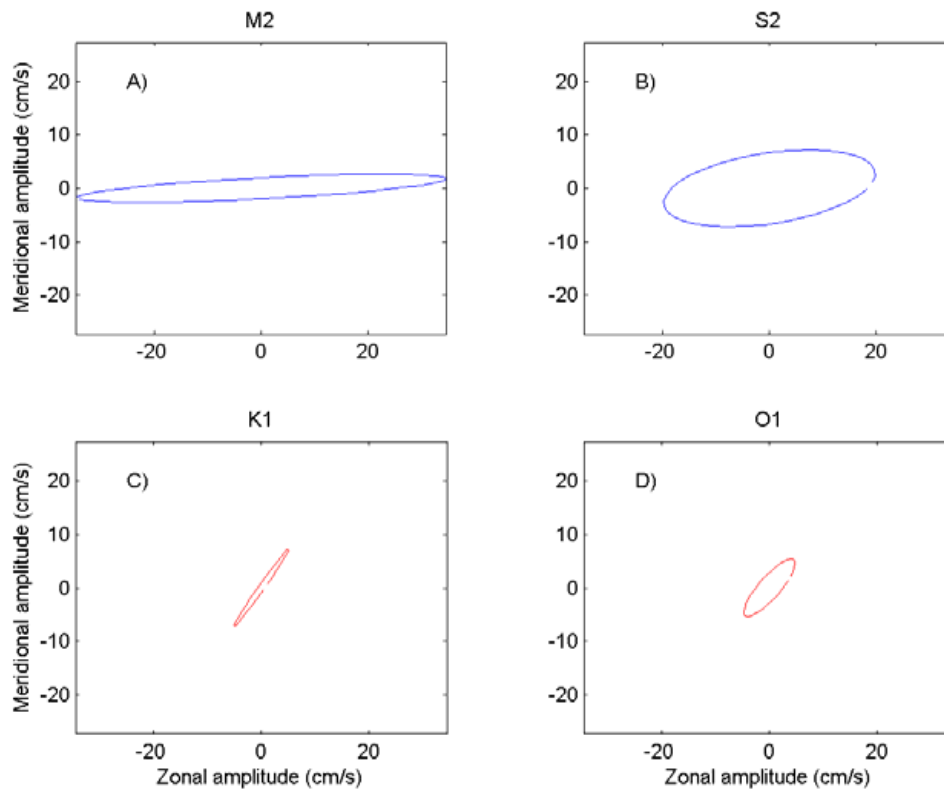


Fig. 4.48. 07CM05 tidal ellipses plotted for the four major constituents: a) M2; b) S2; c) K1; and d) O1. Red indicates that the ellipses are travelled clockwise, blue indicates that the ellipses are travelled anti-clockwise.

Table 4.30. Tidal Ellipse parameters of bed and surface currents from Mooring 07CM05.

Bin	Constituent	Semi-major Axis (cm s <sup>-1</sup> )	Eccentricity	Inclination (degrees)	Phase (degrees)
1	M2	34.57	0.0567	2.98	170.13
	S2	19.99	0.3302	9.89	16.20
	K1	8.78	-0.0602	54.77	269.35
	O1	6.88	-0.2842	48.83	298.15

#### 4.4.5.8 Review of Current Analysis

Tidal current speeds measured at the seabed and at the surface were generally slightly greater in Area B than Area A over the deployment period. The principal axes of currents in Area B (06CM06, [table 4.26](#)) indicate a major axis length of 42.15 (45.78)  $\text{cm s}^{-1}$  in the near-bed (near-surface) layer. In Area A (02CM07, [table 4.20](#)), the major axis length is 32.50 (35.86)  $\text{cm s}^{-1}$ . These magnitudes reflect the magnitude of the tidal currents. Residual currents however, are slightly greater in Area A.

For Area A (02CM07), time-series from the 10 minute averaged data indicate that both near bed and near surface, strongest currents occur around Julian Days 286 and 298 corresponding to periods of turbidity maxima. These periods of maximum currents do not correspond in time with spring tide in terms of sea-levels, demonstrating the complexity of the Torres Strait tides.

In Area B (06CM06), time-series from the 10-minute averaged data indicate that both near bed and near surface, strongest currents occur around Julian Days 286 and 298. Again these correspond with periods of turbidity maxima. It is worth noting however, that maximum wave heights were also achieved during these same periods, indicating a relationship between spring tidal currents, wind speeds, and consequently wave heights and turbidity.

The principal axes analysis of 02CM07 indicates that in Area A, surface currents are approximately 10% larger than near bed currents. Regardless, the currents are well aligned, with the major axis oriented towards  $-70^\circ\text{N}$  in both the near-bed and near-surface currents and an ellipticity of approximately 0.75, (i.e., the major axis is approximately 4 times the magnitude of the minor axis). The low-pass filtered ellipses indicate similar alignment to the 10-min averaged currents.

In Area B (06CM06), the principal axes indicate that surface currents are approximately 8% larger than the near bed currents in all directions. The currents are similarly aligned all through the water column, with the major axis oriented towards  $-98^\circ\text{N}$  in both near-bed and near-surface ellipses, and the ellipticity of each being approximately 0.75. Despite the levels of bad data removed from some of the ADCP records the principal axes analyses for 04CM03 and 07CM05 display very similar results to those at 06CM06 representing currents in Area B.

Again, the shorter deployment of this survey means that results of the tidal analysis of currents are not as accurate as those determined for the monsoon survey. A description of the tidal ellipses in Area A and B is included in the report from the March-April survey (Heap et al., 2005). Agreement between the two surveys is good, and within the error bounds presented.

## 4.4.6. Bedload Transport Estimates

### 4.4.6.1. Station 01CM01

No current meter was deployed at CSIRO Mooring 1.

### 4.4.6.2. Station 02CM07

Table 4.31 displays the calculated total bedload and direction at 02CM07 for the entire deployment using each of the defined formulations. Vector stick plots for bedload transport using each method are shown in [Fig. 4.49](#). The direction of bedload transport (between 260.89° and 273.56°) agrees with the sandwave migration measured in the north of Area A with the multibeam sonar surveys (approximately 270°). Mean bedload transport rates in Area A (02CM07) for the period of the deployment range from  $1.24 \times 10^{-2} \text{ g cm}^{-1} \text{ s}^{-1}$  using the method of Gadd et al. (1978) to  $1.36 \times 10^{-2} \text{ g cm}^{-1} \text{ s}^{-1}$  using the method of Engelund-Hansen. Significant bedload transport occurred during periods of maximum tidal current speeds (JD 286 and 298, [Fig. 4.49](#)). The average rate bedload transport is comparable to 07CM05 ([Fig. 4.53](#)) though substantially less compared to the other two stations, this results is also reflected in the average current strength for the 4 stations ([Tables 4.19, 4.22, 4.25, 4.28](#)).

Table 4.31. Bedload transport calculated at 02CM7

	Bagnold (Gadd et al., 1978)	Engelund- Hansen	Einstein- Brown	Yalin	Bagnold (Hardisty, 1983)
Q – Av ( $10^{-2} \text{ g cm}^{-1} \text{ s}^{-1}$ )	1.24	1.36	0.31	0.69	0.10
Q - Total ( $10^4 \text{ g cm}^{-1}$ )	0.87	0.73	0.18	0.30	0.09
Dir (True)	272.12	268.87	269.84	260.89	273.56

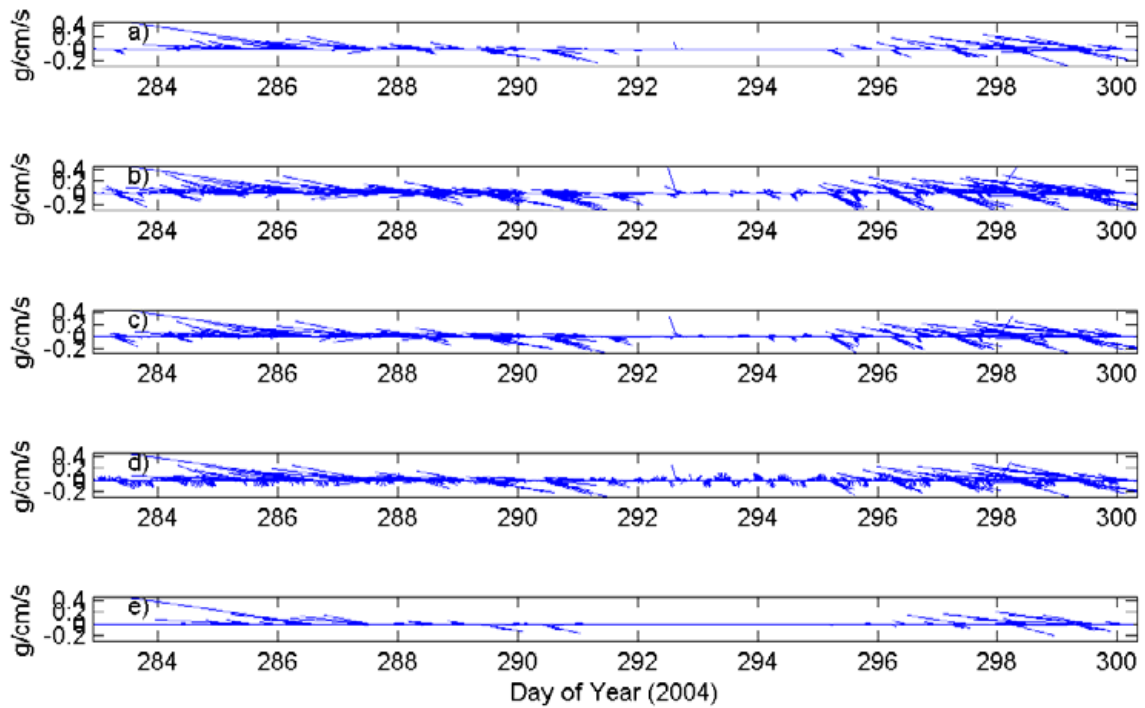


Fig. 4.49. Vector stick plots of bedload transport at 02CM07, as calculated using: a) Bagnold (Gadd et al., 1978); b) Engelund Hansen; c) Einstein-Brown; d) Yalin; e) Bagnold (Hardisty, 1983).

#### 4.4.6.3. Station 03CM02

Current meter data from 03CM02 was corrupt, and consequently bedload transport rates cannot be calculated.

#### 4.4.6.4. Station 04CM03

Table 4.32 displays the calculated total bedload and direction at 04CM03 for the entire deployment using each of the defined formulations. Vector stick plots for bedload transport using each method are shown in Fig. 4.50. Mean bedload transport rates in Area B (04CM03) for the period of the deployment range from  $9.24 \times 10^{-2} \text{ g cm}^{-1} \text{ s}^{-1}$  using the method of Gadd et al (1978) to  $4.87 \times 10^{-2} \text{ g cm}^{-1} \text{ s}^{-1}$  using the method of Engelund-Hansen. Significant bedload transport occurred during periods of maximum tidal current speeds (JD 285 and 297, Fig. 4.50). 04CM03 experienced the highest rates of bedload transport compared to the other three stations. The station was located on top of the sand bank in Area B and recorded the highest rates of bedload transport (Fig. 4.53 shows nearly 10 times that of 02CM07 of 07CM05).

Table 4.32. Bedload transport calculated at 04CM03

	Bagnold (Gadd et al., 1978)	Engelund- Hansen	Einstein- Brown	Yalin	Bagnold (Hardisty, 1983)
$Q - A_v$ ( $10^{-2} \text{ g cm}^{-1} \text{ s}^{-1}$ )	9.24	4.87	1.36	2.84	1.50
$Q - \text{Total}$ ( $10^4 \text{ g cm}^{-1}$ )	4.42	1.77	0.55	1.15	0.80
Dir (True)	271.18	270.41	270.78	270.48	-270.65

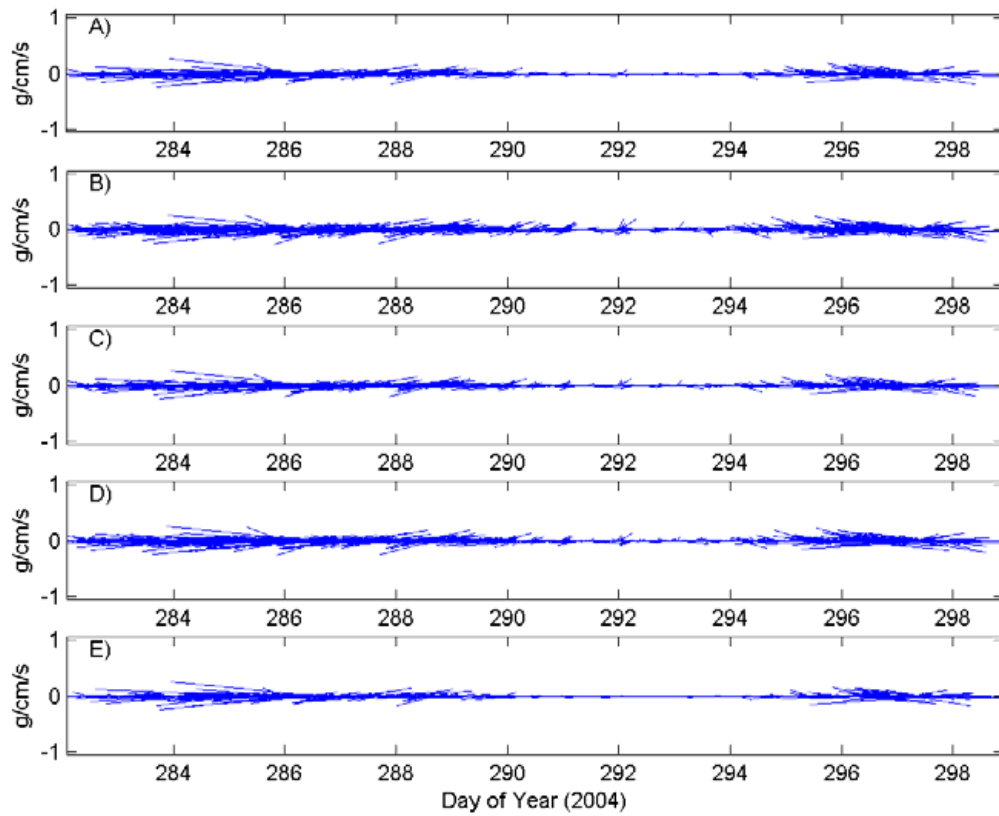


Fig. 4.50. Vector stick plots of bedload transport at 04CM03, as calculated using: a) Bagnold (Gadd et al., 1978); b) Engelund Hansen; c) Einstein-Brown; d) Yalin; e) Bagnold (Hardisty, 1983).

#### 4.4.6.5. Station 05CM04

Current meter data from 05CM04 was corrupt, and consequently bedload transport rates cannot be calculated.

#### 4.4.6.6. Station 06CM06

Table 4.33 displays the calculated total bedload and direction at 06CM06 for the entire deployment using each of the defined formulations. Vector stick plots for bedload transport using each method are shown in [Fig. 4.51](#). Mean bedload transport rates in Area B (06CM06) for the period of the deployment range from  $3.32 \times 10^{-2} \text{ g cm}^{-1} \text{ s}^{-1}$  using the method of Gadd et al (1978) to  $2.54 \times 10^{-2} \text{ g cm}^{-1} \text{ s}^{-1}$  using the method of Engelund-Hansen. Significant bedload transport occurred during periods of maximum tidal current speeds (JD 289 and 290, [Fig. 4.51](#)) Bedload transport at 06CM06 was approximately three times higher and 02CM07 and 07CM05, and approximately one third that of 04CM03. The direction of the bedload transport was to the easterly, and in contrast to the other three stations that have a net westwards displacement ([Fig. 4.53](#)). The eastwards transport is, however, consistent with the crest migration measured using multibeam sonar ([Fig. 2.2](#)). The eastwards current, occurring during ebb tide carrying sediment as bedload in the flat seabed areas of Area B.

Table 4.33. Bedload transport calculated at 06CM06.

	Bagnold (Gadd et al., 1978)	Engelund- Hansen	Einstein- Brown	Yalin	Bagnold (Hardisty, 1983)
Q – Av ( $10^{-2} \text{ g cm}^{-1} \text{ s}^{-1}$ )	3.32	2.54	0.65	1.45	0.52
Q – Total ( $10^4 \text{ g cm}^{-1}$ )	2.14	0.92	0.29	0.61	0.41
Dir (True)	69.71	64.60	66.34	71.27	71.62

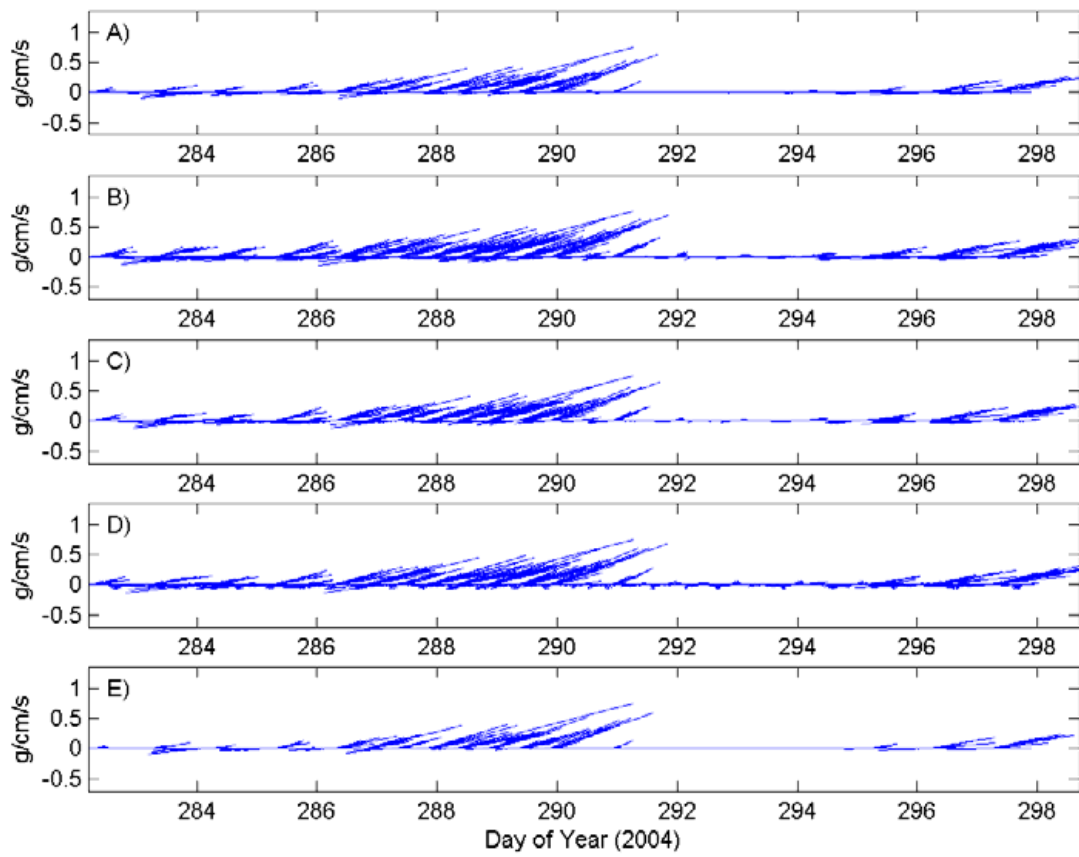


Fig. 4.51. Vector stick plots of bedload transport at 06CM06, as calculated using: a) Bagnold (Gadd et al., 1978); b) Engelund Hansen; c) Einstein-Brown; d) Yalin; e) Bagnold (Hardisty, 1983).

#### 4.4.6.7. Station 07CM05

Table 4.34 displays the calculated total bedload and direction at 07CM07 for the entire deployment using each of the defined formulations. Vector stick plots for bedload transport using each method are shown in Fig. 4.52. Mean bedload transport rates in Area B (07CM05) for the period of the deployment range from  $1.13 \times 10^{-2} \text{ g cm}^{-1} \text{ s}^{-1}$  using the method of Gadd et al (1979) to  $1.11 \times 10^{-2} \text{ g cm}^{-1} \text{ s}^{-1}$  using the method of Engelund-Hansen. Significant bedload transport occurred during periods of maximum tidal current speeds (JD 284-286 and 292, Fig. 4.52). 07CM05 had the lowest levels of bedload transport out of the four stations (Fig. 4.53). The placement of the current meter on the northern margin of the bank provided an intermediate of bedload transport between the top of the bank (04CM03) and between the banks (06CM06). The low level of bedload transport and the westerly direction indicates there a convergence zone exists between the strong eastwards bedload transport on the north western side of the bank, and westerly transport on the wester side of the bank. This convergence zone is also visible in the crest migration data (Fig. 2.2).

Fig. 4.34. 07CM05 bedload transport.

	Bagnold (Gadd et al., 1978)	Engelund- Hansen	Einstein- Brown	Yalin	Bagnold (Hardisty, 1983)
Q – Av ( $10^{-2} \text{ g cm}^{-1} \text{ s}^{-1}$ )	1.13	1.11	0.24	0.54	0.059
Q - Total ( $10^4 \text{ g cm}^{-1}$ )	0.46	0.47	0.099	0.19	0.015
Dir (True)	276.87	255.04	259.78	240.86	322.08

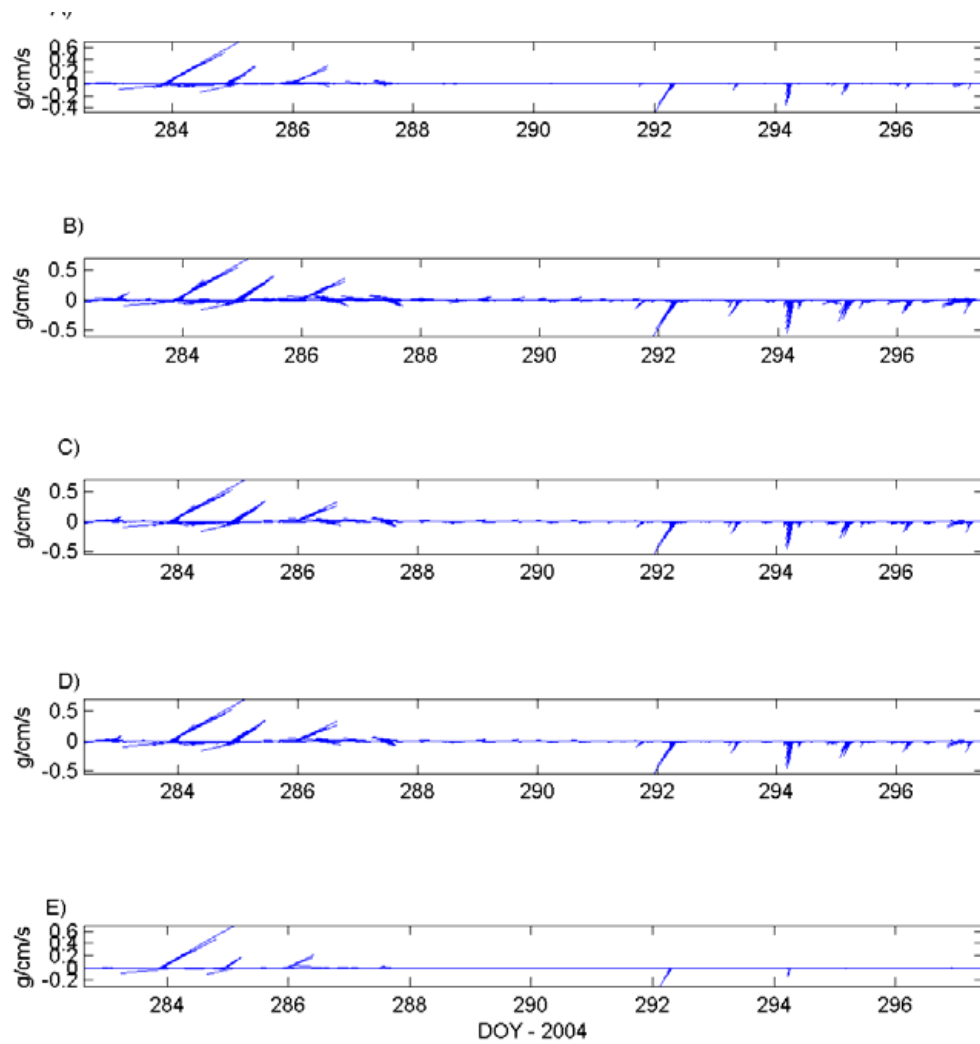


Fig. 4.52. Vector stick plots of bedload transport at 07CM05, as calculated using: a) Bagnold (Gadd et al., 1978); b) Engelund Hansen; c) Einstein-Brown; d) Yalin; e) Bagnold (Hardisty, 1983).

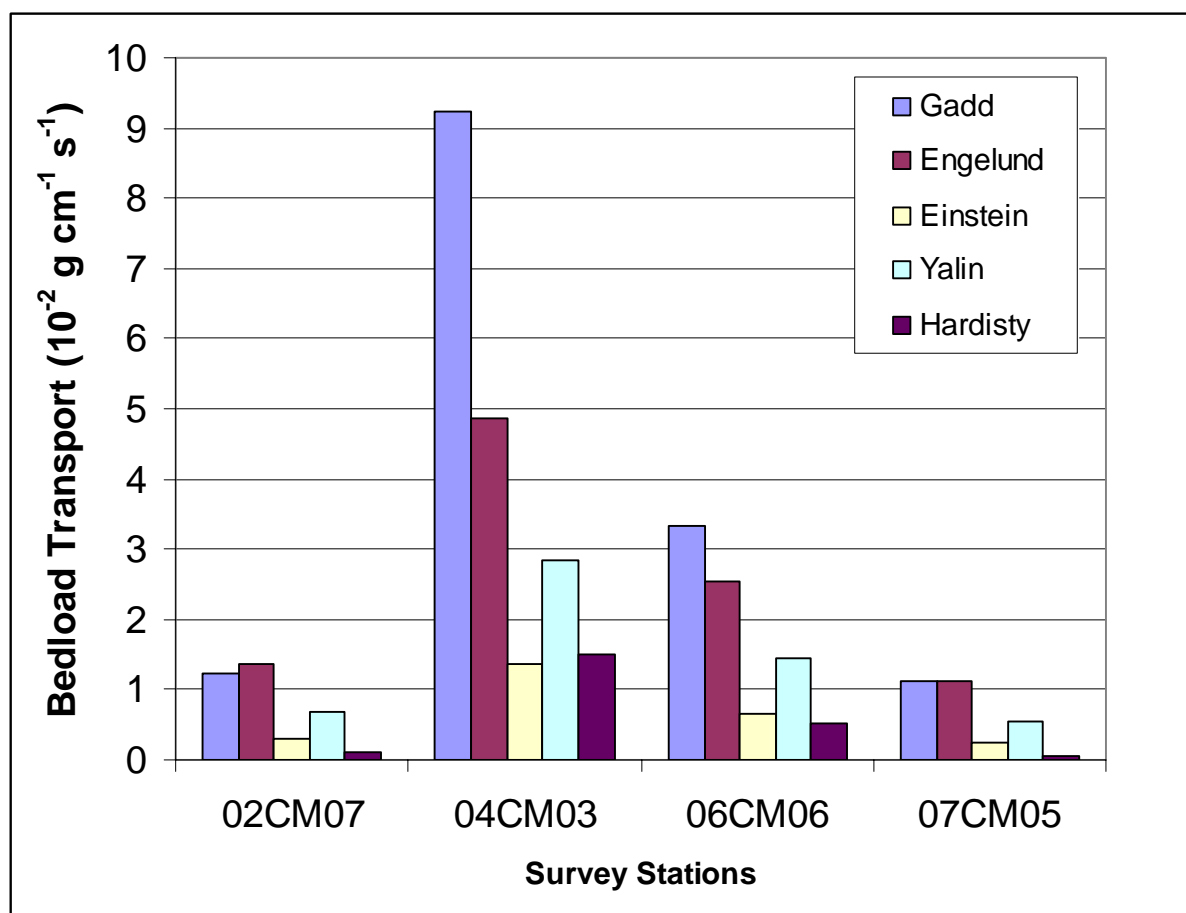


Fig 4.53. Average bedload transport in  $10^{-2} \text{ g cm}^{-1} \text{ s}^{-1}$  for the four stations and five different bedload transport calculations.

#### 4.4.6.8. Review of bedload transport calculations

There is upwards of an order of magnitude difference in the bedload transport rates predicted by the different methods (Fig. 4.53). An independent means of inferring the actual transport rate based on sandwave celerity was used to estimate the best equations for measuring bedload transport for this region (see [section 4.4.7](#)).

#### 4.4.7. Sandwave Migration

Sandwave migration rates in Area A (02CM07) as determined from the current meter measurements range, from 2 cm d<sup>-1</sup> (using method of Hardisty, 1983) to 16 cm d<sup>-1</sup> (using method of Gadd et al., 1978). In Area B (04CM03), the rates range from 10 cm d<sup>-1</sup> (using method of Einstein-Brown) to 75 cm d<sup>-1</sup> (using method of Gadd et al., 1978). Using currents measured at 06CM06, which does not lie within the sandwave field, sandwave migration rates vary from 3 cm d<sup>-1</sup> (using method of Hardisty, 1983) to 19 cm d<sup>-1</sup> (using method of Gadd et al., 1978). As expected, the sandwave migration rates reflect the bedload transport rates (Table 4.35). In all estimates, the Bagnold equation formulated by Gadd et al. (1978) has results in the largest estimates of bedload transport and sandwave migration.

Measured sandwave migration rates were approximately 20-30 cm day<sup>-1</sup>, suggesting that the bedload transport equations of Gadd et al. and Engelund-Hansen are perhaps the most applicable in this environment. Although predicted sandwave celerities still differed from measured celerities by up to a factor of 3 on occasions.

Table 4.35. Predicted average migration rates for all moorings. All measurement are in cm day<sup>-1</sup>.

Station	Bagnold (Gadd et al., 1978)	Engelund- Hansen	Einstein- Brown	Yalin	Bagnold (Hardisty, 1983)	Notes
01CM01	-	-	-	-	-	No current meter was deployed at 01CM1
02CM07	16.0	11.9	2.9	6.4	1.8	
03CM02	-	-	-	-	-	Current meter data from mooring 03CM2 was unusable.
04CM03	75.4	35.3	10.3	21.4	12.9	
05CM04	-	-	-	-	-	Current meter data from mooring 05CM4 was unusable.
06CM06	19.2	14.6	3.8	8.4	3.0	
07CM05	6.5	6.4	1.4	3.1	0.3	

## 4.5. Seasonal differences between monsoon and trade wind surveys

### 4.5.1. Salinity

Orman Reefs and Areas A and B show consistently higher salinities during the trade wind survey (Tables 4.2-4.4) in comparison to the monsoon survey (Heap et al., 2005, table 3.1). At the Orman Reefs station (01CM01), mean salinity is 0.6 PSU higher during the trade wind survey. In Area A and B, salinities are approximately 2 higher during the trade wind survey. Salinities are likely to be lower during the monsoon season with increased rainfall in the region during that period.

### 4.5.2. Temperature

At all stations, temperatures are consistently 1.6°C lower during the trade wind survey (Tables 4.2-4.4 compared to Heap et al., 2005, table 3.1). The persistent winds from the south-east move cooler waters from the south-east, resulting in the lower temperatures. Higher wind strengths during the trade wind season also mix surface waters to greater depths reducing the potential for shallow thermal stratification.

### 4.5.3. Turbidity

The largest seasonal change in the hydrological conditions is shown by turbidity. Turbidity during the monsoon survey (Heap et al., 2005, table 3.1) is consistently 3 times the magnitude of that observed during the trade wind survey (Tables 4.2-4.4). Current velocities and wind speeds (and consequently wave heights) are not significantly different between surveys, and consequently local resuspension is ruled out as the source for the turbidity. Hydrodynamic modelling undertaken as part of the Torres Strait CRC has provided some indications of the processes controlling turbidity in the region. Key results from the hydrodynamic modelling relevant to the generation of turbidity in the Turnagain Island region are summarised in section 6.1.3.

### 4.5.4. Sea Level

Low frequency sea-level variation can not be compared between surveys. Sea-level tidal analysis yields similar results for amplitude and phase of the main tidal constituents, and differ only by the error bounds presented.

### 4.5.5. Waves

Unfortunately, waves were not recorded during the monsoon survey. Consequently, for this comparison wind speeds and direction are compared. During both surveys, winds were predominantly directed from the south-east. Mean wind speeds were greater during the trade wind survey (Horn Island, 6.19 m s<sup>-1</sup> during trade wind survey, 4.85 m s<sup>-1</sup> during the monsoon survey), however maximum wind speeds obtained during each survey were almost identical (10.84 and 10.83 m s<sup>-1</sup>

respectively) (Section 3 in this report). Maximum gust obtained is largest during the monsoon survey ( $15.28 \text{ m s}^{-1}$  during monsoon,  $14.44 \text{ m s}^{-1}$  during the trade wind survey). There are only small differences observed between the wind conditions between the two surveys. Consequently, local wave conditions are expected to have been similar.

#### 4.5.6. Currents

Tidal currents are the same magnitude for each survey. Any difference between surveys will be a result of the local wind conditions.

In Area A, comparisons between 02CM07 (section 4.4.5.2) during the trade wind survey, and CSIRO-3 (Heap et al., 2005, section 3.3.2.3) during the monsoon survey show mean residual currents in the near-bed layer are 5% larger during the trade wind survey ( $8.7 \text{ cm s}^{-1}$  to  $254^\circ\text{N}$ ) than the monsoon survey ( $8.2 \text{ cm s}^{-1}$  to  $270^\circ\text{N}$ ), and directed south-westwards as opposed to southwards respectively. In the surface layer, mean residual currents are greater during the monsoon survey ( $10.65 \text{ cm s}^{-1}$  to  $265^\circ\text{N}$ ) than the trade wind survey ( $9.38 \text{ cm s}^{-1}$  to  $241^\circ\text{N}$ ). The currents are directed to the south-west during the trade wind survey, as opposed to westwards during the monsoon survey. Water depth of the mooring during the monsoon survey ( $\sim 9 \text{ m}$ ) is three times greater than the water depth of the trade wind mooring ( $\sim 3.5 \text{ m}$ ). Therefore, despite wind-driven currents being larger during the monsoon survey, their magnitude decreases through the water column so that they are of smaller magnitude near the bed. It could be assumed that if the moorings were deployed in the same water depth, near-bed currents would also be larger during the monsoon survey.

In Area B the comparison is made between 04CM03 (section 4.4.5.4) from the trade wind survey and CSIRO-2 (Heap et al., 2005, section 3.3.2.3) from the monsoon survey. Mean residual currents in the near bed layer are 35% larger during the trade wind survey ( $6.49 \text{ cm s}^{-1}$  to  $252^\circ\text{N}$ ) than the monsoon survey ( $4.79 \text{ cm s}^{-1}$  to  $236^\circ\text{N}$ ). Mean residual currents in the near-surface layer are also 35% larger during the trade wind survey ( $6.92 \text{ cm s}^{-1}$  to  $248^\circ\text{N}$ ) than the monsoon survey ( $5.11 \text{ cm s}^{-1}$  to  $235^\circ\text{N}$ ). In both the near-bed and near-surface layers, currents are directed more westwards during the trade wind survey.

Mean residual currents are not necessarily larger during one season than the other. In one area (Area A), greatest residual currents are observed during the monsoon survey, and in the other area (Area B), the greater residual currents are observed during the trade wind survey. Given wind speeds were very similar for the two surveys, the apparent seasonal variability is possibly a result of local variability of flow, dependent on the local deployment location of the current meter, rather than changes in large scale circulation. This aspect should be investigated in more detail in the future.

#### 4.5.7. Bedload transport and sandwave migration rates

The mean rates of transport are used to compare bedload transport between surveys. Using total transport would be inaccurate as the periods of deployment differ for each survey. In Area A, bedload transport rates are consistently higher, by a factor of approximately 2, during the monsoon survey (section 4.3.6 compared to Heap et al., 2005, section 3.3.3), regardless of the method of calculation. Mean direction of transport is within 20 degrees. During the monsoon season, transport is north-westward, however during the trade wind survey, transport is westward.

In Area B, bedload transport rates are consistently three times higher if comparing to 04CM03, or a two times higher if comparing to 06CM06, during the trade wind survey (section 4.3.6 compared to Heap et al., 2005, section 3.3.3), regardless of the method of calculation. If comparisons are made between CSIRO-3 from the monsoon survey and 06CM06 from the trade wind survey, the direction of bedload transport is within 5 degrees, both indicating an east-north-eastwards bedload transport. If comparisons are made to 04CM03 from the trade wind survey, bedload transport directions are in almost opposite directions, with currents from 04CM03 indicating bedload transport is in a westwards direction.

Local variation of currents is expected to account for the between survey variability of bedload transport, rather than changes in the circulation. Between survey comparison of sandwave migration rates indicates a similar result with no general trend observed.

## 5. Sedimentology

### 5.1. SAMPLE ACQUISITION

A total of 38 stations were occupied during the survey (Fig 5.1). The locations of the stations were designed to capture the full spectrum of sedimentary environments and seabed habitats. A variety of operations were undertaken at each station to characterise the seabed sediments, sedimentary processes, and biota and habitats. The survey locations were extended from the monsoon survey to include:

1. Push cores and grabs from the northern margin of Turnagain Island to compare to samples taken from the southern margin.
2. A sampling transect from Turnagain Island to Saibai Island to identify the transition zone between carbonate and terrigenous dominated sediments.
3. Surface grabs from around Saibai Island to compare their compositions to sediments from Turnagain Island, and Areas A and B.

#### 5.1.1. Water samples

A total of 212 water samples (WS1-WS212) were taken using a 2 litre Niskin bottle fitted with a messenger. The Niskin bottle was lowered to the bed and then raised approximately 0.5 m off the bottom before the messenger was sent down the wire to trigger the Niskin bottle and collect the water sample. Water samples were collected at select locations on the transit from Thursday Island to the study sites (Table 5.1) and every 20 minutes at four stations that were occupied for 25 hours (stations 25, 26, 36, 37). Two litres of water were filtered through pre-weighed 0.45  $\mu\text{m}$  mesh glass filter papers using a vacuum system. The filter papers were then stored in a dry freezer and on return from the survey were oven dried at 60° C in the laboratory and re-weighed to  $\pm 0.0001$  g to obtain suspended sediment masses.

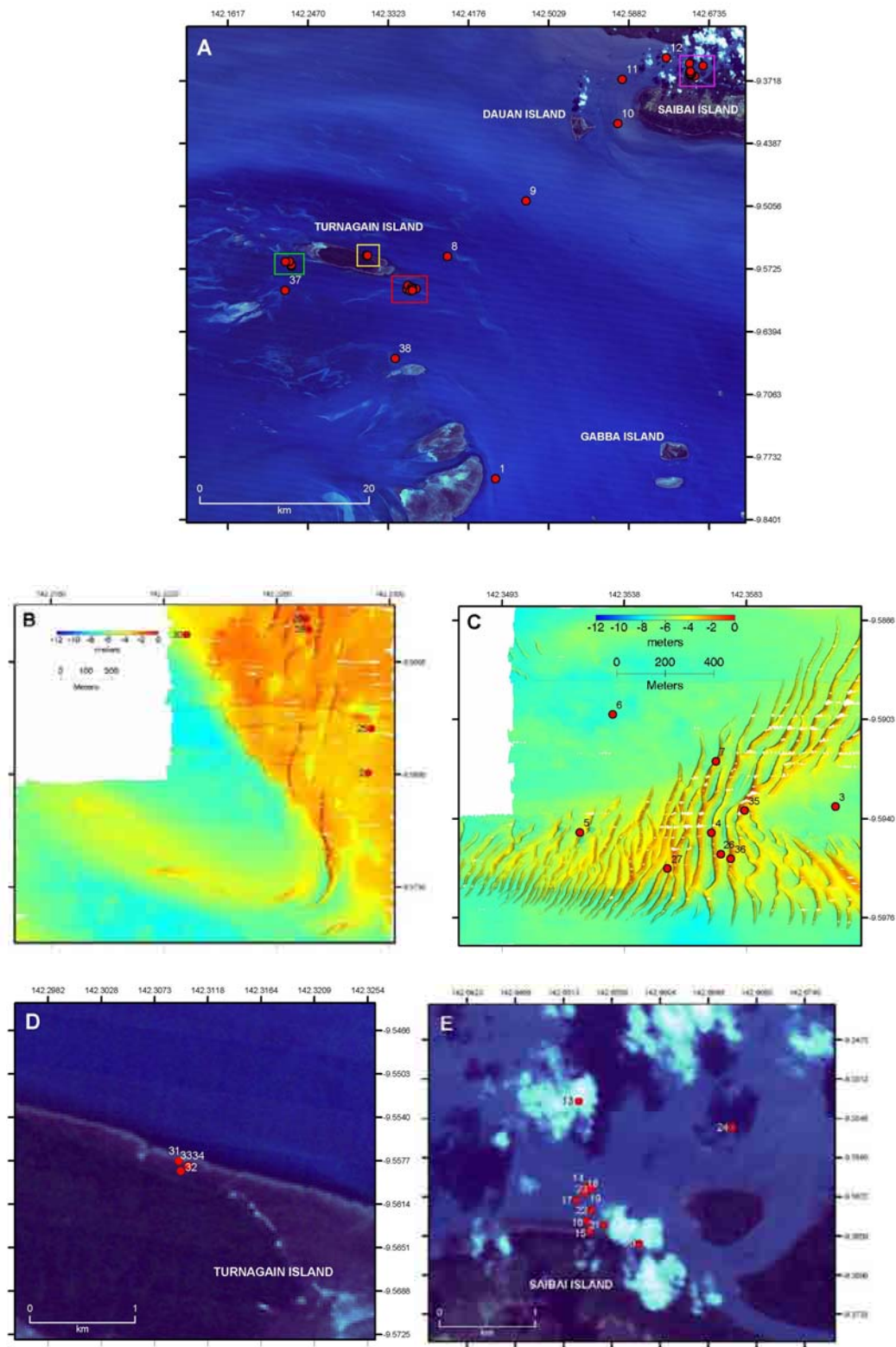


Figure 5.1a Shows the locations of sample stations over the Torres Strait region for survey 273. The area enclosed by the green triangle (Area A) is shown in detail in Fig. 5.1b. The area enclosed by the red triangle (Area B) is shown in detail in Fig. 5.1c. The area enclosed by the yellow triangle (north Turnagain Island) is shown in detail in Fig. 5.1d. The area enclosed by the purple triangle (Saibai Island) is shown in detail in Fig. 5.1e.

### 5.1.1. Water samples

A total of 212 water samples (WS1-WS212) were taken using a 2 litre Niskin bottle fitted with a messenger. The Niskin bottle was lowered to the bed and then raised approximately 0.5 m off the bottom before the messenger was sent down the wire to trigger the Niskin bottle and collect the water sample. Water samples were collected at select locations on the transit from Thursday Island to the study sites ([Table 5.1](#)) and every 20 minutes at four stations that were occupied for 25 hours (stations 25, 26, 36, 37). Two litres of water were filtered through pre-weighed 0.45  $\mu\text{m}$  mesh glass filter papers using a vacuum system. The filter papers were then stored in a dry freezer and on return from the survey were oven dried at 60° C in the laboratory and re-weighed to  $\pm 0.0001$  g to obtain suspended sediment masses.

### 5.1.2. Digital Video Footage

Video footage of the seabed was collected to characterise the substrate, morphology, habitats, and benthic biota in the study area. A video camera was lowered to the seabed and recorded a minimum of three minutes of video. The video camera was built by Geoscience Australia and is comprised of a digital video camera in a watertight housing attached to a steel frame. Two 25W halogen lights were used to illuminate the seabed where necessary. In addition, the camera was deployed at four stations to collect digital footage of the seabed to monitor the resuspension of bed sediment. At each station approximately 90 seconds of video was collected every 20 minutes for 25 hours (i.e., over one tidal cycle) and was timed to correspond to measurements of tide and wave currents with an acoustic current meter. Due to difficulties in maintaining a constant position at the 25-hour stations, the camera frame was lowered to the seabed just before the measurements were taken. At all sites, a cm-scale was set up on the camera frame in the view finder to determine the size of seabed features and objects in the water column. The underwater camera captured real-time broadcast quality digital footage that was recorded on digital videotape in the camera and was also fed to VHS tape on board the vessel. All video footage is contained in [Appendix B](#).

### 5.1.3. Surface Sediment Sampling

Samples of the seabed were collected using a Van-Veen grab. A total of 27 grabs were collected over the two study sites to characterise the texture and composition of the seabed sediments and associated habitats ([Table 5.1](#)). Each grab was sub-sampled for bulk sediment and seagrass types. All sub-samples were double bagged, labelled (including an aluminium tag), stored in a

refrigerated container, and the details entered into Geoscience Australia's Marine samples database (MARS) ([www.ga.gov.au/oracle/mars](http://www.ga.gov.au/oracle/mars)).

#### **5.1.4. Subsurface Sediment Sampling**

Subsurface sediments were sampled using an electric-powered vibrocorer. The 240V electric cable connected to the vibrating head unit was attached to the coring wire as a lazy line and powered from the vessel. The core frame was held upright on the seabed by three legs that extended outwards and maintained orientation into the current by a fin attached to one of the legs. The core barrels were 60 mm diameter stainless steel and contained a 58 mm diameter PVC liner fitted with a core catcher. The empty core liners were 4.5 m long and contained a piston that was tethered to the frame to assist with core recovery. From previous experience, each core was vibrated into the seabed for about 3 minutes to achieve maximum penetration into the seabed. A total of 10 vibrocores and 3 push cores were recovered (Table 5.12). Cores represented a total length of 5.16 m. On board, the cores were cut into 0.5 m sections, sealed with end caps (and packed with high-density foam biscuits where necessary), labelled, and stored in a refrigerated container before being transported to Canberra for geophysical logging.

### **5.2. SAMPLE PROCESSING AND ANALYSIS**

#### **5.2.1 Water Samples**

One litre of water was filtered through pre-weighed 0.45 µm mesh glass filter papers using a vacuum system on board the vessel. The filter papers were then stored in a dry freezer and on return to the laboratory where oven dried at 60°C and reweighed to ±0.0001 g to obtain the weight of suspended sediments. Suspended sediment concentrations were then calculated from these weights for the 1 litre of seawater filtered through the paper. Select filter papers were then visually inspected using a standard binocular microscope to provide an assessment of the type and nature of particles in suspension.

##### **5.2.1.1. EDX analysis of filter paper and grab samples**

Understanding the chemical composition of suspended sediments (filter papers) and surficial sediment was considered important for understanding the sources of sediment plumes in Torres Strait. EDX analysis is a technique commonly used to identify the elemental composition of samples (sediments in this case) and works as an integrated feature of a scanning electron microscope (SEM) (Brink F.J., Norén L. and Withers R.L., 2004.). A variety of grabs and filter paper samples from stations 25 and 26 were used in the study.

Table 5.1. Summary of station operations.

Station	Camera	Grab	Core	Water Sample	Currentmeters
1	01CAM01	01GRVV01		01WS01	01CM01
2	02CAM02	02GRVV02		02WS02	02CM07
3	03CAM03	03GRVV03		03WS04	03CM02
4	04CAM04	04GRVV04		04WS05	04CM03
5	05CAM05	05GRVV05			05CM04
6	06CAM06	06GRVV06		06WS07	06CM06
7	07CAM07	07GRVV07		07WS08	07CM05
8		08GRVV08			
9		09GRVV09			
10		10GRVV10			
11		11GRVV11			
12		12GRVV12			
13		13GRVV13			
14		14GRVV14			
15		15GRVV15			
16		16GRVV16			
17		17GRVV17			
18		18GRVV18			
19		19GRVV19			
20		20GRVV20			
21		21GRVV21			
22		22GRVV22			
23		23GRVV23			
24		24GRVV24			
25	25CAM08			25WS 9-60	
26	26CAM9			26WS 61-112	
27			27VC1-2		
28		28VC3cc-4cc	28VC3-4		
29	29CAM10		29VC6		
30	30CAM11	30VC7cc	30VC7		
31		31GR25			
32			32PK1		
33		33GR26	33PK2		
34			34PK3		
35	35CAM12	35VC8cc	35VC8-9		
36	36CAM13		36VC10	36WS 113-162	
37	37CAM14			37WS 163-212	
38	38CAM15	38GR27			

For the purpose of this study EDX analysis was specifically used to:

1. Compare the changes in chemical composition of suspended sediments over time with changes in suspended sediment concentration.
2. Compare the chemical composition of sediment samples in Areas A and B with the sediments found on filter papers at stations 25 and 26 to determine if suspended sediment was advected locally or sourced from elsewhere; and
3. Compare the chemical composition of sediment samples from Saibai Island, between Saibai and Turnagain Island, and Areas A and B.

The output of an EDX analysis is an EDX spectrum, which is a plot of how frequently an X-ray is received for each energy level. An EDX spectrum normally displays peaks corresponding to the energy levels for which the most X-rays have been received. Each of these peaks is unique to an atom and, therefore, corresponds to a single element. The higher a peak is in a spectrum, the more concentrated the element is in the specimen.

Due to the high variability in the sediment concentrations, sub-samples were scraped from the main filter papers to be mounted on metal stubs and fixed with double sided carbon tape to ensure conductivity. Samples were coated with a thin film of carbon in a glass vacuum vessel using a DYNAVAC CS300 Coating Unit. The coating is also required to eliminate or reduce the electric charge which builds up rapidly in a non-conducting specimen when scanned by a beam of high-energy electrons. The EDX analyses were carried out at 15kV (kilo Volt) and 1nA (nano Ampere) using a JEOL 6400 Scanning Electron Microscope (SEM) equipped with an Oxford Instruments light element EDS detector and Link ISIS SEMquant software as well as a Cameca SX100 using WDS (Wavelength Dispersive X-Ray Spectroscopy). The SEM is located at the Research School of Biological Sciences at the Australian National University in Canberra. In order to minimise atomic number, absorption and fluorescence (ZAF) corrections, a stoichiometric method was used throughout the analyses.

Four 24-hour stations were occupied in Survey 273 to measure the SSC but only the samples collected on the hour have been considered for the EDX analysis (a total of 45 water samples). This low number was due to the fact that two of the four 24h-stations (36 and 37) did not contain enough sediment to be analysed. A summary of the filter papers analysed is given in [Table 5.2](#). The mud component of 15 Grab samples were also analysed (Grabs 1-13, 17, 18, 23).

As a general rule, each sample has been analysed five times in different sectors at the SEM to minimise errors and obtain a more homogeneous result

and the averages were then calculated. A magnification of 100 times was also maintained constant at each measurement for the sake of reproducibility.

Table 5.2. Water samples analysed from near Turnagain Island. Samples marked in grey were not analysed due to insufficient sample size.

Area A 15-16/10/04			Area B 16-17/10/04			Area B 20-21/10/04			Area A 21-22/10/04		
Station 25			Station 26			Station 36			Station 37		
Time (GMT)	Filter Paper No.	Concentration (mg l <sup>-1</sup> )	Time (GMT)	Filter Paper No.	Concentration (mg l <sup>-1</sup> )	Time (GMT)	Filter Paper No.	Concentration (mg l <sup>-1</sup> )	Time (GMT)	Filter Paper No.	Concentration (mg l <sup>-1</sup> )
20:00	312	3.9	0:00	366	2.7	8:00	420	0	11:00	471	1.7
21:00	314	3.6	1:00	368	1.7	9:00	422	-0.3	12:00	473	0.5
22:00	316	3.2	2:00	370	4.7	10:00	242	0.2	13:00	475	1.6
23:00	318	4.2	3:00	372	2.5	11:00	426	-0.4	14:00	477	1.8
0:00	320	3.8	4:00	374	2.9	12:00	428	-0.1	15:00	479	2.1
1:00	322	4.1	5:00	376	2.9	13:00	430	0.5	16:00	481	1.4
2:00	324	3.2	6:00	378	2.1	14:00	432	0	17:00	483	1.6
3:00	326	5.5	7:00	380	6.8	15:00	434	0.17	18:00	485	2.2
4:00	328	4.1	8:00	382	1	16:00	436	0.2	19:00	487	4
5:00	330	6.5	9:00	384	2.1	17:00	438	0.4	20:00	489	1
6:00	332	4.2	10:00	386	1.4	18:00	440	-0.5	21:00	491	1.4
7:00	334	1.4	11:00	388	1.2	19:00	442	-0.3	22:00	493	2.1
8:00	337	3.7	12:00	391	1.2	20:00	444	-0.1	23:00	495	2.2
9:00	339	3.8	13:00	393	0.7	21:00	446	-0.3	0:00	497	2
10:00	341	10	14:00	395	1.7	22:00	448	1.3	1:00	499	2.1
11:00	344	24.4	15:00	397	0.8	23:00	450	0	2:00	501	2.9
12:00	346	2.5	16:00	399	1.5	0:00	452	0.3	3:00	503	2.8
13:00	348	8	17:00	401	1.3	1:00	454	0.5	4:00	506	3.9
14:00	350	13.1	18:00	403	1.2	2:00	456	0.1	5:00	510	9.8
15:00	352	8.6	19:00	405	0.6	3:00	458	-0.1	6:00	511	3.9
16:00	354	4.2	20:00	407	2	4:00	460	0.3	7:00	513	3.4
17:00	356	3.6	21:00	409	6.5	5:00	462	0.6	8:00	515	2.9
18:00	358	4.7	22:00	411	1.2	6:00	465	0.4	9:00	517	2.8
19:00	360	7.5	23:00	413	1	7:00	467	1.5	10:00	519	2.9
20:00	362	2.4	0:00	415	1.3	8:00	469	1.8	11:00	521	3.5

#### 5.2.1.2. SXAM - X-ray fluorescence of grab samples

Pixel-intensities from X-ray fluorescence (XRF) images document the distribution of selected elements in a material. Images The XRF images are obtained using a scanning X-ray analytical microscope (SXAM) and can be calibrated to produce quantitative elemental distribution maps by an automated process during acquisition. Image output can be in colour or black/white, and colour schemes for the images can be user-defined. The XRF techniques used for this analysis are detailed in Norrish and Hutton (1964, 1969)

For this study, both mud and sand fractions of two grab samples have been analysed to determine the differences levels of biogenic silica and quartz (273/08GRVV08 near Turnagain Island and 273/11GRVV11 near Saibai Island; Fig. 5.1a). EDX analysis only measures total concentrations of Si and hence is unable to differentiate between the different types of Silica.

XRF maps for the mud fraction have been collected using a constant magnification of x120, while for the sand fraction a magnification of x50 has been applied, in both cases to retain comparability among the pictures.

### **5.2.2. Digital Video Footage**

Approximately 3-5 minutes of video footage was captured at each site, and 1.5 minutes of video was captured every 20 minutes for the 24 hour stations, the video footage recorded was edited down to 20-30 second snippets that showed the major habitats, biota, and sedimentary processes (such as bedload transport) that were observed at each station. The video was edited using standard video editing software.

### **5.2.3. Surface Sediments**

#### **5.2.3.1. Sediment texture**

Initially, the bulk sample was split into two sub-samples for grain size analysis. Bulk grain size distributions were determined for the first sub-sample using a Malvern Mastersizer-2000 laser particle size analyser (e.g., Heap et al., 1999). The bulk sample was sieved through a 2 mm mesh to remove the gravel fraction, which was retained for visual inspection. Organic matter in the fine fraction was then removed by immersing the sample in 10-20 ml of dilute hydrogen peroxide ( $\text{H}_2\text{O}_2$ ). After rinsing thoroughly with distilled water, the sample was placed in an ultrasonic bath for up to 2 mins to break up any remaining aggregates. The grain size distribution of the fine fraction was then determined using the laser particle size analyser.

Approximately 10-20 g of the second sub-sample was sieved through a 2 mm and 63  $\mu\text{m}$  sieve with distilled water. Each size fraction was retained. The mud fraction was spun in a centrifuge at 3,500 rpm for 10 mins to separate out the sample. All of the fractions were dried in an oven at 40° C for at least 24 hours and then allowed to cool to room temperature. The dried material for each fraction was then weighed with an analytical balance to obtain the amount of gravel, sand and mud in the sample.

#### **5.2.3.2. Sediment composition**

Carbonate concentrations were determined on all of the bulk samples, as well as the sand and mud fractions using the "carbonate bomb" method of Muller and Gastner (1971). Initially the 3-5 g of bulk sample was dried in an oven at 40° C for 24 hours. This sample was then ground to a fine powder and exactly 0.8 g was reacted with 10 ml of orthophosphoric acid ( $\text{H}_3\text{PO}_4$ ). The flask was agitated until the entire sample had reacted with the acid (usually about 60 s). The pressure of the gas liberated was then compared to a standard curve that

converted the pressure into carbonate concentrations (the curve is constructed by reacting known amounts of pure calcium carbonate between 0.1 - 0.8 g and recording the corresponding pressure). The carbonate content of the gravel fraction was estimated from a visual inspection for all samples.

Select samples were also visually inspected for composition on board the vessel and in the laboratory using a standard binocular microscope. The bulk, gravel, sand and mud fractions were inspected separately, with only the coarse silt-sized grains visible in the mud fraction. An estimate of the abundance of each constituent in each fraction was made based on a visual assessment of the grains. At the time of writing, no point counting of the grains had been carried out.

#### 5.2.4. Subsurface Sediments

To characterise changes in sandwave sediment texture through the Late Quaternary the wet bulk density, P-wave velocity, fractional porosity, texture, composition, and age of the sediments contained in the cores were determined.

##### 5.2.4.1. Physical Properties

After equilibration with ambient laboratory conditions (between 18° and 20° C), wet bulk density (WBD), P-wave Velocity (Vp), and Fractional Porosity (FP) were determined at 0.01 m intervals down VC1-5 using a GEOTEK MS2 multi-sensor core logger (e.g., Heap et al., 2001).

Wet bulk density (WBD) was determined by measuring the gamma attenuation of the sediment from a Cs-137 source. WBD of the sediment is positively correlated with gamma attenuation. The relationship between density and gamma attenuation was initially calibrated using a graduated density standard consisting of 13 water/aluminium density components (e.g., Best and Gunn, 1999). This procedure corrects for gamma attenuation (caused by the Al liner), count rate effects (e.g., Weber et al., 1997), and the different scattering properties of seawater and sediment (e.g., Gerland and Villinger, 1995). The calibration was undertaken using a water density of 1.001 g cm<sup>-3</sup>, and aluminium density of 2.71 g cm<sup>-3</sup>, which is approximately equal to the mineral densities of siliciclastic (2.65 g cm<sup>-3</sup>) and carbonate (2.67 g cm<sup>-3</sup>) grains. Using this calibration, repeat density measurements were within 0.05 g cm<sup>-3</sup>.

P-wave velocity (Vp) was determined by measuring the travel time of a 500 kHz ultrasonic compressional pulse across the core. The pulse propagates through the core from the transmitter and is detected by the receiver. Vp is directly related to changes in the composition and texture of the sediments (e.g., mineral composition, grain shape and size, packing, etc.). To prevent variations in the ambient conditions masking differences between

sedimentary units, the  $V_p$  was also corrected for temperature of the water and sediment and salinity of the interstitial fluid for each core.

Fractional Porosity (FP) was calculated directly from the WBD using the equation:

$$FP = (MGD - WBD) / (MGD - WD) \quad [1]$$

where FP = fractional porosity, MGD = mineral grain density, WBD = wet bulk density, and WD = fluid density (i.e., sea water). This calculation assumes that the sediment was fully saturated with seawater, a mineral density of siliciclastic and carbonate sediment of  $\sim 2.65 \text{ g cm}^{-3}$ , and a fluid (i.e., seawater) density of  $1.024 \text{ g cm}^{-3}$ .

#### **5.2.4.2. Sediment texture**

Grain size distributions were determined for bulk samples using a Malvern Mastersizer-2000 laser particle size analyser (e.g., Heap et al., 1999). The samples were prepared and analysed using the same methods as those undertaken for the surface samples ([section 5.2.3](#)).

#### **5.2.4.3. Sediment Composition**

Core sub-samples were analysed for percent gravel, sand and mud. In the case of the sub-samples, approximately 2-5 g of bulk sediment was washed with distilled water through sieves of mesh sizes of 2 mm and  $63 \mu\text{m}$ . The sub-samples were then treated and analysed using the same methods as those undertaken for the surface samples ([section 5.2.3](#)).

Carbonate concentrations were determined on the bulk samples, as well as the sand and mud fractions according to the bomb method of Muller and Gastner (1971). The procedure used is the same as that for the surface sediments ([section 5.2.3](#)).

## 5.3. Results

### 5.3.1. Water Samples

Four stations were occupied to measure near-bed suspended sediment concentrations (SSC) in both Areas A and B over a spring and neap tide cycle (i.e. 25 hours) (see table 5.3, [fig 5.1](#)).

Table 5.3. Summary of 24 hour stations. Note that the tide cycle is important for understanding the current strengths experienced during the 24 hour station with springs having higher peak current than the neaps.

Station	Area	Lat	Lon	Start UTC	Stop UTC	Tide Cycle
25	A	-9° 34.10S	142° 13.77E	20:00 15/10/2004	21:00 16/10/2004	Neap
26	B	-9° 35.717S	142° 21.444E	00:00 16/10/2004	03:00 17/10/2004	Neap
36	B	-9° 35.717S	142° 21.444E	11:00 20/10/2004	11:00 21/10/2004	Spring
37	A	-9° 34.10S	142° 13.77E	08:00 21/10/2004	08:00 22/10/2004	Spring

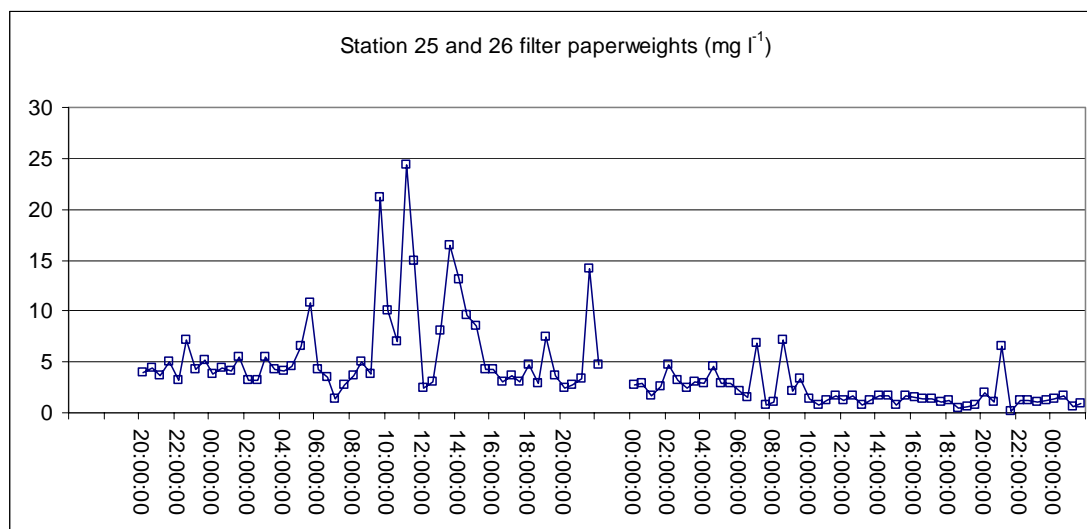


Figure 5.2 Graph showing suspended sediment concentrations for neap tide cycle in the vicinity of Turnagain Island. Data for Area A starts at 20:00 15/10/2004 and finishes at 21:00 16/10/2004. Data for Area B starts at 00:00 16/10/2004 and finishes at 03:00 17/10/2004. Note that all times are in GMT.

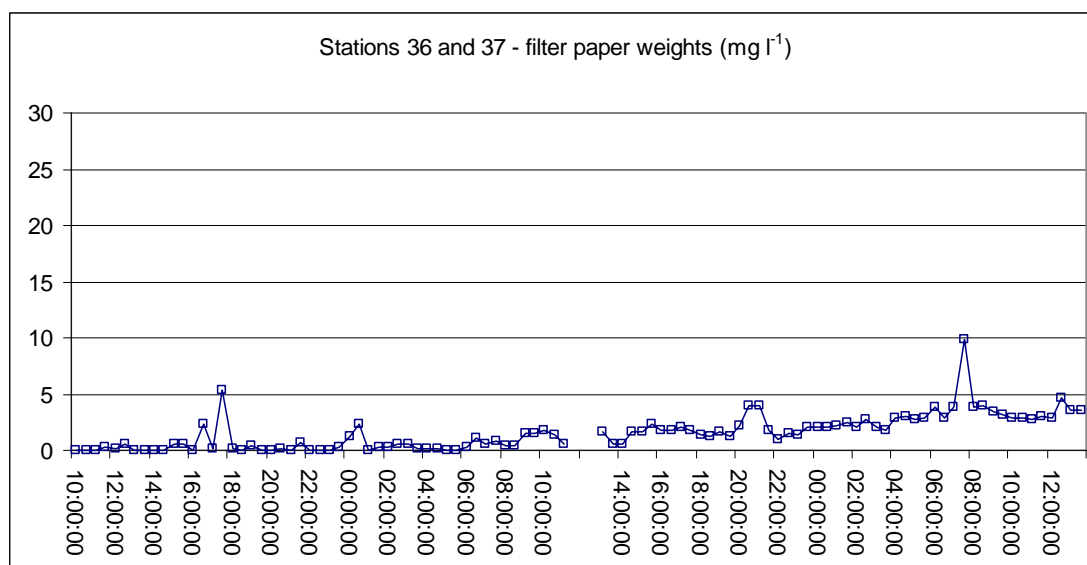


Figure 5.3 Graph showing suspended sediment concentrations for spring tide cycle in the vicinity of Turnagain Island. Data for Area B starts at 10:00 20/10/2004 and finishes at 11:00 21/10/2004. Data for Area A starts at 13:00 21/10/2004 and finishes at 14:00 22/10/2004. Note that all times are in GMT.

#### 5.3.1.1. Area A

During the neap cycles the average SSC was 6.1 mg l<sup>-1</sup> with a maximum of 24.4 mg l<sup>-1</sup>. During the springs the average SSC was 2.5 mg l<sup>-1</sup> with a maximum of 9.8 mg l<sup>-1</sup>. No cyclicity is evident in the dataset although the Seabird sensor in Area A (02CM07, [Fig. 4.9g](#)) indicates otherwise. This may be a result of a different range of grain sizes being trapped by the Niskin bottle than were measured using the Seabird sensor or the influence of wave activity on our sampling method.

#### 5.3.1.2. Area B

During the neap cycles the average SSC was 2.0 mg l<sup>-1</sup> with a maximum of 7.2 mg l<sup>-1</sup>. During the springs the average SSC was 0.5 mg l<sup>-1</sup> with a maximum of 5.3 mg l<sup>-1</sup>. No cyclicity is evident in the dataset although the Seabird sensor in Area B (06CM06, [Fig. 4.11g](#)) indicates otherwise. As in Area A this may be a result of different range of grain sizes being trapped by the Niskin bottle than were measured using the Seabird sensor or the influence of wave activity on our sampling method.

### 5.3.1.3. Comparison with Monsoon survey

Compared to the monsoon survey the SSC's are much less during the trade wind survey. The monsoon survey had average values ranging from 8.9-18.31 mg l<sup>-1</sup> (see table 5.4 and 5.5) whereas values for the trade wind survey ranged from 0.5-6.1 mg l<sup>-1</sup> (Tables 5.4 and 5.5). The monsoon survey had highest SSC during the spring tides whilst trade wind survey had higher SSC during the neap tide. It is possible that these differences in SSC are a result of differences in wave activity during the surveys.

Table 5.4. Average suspended sediment concentrations for Area A during neaps and spring for both survey seasons

Average SSC (mg l <sup>-1</sup> )	Spring	Neap
Area A monsoon	13.2	11.6
Area A trade wind	2.6	6.1

Table 5.5. Average suspended sediment concentrations for Area B during neaps and spring for both survey seasons

Average SSC (mg l <sup>-1</sup> )	Spring	Neap
Area B monsoon	18.3	8.9
Area B trade wind	0.5	1.9

### 5.3.1.4. EDX analyses results

For this study eleven chemical elements have been detected through the JEOL 6400. The results (Figs. 5.4a & 5.5a) are shown in terms of atomic percentages, which indicate the total percent of atoms belonging to a certain element against the general composition measured for a sample.

Carbon (C) has also been identified in all samples. However, because of the high concentration of carbon in the composition of the filters from which the samples have been scraped for the analyses, such element is considered not diagnostic. The output of such analysis, due to the nature of the filter papers, provides only the raw elemental composition of a sample implying that any form of identification of compounds and interpretation is left to the scientist.

The average atomic percentages for each element indicate a constant composition of the near-bed suspended sediments throughout the time. The inverse relationship between O and Na/Cl and the direct relationship between

O and Ca are also easily detected in both stations. However, other elements, such as Si, Fe and Al, display more complex and apparently random patterns.

In station 25, the oxygen record presents a number of oscillations, the largest of which is centred at 10:00 GMT, when O concentration reaches the lowest value of 44.89%. At this same time, all other elements, except S, register an abrupt change in abundance indicating a common cause of disruption. This peak also corresponds to one of the highest peaks within the SSC plot for station 25 (Fig. 5.2). Assuming the peak in Fig. 5.2 is reliable it has been inferred that the increased level of turbidity at that time may have been wave related (due to the lack of a tidal signature within that data set). The peak in the EDX analysis at 10:00 GMT may be related to subtle changes in the chemistry of the seabed sediment and the suspended load. A similar but less pronounced peak also occurs at 15:00 GMT. This peak also corresponds to a peak in the SSC in Fig. 5.2.

In station 26, the EDX results, shown in Fig. 5.5a, are partially incomplete as four samples were not able to be analysed. Two major negative peaks have been detected in an otherwise almost flat oxygen record at 02:00 and 21:00 GMT, respectively. These peaks also correspond to peaks in the SSC for station 26 (Fig. 5.2) although peaks in the SSC at 7:00 and 8:30 GMT are not recorded in the EDX analysis due to missing samples at those times. These peaks may also be to subtle changes in the chemistry of the seabed sediment and the suspended load however there are different responses in the EDX curves for each station during the high SSC events. For both stations 25 and 26 the negative peak in O is matched by positive peak in Na and Cl. At station 25 the negative peak in O is matched by strong negative peak in Si and Ca, and peaks for Fe and Al. At station 26 the Si, Ca, Fe and Al data are noisier than station 25 and no clear relationship can be made.

The EDX analysis appears to show anomalies in the sediment chemistry at times where there is high suspended sediment concentrations. The sediments at high SSC appear to be characterised by relatively low O, Si, Ca, Fe and Al and high Na and Cl. The concentrations of S, Ti, K and Mg typically show very weak to non existent relationships to the peaks in SSC.

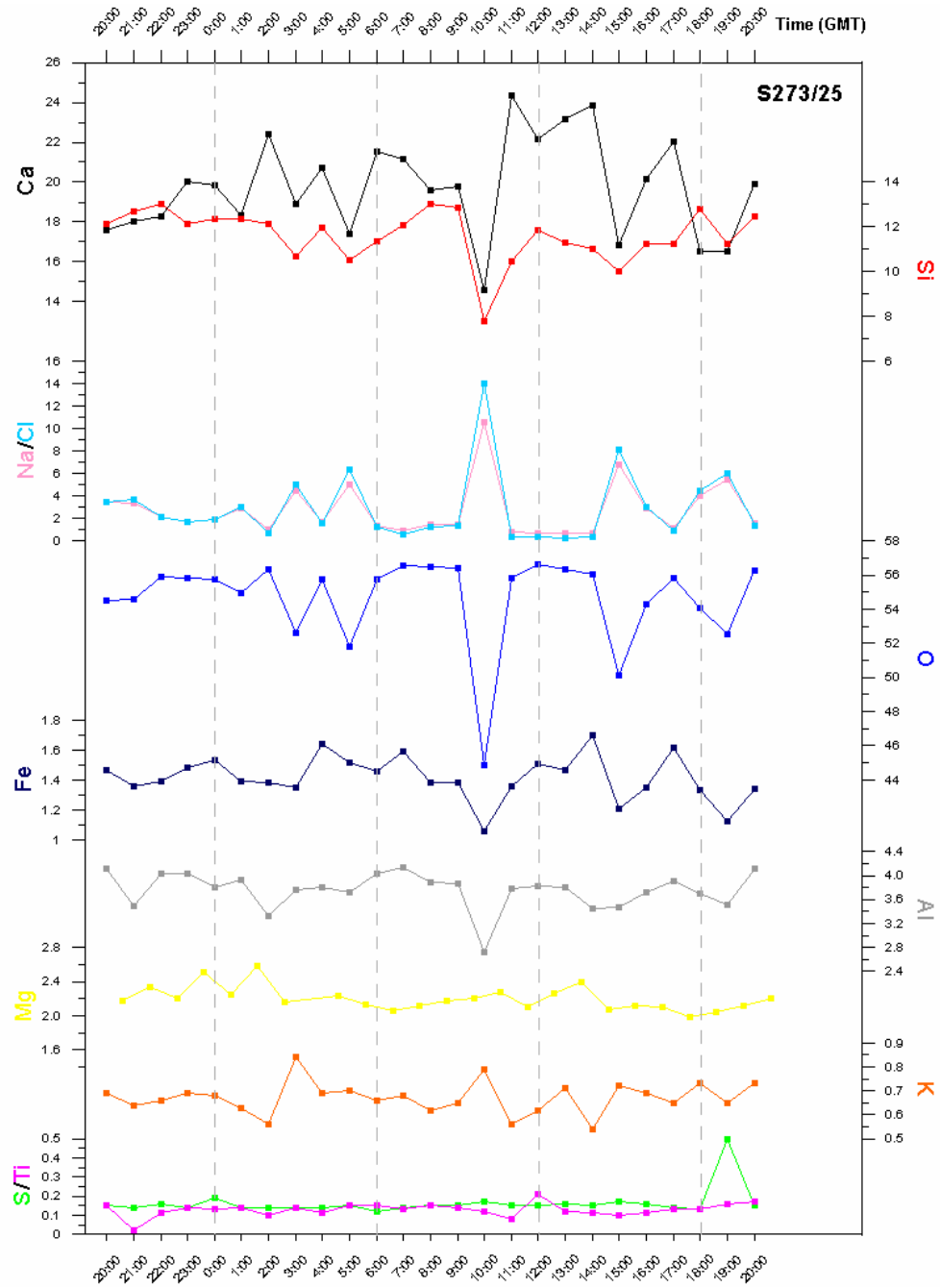


Figure 5.4. Summary plot of all the main chemical elements (atomic %) detected in the water samples from 24-hour station S273/25 using EDX analysis.

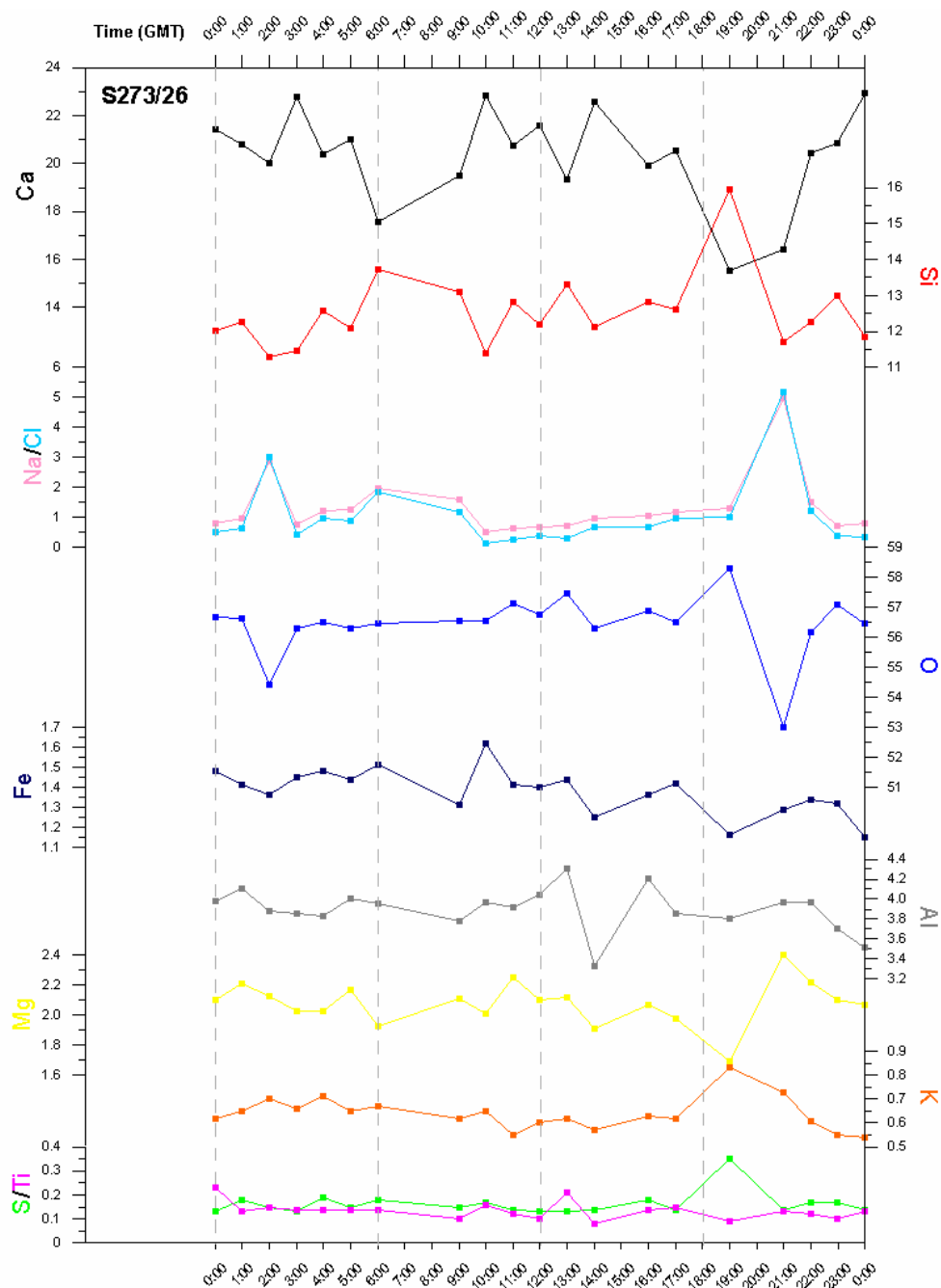


Figure 5.5. Summary plot of all the main chemical elements (atomic %) detected in the water samples from 24-hour station S273/26 using EDX analysis.

The mud fraction of 15 grab samples was also analysed and the results are shown in [Table 5.6](#). Samples 1-7 were acquired in the Turnagain Island region, samples 8–12 were transitional between Turnagain Island and Saibai Island, samples 13, 17, 18, and 23 were from Saibai Island.

Table 5.6. EDX Analysis of select grab samples (atomic %) from Survey 273 using ADX analysis.

Grab No.	01GRVV01	02GRVV02	03GRVV03	04GRVV04	06GRVV06	07GRVV07	08GRVV08	09GRVV09	10GRVV10	11GRVV11	12GRVV12	13GRVV13	17GRVV17	18GRVV18	23GRVV23
Na	0.55	0.79	2.91	1.21	0.78	1.98	2.33	0.82	0.64	0.59	0.82	0.77	0.59	0.62	0.88
Mg	2.32	2.28	2.40	2.96	2.24	2.37	2.28	2.06	1.54	1.36	1.30	1.97	1.31	1.22	1.16
Al	3.64	4.02	2.62	3.40	4.50	2.79	3.96	5.26	8.05	7.83	8.58	7.91	7.43	6.95	7.13
Si	9.28	10.82	8.98	8.19	10.84	8.13	10.39	13.68	18.71	19.19	19.16	19.00	19.21	19.60	19.78
S	0.14	0.16	0.17	0.16	0.13	0.13	0.12	0.13	0.08	0.09	0.07	0.09	0.09	0.06	0.17
Cl	0.16	0.52	3.13	1.16	0.54	2.51	1.49	0.58	0.03	0.03	0.02	0.03	0.05	0.03	0.04
K	0.51	0.62	0.48	0.49	0.67	0.50	0.62	0.88	1.31	1.33	1.33	1.30	1.22	1.18	1.26
Ca	26.73	23.21	24.17	26.21	22.26	27.02	22.08	16.67	4.59	4.69	3.69	5.00	5.48	5.77	4.83
Ti	0.10	0.12	0.08	0.10	0.14	0.05	0.13	0.17	0.31	0.33	0.40	0.34	0.31	0.32	0.29
Fe	1.58	1.54	1.83	1.57	1.87	1.46	1.68	1.94	3.64	3.19	3.01	3.00	2.97	2.92	2.87
Cu	-	-	0.36	0.45	-	-	0.07	0.18	-	0.12	0.19	-	0.13	0.11	0.20
O	55.35	55.98	52.89	54.11	56.07	53.01	54.86	57.63	61.08	61.29	61.44	61.19	61.21	61.29	61.39

Figure 5.6 shows a scattergram comparing the relative concentrations of calcium (analogous to carbonate) and silica (analogous to quartz and biogenic silica) between all the grab samples and filter papers that underwent EDX analysis for the trade wind survey. There are two distinct groupings within the plot. The samples from Turnagain Island show high calcium and low silica, the samples from Saibai Island have high silica and low carbonate. This is inferred to be a result of the influence of turbid waters from rivers on the south coast of Papua New Guinea bringing terrigenous sediment into northern Torres Strait, although this measurement can be misleading as it does not differentiate between biogenic silica (e.g., diatoms) and quartz (see section 5.3.1.6).

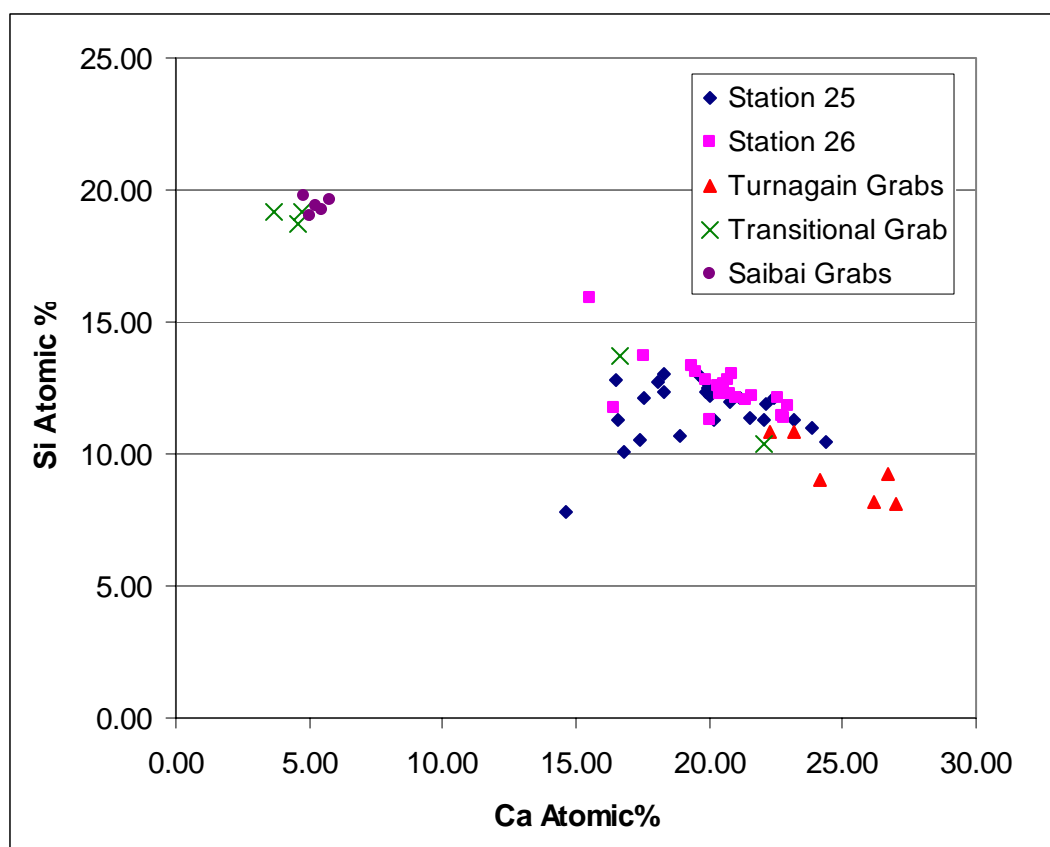


Figure 5.6 Scattergram of EDX analysis of grab samples and filter papers comparing calcium and silica compositions

Figure 5.7 shows a scattergram comparing the relative concentrations of calcium (analogous to carbonate) and aluminium (analogous to clay) between all the grab samples and filter papers that underwent EDX analysis for trade wind survey. Again there are two distinct grouping within the plot. Samples from the Turnagain Island region have low aluminium and high calcium and the samples from Saibai Island have high aluminium and low calcium. These results suggest that both the grab samples and filter papers from the Turnagain Island region not only have a very similar composition but that the sediments are highly calcareous and locally derived, the sediment from Saibai Island have a strong terrigenous component indicated by the high concentration of aluminium and silica. The terrigenous component is likely to be sourced from rivers on the southern coast of Papua New Guinea. The low terrigenous component of the Turnagain Island filter papers and grab samples indicates that turbid plumes such as rivers are unlikely reach as far south as Turnagain Island.

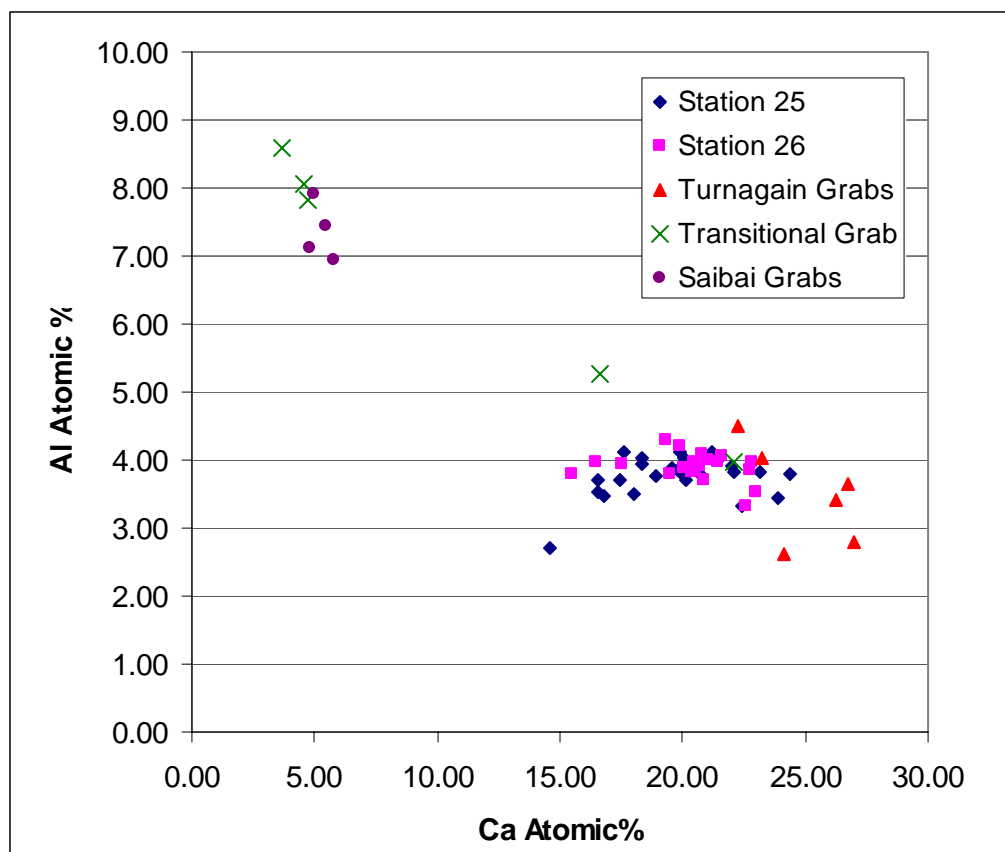


Figure 5.7 Scattergram of EDX analysis of grab samples and filter papers comparing aluminium and calcium compositions

The chemical compositions of the filter papers from stations 25 and 26 are subtly different from the grab samples (Table 5.7). Although stations 25 and 26 are located within Areas A and B (where the grab samples were sourced) they have a significantly lower concentration of Ca and increased levels of Si. It is possible that diatoms in the water column may be biasing these results and further analysis of the silica compositions is needed. The Al component of the filter papers and grabs remain similar and hence suggests there is no significant difference in the clay component when using the two sampling methods.

Table 5.7. Average chemical composition of filter papers from stations 25 and 26 and grab samples in the vicinity of Turnagain Island.

	Average % Ca	Average % Si	Average % Al
Station 25	19.75	11.64	3.76
Station 26	20.35	12.50	3.90
Grab samples	24.93	9.37	3.50

#### 5.3.1.5 Biological content of the water samples

The very small size fraction of the samples (0.45  $\mu\text{m}$ ) prevented detailed analyses of the biological forms present through a regular light microscope. However, several major groups of organisms have been easily recognised.

Diatoms are by far the most abundant organisms in the samples. These siliceous unicellular algae are present with specimens of both Centrales and Pennales orders, although centric diatoms are more numerous. The presence of both orders is justified by the fact that pennate diatoms thrive in benthic marine habitats, while centric diatoms thrive as plankton in marine waters. Diatoms spicules are also extremely abundant at all locations.

Foraminifera are present in limited numbers and with mostly benthic forms, generally Miliolida and Textularia, although juvenile planktonic specimens of the *Globigerinidae* Family have also been rarely detected.

Other well-recognisable groups present with less frequency are juvenile pteropods (planktonic - all of the *Limacinidae* Family) and juvenile ostracods (benthonic).

Other particles of biological origin are mostly fragments of bivalves, corals and gastropods, although many of the fragments are too small to be unequivocally recognised.

The size fractions of the samples also made any attempt to quantitatively estimate the different biota unreliable. In general, the samples are much richer in organic content than in terrigenous particles in a proportion of about 3 to 1.

#### 5.3.1.6. SXAM - X-ray fluorescence results

[Figs. 5.8](#) and [5.9](#) summarise the results obtained for Ca, Si, Fe and Al which are the most variable elements in the samples (lighter colours in the pictures indicate higher concentrations of an element). When comparing the mud fraction of the two samples, 08GRVV08 (northwest of Turnagain Island) appears to be very rich in calcium and the silicon detected is mostly of organic origin as diatom spicules are common in the sample ([Fig. 5.8c](#)), on the other hand, the sample is relatively poor in iron and aluminium in comparison to 11GRVV11 where the silicon appears mostly in the form of quartz. A very similar result has also been obtained for the sand fraction of the two samples ([Fig. 5.9](#)) where the visualisation of single grains is made easier by the increase in grain size.

In conclusion, sample 11GRVV11 has higher concentrations of terrigenous material (both clay and quartz) than sample 08GRVV08, which appears to be mostly organic in composition. The increased amount of silicon detected in sample 11GRVV11 though the EDX analysis is due to the presence

of quartz sourced from rivers on the south coast of Papua New Guinea, as the diatom content, also quantified through initial visual inspection, is very similar to that detected for sample 08GRVV08.

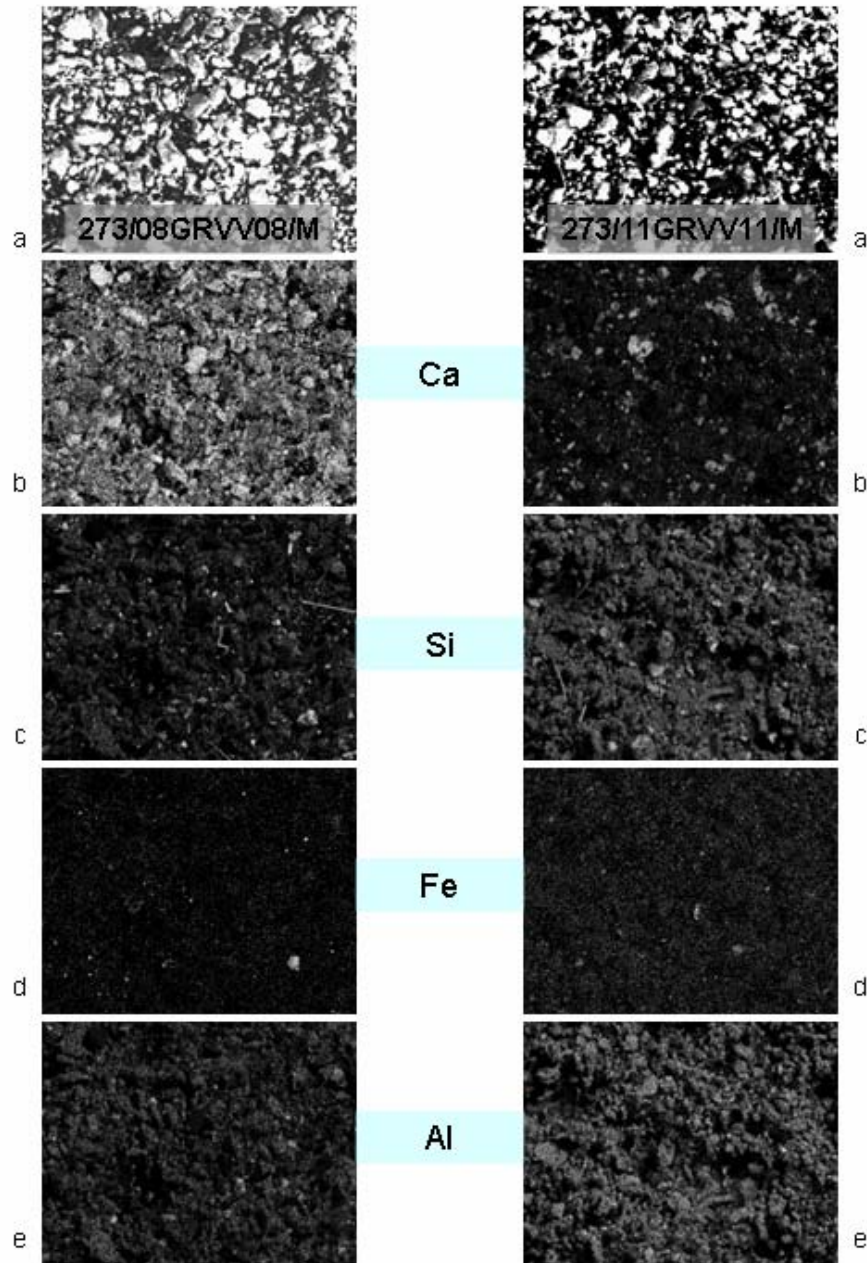


Fig. 5.8. Summary of the SXAM-XRF images obtained for the mud fraction of samples 273/08GRVV08 (left column) and 273/11GRVV11 (right column). Lighter colours indicate a higher concentration of the element. a) original SEM images or secondary images; b) intensity maps of calcium; c) intensity maps of silicon; d) intensity maps of iron; e) intensity maps of aluminium.

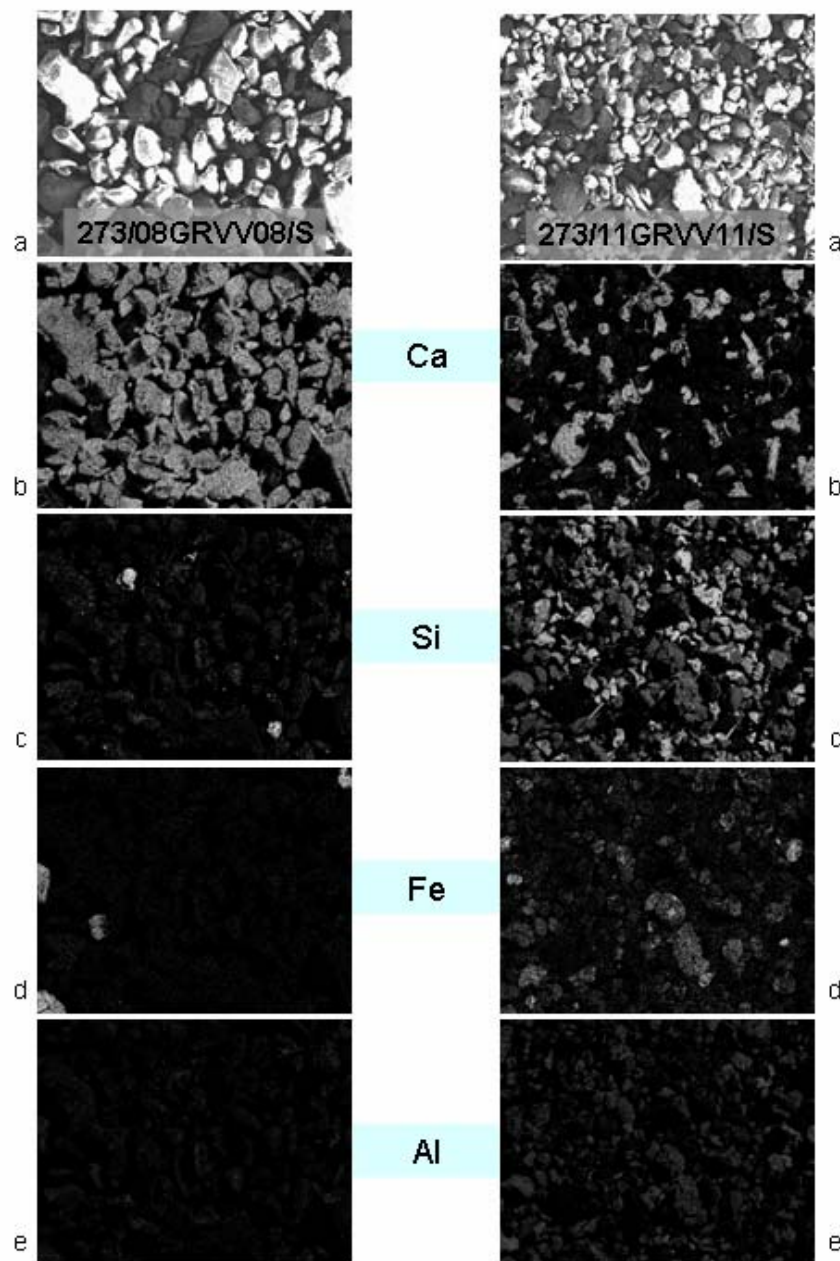


Fig. 5.9. Summary of the SXAM-XRF images obtained for the sand fraction of samples 273/08GRVV08 (left column) and 273/11GRVV11 (right column). Lighter colours indicate a higher concentration of the element. a) original SEM images or secondary images; b) intensity maps of calcium; c) intensity maps of silicon; d) intensity maps of iron; e) intensity maps of aluminium.

### 5.3.2. Digital Video Footage

Locations of underwater video stations are found in [figures 5.1a-e](#).

#### 5.3.2.1. Area A 24 hour station (Station 25 - neap tide)

Area A is dominated by seagrass and/or algae habitats. The amount of habitat cover throughout the video footage for Station 25 is typically > 50% (example shown in [Fig. 5.10a](#)). Strong currents were inferred to be present during the 24 hour station by observing the motion of the biota on the seabed (specifically 09:08 – 18:08). Little bedload transport was observed due to the high degree of coverage supplied by the seagrass and algae.

#### 5.3.2.2. Area A 24 hour station (Station 37 - spring tide)

The habitats observed in Area A during the spring tide were not appreciably different to the habitats observed during the neap tide. Habitats dominated by algae and/or seagrass were observed and coverage was again typically > 50% (example shown in [Fig. 5.10c](#)). No bedload transport was observed during station 37 specifically due to the high degree of cover by benthic biota. Moderate currents are observed at many stations by the movement of benthic biota.

#### 5.3.2.3. Area B 24 hour station (Station 26 - neap tide)

Area B appears to lack any significant coverage of algae or seagrass (see 273\_26CAM09\_0608.mov in Appendix B for example). The rippled substrate indicates that the area is undergoing mobilisation by currents ([Fig. 5.10b](#)). Bedload transport was observed in many of the camera stations though it is generally weak (often non-existent). Strong bedload transport was observed at 2:00, 3:00, 11:00, 15:00, 16:00, 17:00 (GMT). The periods of strong bedload transport are approximately 12 hours apart and coincident with the strongest ebb and flood currents. Bedload transport (and turbidity) in response to tidal currents was also observed in the Seabird-19 sensors at stations 02CM07 and 06CM06. Suspended sediment concentration observed over 24 hours (section 5.3.1) was not observed to follow this trend, possibly due to the influence of wave activity.

#### 5.3.2.4. Area B 24 hour station (Station 36 - spring tide)

Similar to Station 26, Station 36 was a rippled sandy substrate (example shown in [Fig. 5.10d](#)). There does, however, appear to be a coarse, gravelly, lag between many of the ripples. Bedload transport fluctuates throughout the video footage with peaks bedload transport occurring at 14:00, and 20:00 to 23:00. From 23:00GMT, very strong unidirectional bedload transport occurs,

but by 00:00GMT this bedload transport had dropped off significantly. Similar to station 26, Area B lacks any significant coverage of algae or seagrass (see 273\_36CAM13\_0708.mov in [Appendix B](#) for example).

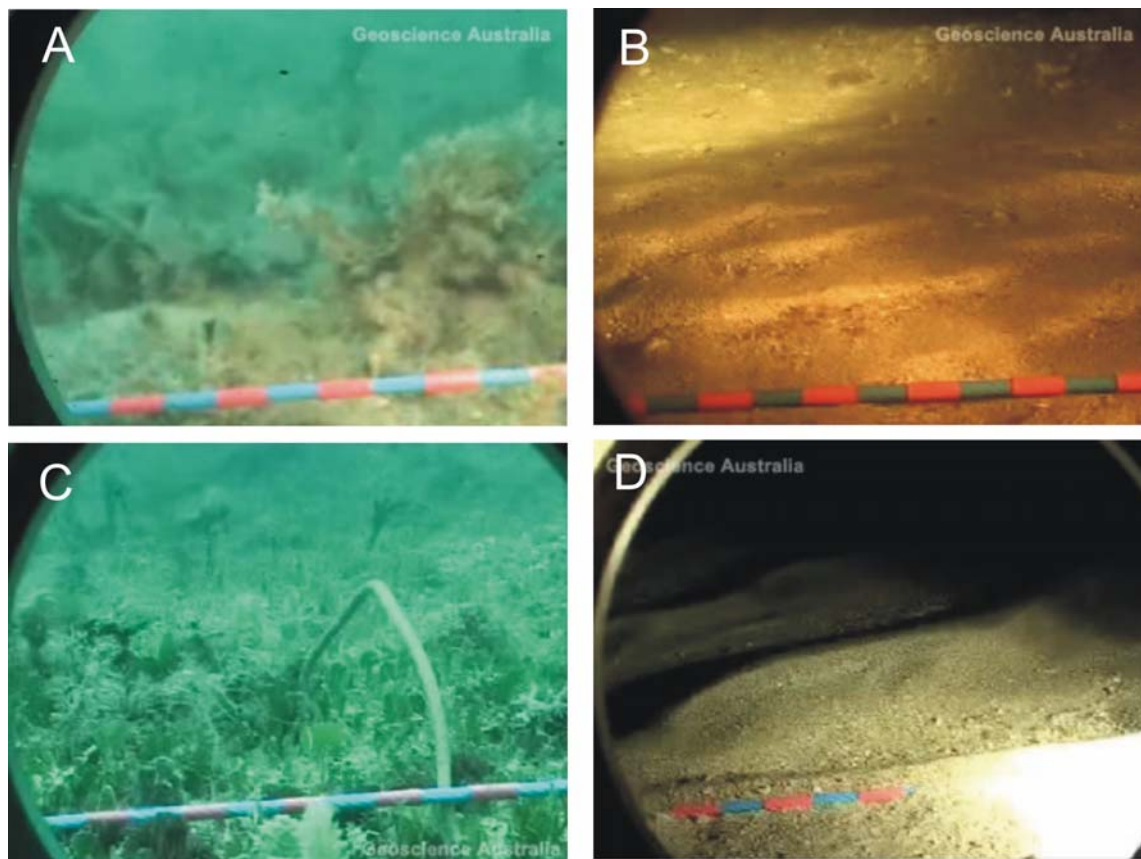


Figure 5.10. a) Screenshot of video footage showing algae dominated substrate from Area A (273\_25CAM8\_0108.mov). b) Screenshot of video footage showing a sandy, rippled substrate from Area B (273\_26CAM9\_1708.mov). c) Screenshot of video footage showing algae and seagrass substrate from Area A (273\_37CAM14\_0108.mov). A sea whip is observed in the centre of the image. d) Screenshot of video footage showing a sandy, rippled substrate from Area B (273\_36CAM13\_1308.mov)

### 5.3.2.5. Other Stations

Stations 1-7, 10-12 and 15 showed a variety of benthic habitats ranging from bare seabed with gravelly, or sandy substrates to a thick cover of seagrass and algae. All the sites except 3-5, 7, 10-12 showed the presence of either seagrass or algae. Station 15, in the vicinity of Numar Reef had the most complete coverage of benthic biota (~100%) dominated by seagrasses and algae.

### 5.3.3. Surface Sediments

#### 5.3.3.1. Area A sediment samples

Only four sediment samples were recovered from Area A, three of these samples were from the core catcher of the vibro-core (Fig. 5.11). All samples were sandy or gravelly sands and had high concentrations of carbonate (Table 5.8). The presence of bedforms in the multibeam bathymetry indicates that there are strong tidal currents present in the region. The strong current would prevent the settling of fine sediment and this is reflected in the gravel, sand, and mud percentages Table 5.8).

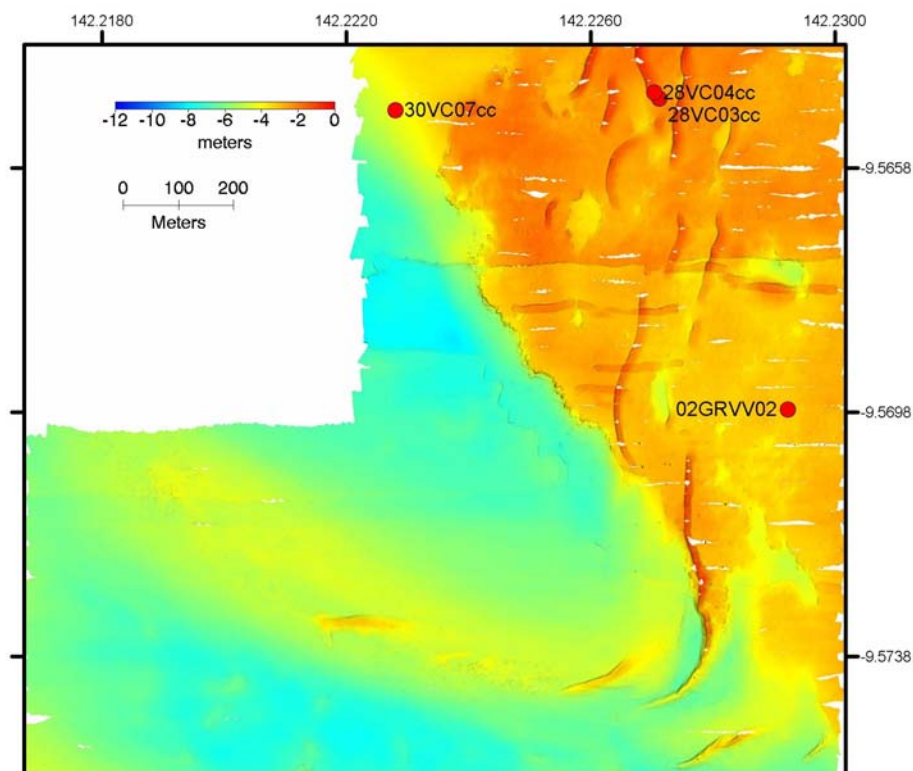


Figure 5.11. Map showing sediment sample locations for Area A (including any core catcher samples)

Table 5.8. Compositions of sediment samples from Area A.

Grab	%Gravel	%Sand	%Mud	CaCO <sub>3</sub> %Bulk	CaCO <sub>3</sub> %Gravel	CaCO <sub>3</sub> %Sand	CaCO <sub>3</sub> %Mud
273/28VC3cc	41.27	56.63	2.10	96.32	90.00	95.81	*
273/29VC4cc	25.45	68.13	6.42	91.25	90.00	96.83	75.01
273/30VC7cc	6.12	86.31	7.58	88.20	85.00	91.75	76.53
273/02GRVV02	23.12	67.90	8.98	85.16	70.00	94.29	65.88

\* insufficient sample size for analysis

### 5.3.3.2. Comparison with Monsoon survey (Area A)

The composition of seabed sediment from Area A is consistent between the monsoon and trade wind surveys based on the concentrations of gravel, sand, and mud. Fig. 5.12 compares all sediment samples acquired in Area A for both surveys. The samples are dominantly gravelly sands with a minor (typically <10%) amounts of mud.

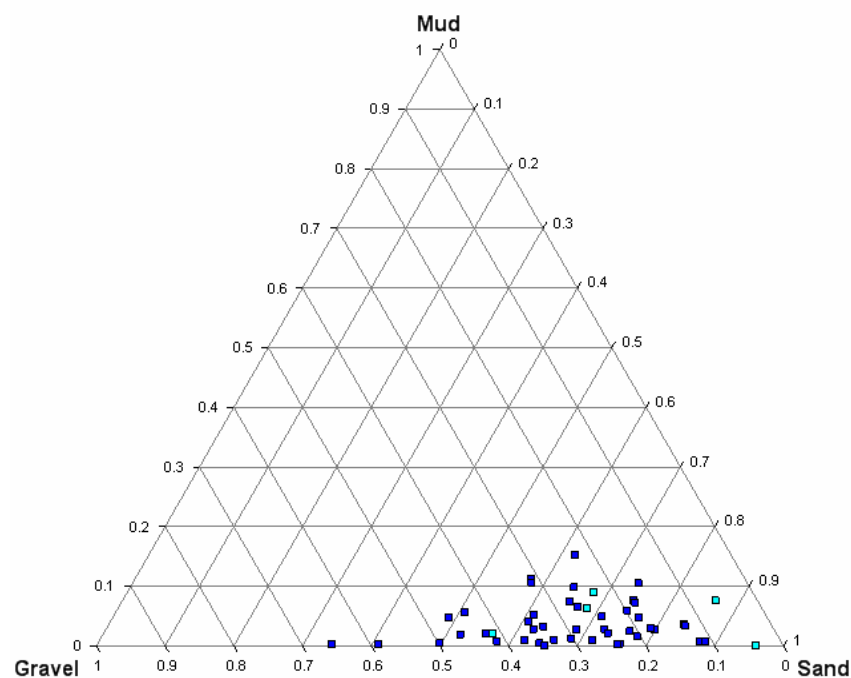


Figure 5.12. Ternary diagram of bulk sediment compositions from Area A. Trade wind season samples are light blue, monsoon samples are dark blue

### 5.3.3.3. Area B sediment samples

A total of six sediment samples were acquired from Area B (Fig. 5.13). Samples 03GRVV03 and 06GRVV06 are both located off the sandbank and stand out from the other four with respect to their composition (Table 5.9). Both 03GRVV03 and 06GRVV06 have a much higher gravel content (59% and 54%, respectively) than the other grabs and may represent a coarse gravel lag between the large sandbanks in Torres Strait. The fine sediments are either transported out of the area by tidal or wind driven currents or trapped within the numerous sandbanks in the region. The other sediment samples acquired within Area B have a higher sand content and lower gravel content than samples located off the bank. All sediments have a low mud content (typically < 2%) and a high  $\text{CaCO}_3$  content (typically > 75%).

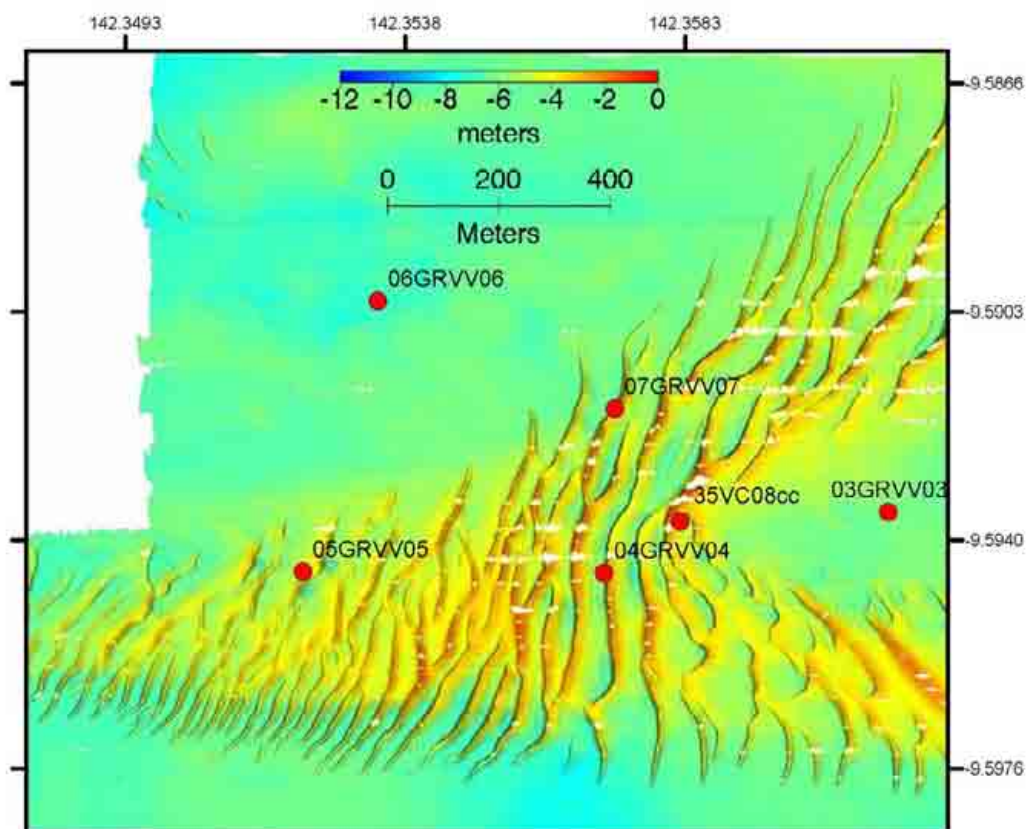


Figure 5.13. Map showing sediment sample locations for Area B

Table 5.9. Compositions of sediment samples from Area B

Grab	%Gravel	%Sand	%Mud	CaCO <sub>3</sub> %Bulk	CaCO <sub>3</sub> %Gravel	CaCO <sub>3</sub> %Sand	CaCO <sub>3</sub> %Mud
273/35VC8cc	29.17	70.26	0.57	80.59	95.00	90.23	*
273/03GRVV03	58.84	40.91	0.25	93.28	90.00	94.29	*
273/04GRVV04	18.38	81.42	0.19	79.07	80.00	86.17	*
273/05GRVV05	11.54	88.44	0.02	75.22	75.00	75.01	*
273/06GRVV06	53.79	43.86	2.35	86.68	85.00	93.28	69.94
273/07GRVV07	38.66	61.20	0.14	79.58	80.00	82.62	*

\* insufficient sample size for analysis

#### 5.3.3.4. Comparison with Monsoon survey (Area B)

The composition of sediment samples from Area B are consistent through the trade wind and monsoon surveys. Fig. 5.14 compares all the sediment samples acquired in Area B throughout both survey seasons. Samples are dominantly gravelly sands to sandy gravels with very little mud (typically <2%). Samples from Area B are coarser than Area A (Fig. 5.12) and have less mud. Sediment samples from the sandbank in Area B are probably well winnowed due to tidal currents hence the lack of mud in any of the grab samples.

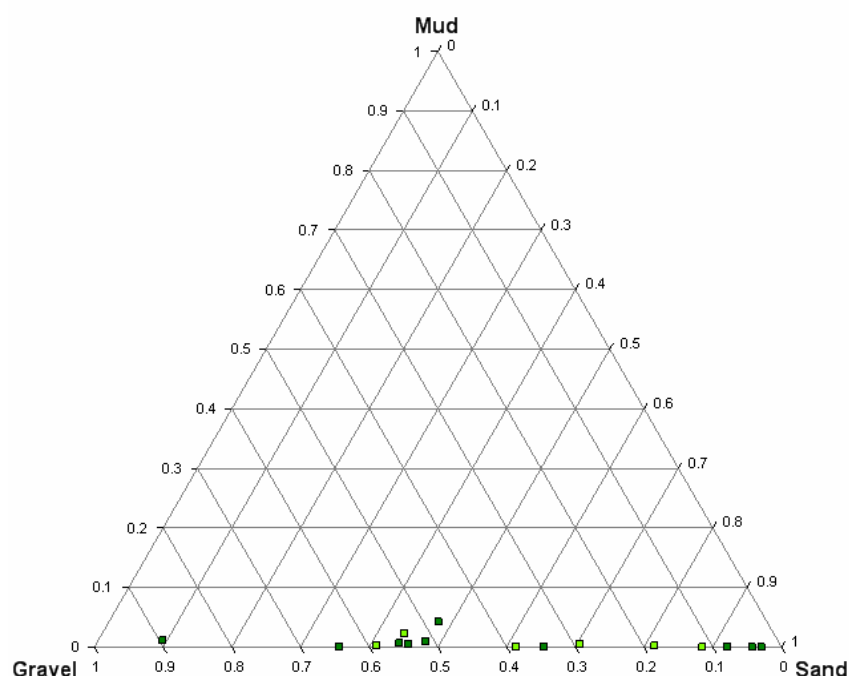


Figure 5.14. Ternary diagram of bulk sediment compositions of sediment samples from Area B. Trade wind survey samples are dark green, monsoon survey samples are light green

### 5.3.3.5. Transect from Turnagain Island to Saibai Island

Five sediment samples were collected in a transect between Turnagain Island and Saibai Island to determine the location of the transition zone between terrigenous dominated and carbonate dominated sediments (Fig. 5.15). The composition of the sediment samples is presented in Table 5.10 and shows the sediments range from mud dominated (11GRVV11) to gravel-dominated (12GRVV12). The bulk  $\text{CaCO}_3$  shows the transition of terrigenous-dominated sediment ( $<50\% \text{CaCO}_3$ ) to occur between samples 09GRVV09 and 10GRVV10 and closest to and south of 10GRVV10 with its bulk percentage of  $\text{CaCO}_3 = 45.58\%$ . Carbonate dominated sediment occurs to the southwest of the dashed line in Fig. 5.18, terrigenous dominated sediment occurs to the north east.

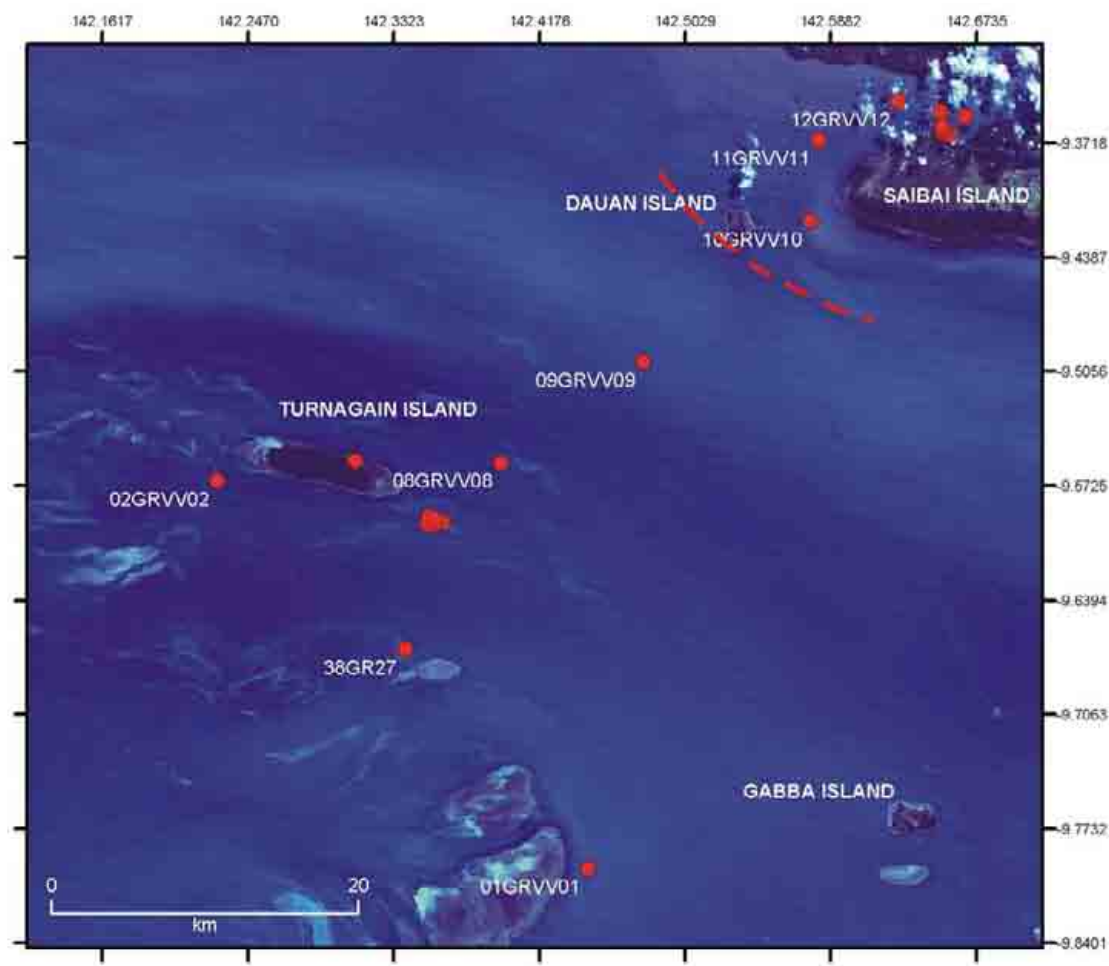


Figure 5.15. Regional scale location map for sediment samples acquired during the trade wind survey. Samples 08GR08-12GR12 are samples collected within a transect from Turnagain Island to Saibai Island to determine the location of a transition zone of terrigenous sediments to carbonate dominated sediments. The dashed line shows the approximate location of the transition zone from carbonate/terrigenous dominated sediment.

Table 5.10. Sediment compositions of samples collected in a transect from Turnagain Island to Saibai Island.

Grab	%Gravel	%Sand	%Mud	CaCO <sub>3</sub> %Bulk	CaCO <sub>3</sub> %Gravel	CaCO <sub>3</sub> %Sand	CaCO <sub>3</sub> %Mud
273/08GRVV08	43.62	55.91	0.48	59.79	70.00	77.04	*
273/09GRVV09	34.81	63.87	1.32	78.06	90.00	80.08	*
273/10GRVV10	37.34	42.35	20.31	45.58	75.00	46.09	13.11
273/11GRVV11	12.75	40.64	46.61	28.84	55.00	29.35	19.20
273/12GRVV12	42.83	34.68	22.49	38.48	70.00	38.99	15.14

\* insufficient sample size for analysis

### 5.3.3.6. Saibai Island

A total of 12 sediment samples were acquired from around Saibai Island to compare their carbonate and grainsize compositions to the sediment samples from around Turnagain Island (Fig. 5.16). Saibai Island is located in a region that is in close proximity to and probably influenced by runoff from rivers on the south coast of Papua New Guinea. The sediments from around Saibai Island are typically sandy mud and muddy sand. The mud content of the samples has a strong terrigenous component with only two samples having a CaCO<sub>3</sub> content > 20% (Table 5.11). The sand and gravel components of the samples typically have a greater proportion of CaCO<sub>3</sub> than the mud fractions.

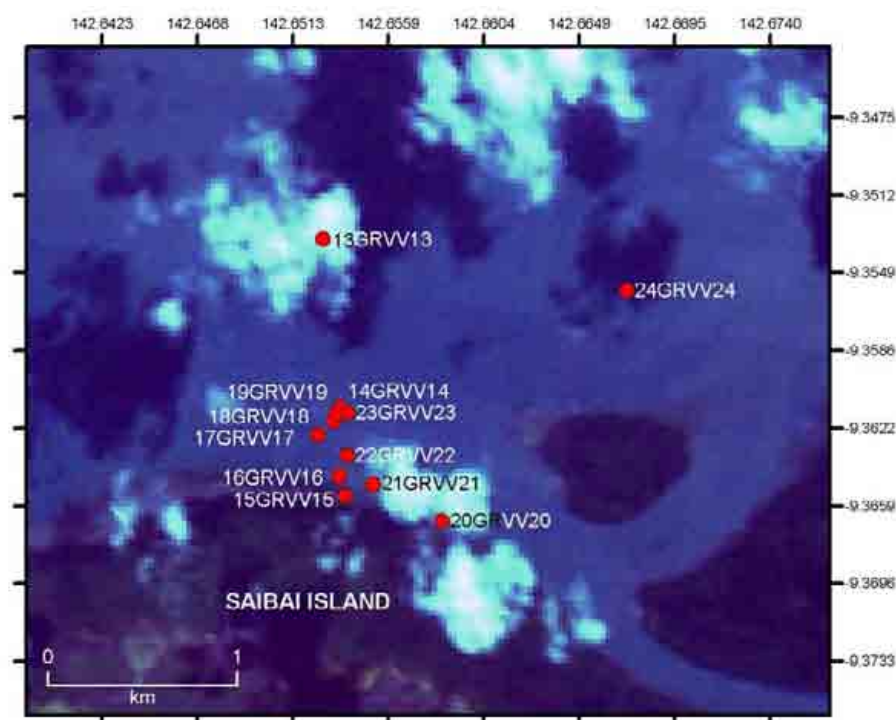


Figure 5.16. Sediment sample location for Saibai Island

Table 5.11. Compositions of sediment samples from Saibai Island.

Grab	%Gravel	%Sand	%Mud	CaCO <sub>3</sub> %Bulk	CaCO <sub>3</sub> %Gravel	CaCO <sub>3</sub> %Sand	CaCO <sub>3</sub> %Mud
273/13GRVV13	14.41	52.35	33.25	38.99	70.00	42.54	18.19
273/14GRVV14	0.51	34.76	64.73	21.23	80.00	27.32	21.23
273/15GRVV15	0.29	74.52	25.19	12.10	80.00	11.09	13.62
273/16GRVV16	0.41	33.03	66.56	19.71	80.00	25.29	21.23
273/17GRVV17	6.40	63.70	29.90	26.81	75.00	31.38	18.19
273/18GRVV18	2.87	53.99	43.15	29.35	80.00	27.32	19.20
273/19GRVV19	1.32	44.33	54.35	23.26	75.00	26.31	19.20
273/20GRVV20	1.66	49.88	48.45	18.19	10.00	15.14	14.13
273/21GRVV21	0.19	30.20	69.61	20.72	90.00	24.28	18.19
273/22GRVV22	3.00	54.59	42.41	24.28	70.00	27.32	18.19
273/23GRVV23	0.47	43.82	55.71	22.25	80.00	24.28	19.20
273/24GRVV24	47.04	37.97	14.98	46.60	60.00	40.00	15.65

### 5.3.3.7. Saibai Island comparison

EDX analysis indicates that there is a strong contrast between the chemical compositions of sediments from Saibai and Turnagain Island with the presence of terrigenous clays in higher concentrations around Saibai Island (Fig. 5.7). The process of contrasting the composition of sediment samples from Saibai Island with the other samples collected during the trade wind and monsoon surveys is aimed at gauging the influence of terrestrial (riverine) sources on the sediments in northern Torres Strait. Figure 5.17 compares the gravel, sand, and mud compositions of all the grab samples acquired during both trade wind and monsoon surveys. Samples acquired in the vicinity of Saibai Island are coloured red for comparison. The samples acquired from Saibai Island have a much higher mud content (14%-69% with an average of 42%) than all other sample (typically less than 10% mud). As expected, the samples from the transect between Turnagain and Saibai Islands have a range of mud content values from 47%-<1% (Fig. 5.17, Table 5.10).

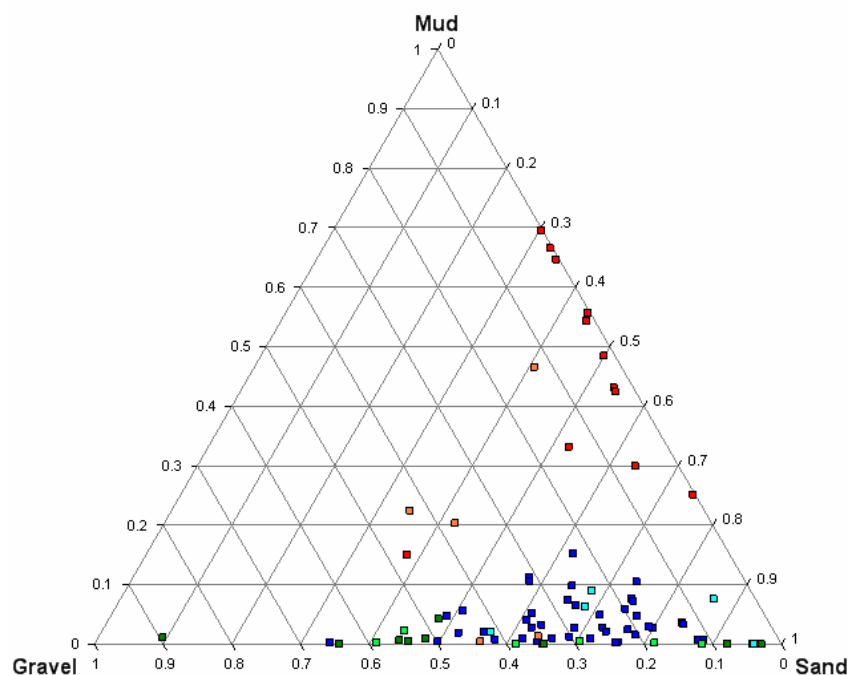


Figure 5.17. Ternary diagram of bulk sediment compositions of sediment samples from Area A (trade wind = light blue, monsoon = dark blue), Area B (trade wind = dark green, monsoon = light green), Saibai Island (red), and transect from Turnagain to Saibai Island (orange).

The samples from the Saibai Island region stand out from all the other samples. The low carbonate content for the mud fraction within the Saibai Island grabs (12-22%) indicates a strong terrigenous influence (Fig. 5.18). All the other sediment samples, though having a minor mud component, have carbonate composition of between 65% and 78%. The higher carbonate content indicates that although there is mud from terrigenous sources it is only a fraction of what is found closer to the Papua New Guinea coast.

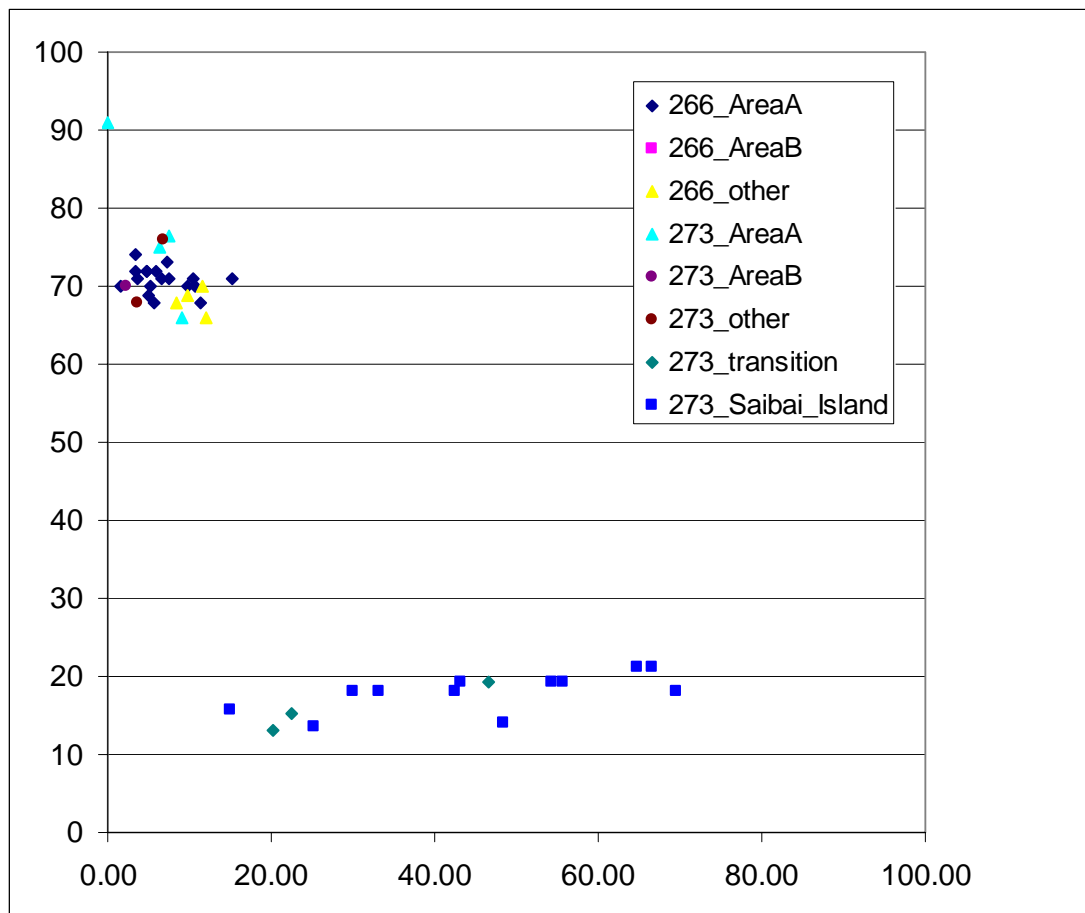


Figure 5.18. comparison of sediment sample collected during surveys 266 and 273. A plot of % mud versus %  $\text{CaCO}_3$  (within the mud fraction) is used to differentiate sediment in the Saibai Island region.

#### 5.3.3.8. Other Sediment samples

A total of 4 other sediment samples were acquired during survey 273 (Figs. 5.15 and 5.19). These samples were not located in vicinity of Area A, Area B, or Saibai Island. They are gravelly sands with a high  $\text{CaCO}_3$  content (see table 5.12). The sediment composition is typical for sediments in Area's A and B.

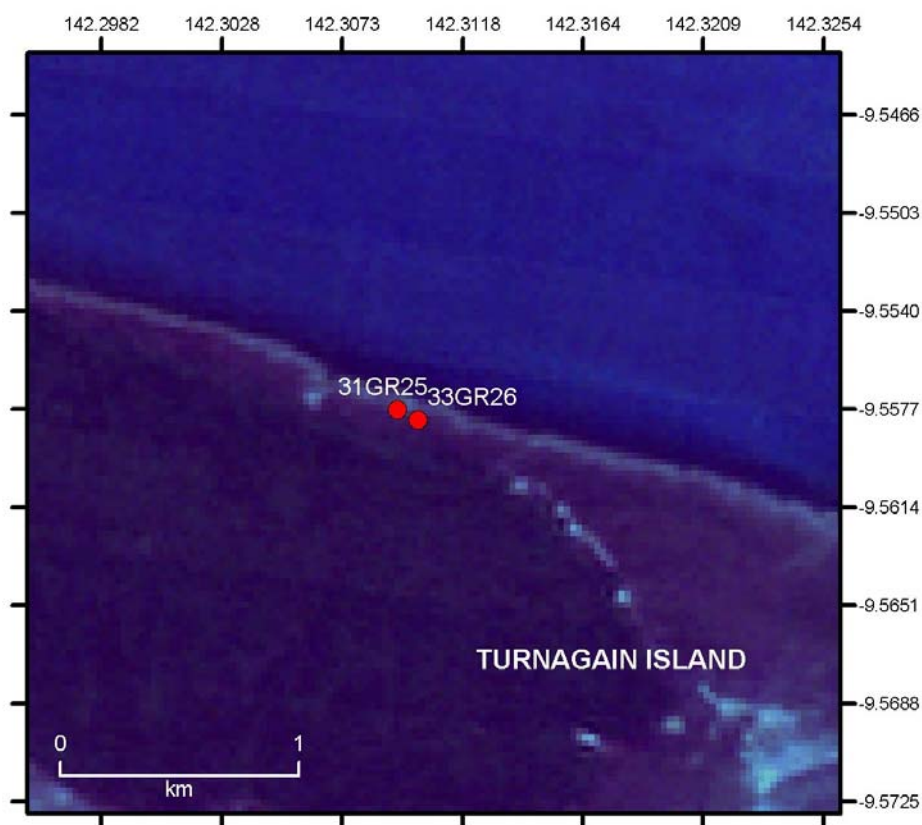


Figure 5.19. Grab sample locations from the northern margin of Turnagain Island.

Table 5.12. Sediment compositions of miscellaneous sediment samples in Torres Strait (sample locations are found in Figs. 5.15 and 5.19)

Grab	%Gravel	%Sand	%Mud	CaCO <sub>3</sub> %Bulk	CaCO <sub>3</sub> %Gravel	CaCO <sub>3</sub> %Sand	CaCO <sub>3</sub> %Mud
273/01GRVV01	36.19	56.96	6.85	78.06	80.00	82.11	76.03
273/31GR25	13.67	84.31	2.02	75.01	90.00	87.19	insufficient
273/33GR26	25.35	72.33	2.31	91.75	90.00	93.78	insufficient
273/38GR27	18.99	77.33	3.68	87.19	75.00	93.28	67.91

#### 5.3.4. Sub-surface Sediments

A total of 8 vibrocores and 3 push cores were recovered during the survey (Table 5.13, Fig. 5.1a-e). The gravelly texture of the sediments made vibrocoreing difficult and as a result the longest core recovered was only 1.06 meters. Key statistics from the multisensor core logger are presented in table 5.14 though the often disturbed nature of the core material made many of the core log measurements inaccurate. The complete core logs are presented in Appendix C.

Table 5.13. Details of vibrocores recovered during the survey.

Core	Latitude	Longitude	Location	Water Depth (m)	Length
27VC01	-9° 35.749S	142° 21.325E	top of sandwaves - Area B	5.8	0.25
27VC02	-9° 36.764S	142° 21.339E	top of sandwaves - Area B	6.0	0.54
28VC04	-9° 33.874S	142° 13.622E	top of sandwaves - Area A	3.0	0.53
28VC05	-9° 33.888S	142° 13.581E	top of sandwaves - Area A	3.5	0.12
29VC06	-9° 33.857S	142° 13.622E	top of sandwaves - Area A	3.0	0.76
30VC07	-9° 33.891S	142° 13.368E	central channel – Area A	7.2	1.06
32PK01	-9° 33.515S	142° 18.572E	north margin Turnagain Is.	Intertidal	0.32
33PK02	-9° 33.487S	142° 18.609E	north margin Turnagain Is.	Intertidal	0.37
34PK04	-9° 33.488S	142° 18.609E	north margin Turnagain Is.	Intertidal	0.15
35VC09	-9° 35.609S	142° 21.496E	top of sandwaves - Area B	3.0	0.6
36VC10	-9° 35.727S	142° 21.466E	top of sandwaves - Area B	4.0	0.45

Table 5.14. Statistics of geophysical parameters from multi-sensor core logger.

Core	Ave P-wave velocity m s <sup>-1</sup>	Max P-wave velocity m s <sup>-1</sup>	Min P-wave velocity m s <sup>-1</sup>	Ave Bulk Density g c <sup>-3</sup>	Max Bulk Density g c <sup>-3</sup>	Min Bulk Density g c <sup>-3</sup>	Ave Magnetic susceptibility CGS	Max Magnetic susceptibility CGS	Min Magnetic susceptibility CGS	Ave Fractional Porosity	Max Fractional Porosity	Min Fractional Porosity
27VC01	1318.17	1468.71	1106.50	2.23	2.50	1.86	0.87	1.40	0.20	0.30	0.52	0.14
27VC02	1744.43	1867.15	1359.39	1.62	1.73	1.10	0.67	1.20	0.30	0.64	0.95	0.58
28VC04	1660.95	2119.50	1406.84	1.23	1.51	1.03	0.20	0.60	0.00	0.87	0.99	0.71
28VC05	1462.88	1716.69	1023.43	-	-	-	-	-	-	-	-	-
29VC06	1543.74	1732.19	1327.01	1.16	1.24	1.03	-	-	-	0.92	0.99	0.87
30VC07	1648.79	2108.38	1648.79	1.28	1.46	1.06	1.20	3.60	0.00	0.84	0.97	0.74
32PK01	1980.79	2430.07	1641.78	1.76	1.82	1.70	-	-	-	0.56	0.60	0.53
33PK02	1798.92	2253.09	1312.56	2.13	2.43	1.62	-	-	-	0.35	0.65	0.18
34PK04	1643.75	2169.73	1442.92	1.60	1.89	1.34	0.17	0.30	0.0	0.66	0.81	0.49
35VC09	1665.92	1873.29	1432.11	1.48	1.54	1.23	0.74	1.60	0.10	0.73	0.87	0.69
36VC10	1820.22	1876.47	1506.03	1.52	1.56	1.31	0.83	2.00	0.10	0.71	0.83	0.68

#### **5.3.4.1. Cores from Area A**

Two different sedimentary environments were recorded in the cores from Area A. 28VC04, 28VC05 and 29VC06, were all taken from the tops of sandwaves whilst 30VC07 was taken from the side of the central channel in Area A. The core lengths ranged from 0.12 to 1.06 m. The three cores from the sandwaves were typically calcareous gravels. 28VC04 shows changes in sediment texture though the core showing two fine sequences of medium, and coarse sand. 20VC05 also shows a fine sequence at its base whilst 29VC06 is gravelly throughout. By comparison the core from the channel (30VC07) consisted of poorly sorted, calcareous, muddy, medium sand. The fine nature of the sediment within the channel indicates that the channel itself acts as a local sink for fine sediment being transported off the surrounding reef. The coarser sediment is trapped in the sandwave on the reef.

#### **5.3.4.2. Cores from Area B**

The four cores from Area B (27VC01-02, 35VC09, 36VC10) were all from the crests of large sandwaves near the centre of the sandbank ([Fig. 5.1b](#)) and ranged in length from 0.25 to 0.60 m. The cores were typically poorly sorted, calcareous, coarse sands with a mixture of relict and modern material. Very little variation in sediment texture is observed down the cores though there are occasional bands of lighter coloured material, or coarser, gravelly material.

#### **5.3.4.3. Cores from Turnagain Island**

Three push cores were taken from the northern margin of Turnagain Island (32PK01, 33PK02, 34PK03), ranging in length from 0.15 to 0.37 m. 32PK01 had the coarsest sediment of the three cores and consisted of poorly sorted calcareous gravel with minor amounts of calcareous rubble. 33PK02 consisted of poorly sorted, muddy, coarse sand with occasional coral clasts. 34PK03 consisted of a poorly sorted, muddy, fine to medium sand with occasional coral clasts. A thin band of organic rich material from 0.05-0.07 m is also present in 34PK03.

## **6. Discussion and Summary**

The trade wind survey (survey 273) was largely considered a successful survey as it managed to fulfil all of its key research objectives.

These objectives were:

- Resurvey the key study areas from survey 266 (namely Areas A and B) using multibeam sonar
- Successful deployment of current meters and oceanographic moorings
- Acquisition of sediment samples from the Saibai Island region to compare against samples acquired from Turnagain Island
- Successful acquisition of vibro-cores
- Acquisition of Filter Papers and video data for 24 hour stations

The survey also provided a key insight in to how oceanographic processes changed between the monsoon and trade wind seasons (surveys 266 and 273). It is this comparison between the two surveys that provides the most information on the long term stability of sand dunes, sandbanks and benthic habitats.

### **6.1 Key comparisons and conclusions for the monsoon and trade wind seasons**

#### **6.1.1. Sandwave mobility**

The monsoon and trade wind surveys have given key insights into the stability of habitats in Torres Strait. Multibeam surveys have shown that areas of Torres Strait that contain sandwaves are highly dynamic and are prone to rapid changes in morphology over short time periods (i.e spring/neap cycles).

Contrasts were observed between the migration rates and directions of the sandwave crests between the two surveys (figs. 2.3 and 2.4). The monsoon survey was characterised by strong westward migration of sandwave crests, up to 16 m in Area A. The trade wind survey, in contrast, had much lower overall migration, 4 m at a maximum and in both east and west directions.

As the wind and wave conditions were similar for both the trade wind and monsoon seasons the obvious differences in crest migration appears to be counterintuitive. The mechanism by which these differences can be explained relates to the orientation of the sandwaves. It is known that at the beginning of monsoon survey the sandwaves were facing the east because of the net eastwards flow through Torres Strait during the monsoon season (Heap et al., 2005). As the monsoon survey measured the onset of the trade wind season the eastward facing sandwave were acted upon by flows forced by the south-east trade winds. Hence the sandwaves that were hydrodynamically stable during the monsoon became unstable with the change in seasons (and the associated change in hydrodynamics). Once the sandwaves became unstable with the onset of the trade wind season an increased rate of reworking and migration was observed to compensate for orientation of the sandwaves. Hence, the crests of the east facing sandwaves migrated to the west. Although there were similar flow conditions experienced during the trade wind survey the sandwaves were already in a hydrodynamically stable configuration and hence very little crest migration was observed.

These results would indicate that the greatest rates of sand dune crest migration will occur at the transition between the seasons. Harris (1989, 1991) noted that sandwaves in Adolphus Channel in the south east of the Torres Strait reverse their orientations with the seasonal changes in hydrodynamics. The data presented in [section 2](#) of this report would suggest that not only do the sandwaves in the vicinity of Turnagain Island behave in a similar way but the rate of reversal appears to be rapid. Once the sandwaves have changed their orientation to suit the new hydrodynamic regime, the migration of the sandwave crests diminishes as it has reached a new equilibrium (highlighted in [section 2.3.3](#)). The relative magnitudes of the monsoon and trade wind currents hence play an important role in the migration of sandwave throughout Torres Strait. For example a weak monsoon could prevent the sandwaves from reversing at the end of the trade wind season and allow for a greater net displacement in the sandwaves over that year and potentially impact on seagrass communities.

Changes in the positions of the sandwaves in Area A between the surveys (approximately 6 months) was measured at ~50 m ([Fig. 2.5](#)). This result indicates that although the sandwaves can moved rapidly over a short time period (eg. 16 m over 14 days) in response to the transition from the monsoon to the trade wind season their migration during typical trade wind conditions is ~8 m per month (comparable to measurements made over 14 days in [section 2.3.3](#)). The change in position of the sandbank in Area B over 6 months was also measured. Only the northeast arm of the bank appeared to have changed position between the surveys (by ~15 m). Similar to Area A, the bank itself appears to be stable over long periods of time regardless of the activity of the sandwaves superimposed upon it ([Fig. 2.6](#)). The overall low rate of migration of the sandbank in Area B in comparison to the sandwaves that are

superimposed upon it would indicate that it is highly unlikely that rapid migration of the sandbank would occur under typical hydrodynamic conditions. Repeat surveys by multibeam sonar indicated that the large sandbanks in Torres Strait migration on average ~13 m per year.

### 6.1.2. Wind regime

The wind record for the two weeks preceding the monsoon survey were typically from the northwest but highly variable, this is considered to be typical of the monsoon season. For the two weeks during monsoon survey the wind changes to consistent south easterlies, typical of the trade winds (see [Figs. 3.1, 3.2, 3.5](#)). The first multibeam sonar surveys of Area B during monsoon survey showed sandwaves facing to the east (i.e. consistent with the dominant wind direction during the monsoon). However by the time the second survey was completed (~14 days later) the sandwaves had begun to reverse – it is assumed that they were aided by the change in wind direction that occurred during this time. The wind regime for the trade wind survey was typically strong south easterly winds (see [Figs. 3.3, 3.4, 3.6](#)). As noted in [section 6.1.1](#), sandwave migration during this time was substantially less than during the monsoon survey, probably as a result of the sandwaves being in a more hydrodynamically stable configuration due to the constant direction of the winds during the trade wind season. Numerous authors have previously noted the influence of low frequency wind driven currents on the circulation in Torres Strait (Wolanski et al., 1988, Hemer et al., 2004, Harris, 1991). The changes in wind regime observed during the course of monsoon survey appear to have had a direct impact on the orientation and mobilisation of sandwave crests. This observation supports the conclusions of Harris (1991) who documented sandwaves changing their orientations with the changing wind regimes of the season in Adolphus Channel in south east Torres Strait.

### 6.1.3. Turbidity

During both surveys turbidity was measured during 24 hour stations using sensors on oceanographic moorings ([sections 4.3.1](#) and [5.3.1](#)). Levels of turbidity changed between the two surveys with turbidity during the monsoon survey being consistently 3 times the magnitude of that observed during the trade wind survey ([Tables 5.4 and 5.5](#)). Current magnitudes and wind speeds (and consequently wave heights) are not significantly different between the two surveys and consequently local resuspension is ruled out as a source for the turbidity. Hydrodynamic modelling of the Torres Strait region had indicated that the seasonal changes in turbidity is due to the greater availability of fine sediment west of Turnagain Island compared to the east. During the monsoon season fine sediment is mobilised from the Gulf of Carpentaria and western Torres Strait and transported east into the Turnagain Island region. Wind driven currents during the monsoon are typically

directed eastwards and hence provide a mechanism to transport fine sediment towards Turnagain Island and explain the turbidity levels observed during the monsoon season survey. Due to the comparatively small amounts of fine sediment available to be mobilised in the central and east of Torres Strait, very little turbidity is seen around Turnagain Island during the trade wind season. The westward, wind-driven currents during the trade wind season are more consistent than the winds during the monsoon season but due to the overall lack of available sediment to the east of Turnagain Island prevented significant levels of turbidity being observed during this trade wind survey. The results of the hydrodynamic modelling in Torres Strait will be reported as a Geoscience Australia record at a later date.

#### 6.1.4. Wave activity

As wave data were not acquired during the monsoon survey, wind data were used as a proxy. There were only small differences observed between the wind conditions between the two surveys ([Tables 3.1 and 3.2](#)). During both surveys, winds were predominantly directed from the southeast and of a similar magnitude (see [section 4.5.5](#)). Hence, wave conditions are expected to have been similar for each survey.

#### 6.1.5. Currents

Very little change in the tidal currents was observed between the two survey seasons ([section 4.5.6](#)). Hence it is assumed that any difference in sediment mobility between surveys will be a result of the winds or waves that occurred during the survey. Given wind speeds were very similar for the two surveys, the apparent seasonal variability in currents is possibly a result of local variability of flow, dependent on the local deployment location of the current meter, rather than changes in large scale circulation. Season differences in current regimes will be further addressed in a hydrodynamic model for the Torres Strait region. The results of this modelling work will be reported as a Geoscience Australia record at a later date.

#### 6.1.6. Sedimentology

Comparisons between sediment samples acquired from Saibai Island and samples from Turnagain Island showed the following:

1. The sediment samples from Saibai Island were significantly higher in mud content than the samples collected from around Turnagain Island ([section 5.3.3.7](#));
2. The mud content of the sediment samples from Saibai Island were much lower in CaCO<sub>3</sub> and hence had a much higher terrigenous component ([section 5.3.3.7](#));

3. The EDX analysis indicated that the samples from Saibai Island had a much higher concentration of aluminium indicating a higher clay content than the samples from the Turnagain Island region ([section 5.3.1.4](#)); and
4. The SXAM-XRF analysis indicated that the increased levels of silica seen in the samples around Saibai Island were due to the presence of quartz and not biogenic silica in the form of diatoms ([section 5.3.1.6](#)).

These results indicate that runoff from the south coast of Papua New Guinea, in the form of mud and quartz, was seen in the sediments deposited off Saibai Island but not in the sediments from around Turnagain Island. The sediments around Turnagain Island had only a negligible mud component, indicating that the region is less influenced by terrigenous input. The filter papers around Turnagain Island had similar chemical components to the grab samples from the seabed indicating that the suspended sediments in the region are likely to be locally derived and not sourced from Papua New Guinea.

## **7. Statement addressing scientific objectives of the Torres Strait CRC**

One of the principal objectives of the study was to better understand the relationship between oceanography, mobile sediments and seagrasses and determine what effect (if any) the sandwaves might have on the distribution, abundance and survival (or otherwise) of seagrass in Torres Strait.

The key objectives of the marine surveys undertaken for the Torres Strait CRC were to:

- 1) acquire key datasets to measure and characterise the mobile sediments and turbid plumes within Torres Strait; and
- 2) acquire data to assist in the ground truthing of a hydrodynamic model.

The data acquired during the surveys assisted in meeting the task objectives set out in the Torres Strait CRC proposal.

### **7.1. CRC Task objectives**

#### **1. In association with other projects, identify focus issues to guide field sampling, model development, and the selection of run scenarios and model outputs.**

- The issues of turbidity and sandwave mobility were seen to be two potential threats to seagrass communities. Survey work was designed to capture key datasets to characterise bedforms mobility and the timing and sources of suspended sediments.
- Repeat multibeam sonar surveys were used to monitor changes in seabed topography. These surveys allowed accurate measurement of bedform height and rates of migration to be made.

- Seabed and suspended sediment samples were used to characterise the sediments around Turnagain Island and Saibai Island. These samples were analysed to measure the level of influence of runoff from Papua New Guinea on the sediments in northern Torres Strait.
- Current meters and other oceanographic sensors were used to acquire data on waves, currents, tides, turbidity, light, temperature, salinity, oxygen, and fluorescence. This data was used to characterise the water column through time at each of the mooring sites.

## **2. Identify and collate relevant existing biophysical data.**

- Bathymetry data for the Torres Strait region was collated and a new bathymetry grid was created to assist with hydrodynamic modelling and seabed characterisation.
- All sediment sample data from previous surveys to the Torres Strait region was collated and entered into the MARS sediment database ([www.ga.gov.au/oracle/mars](http://www.ga.gov.au/oracle/mars)).
- Data from both Torres Strait CRC marine surveys (monsoon and trade wind season) were entered into MARS database.
- Landsat Imagery acquired between 1987 and 2003 was used to estimate long term sandbank migration rates.
- Meteorological data from the Bureau of Meteorology was used to characterise wind regimes in the Torres Strait region.

## **3. Make field measurements of key oceanographic and seabed quantities for model calibration under both summer monsoon and southeast trade wind conditions.**

- Oceanographic moorings were used in both marine surveys to acquire datasets for model calibration. These datasets included: sea level, temperature, wave, tide, current, turbidity, salinity, light, dissolved oxygen, and primary productivity.
- Rates and direction of bedform migration were measured using repeat high-resolution multibeam sonar surveys.
- High-resolution measurements of bedform sizes were made.

**4. Provide information on processes and model outputs relevant to other tasks and projects.**

- Data acquired from the both marine surveys has been published as GA Records (this report and Heap et al, 2005) and made available to CRC staff.
- Bathymetry grid of the Torres Strait has been made available to Torres Strait CRC to incorporate into hydrodynamic and sediment transport modelling.
- Information on sandbank and sandwave morphology supplied to Torres Strait CRC to incorporate into hydrodynamic and sediment transport modelling.
- Bathymetry map of Torres Strait made available to CRC staff (November 2005).
- Landsat map of Torres Strait made available to CRC staff (Mid 2004).
- Flythrough of Torres Strait of Torres Strait made available to CRC staff (November 2005).

## 8. Acknowledgements

We thank the crew and master of the RV *James Kirby* for their assistance throughout the survey. We are grateful of Prof. Bob Henderson (School of Earth Sciences, James Cook University) for permission to use the RV *James Kirby* and hire the shallow swath sonar, Chirper and vibrocoring equipment. We are indebted to Toshi Nakada (Torres Strait Regional Authority) for advice on indigenous issues and the Torres Strait Island community for their support of the survey. Financial support was provided by Geoscience Australia, Reef CRC, and Queensland Department of Primary Industry and Fisheries. Dr Alan Butler (CSIRO – Marine Research) provided guidance on survey design. Alex McLachlan, Neil Ramsay, Tony Watson, and Richard Brown of the sedimentology laboratory at Geoscience Australia managed all sample analyses and are thanked for their timely and efficient production of the texture and composition data. The video footage was edited by Tara Dowling (Geoscience Australia). The original report benefited from reviews by Dr Phil O'Brien and Dr Brendan Brooke. Published with the permission of CEO Neil Williams

## 9. References

- Agrawal, Y.C., and Pottsmith, H. C., 2000. Instruments for particles size and settling velocity observations in sediment transport. *Marine Geology* 168, 89-114.
- Best, A.I. & Gunn, D.E., 1999. Calibration of marine sediment core loggers for quantitative acoustic impedance studies. *Marine Geology* 160, 137-146.
- Brink F.J., Norén L. and Withers R.L., 2004. Electron diffraction evidence for continuously variable, composition-dependent O/F ordering in the  $ReO_3$  type,  $Nb_{1-x}V^{IV}Nb_x^{IV}O_{2-x}F_{1+x}$ ,  $0 \leq x \leq 0.48$ , solid solution. *Journal of Solid State Chemistry* 177, 2177-2182.
- Brown, C.B., 1950. Sediment transportation. In: Rouse, H., (Ed.), *Engineering Hydraulics*, Wiley, New York. 797pp.
- Engelund, F. & Hansen, E., 1967. *A Monograph on Sediment Transport in Alluvial Streams*. Teknisk Vorlag, Copenhagen, 62pp.
- Gadd, P.E. Lavelle, J.W. & Swift, D.J.P., 1978. Estimates of sand transport on the New York shelf using near-bottom current meter observations. *Journal of Sedimentary Petrology* 48, 239-252.
- Gerland, S. & Villinger, H., 1995. Non-destructive density determination on marine sediment cores from gamma-ray attenuation measurements. *Geo-Marine Letters* 15, 111-118.
- Gordon, L., 1996, Principles of operation - A practical primer: RD Instruments publication number 951-6069-00, second ed.
- Hardisty, J., 1983. An assessment and calibration of formulations for Bagnold's bedload equation. *Journal of Sedimentary Petrology* 53, 1007-1010.
- Harris, P.T., 1991. Reversal of subtidal dune asymmetries caused by seasonally reversing wind-driven currents in Torres Strait, northeastern Australia. *Continental Shelf Research* 11, 655-662.
- Harris, P.T., 1989. Sandwave movement under tidal and wind-driven currents in a shallow marine environment: Adolphus Channel, northeastern Australia. *Continental Shelf Research* 9, 981-1002.
- Harris, P.T., 1988. Sediments, bedforms and bedload transport pathways on the continental shelf adjacent to Torres Strait, Australia-Papua New Guinea. *Continental Shelf Research* 8, 979-1003.
- Heap, A.D., Hemer, M., Daniell, J., Mathews, E., Harris, P.T., Kerville, S., and O'Grady, L., 2005. *Biophysical Processing in the Torres Strait Marine Ecosystem – post cruise report*. Geoscience Australia, Record 2005/11, 112pp.

- Heap, A.D., Daniell, J., Mazon, D., Harris, P.T., Scaffi, L., Fellows, M. & Passlow, V., 2004. *Geomorphology and Sedimentology of the Northern Planning Region of Australia*. Geoscience Australia Record 2004/11, Canberra. 68pp.
- Heap, A.D., Dickens, G.R. & Stewart, L.K., 2001. Late Holocene sediment in Nara Inlet, central Great Barrier Reef platform, Australia: sediment accumulation on the middle shelf of a tropical mixed clastic/carbonate systems. *Marine Geology* 176, 39-54.
- Heap, A.D., Larcombe, P. & Woolfe, K.J., 1999. Storm-dominated sedimentation in a protected basin fringed by coral reefs, Nara Inlet, Whitsunday Islands, Great Barrier Reef. *Australian Journal of Earth Sciences* 46, 443-451.
- Hemer, M.A, Harris, P.T., Coleman, R. & Hunter, J., 2004. Sediment mobility due to currents and waves in the Torres Strait-Gulf of Papua region. *Continental Shelf Research* 24, 2297-2316.
- Li, M.Z. & Amos, C.L., 2001. SEDTRANS96, the upgraded and better calibrated sediment-transport model for continental shelves. *Computers and Geosciences* 27, 619-645.
- Long, B.G. & Poiner, I.R., 1997. *Seagrass communities of Torres Strait, Northern Australia*. Report to the Torres Strait Scientific Advisory Committee No 27, December 1997, CSIRO, Cleveland. 49 pp.
- Long, B.G., Skewes, T., Thomas, M., Isdale, P., Pitcher, R., and Poiner, I., 1997. *Torres Strait Seagrass Dieback. Final Report to TSFSAC 26*. CSIRO Division of Marine Research, Cleveland.
- Miller, M.C., McCave, I.N. & Komar, P.D., 1977. Threshold of sediment motion under unidirectional currents. *Sedimentology* 24, 507-527.
- Muller and Gastner, 1971. The "Karbonat-Bombe", a simple device for the determination of the carbonate content in sediments, soils, and other materials. *Neues Jahrbuch fuer Mineralogie* 10, 466-469.
- Norrish, K., and Hutton, J.T., 1964. Preparation of samples for analysis by X-ray fluorescence spectrography. Divisional Report CSIRO Division of Soils 3/64.
- Norrish, K., and Hutton, J.T., 1969. An accurate X-ray spectrographic method for the analysis of a wide range of geological samples. *Geochemica et Cosmochemica Acta* 33, 431.
- Nortek, 2000. Vector Operations Manual, 1 November 2000. <http://www.nortek-as.com>
- Pawlowicz, R., Beardsley, B. and Lentz, S., 2002. Classical tidal harmonic analysis including error estimates in MATLAB using T\_TIDE. *Computers and Geosciences* 28, 929-937.
- Pond, S. and Pickard, G.L., 2000. *Introductory Dynamical Oceanography*, 2<sup>nd</sup> Edition. Butterworth Heinemann, Oxford. 329pp.

- Weber, ME., Niessen, F., Kuhn, G. & Wiedicke, M., 1997. Calibration and application of marine sedimentary physical properties using a multi-sensor core logger. *Marine Geology* 136, 151-172.
- Wolanski, E., Ridd, P., and Inoue, M., 1988. Currents through Torres Strait. *Journal of Physical Oceanography* 18, 1535-1545.
- Xu, Z., 2002. Ellipse Parameters Conversion and Velocity Profiles for Tidal Currents in Matlab. Maurice-Lamontagne Institute, Ocean Science Division, Fisheries and Ocean Canada. 24pp.
- Yalin, M.S., 1963. An expression for bed-load transportation. *Journal of the Hydraulic Division, ASCE* 89, 49-59.

## 10. Appendices

### 10.1 Appendix A – Survey Leaders Log

Geoscience Australia Survey 273, Torres Strait, 2004

Survey Leaders Log

*RV James Kirby*

Peter Harris (8 October to 28 October)

#### **Scientific Personnel.**

Dr Peter Harris (PH)

Dr Andrew Heap (AH)

Dr Mark Hemer (MH)

Dr Frederick Saint-Cast (FSC)

Dr Michael Hughes (DH)

Mr James Daniell (JD)

Mr Franz Villigran (FV)

Mr Mike Sexton (MS)

Mr Jack Pittar (JP)

#### **Ships Crew.**

Mr Don Battersby (DB)

Mr Kevin Hooper (KH)

**Thursday, 7 October 2004.** MH, JD, FV and FSC met the *RV James Kirby* in Thursday Island to set up current meter frames and moorings. Moorings were assembled on board. AH joined science party in the afternoon. The galvanised steel frame for Geoscience Australia's ADCP was affecting the magnetic compass (total error 25-35%). So it was decided to use the CSIRO stainless steel frame containing the multimeter frame for Geoscience Australia's ADCP. Science Party stayed ashore.

**Friday, 8 October 2004.** Beginning of Leg 1. AH, MH, JD, FV and FSC joined the *RV James Kirby* for Leg 1 of the survey. Departed Thursday Island at 22:00 UTC and arrived at Mooring Site 1 (Orman Reef) at 01:00 UTC and deployed CSIRO multimeter eventually at 07:38 UTC. Problems with camera remote not working, which were fixed by FV that night. Anchored behind Orman Reef at 08:40 UTC. That night modifications were also made to the CSIRO frame to accommodate Geoscience Australia's ADCP.

**Saturday, 9 October 2004.** Underway at 20:00 UTC. Arrived at Area A and deployed CSIRO current meter at 22:05 UTC. Transited to Area B and deployed BRUCE at 01:42 UTC. Deployed GA ADCP on modified CSIRO frame at 02:10 UTC. Deployed University of Sydney ADCP at 03:25 UTC. Deployed CSIRO ADCP and multimeter mooring at 04:24 UTC. During the late-afternoon, one of the GA science party was advised of the sudden and unexpected death of an immediate family member. In

response, we steamed directly for Thursday Island harbour for them to catch a flight out the next morning. Arrived at Thursday Island harbour at 12:30 UTC. This event has been very upsetting for all on board. AH advised relevant staff at Geoscience Australia of events and they are organising a replacement staff member for Leg 2.

**Sunday, 10 October 2004.** Departed Thursday Island harbour at 18:00 UTC for Turnagain Island. Arrived in Area B and deployed University of Sydney FSI current meter at 00:50 UTC. Started swath mapping Area B at 01:30 UTC and stopped at 03:30 UTC to fix University of Sydney ADCP mooring. We attempted to recover the weight to weigh down the silver rope ground line. However, the rope had dropped below the surface in the strong current and could not be retrieved. Continued swath mapping of Area B 04:00 UTC. Finished swath mapping for the day at 07:15 UTC. Anchored at Numar Reef for the night at 08:00 UTC.

**Monday, 11 October 2004.** Departed Numar Reef for Area B at 21:00 UTC. Continued swath mapping of sandwaves in Area B at 21:30 UTC. Although the barchan shape of the bedform has not changed from the first survey (S266) in April 2004, the morphology of the individual sandwaves has changed significantly – indicating that they are migrating to the west and have changed direction. Individual sandwaves identified in the April survey are still recognisable. The smaller sandwaves in the SW of the study area were more symmetrical or oriented towards the west. These smaller sandwaves are possibly more mobile, and may change their direction with the tide. Finished swath mapping for the day at 07:10 UTC. Could not use Geoscience Australia's DVD burner to back up files because DVD program is not compatible with the hardware. Backed up files using KH's DVD burner. During the day AH organised with Stephen Dutton (GA) for a replacement swath processor. Mike Sexton (GA) will join the survey for Leg 2. Anchored at Numar Reef for the night at 08:05 UTC.

**Tuesday, 12 October 2004.** Departed Numar Reef for Area B at 20:45 UTC. Commenced swath mapping of sandwaves in Area B at 21:30 UTC. However, due to problems with the swath mapper (possibly a faulty ethernet connection) we could only collect bathymetry without side scan sonar. Water depths were too shallow to fill in gaps over the largest sandwaves, so we continued swath mapping of sandwaves in deeper water. Completed swath mapping of Area B at 23:05 UTC. The area mapped is bounded approximately by the following co-ordinates: -9°35.17, 142°21.00; -9°35.17, 142°21.75; -9°35.91, 142°21.75; -9°35.91, 142°20.58; -9°35.58, 142°20.58; and -9°35.58, 142°21.00. Transited to Area A and commenced swath mapping of sand ridges and reefs at 01:15 UTC. Side scan sonar still not working. Due to shallow water, we commenced mapping the gutter between the reefs and decided to map the reef areas at night during high tide. Completed swath mapping of the gutter at 05:30 UTC. Anchored in Area A. Woke at 12:15 UTC to find that the ship had dragged anchor some 1.8 nautical miles to the NWW due to strong currents and high winds - thankfully not over a reef! After returning to position, we commenced swath mapping of the eastern reef at 13:00 UTC. The sand ridges do not appear to have moved significantly from the April survey (S266). Completed swath mapping of the eastern reef at 05:10 UTC. Anchored at Aldai Reef at 06:00 UTC.

**Wednesday, 13 October. 2004** Departed Aldai Reef at 22:45 UTC for Area A. Continued swath mapping gutter between reefs at 23:17 UTC as far south as -9° 34.53. Side scan sonar still unavailable. Commenced swath mapping of eastern reef at 02:34 UTC including areas as far south as -9° 34.526 and many of the gaps not filled the previous night. The sand ridges appear not to have moved significantly from the April survey (S266), although the crests of two in the southeastern part of the gutter have moved a small amount to the west, and the stoss slopes contain small mega-ripples oriented (and migrating?) to the west. Continued mapping eastern reef until water depths became too shallow at 05:50 UTC. Anchored in Area A at 06:10 UTC until high tide. Continued mapping eastern reef at 14:00 UTC at high tide and completed the area at 15:45 UTC. The mapped area is bounded approximately by the following co-ordinates: -9° 33.95, 142° 12.92; -9° 33.95, 142° 13.83; -9° 34.53; 142° 13.83; -9° 34.53, 142° 12.92; and -9° 34.16, 142° 13.10. As there has been very little observable change in the morphology of Area A since the survey in April 2004 (S266) it is recommended that this area NOT be resurveyed during Leg 2.

**Thursday, 14 October. 2004** Departed for Saibai Island at 18:25 UTC. Collected grab samples at various points along route (GRVV8 @ 19:54, -9° 33.598, 142° 23.708; GRVV9 @ 20:48, -9° 30.000, 142° 28.722; GRVV10 @ 21:55, -9° 25.049, 142° 34.589; GRVV11 @ 22:28, -9° 22.203, 142° 34.872; GRVV12 @ 22:57, -9° 20.834, 142° 37.678; GRVV13 @ 23:13, -9° 21.196, 142° 39.166; GRVV14 @ 23:35, -9° 21.676, 142° 39.214). After arriving at the reef flat on the north coast of Saibai Island, AH and MH went out in the dinghy and collected 8 grab samples of the reef flat environments, roughly in a cross-shore transect from the channel to the mangroves. A further grab sample was collected further to the east along the coast. A recommendation is that the second leg returns to Saibai Island to continued sampling along the northern coast of the island. Departed for Area A at Turnagain Island at 02:35 UTC to commence 24-hour stations. Arrived at Aldai Reef anchorage at 06:30 UTC and anchored for the night.

**Friday, 15 October 2004.** Transited to Area A at 18:30 UTC. Commenced 24-hour station in Area A at 20:00 UTC in the vicinity of the CSIRO oceanographic mooring (CM7) at approximately -9° 34.090, 142° 13.759. The science party separated into two shifts, working 6 hours on then 6 hours off (AH, FSC – 6-12; MH, FV – 12-6). Camera stations were taken on the hour for 8 minutes (sampling time of instruments). Water samples were collected 1 m from the seabed at 2 minutes and 6 minutes past the hour and then filtered through filter papers. Initial problems with the underwater camera remote were expertly and quickly fixed by FV. It was then discovered that the bulb of one of the halogen lights had blown as well as the spare! Again, there was too much ambient light during the day for the camera lights, although the combination of one halogen light and two incandescent light provided suitable visibility and colour at night. However, the poor record of the camera lights continued with the one remaining halogen light blowing its bulb during the station. This restricted us to using the incandescent lights for the remainder of the survey, as no halogen bulbs could be sourced from the mainland. The station commenced with light and variable

winds, no sea or swell and a moderate SE current. KH fixed side scan sonar based on advice from Reson (USA).

**Saturday, 16 October 2004.** Completed 24-hour station in Area A at 21:00 UTC. The station ended with light and variable winds, no sea or swell, with a strong SE current. VHS tape did not record for station 25, copied DV tapes on to VHS using the camera and ship's video recorder. Transited to Area B and spent some time getting into a suitable position to conduct 24-hour stations due to significant turbulence and strong currents over the crests of the sandwaves that caused the ship to swing in  $>90^\circ$  arcs. Commenced 24-hour station in Area B at 00:00 on the stoss slope of a sandwave south of Geoscience Australia's ADCP oceanographic mooring (CM3) at  $-9^\circ 35.717$ ,  $142^\circ 21.444$ . Camera stations were taken on the hour for 8 minutes (sampling time of instruments). Water samples were collected 1 m from the seabed at 2 minutes and 6 minutes past the hour and then filtered through filter papers. Again, there was too much ambient light for the camera lights during the day. The station began with light and variable winds, and no sea or swell, with a strong easterly current over the sandwaves.

**Sunday, 17 October 2004.** Completed 24-hour station in Area B at 01:00 UTC. The station ended with SE winds of 10-15 knots, slight to moderate SE seas and a moderate easterly current over the sandwaves. VHS tape did not record for station 26, copied DV tapes for on to VHS tapes using the camera and ship's video recorder. Departed for Thursday Island Harbour at 01:45 UTC. Arrived in Thursday Island Harbour at 09:00 UTC. Packed up and stowed gear for Leg 2. Overall, a very successful leg, with all major science objectives achieved. All members of the crew and Science Party worked together in a friendly, co-operative and professional manner through out the leg.

**Monday, 18 October 2004.** Science Party for Leg 1 disembarked ship at 22:35 UTC, and flew back to Canberra (AH, FV), Sydney (MH) and Hobart (FSC). Science Party for Leg 2 boarded ship at 0730 local time. Loaded fuel, water and vibrocorer. Departed for Turnagain Island at 1100 hrs. Windy passage caused some discomfort as several of the party were sea sick. Arrived at Orman Reefs at around 1830 hrs and dropped anchor. We have decided to attach 30 kg lead weights to the JCU vibrocorer, one to each of the 3 legs.

**Tuesday, 19 October 2004.** Completed modifications to JCU vibrocorer and underway by 0630. Arrived at first core site in Area B by 0930 and deployed the corer among sandwaves. Core VC 1 was about 30 cm long, comprised of well sorted sand. Second attempt at this site recovered a slightly longer 70 cm core. Strong tides flowing against the wind so we abandoned coring at this site at around 1030. Move to Area A and collected a further 5 vibrocores and 2 camera stations over sand waves. Anchored at Aldai Reef at around 1700 hrs.

**Wednesday, 20 October 2004.** Underway @ 0600 hrs transit to NE end of Turnagain Island to land shore party. PH and MH collected sediment samples including 3 push-cores from intertidal flats and among the mangrove roots at the shoreline from 4 locations. Underway again at 1000 hrs to a vibrocore station. The core tower became trapped under the end of the ship and damaged a section of metal frame – repairs took about 1.5 hours. Even so we took two cores before moving on to run 5 swath sonar lines over sandwaves in the SE corner of the study area. This was completed by 1500 hrs when we moved to the 24-hr station site for one last vibrocore VC10. This was completed at 1600 hrs and the 24 hr station started at 1800 hrs.

**Thursday, 21 October 2004.** 24-hr Station, Stn 36 at Area B. Last sample collected @ 1800 hrs. Complete 5 swath sonar lines of small area in SE corner of Area B. Transit to Area A, arrive @ 2030 hrs to start 24-hr station 37.

**Friday, 22 October 2004.** Welds holding the camera pod inside the frame have broken, so the camera was not used for the last 4 hours. Complete 24 hr station @ 2100 hrs and transit to area B to start swath mapping. High-high water is a 3m tide at around 2400 hrs so swath mapping is best done at this time. Rough seas kept most of the science party in their bunks, airborne during the largest waves.

**Saturday, 23 October 2004.** Stopped swath mapping @ 0130 hrs after completing 10 lines and transit to anchorage at Numar Reef. Station 38 was carried out at the anchorage @ 0830 hrs. Up anchor and returned to swath mapping Area B @ 0900 hrs. Complete 5 swath sonar lines of small area in SE corner of Area B. Mapping stopped @ 1730 hrs and we returned to Numar Reef anchorage for meal and rest. Underway again @ 2230 hrs to map shallow areas at midnight high water.

**Sunday, 24 October 2004.** Stopped swath mapping @ 0100 hrs after completing 10 lines and transit to anchorage at Numar Reef. Underway again @ 0800 hrs to continue swath mapping. We decided to recover BRUCE current meter @ 1300 hrs (slack water) today as its batteries are due to run out and we hoped to spread the current meter recovery work over a few days. Recovery of BRUCE was complicated by the ground line having fouled the instrument frame which kept the floats from rising to the surface when the acoustic release was triggered. This meant we had to drag for the instrument using a grappling line. Eventually we were successful after about 4 hours of attempts. Strong currents and 20 knot winds made the work more difficult. BRUCE was safely recovered @ 1730 and we also recovered the Sydney

University ADCP instrument @ 1800. We returned to Numar Reef anchorage for meal and rest. Underway again @ 2230 hrs to map shallow areas at midnight high water.

**Monday, 25 October 2004.** Stopped swath mapping @ 0100 hrs after completing 10 lines and transit to anchorage at Numar Reef. Underway again @ 0800 hrs to continue swath mapping. Underway again @ 0600 hrs to Area B to collect the last 3 CMs in that area. This was accomplished without incident and we headed for Area A @ 0820. Arrive in Area A and commenced swath mapping. Mapping of shallow dune crests was started @ 1300 hrs when the tide had risen enough to provide sufficient depth for mapping. Mapping was stopped @ 1640 hrs and we transited to our anchorage at Aldai Reef.

**Tuesday, 26 October 2004.** Strong winds and heavy rainfall today – seas 1-2 m breaking over the reef. At anchorage until 10AM waiting for tide to rise so we could complete swath mapping of sandwaves in Area A. Underway and completed patch test @ 1230 and completed shallow swath mapping by 1620. We recovered CM 7 at 1640 without incident, in spite of strong winds gusting to 35 knots and 1-2 m seas. Arrived at the anchorage at Numar Reef by 1800 hrs. Tonight at dinner we presented Captain Don Battersby and Kevin Hooper with GA T-shirts as gifts to show our appreciation of their efforts through the survey.

**Wednesday, 27 October 2004.**

**Thursday, 28 October 2004.** Arrived Thursday Island harbour at 0000 UTC and science party departed ship with all equipment and samples. End of Leg 2.

**Friday 29 October 2004.** Science Party flew back to Canberra. End of Survey.

## **10.2. Appendix B – Digital Video Footage**



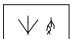




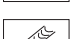

Excerpts of the digital video footage for select sites are provided on the CD in mpeg format. The filenames follow the convention: *GA Survey Number\_Station Number, Operation Type and Operation Number* (e.g., 273\_26CAM09).

### 10.3. Appendix C – Core Logs




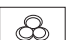
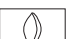




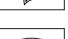
The core logs are produced from the visual logs of the cores. They contain the physical property data (Bulk Density, P-wave Velocity, Magnetic Susceptibility, Fractional Porosity), texture and composition information, visual log (including digital images and x-radiographs) and comments on specific features.

#### Core Log Legend

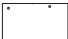




##### Sedimentary Features


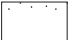
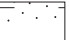

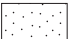
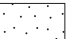
	Shell Hash
	Wood
	Organic Fragments
	Articulated Shell (in-situ)
	Articulated Shell
	Intact Shell Valve(s)
	Laminations
	Burrows
	Unconformity

##### Fossils




	Gastropods
	Corals
	Bryozoans
	Foraminifers
	Bivalves
	Echnoids
	Halimeda
	Worm Tubes
	Scaphopods
	Crustaceans

##### Lithology

Gravel	
Sandy mud	
Silt	
Clay	
Limestone	

	Fine	Medium	Coarse
Muddy gravelly sand			
Sand			

##### Sub-samples

	Grain-size/CaCO <sub>3</sub> /XRF
	C-14 age
	Mineralogy

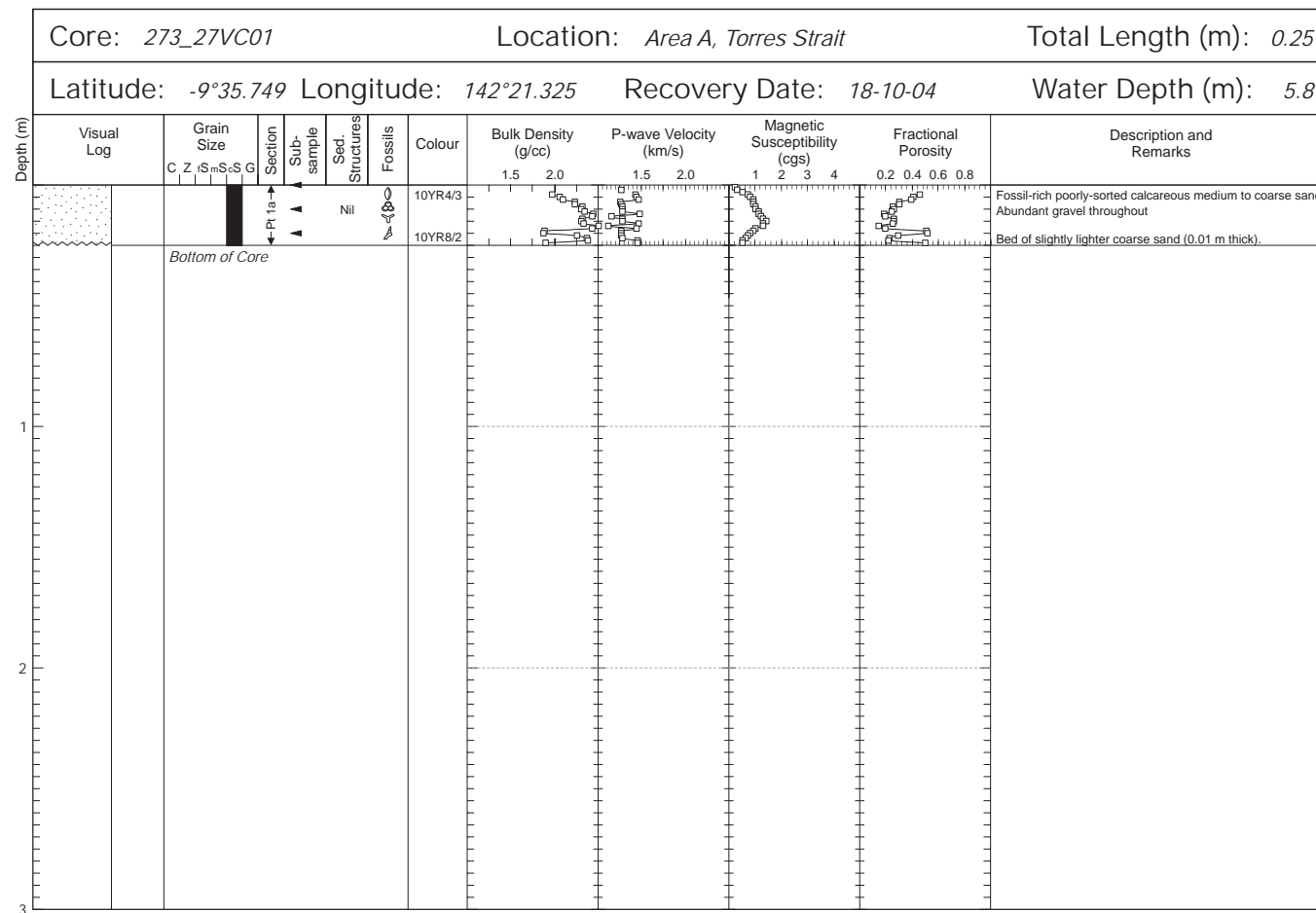


Fig 10.1. Core log for 27VC01 containing stratigraphic interpretations, texture and composition data, and physical properties (Bulk Density, P-wave Velocity, Magnetic Susceptibility, Fraction al Porosity)

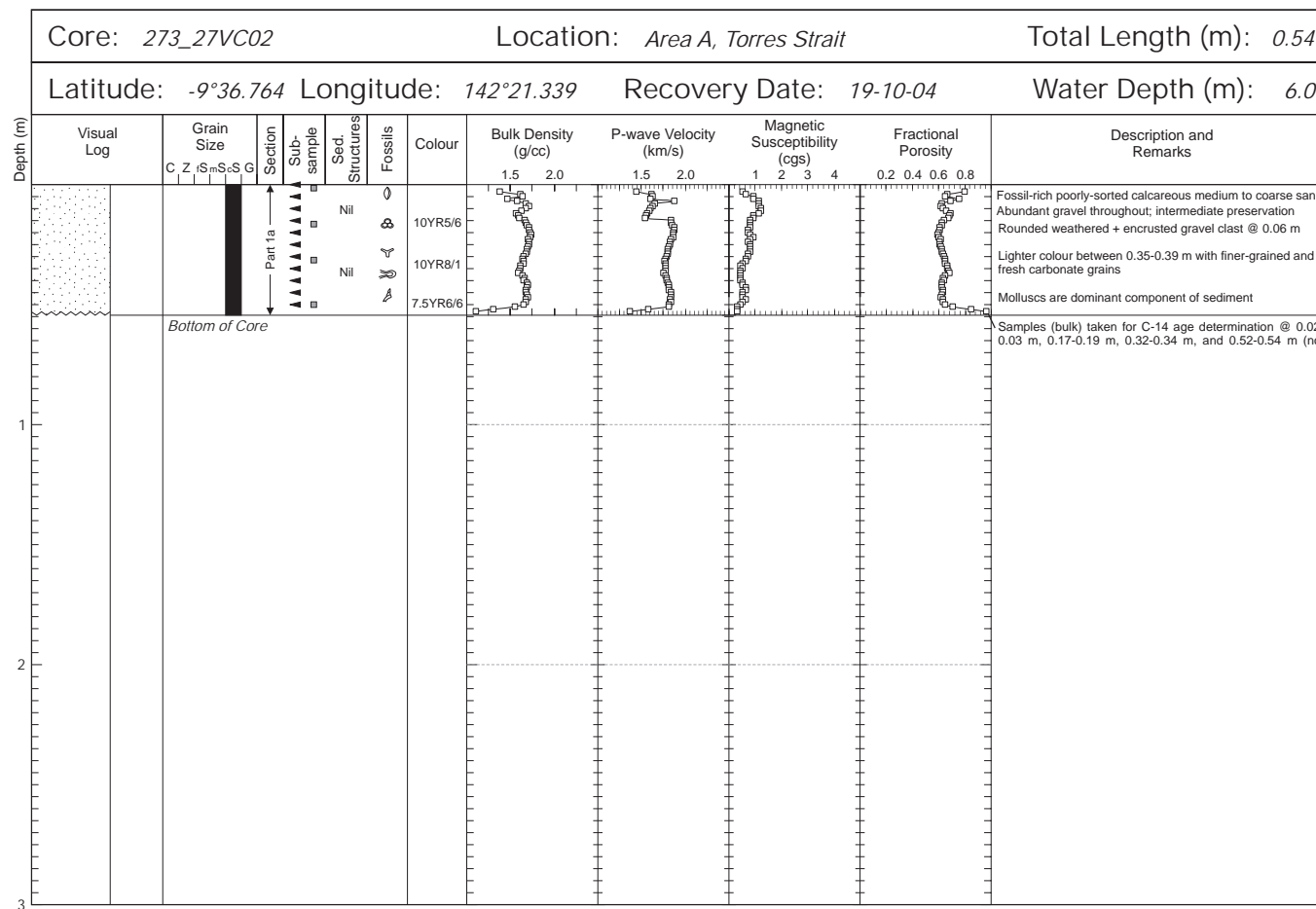


Fig 10.2. Core log for 27VC02 containing stratigraphic interpretations, texture and composition data, and physical properties (Bulk Density, P-wave Velocity, Magnetic Susceptibility, Fractional Porosity)

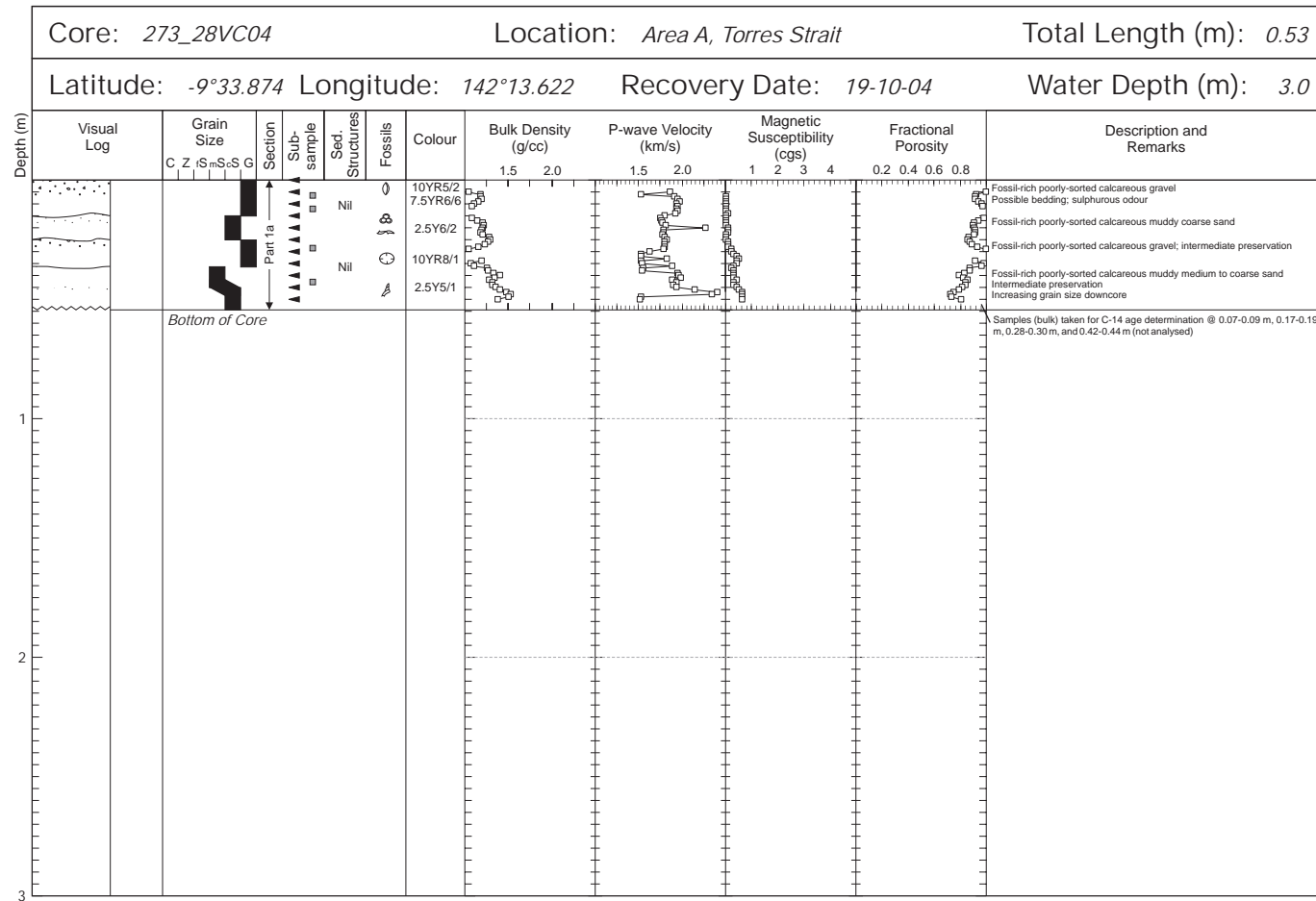


Fig 10.3. Core log for 28VC04 containing stratigraphic interpretations, texture and composition data, and physical properties (Bulk Density, P-wave Velocity, Magnetic Susceptibility, Fractional Porosity)

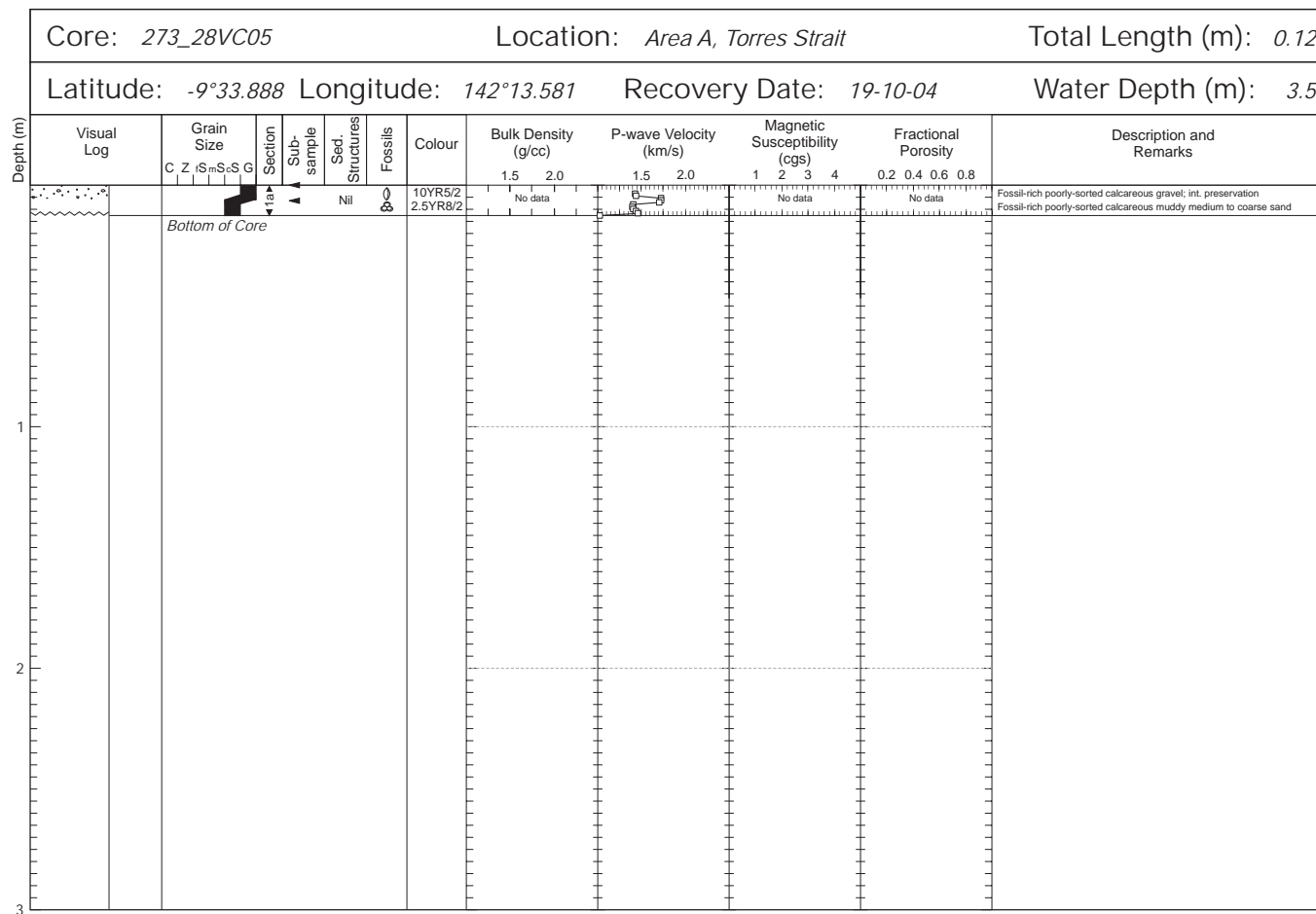


Fig 10.4. Core log for 28VC05 containing stratigraphic interpretations, texture and composition data, and physical properties (Bulk Density, P-wave Velocity, Magnetic Susceptibility, Fractional Porosity)

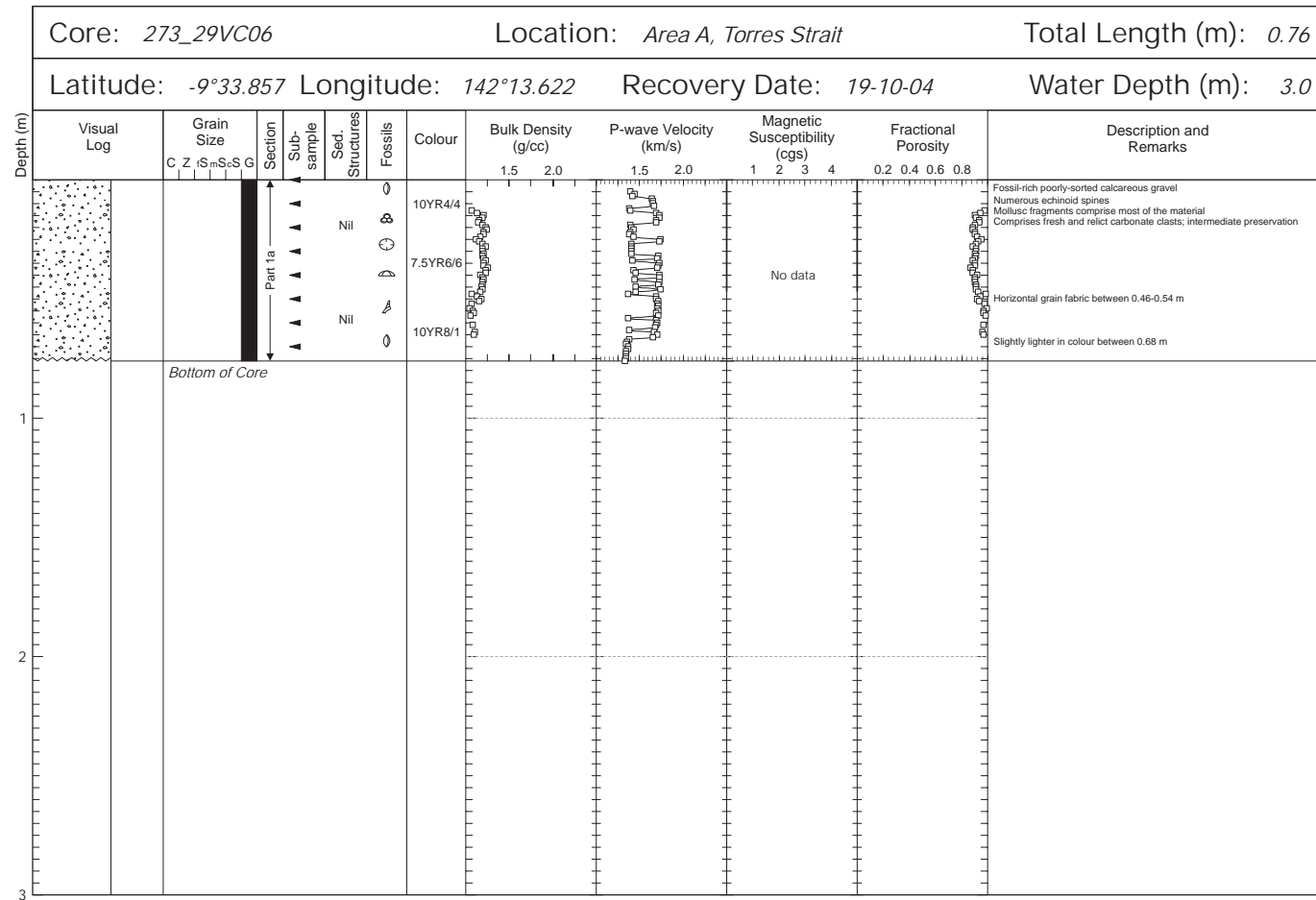
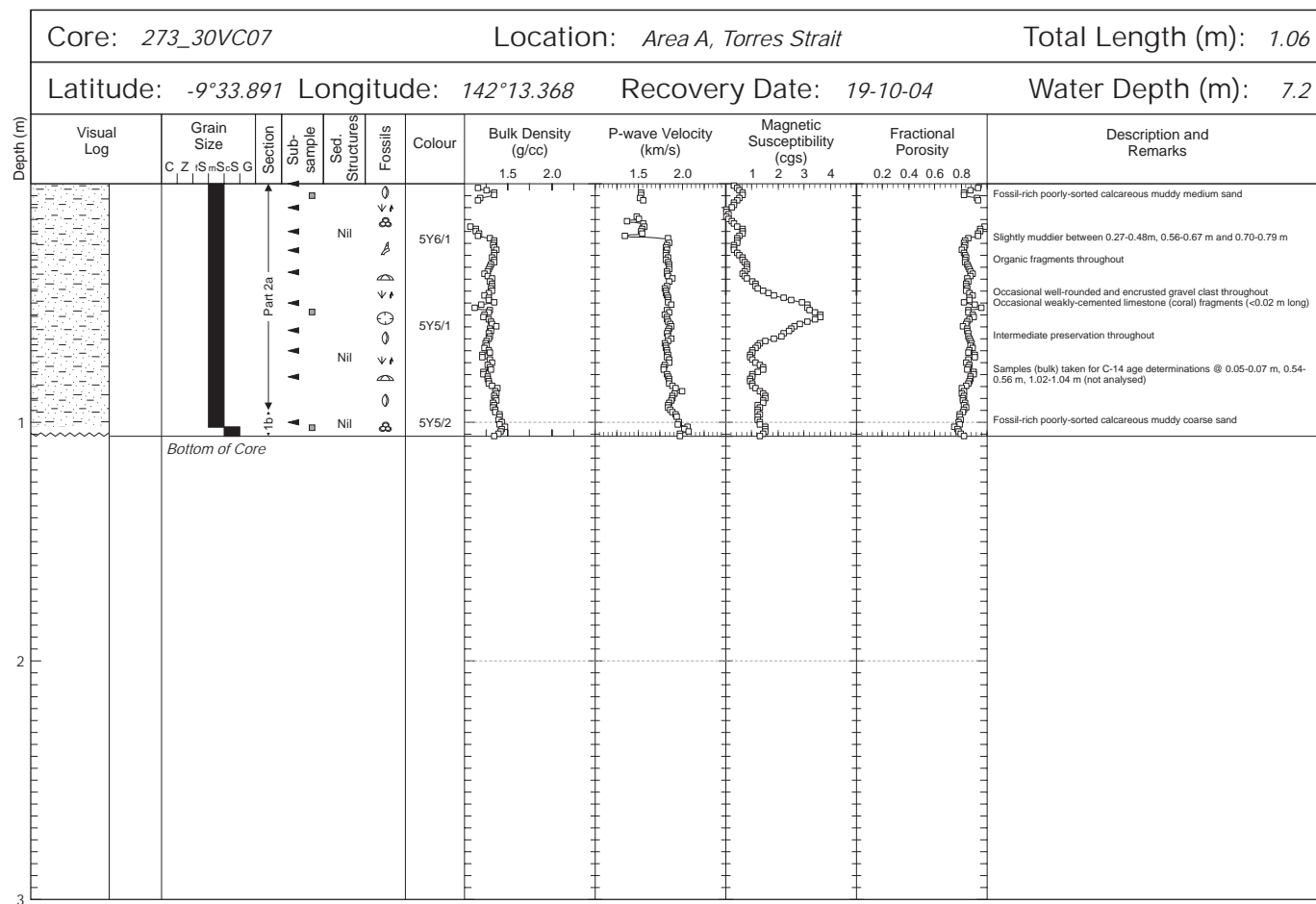


Fig 10.5. Core log for 29VC06 containing stratigraphic interpretations, texture and composition data, and physical properties (Bulk Density, P-wave Velocity, Magnetic Susceptibility, Fractional Porosity)



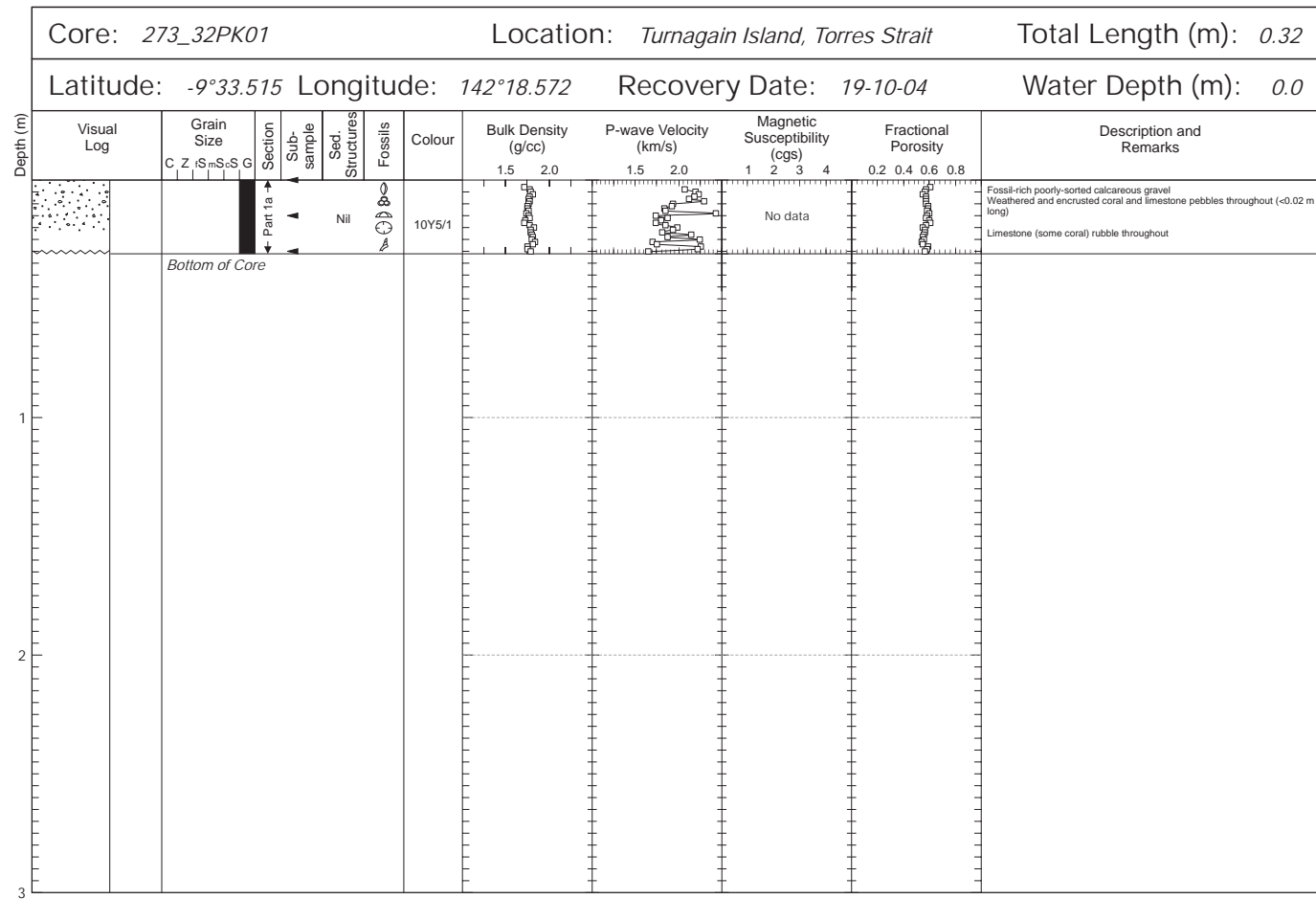


Fig 10.7. Core log for 32PK01 containing stratigraphic interpretations, texture and composition data, and physical properties (Bulk Density, P-wave Velocity, Magnetic Susceptibility, Fractional Porosity)

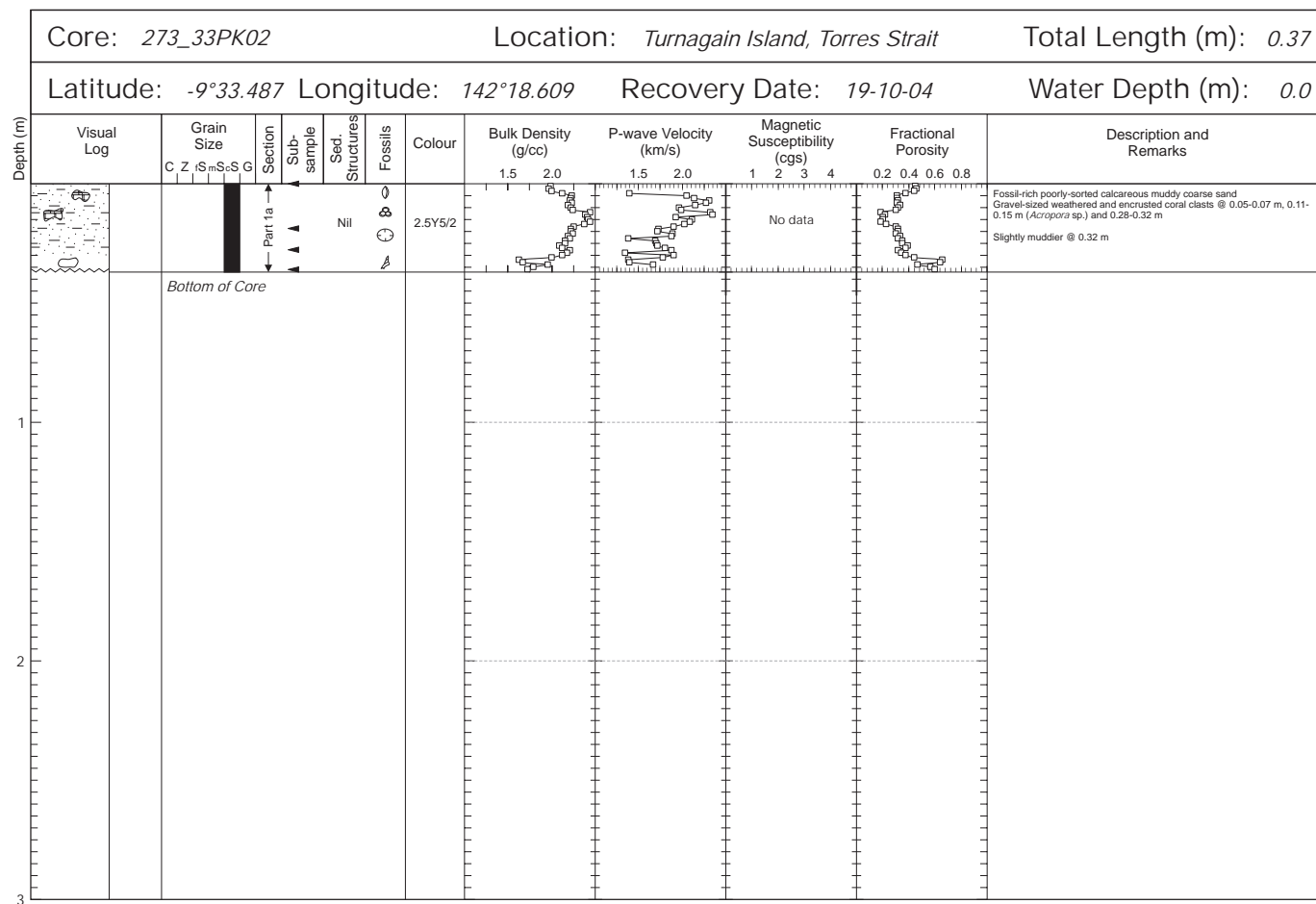


Fig 10.8. Core log for 33PK02 containing stratigraphic interpretations, texture and composition data, and physical properties (Bulk Density, P-wave Velocity, Magnetic Susceptibility, Fractional Porosity)

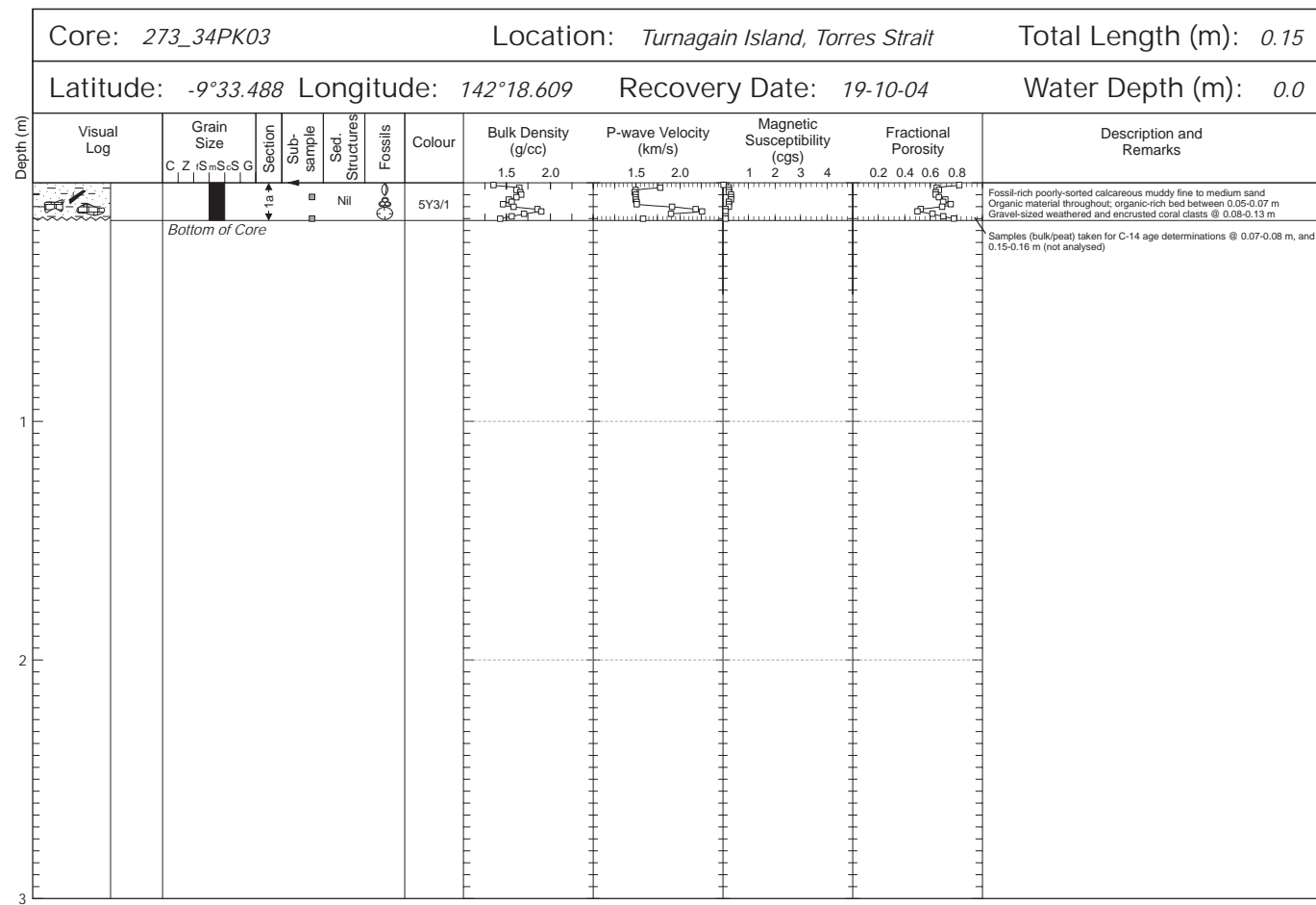


Fig 10.9. Core log for 34PK03 containing stratigraphic interpretations, texture and composition data, and physical properties (Bulk Density, P-wave Velocity, Magnetic Susceptibility, Fractional Porosity)

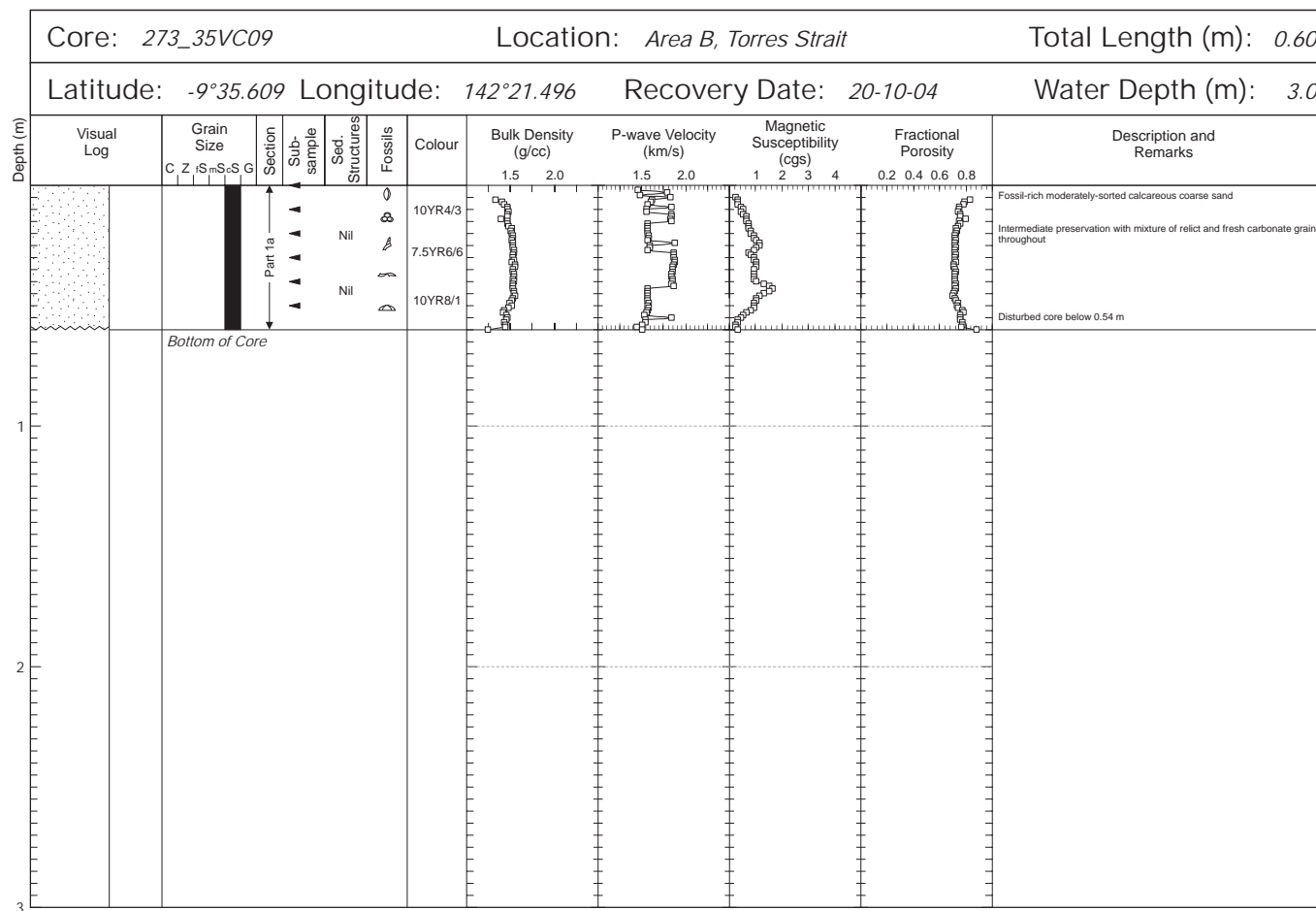


Fig 10.10. Core log for 35VC09 containing stratigraphic interpretations, texture and composition data, and physical properties (Bulk Density, P-wave Velocity, Magnetic Susceptibility, Fractional Porosity)

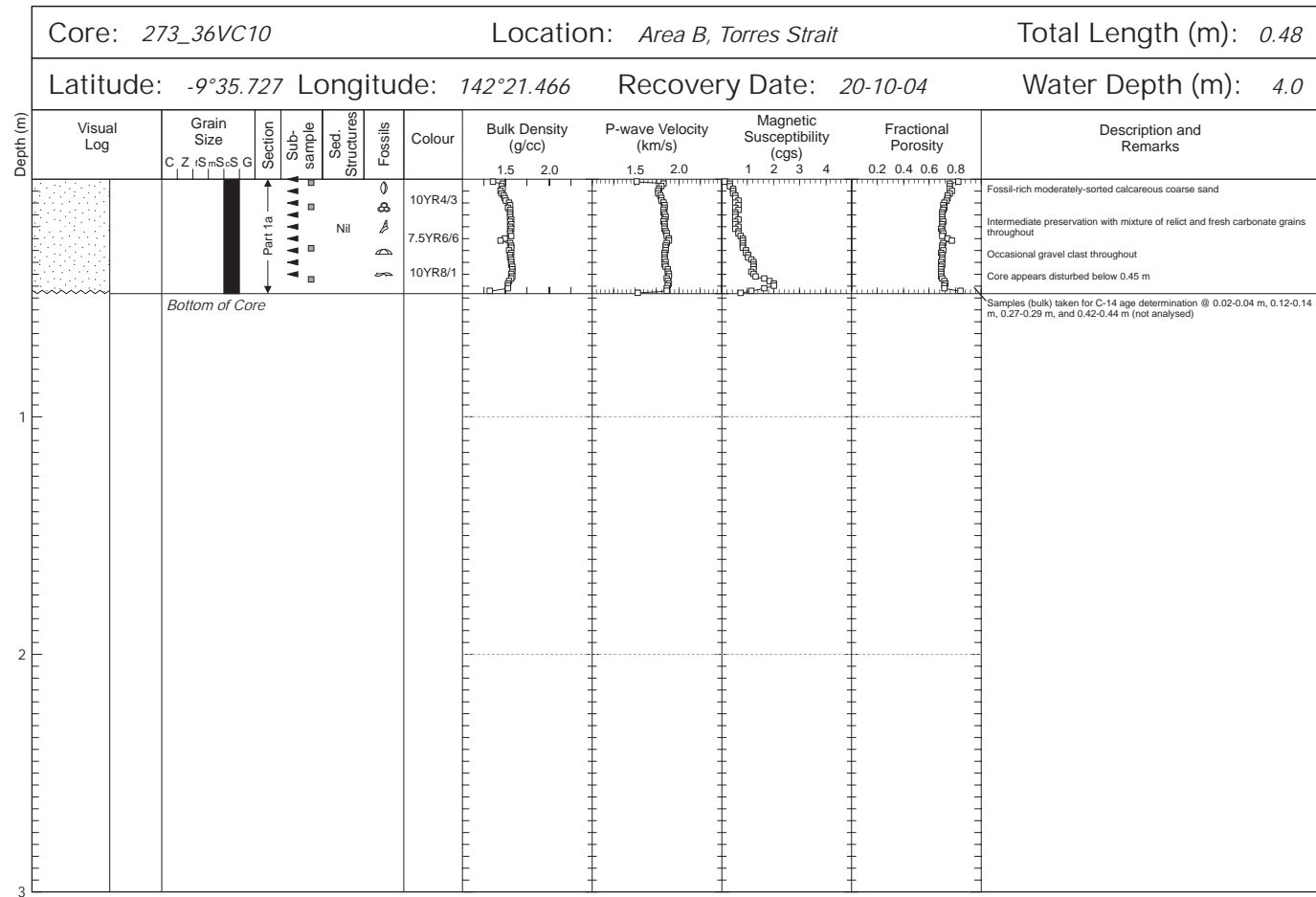


Fig 10.11. Core log for 36VC10 containing stratigraphic interpretations, texture and composition data, and physical properties (Bulk Density, P-wave Velocity, Magnetic Susceptibility, Fractional Porosity)

## 10.4. Appendix D – Laser analysis of S273 Grab Samples (On the CD)

The laser analysis plots are generated by the Malvern™ Mastersizer-2000 laser particle size analyser. They show distribution curves of the grab sample sediment grainsizes. They also show basic statistical analysis on the distribution curve such as mean, standard deviation, skewness, kurtosis etc.

## 10.5. Appendix E – Sediment samples taken from S273 cores

Table 10.1. Sediment samples taken from S273 cores

SampleID	Depth (m) top	Depth (m) bottom	Lat	Lon	Notes
273/27VC01_0-2	0	0.02	-9.35749	142.2133	top
273/27VC01_10-12	0.1	0.12	-9.35749	142.2133	middle
273/27VC01_20-22	0.2	0.22	-9.35749	142.2133	bottom
273/27VC02_0-2	0	0.02	-9.36764	142.2134	top
273/27VC02_2-4	0.02	0.04	-9.36764	142.2134	Bulk - C14
273/27VC02_5-7	0.05	0.07	-9.36764	142.2134	
273/27VC02_10-12	0.1	0.12	-9.36764	142.2134	
273/27VC02_15-17	0.15	0.17	-9.36764	142.2134	Bulk C14
273/27VC02_17-19	0.17	0.19	-9.36764	142.2134	
273/27VC02_20-22	0.2	0.22	-9.36764	142.2134	
273/27VC02_25-27	0.25	0.27	-9.36764	142.2134	Bulk C14
273/27VC02_30-32	0.3	0.32	-9.36764	142.2134	
273/27VC02_32-34	0.32	0.34	-9.36764	142.2134	
273/27VC02_35-37	0.35	0.37	-9.36764	142.2134	
273/27VC02_40-42	0.4	0.42	-9.36764	142.2134	
273/27VC02_45-47	0.45	0.47	-9.36764	142.2134	
273/27VC02_50-52	0.5	0.52	-9.36764	142.2134	Bulk C14
273/27VC02_52-54	0.52	0.54	-9.36764	142.2134	
273/28VC04_0-2	0	0.02	-9.33874	142.1362	top
273/28VC04_5-7	0.05	0.07	-9.33874	142.1362	Bulk - C14
273/28VC04_7-9	0.07	0.09	-9.33874	142.1362	
273/28VC04_10-12	0.1	0.12	-9.33874	142.1362	
273/28VC04_15-17	0.15	0.17	-9.33874	142.1362	Bulk - C14
273/28VC04_17-19	0.17	0.19	-9.33874	142.1362	
273/28VC04_20-22	0.2	0.22	-9.33874	142.1362	
273/28VC04_25-27	0.25	0.27	-9.33874	142.1362	Bulk - C14
273/28VC04_28-30	0.28	0.3	-9.33874	142.1362	
273/28VC04_30-32	0.3	0.32	-9.33874	142.1362	
273/28VC04_35-37	0.35	0.37	-9.33874	142.1362	Bulk - C14
273/28VC04_40-42	0.4	0.42	-9.33874	142.1362	
273/28VC04_42-44	0.42	0.44	-9.33874	142.1362	
273/28VC04_45-47	0.45	0.47	-9.33874	142.1362	nodules for thin section
273/28VC04_50-52	0.5	0.52	-9.33874	142.1362	
273/28VC04_50-52	0.5	0.52	-9.33874	142.1362	
273/28VC05_0-2	0	0.02	-9.33888	142.1358	top
273/28VC05_6-8	0.06	0.08	-9.33888	142.1358	middle
273/29VC06_0-2	0	0.02	-9.33857	142.1362	
273/29VC06_10-12	0.1	0.12	-9.33857	142.1362	
273/29VC06_20-22	0.2	0.22	-9.33857	142.1362	
273/29VC06_30-32	0.3	0.32	-9.33857	142.1362	
273/29VC06_40-42	0.4	0.42	-9.33857	142.1362	
273/29VC06_50-52	0.5	0.52	-9.33857	142.1362	

*Post-cruise Report Survey 273: Torres Strait*

273/29VC06_60-62	0.6	0.62	-9.33857	142.1362	
273/29VC06_70-72	0.7	0.72	-9.33857	142.1362	
273/30VC07_0-2	0	0.02	-9.33891	142.1337	
273/30VC07_5-7	0.05	0.07	-9.33891	142.1337	
273/30VC07_10-12	0.1	0.12	-9.33891	142.1337	
273/30VC07_20-22	0.2	0.22	-9.33891	142.1337	
273/30VC07_27-29	0.27	0.29	-9.33891	142.1337	
273/30VC07_37-39	0.37	0.39	-9.33891	142.1337	
273/30VC07_50-52	0.5	0.52	-9.33891	142.1337	
273/30VC07_54-56	0.54	0.56	-9.33891	142.1337	Bulk C14
273/30VC07_61-63	0.61	0.63	-9.33891	142.1337	
273/30VC07_70-72	0.7	0.72	-9.33891	142.1337	
273/30VC07_81-83	0.81	0.83	-9.33891	142.1337	
273/30VC07_100-102	1	1.02	-9.33891	142.1337	
273/30VC07_102-104	1.02	1.04	-9.33891	142.1337	Bulk C14
273/35VC09_0-2	0	0.02	-9.35609	142.215	top
273/35VC09_10-12	0.1	0.12	-9.35609	142.215	
273/35VC09_20-22	0.2	0.22	-9.35609	142.215	
273/35VC09_30-32	0.3	0.32	-9.35609	142.215	
273/35VC09_40-42	0.4	0.42	-9.35609	142.215	
273/35VC09_50-52	0.5	0.52	-9.35609	142.215	
273/36VC10_0-2	0	0.02	-9.35727	142.2147	top
273/36VC10_2-4	0.02	0.04	-9.35727	142.2147	Bulk C14
273/36VC10_5-7	0.05	0.07	-9.35727	142.2147	
273/36VC10_10-12	0.1	0.12	-9.35727	142.2147	
273/36VC10_12-14	0.12	0.14	-9.35727	142.2147	Bulk C14
273/36VC10_15-17	0.15	0.17	-9.35727	142.2147	
273/36VC10_20-22	0.2	0.22	-9.35727	142.2147	
273/36VC10_25-27	0.25	0.27	-9.35727	142.2147	
273/36VC10_27-29	0.27	0.29	-9.35727	142.2147	Bulk C14
273/36VC10_30-32	0.3	0.32	-9.35727	142.2147	
273/36VC10_35-37	0.35	0.37	-9.35727	142.2147	
273/36VC10_40-42	0.4	0.42	-9.35727	142.2147	
273/36VC10_42-44	0.42	0.44	-9.35727	142.2147	Bulk C14
273/32PK01_0-2	0	0.02	-9.33515	142.1857	top
273/32PK01_15-17	0.15	0.17	-9.33515	142.1857	middle
273/32PK01_20-21	0.2	0.21	-9.33515	142.1857	nodule to be thin sectioned
273/32PK01_30-32	0.3	0.32	-9.33515	142.1857	bottom
273/33PK02_0-2	0	0.02	-9.33487	142.1861	top
273/33PK02_18-20	0.18	0.2	-9.33487	142.1861	middle
273/33PK02_27-29	0.27	0.29	-9.33487	142.1861	nodule to be thin sectioned
273/33PK02_36-37	0.36	0.37	-9.33487	142.1861	bottom
273/34PK03_0-2	0	0.02	-9.33488	142.1861	top
273/34PK03_7-8	0.07	0.08	-9.33488	142.1861	C14- peat
273/34PK03_15-16	0.15	0.16	-9.33488	142.1861	C14 - coral

## 10.6. Appendix F – S273 filter paper results

Table 10.2. Weights of S273 filter papers

Survey ID	I.D No.	SAMPLE NAME	SAMPLE NO.	PreWeight (g)	PostWeight (g)	Sample Weight (g)	Survey ID	I.D No.	SAMPLE NAME	SAMPLE NO.	PreWeight (g)	PostWeight (g)	Sample Weight (g)
273	304	1WS1	1443795	0.1007	0.1020	0.0013	273	413	26WS107	1444129	0.1007	0.1017	0.0010
273	305	2WS2	1443796	0.1010	0.1040	0.0030	273	414	26WS108	1444130	0.1063	0.1075	0.0012
273	306	3WS3	1444318	0.1005	0.1038	0.0033	273	415	26WS109	1444131	0.1007	0.1020	0.0013
273	307	3WS4	1443797	0.1005	0.1035	0.0030	273	416	lost		0.1003		
273	308	4WS5	1443798	0.1004	0.1030	0.0026	273	417	26WS110	1444132	0.1005	0.1021	0.0016
273	309	5WS6	1443806	0.1072	0.1162	0.0090	273	418	26WS111	1444133	0.1009	0.1015	0.0006
273	310	6WS7	1443799	0.1010	0.1110	0.0100	273	419	26WS112	1444134	0.1006	0.1015	0.0009
273	311	7WS8	1443800	0.1007	0.1099	0.0092	273	420	36WS113	1444135	0.1009	0.1009	0.0000
273	312	25WS9	1444031	0.1006	0.1045	0.0039	273	421	36WS114	1444136	0.1007	0.1005	-0.0002
273	313	25WS10	1444032	0.1009	0.1053	0.0044	273	422	36WS115	1444137	0.1012	0.1009	-0.0003
273	314	25WS11	1444033	0.1004	0.1040	0.0036	273	423	36WS116	1444138	0.1012	0.1015	0.0003
273	315	25WS12	1444034	0.0998	0.1048	0.0050	273	424	36WS117	1444139	0.1011	0.1013	0.0002
273	316	25WS13	1444035	0.1005	0.1037	0.0032	273	425	36WS118	1444140	0.1011	0.1017	0.0006
273	317	25WS14	1444036	0.1004	0.1076	0.0072	273	426	36WS119	1444141	0.1003	0.0999	-0.0004
273	318	25WS15	1444037	0.1003	0.1045	0.0042	273	427	36WS120	1444142	0.1017	0.1014	-0.0003
273	319	25WS16	1444038	0.0986	0.1038	0.0052	273	428	36WS121	1444143	0.1005	0.1004	-0.0001
273	320	25WS17	1444039	0.1005	0.1043	0.0038	273	429	36WS122	1444144	0.1020	0.1014	-0.0006
273	321	25WS18	1444040	0.1006	0.1050	0.0044	273	430	36WS123	1444145	0.1007	0.1012	0.0005
273	322	25WS19	1444041	0.1005	0.1046	0.0041	273	431	36WS124	1444146	0.1003	0.1009	0.0006
273	323	25WS20	1444042	0.1004	0.1059	0.0055	273	432	36WS125	1444147	0.1075	0.1075	0.0000
273	324	25WS21	1444043	0.1006	0.1038	0.0032	273	433	36WS126	1444148	0.1065	0.1088	0.0023
273	325	25WS22	1444044	0.1010	0.1042	0.0032	273	434	36WS127	1444149	0.1008	0.1010	0.0002
273	326	25WS23	1444045	0.1004	0.1059	0.0055	273	435	36WS128	1444150	0.1072	0.1125	0.0053
273	327	25WS24	1444046	0.1012	0.1055	0.0043	273	436	36WS129	1444151	0.1007	0.1009	0.0002

Post-cruise Report Survey 273: Torres Strait

273	328	25WS25	1444047	0.1000	0.1041	0.0041	273	437	36WS130	1444152	0.1009	0.1004	-0.0005
273	329	25WS26	1444048	0.1004	0.1049	0.0045	273	438	36WS131	1444153	0.1076	0.1080	0.0004
273	330	25WS27	1444049	0.1001	0.1066	0.0065	273	439	36WS132	1444154	0.1006	0.1004	-0.0002
273	331	25WS28	1444050	0.1005	0.1113	0.0108	273	440	36WS133	1444155	0.1009	0.1004	-0.0005
273	332	25WS29	1444051	0.1006	0.1048	0.0042	273	441	36WS134	1444156	0.1011	0.1012	0.0001
273	333	25WS30	1444052	0.1001	0.1036	0.0035	273	442	36WS135	1444157	0.1003	0.1000	-0.0003
273	334	25WS31	1444053	0.1012	0.1026	0.0014	273	443	36WS136	1444158	0.1008	0.1015	0.0007
273	335	lost		0.1069			273	444	36WS137	1444159	0.1013	0.1012	-0.0001
273	336	25WS32	1444054	0.1009	0.1037	0.0028	273	445	36WS138	1444160	0.1006	0.1004	-0.0002
273	337	25WS33	1444055	0.1071	0.1108	0.0037	273	446	36WS139	1444161	0.1005	0.1002	-0.0003
273	338	25WS34	1444056	0.1067	0.1118	0.0051	273	447	36WS140	1444162	0.1010	0.1013	0.0003
273	339	25WS35	1444057	0.1004	0.1042	0.0038	273	448	36WS141	1444163	0.1007	0.1020	0.0013
273	340	25WS36	1444058	0.1002	0.1214	0.0212	273	449	36WS142	1444164	0.1006	0.1029	0.0023
273	341	25WS37	1444059	0.1015	0.1115	0.0100	273	450	36WS143	1444165	0.1009	0.1009	0.0000
273	342	25WS38	1444060	0.1009	0.1079	0.0070	273	451	36WS144	1444166	0.1010	0.1013	0.0003
273	343	lost		0.1003			273	452	36WS145	1444167	0.1007	0.1010	0.0003
273	344	25WS39	1444061	0.1008	0.1252	0.0244	273	453	36WS146	1444168	0.1013	0.1018	0.0005
273	345	25WS40	1444062	0.1010	0.1159	0.0149	273	454	36WS147	1444169	0.1002	0.1007	0.0005
273	346	25WS41	1444063	0.1012	0.1037	0.0025	273	455	36WS148	1444170	0.1006	0.1007	0.0001
273	347	25WS42	1444064	0.1004	0.1035	0.0031	273	456	36WS149	1444171	0.1010	0.1011	0.0001
273	348	25WS43	1444065	0.1007	0.1087	0.0080	273	457	36WS150	1444172	0.1006	0.1007	0.0001
273	349	25WS44	1444066	0.1006	0.1170	0.0164	273	458	36WS151	1444173	0.1012	0.1011	-0.0001
273	350	25WS45	1444067	0.1007	0.1138	0.0131	273	459	36WS152	1444174	0.1010	0.1010	0.0000
273	351	25WS46	1444068	0.1001	0.1097	0.0096	273	460	36WS153	1444175	0.1008	0.1011	0.0003
273	352	25WS47	1444069	0.1006	0.1092	0.0086	273	461	36WS154	1444176	0.1004	0.1015	0.0011
273	353	25WS48	1444070	0.1010	0.1052	0.0042	273	462	36WS155	1444177	0.1067	0.1073	0.0006
273	354	25WS49	1444071	0.1003	0.1045	0.0042	273	463	LOST ??		0.1008		
273	355	25WS50	1444072	0.1002	0.1033	0.0031	273	464	36WS156	1444178	0.1009	0.1017	0.0008
273	356	25WS51	1444073	0.1005	0.1041	0.0036	273	465	36WS157	1444179	0.1010	0.1014	0.0004
273	357	25WS52	1444074	0.1067	0.1097	0.0030	273	466	36WS158	1444180	0.1007	0.1011	0.0004
273	358	25WS53	1444075	0.1008	0.1055	0.0047	273	467	36WS159	1444181	0.1012	0.1027	0.0015
273	359	25WS54	1444076	0.1005	0.1034	0.0029	273	468	36WS160	1444182	0.1007	0.1022	0.0015
273	360	25WS55	1444077	0.1007	0.1082	0.0075	273	469	36WS161	1444183	0.1010	0.1028	0.0018
273	361	25WS56	1444078	0.1060	0.1097	0.0037	273	470	36WS162	1444184	0.1009	0.1023	0.0014
273	362	25WS57	1444079	0.1077	0.1101	0.0024	273	471	37WS163	1444185	0.1005	0.1022	0.0017
273	363	25WS58	1444080	0.1007	0.1034	0.0027	273	472	37WS164	1444186	0.1007	0.1012	0.0005

273	364	25WS59	1444081	0.1013	0.1046	0.0033	273	473	37WS165	1444187	0.1004	0.1009	0.0005
273	365	25WS60	1444082	0.1007	0.1149	0.0142	273	474	37WS166	1444188	0.1005	0.1021	0.0016
273	366	26WS61	1444083	0.1070	0.1097	0.0027	273	475	37WS167	1444189	0.1012	0.1028	0.0016
273	367	26WS62	1444084	0.1064	0.1093	0.0029	273	476	37WS168	1444190	0.1003	0.1026	0.0023
273	368	26WS63	1444085	0.1009	0.1026	0.0017	273	477	37WS169	1444191	0.1005	0.1023	0.0018
273	369	26WS64	1444086	0.1013	0.1039	0.0026	273	478	37WS170	1444192	0.1007	0.1025	0.0018
273	370	26WS65	1444087	0.1000	0.1047	0.0047	273	479	37WS171	1444193	0.1008	0.1029	0.0021
273	371	26WS66	1444088	0.1075	0.1107	0.0032	273	480	37WS172	1444194	0.1007	0.1025	0.0018
273	372	26WS67	1444089	0.1074	0.1099	0.0025	273	481	37WS173	1444195	0.1006	0.1020	0.0014
273	373	26WS68	1444090	0.1075	0.1106	0.0031	273	482	37WS174	1444196	0.1005	0.1018	0.0013
273	374	26WS69	1444091	0.1011	0.1040	0.0029	273	483	37WS175	1444197	0.1006	0.1022	0.0016
273	375	26WS70	1444092	0.1060	0.1106	0.0046	273	484	37WS176	1444198	0.1006	0.1018	0.0012
273	376	26WS71	1444093	0.1005	0.1034	0.0029	273	485	37WS177	1444199	0.1057	0.1079	0.0022
273	377	26WS72	1444094	0.1061	0.1090	0.0029	273	486	37WS178	1444200	0.1009	0.1049	0.0040
273	378	26WS73	1444095	0.1066	0.1087	0.0021	273	487	37WS179	1444201	0.1007	0.1047	0.0040
273	379	26WS74	1444096	0.1011	0.1026	0.0015	273	488	37WS180	1444202	0.1011	0.1029	0.0018
273	380	26WS75	1444097	0.1008	0.1076	0.0068	273	489	37WS181	1444203	0.1011	0.1021	0.0010
273	381	26WS76	1444098	0.1010	0.1017	0.0007	273	490	37WS182	1444204	0.1017	0.1032	0.0015
273	382	26WS77	1444099	0.1015	0.1025	0.0010	273	491	37WS183	1444205	0.1009	0.1023	0.0014
273	383	26WS78	1444100	0.1064	0.1136	0.0072	273	492	37WS184	1444206	0.1009	0.1029	0.0020
273	384	26WS79	1444101	0.1074	0.1095	0.0021	273	493	37WS185	1444207	0.1075	0.1096	0.0021
273	385	26WS80	1444102	0.1006	0.1039	0.0033	273	494	37WS186	1444208	0.1012	0.1033	0.0021
273	386	26WS81	1444103	0.1002	0.1016	0.0014	273	495	37WS187	1444209	0.1007	0.1029	0.0022
273	387	26WS82	1444104	0.1014	0.1021	0.0007	273	496	37WS188	1444210	0.1013	0.1037	0.0024
273	388	26WS83	1444105	0.1067	0.1079	0.0012	273	497	37WS189	1444211	0.1010	0.1030	0.0020
273	389	lost		0.1005			273	498	37WS190	1444212	0.1006	0.1034	0.0028
273	390	26WS84	1444106	0.1064	0.1081	0.0017	273	499	37WS191	1444213	0.1004	0.1025	0.0021
273	391	26WS85	1444107	0.1077	0.1089	0.0012	273	500	37WS192	1444214	0.1003	0.1021	0.0018
273	392	26WS86	1444108	0.1061	0.1077	0.0016	273	501	37WS193	1444215	0.0980	0.1009	0.0029
273	393	26WS87	1444109	0.1067	0.1074	0.0007	273	502	37WS194	1444216	0.0987	0.1017	0.0030
273	394	26WS88	1444110	0.1007	0.1019	0.0012	273	503	37WS195	1444217	0.0979	0.1007	0.0028
273	395	26WS89	1444111	0.1003	0.1020	0.0017	273	504	lost		0.0981		
273	396	26WS90	1444112	0.1072	0.1088	0.0016	273	505	37WS196	1444218	0.0980	0.1009	0.0029
273	397	26WS91	1444113	0.1074	0.1082	0.0008	273	506	37WS197	1444219	0.0982	0.1021	0.0039
273	398	26WS92	1444114	0.1002	0.1018	0.0016	273	507	lost		0.0982		
273	399	26WS93	1444115	0.1057	0.1072	0.0015	273	508	37WS198	1444220	0.0983	0.1012	0.0029

273	400	26WS94	1444116	0.1009	0.1022	0.0013	273	509	37WS200	1444222	0.0981	0.1020	0.0039
273	401	26WS95	1444117	0.1007	0.1020	0.0013	273	510	37WS199	1444221	0.0982	0.1080	0.0098
273	402	26WS96	1444118	0.1005	0.1016	0.0011	273	511	37WS201	1444223	0.0977	0.1016	0.0039
273	403	26WS97	1444119	0.1008	0.1020	0.0012	273	512	37WS202	1444224	0.0973	0.1013	0.0040
273	404	26WS98	1444120	0.1014	0.1018	0.0004	273	513	37WS203	1444225	0.0975	0.1009	0.0034
273	405	26WS99	1444121	0.1003	0.1009	0.0006	273	514	37WS204	1444226	0.0986	0.1018	0.0032
273	406	26WS100	1444122	0.1068	0.1076	0.0008	273	515	37WS205	1444227	0.0965	0.0994	0.0029
273	407	26WS101	1444123	0.1004	0.1024	0.0020	273	516	37WS206	1444228	0.1055	0.1084	0.0029
273	408	26WS102	1444124	0.1005	0.1015	0.0010	273	517	37WS207	1444229	0.0967	0.0995	0.0028
273	409	26WS103	1444125	0.1008	0.1073	0.0065	273	518	37WS208	1444230	0.0965	0.0995	0.0030
273	410	26WS104	1444126	0.1008	0.1009	0.0001	273	519	37WS209	1444231	0.0970	0.0999	0.0029
273	411	26WS105	1444127	0.1008	0.1020	0.0012	273	520	37WS210	1444232	0.0981	0.1028	0.0047
273	412	26WS106	1444128	0.1008	0.1020	0.0012	273	521	37WS211	1444233	0.0979	0.1014	0.0035
273	412	26WS106	1444128	0.1008	0.1020	0.0012	273	522	37WS212	1444234	0.0981	0.1016	0.0035

## 10.7. Appendix G – Results from Laboratory analysis of Grab Samples

The tables below show the textural data for each surface sample based on sieve analysis and carbonate bomb analysis, and are thus expressed as weight percents. Grainsize distribution graphs and associated data from the Malvern are contained on the DVD in jpg format. The filenames follow the convention: *7-digit Lab Number\_GA Survey Number\_Station Number, Operation Type and Operation Number* (e.g., 1443825\_273\_31GR25).

Table 10.3. Textural characteristics of surface sediment samples collected during survey 273.

SAMPLENO	SAMPLEID	SAMPLE_TYPE	LATIT	LONGIT	Water Depth - Start	%Gravel	%Sand	%Mud	CaCO <sub>3</sub> %Bulk	CaCO <sub>3</sub> %Gravel	CaCO <sub>3</sub> %Sand	CaCO <sub>3</sub> %Mud
1443825	273/31GR25	GRAB UNSPECIFIED	-9.5577167	142.309367	0m	13.67	84.31	2.02	75.01	90.00	87.19	insuf.
1443826	273/33GR26	GRAB UNSPECIFIED	-9.5581167	142.31015	0m	25.35	72.33	2.31	91.75	90.00	93.78	insuf.
1443827	273/38GR27	GRAB UNSPECIFIED	-9.6680167	142.339467	4.5m	18.99	77.33	3.68	87.19	75.00	93.28	67.91
1443828	273/01GRVV01	GRAB VAN VEEN	-9.79655	142.446383	10.5m	36.19	56.96	6.85	78.06	80.00	82.11	76.03
1443829	273/02GRVV02	GRAB VAN VEEN	-9.56975	142.229217	3.8m	23.12	67.90	8.98	85.16	70.00	94.29	65.88
1443830	273/03GRVV03	GRAB VAN VEEN	-9.5935	142.36165	8m	58.84	40.91	0.25	93.28	90.00	94.29	insuf.
1443831	273/04GRVV04	GRAB VAN VEEN	-9.5944833	142.35705	6.3m	18.38	81.42	0.19	79.07	80.00	86.17	insuf.
1443832	273/05GRVV05	GRAB VAN VEEN	-9.5944667	142.352167	6.3m	11.54	88.44	0.02	55.22	75.00	75.01	insuf.
1443833	273/06GRVV06	GRAB VAN VEEN	-9.5900833	142.353383	9.8m	53.79	43.86	2.35	86.68	85.00	93.28	69.94
1443834	273/07GRVV07	GRAB VAN VEEN	-9.5918333	142.357217	7.8m	38.66	61.20	0.14	79.58	80.00	82.62	insuf.
1443835	273/08GRVV08	GRAB VAN VEEN	-9.5591333	142.395133	7.8m	43.62	55.91	0.48	59.79	70.00	77.04	insuf.
1443836	273/09GRVV09	GRAB VAN VEEN	-9.5	142.4787	7.1m	34.81	63.87	1.32	78.06	90.00	80.08	insuf.

*Post-cruise Report Survey 273: Torres Strait*

1443837	273/10GRVV10	GRAB VAN VEEN	-9.4174833	142.576483	7.8m	37.34	42.35	20.31	45.58	75.00	46.09	13.11
1443838	273/11GRVV11	GRAB VAN VEEN	-9.37005	142.5812	14.8m	12.75	40.64	46.61	28.84	55.00	29.35	19.20
1443839	273/12GRVV12	GRAB VAN VEEN	-9.3472333	142.627967	30.6m	42.83	34.68	22.49	38.48	70.00	38.99	15.14
1443840	273/13GRVV13	GRAB VAN VEEN	-9.3532667	142.652767	17.8m	14.41	52.35	33.25	38.99	70.00	42.54	18.19
1443841	273/14GRVV14	GRAB VAN VEEN	-9.3612667	142.653567	11.6m	0.51	34.76	64.73	21.23	80.00	27.32	21.23
1443842	273/15GRVV15	GRAB VAN VEEN	-9.3654333	142.653783	1m	0.29	74.52	25.19	12.10	0.00	11.09	13.62
1443843	273/16GRVV16	GRAB VAN VEEN	-9.3645333	142.653517	6m	0.41	33.03	66.56	19.71	80.00	25.29	21.23
1443844	273/17GRVV17	GRAB VAN VEEN	-9.3625667	142.652533	14m	6.40	63.70	29.90	26.81	75.00	31.38	18.19
1443845	273/18GRVV18	GRAB VAN VEEN	-9.3619333	142.653267	15m	2.87	53.99	43.15	29.35	80.00	27.32	19.20
1443846	273/19GRVV19	GRAB VAN VEEN	-9.3615333	142.6534	15m	1.32	44.33	54.35	23.26	75.00	26.31	19.20
1443847	273/20GRVV20	GRAB VAN VEEN	-9.36665	142.658417	1m	1.66	49.88	48.45	18.19	10.00	15.14	14.13
1443848	273/21GRVV21	GRAB VAN VEEN	-9.3649333	142.655133	6m	0.19	30.20	69.61	20.72	90.00	24.28	18.19
1443849	273/22GRVV22	GRAB VAN VEEN	-9.36355	142.6539	10m	3.00	54.59	42.41	24.28	70.00	27.32	18.19
1443850	273/23GRVV23	GRAB VAN VEEN	-9.3615167	142.653933	10m	0.47	43.82	55.71	22.25	80.00	24.28	19.20
1443851	273/24GRVV24	GRAB VAN VEEN	-9.3556833	142.667167	4.3m	47.04	37.97	14.98	46.60	60.00	40.00	15.65
1443784	273/28VC3cc	CORE CATCHER	-9.5646667	142.227117		41.27	56.63	2.10	96.32	90.00	95.81	insuf.
1443786	273/28VC4cc	CORE CATCHER	-9.5645667	142.227033		25.45	68.13	6.42	91.25	90.00	96.83	75.01
1443790	273/30VC7cc	CORE CATCHER	-9.56485	142.2228		6.12	86.31	7.58	88.20	85.00	91.75	76.53
1443792	273/35VC8cc	CORE CATCHER	-9.59365	142.358283		29.17	70.26	0.57	80.59	95.00	90.23	insuf.

## 10.8. Appendix H – Results from 24hour observation stations

### Area A: 24-hr Station 15-16/10/2004

#### Station 25 (-9° 34.10, 142° 13.77)

Notes: Stations taken every hour on the hour. Camera = 00-08 mins past the hour. WS1 = 02 mins past the hour. WS2 = 06 mins past the hour.

Table 10.4. Station 25 log sheet.

Time (local)	Station 25 Water Sample	Filter Paper Number	Camera (y/n)	DV Tape Time (Start)	DV Tape Time (End)	Comments	Filter Paper Seq. No.	Water Sample No.	Time (UTC)	DV Tape No.	VHS Tape No.	Notes
6:00	WS1	312	n	N/A	N/A	remote not working - no video recorded	1	25WS9	20:00	2	2	
	WS2	313	n			camera not recording	2	25WS10		2	2	
7:00	WS1	314	y	2	2:08	strong currents	3	25WS11	21:00	2	2	
	WS2	315	y				4	25WS12		2	2	
8:00	WS1	316	y	11:19	19:30	strong currents	5	25WS13	22:00	2	2	
	WS2	317	y				6	25WS14		2	2	
9:00	WS1	318	y	19:30	27:22	strong currents - did not record on VHS tape	7	25WS15	23:00	2	2	
	WS2	319	y				8	25WS16		2	2	
10:00	WS1	320	y	27:23	35:31	boat moving around a lot - repositioning of camera required	9	25WS17	0:00	2	2	
	WS2	321	y				10	25WS18		2	2	changed DV tape
11:00	WS1	322	y	0:00	8:00	camera moved once	11	25WS19	1:00	3	2	
	WS2	323	y				12	25WS20		3	2	
12:00	WS1	324	y	N/A	N/A	remote not working - recorded on VHS tape only	13	25WS21	2:00	3	2	
	WS2	325	y				14	25WS22		3	2	
13:00	WS1	326	y	08:00	16:18	strong current	15	25WS23	3:00	3	2	
	WS2	327	y				16	25WS24		3	2	
14:00	WS1	328	y	16:19	24:47	strong current	17	25WS25	4:00	3	2	
	WS2	329	y				18	25WS26		3	2	
15:00	WS1	330	y	24:47	32:45	strong current; adjusted focus and added polarising	19	25WS27	5:00	3	2	

Post-cruise Report Survey 273: Torres Strait

	WS2	331	y			filter at end of run	20	25WS28		3	2	
16:00	WS1	332	y	32:45	40:46	slack water	21	25WS29	6:00	3	2	batt 2 put on charge
	WS2	333	y				22	25WS30		3	2	16:15 (LT)
17:00	WS1	334	y	40:46	48:43	slack water; lost filter paper 335 overboard	23	25WS31	7:00	3	2	batt 1 in camera
	WS2	336	y				24	25WS32		3	2	
18:00	WS1	337	y	48:43	56:43	increasing current; VHS & DV recording out of focus	25	25WS33	8:00	3	2	changed DV tape
	WS2	338	y				26	25WS34		3	2	refocused camera
19:00	WS1	339	y	0:00	08:00	strong current; refocused lens	27	25WS35	9:00	4	2	
	WS2	340	y				28	25WS36		4	2	
20:00	WS1	341	y	08:00	15:56	strong current; lots of still water	29	25WS37	10:00	4	2	
	WS2	342	y				30	25WS38		4	2	
21:00	WS1	344	y	15:56	23:36	strong current	31	25WS39	11:00	4	2	
	WS2	345	y				32	25WS40		4	2	
22:00	WS1	346	y	23:36	31:35	boat moving around a lot - repositioning of camera	33	25WS41	12:00	4	2	batt 1 put on charge
	WS2	347	y			required	34	25WS42		4	2	22:18 (LT)
23:00	WS1	348	y	31:35	39:35	boat moving around - repositioning of camera	35	25WS43	13:00	4	2	batt 2 in camera
	WS2	349	y			required	36	25WS44		4	2	
0:00	WS1	350	y	39:35	47:42		37	25WS45	14:00	4	2	
	WS2	351	y				38	25WS46		4	2	
1:00	WS1	352	y	47:32	55:24	strong current	39	25WS47	15:00	4	2	
	WS2	353	y				40	25WS48		4	2	
2:00	WS1	354	y	55:24	1:02:30	strong current; end of DV tape; lost last halogen light	41	25WS49	16:00	4	2	DV tape replaced at end of run
												changed halogen for incandescent light (bulb blown)
3:00	WS2	355	y				42	25WS50		4	2	
	WS1	356	y	00:00	08:01	strong current; new tape #5 inserted;	43	25WS51	17:00	5	2	
	WS2	357	y			changed halogen for strong incandescent light	44	25WS52		5	2	
4:00	WS1	358	y	08:01	16:20	current slackening; camera moved once	45	25WS53	18:00	5	2	replaced battery with spare (#1 not yet fully charged)
	WS2	359	y			replaced battery with spare, put #2 on charge	46	25WS54		5	2	and put #2 on charge at 4:15 (LT)
5:00	WS1	360	y	16:20	24:29	slack water; replaced spare battery with #1	47	25WS55	19:00	5	2	replaced spare battery with #1
	WS2	361	y				48	25WS56		5	2	
6:00	WS1	362	y	24:29	32:35	current increasing	49	25WS57	20:00	5	2	
	WS2	363	y				50	25WS58		5	2	
7:00	WS1	364	y	32:35	40:00	moderate current	51	25WS59	21:00	5	2	
	WS2	365	y				52	25WS60		5	2	

NB: VHS tape did not record on to tape during entire station. Copied DV tape to VHS tape using camera and ship's video recorder.

**Area B: 24-hr Station 16-17/10/2004**

**Station 26 (-9° 35.717, 142° 21.444)**

Notes: Stations taken every hour on the hour. Camera = 00-08 mins past the hour. WS1 = 02 mins past the hour. WS2 = 06 mins past the hour.

Table 10.5. Station 26 log sheet.

Time (local)	Station 26 Water Sample	Filter Paper Number	Camera (y/n)	DV Tape Time (Start)	DV Tape Time (End)	Comments	Filter Paper Seq. No.	Water Sample Seq. No.	Time (UTC)	DV Tape No.	VHS Tape No.	Notes
10:00	WS1	366	y	0:00	08:04	Slack water; too much ambient light for lights	53	26WS61	0:00	6	3	new DV and VHS tapes
	WS2	367	y			Station marker recorded after this sample collected	54	26WS62		6	3	
11:00	WS1	368	y	08:07	16:05	slack water	55	26WS63	1:00	6	3	polarising filter fitted
	WS2	369	y				56	26WS64		6	3	
12:00	WS1	370	y	16:05	24:06	increasing current; repositioning of camera required	57	26WS65	2:00	6	3	batt. 2 put in camera
	WS2	371	y				58	26WS66		6	3	
13:00	WS1	372	y	24:06	32:04	strong current	59	26WS67	3:00	6	3	
	WS2	373	y				60	26WS68		6	3	
14:00	WS1	374	y	32:04	40:09	strong current; camera repositioned several times	61	26WS69	4:00	6	3	
	WS2	375	y				62	26WS70		6	3	
15:00	WS1	376	y	40:08	48:33	strong current	63	26WS71	5:00	6	3	
	WS2	377	y				64	26WS72		6	3	
16:00	WS1	378	y	48:33	57:00	current slackening	65	26WS73	6:00	6	3	changed DV tape
	WS2	379	y				66	26WS74		6	3	batt. 1 put in camera
17:00	WS1	380	y	0:00	08:10	slack water	67	26WS75	7:00	7	3	
	WS2	381	y				68	26WS76		7	3	
18:00	WS1	382	y	08:10	16:05	current increasing	69	26WS77	8:00	7	3	
	WS2	383	y				70	26WS78		7	3	

*Post-cruise Report Survey 273: Torres Strait*

19:00	WS1	384	y	16:05	24:04	strong current, bedload transport	71	26WS79	9:00	7	3	
	WS2	385	y				72	26WS80		7	3	
20:00	WS1	386	y	24:04	32:41	strong current, bedload transport	73	26WS81	10:00	7	3	
	WS2	387	y				74	26WS82		7	3	
21:00	WS1	388	y	32:41	40:46	strong current, bedload transport	75	26WS83	11:00	7	3	
	WS2	390	y				76	26WS84		7	3	
22:00	WS1	391	y	40:46	48:50	current weakening, some bedload transport	77	26WS85	12:00	7	3	changed DV tape
	WS2	392	y				78	26WS86		7	3	batt. 2 put in camera
23:00	WS1	393	y	0:00	08:01	current weakening, some bedload transport	79	26WS87	13:00	8	3	
	WS2	394	y				80	26WS88		8	3	
0:00	WS1	395	n	N/A	N/A	strong current.	81	26WS89	14:00	N/A	N/A	remote not working
	WS2	396	n				82	26WS90		N/A	N/A	replaced remote
1:00	WS1	397	y	08:01	16:12	moderate current; small current ripples	83	26WS91	15:00	8	3	battery to fix
	WS2	398	y				84	26WS92		8	3	
2:00	WS1	399	y	16:12	24:15	moderate current; small current ripples	85	26WS93	16:00	8	3	
	WS2	400	y				86	26WS94		8	3	
3:00	WS1	401	y	24:15	30:59	current slackening	87	26WS95	17:00	8	3	Missed 2 mins as TV
	WS2	402	y				88	26WS96		8	3	screen
4:00	WS1	403	y	30:59	39:09	close to slack water	89	26WS97	18:00	8	3	went blue (not sure of
	WS2	404	y				90	26WS98		8	3	cause)
5:00	WS1	405	y	39:09	47:03	slack water	91	26WS99	19:00	8	3	batt. 1 put in camera
	WS2	406	y				92	26WS100		8	3	
6:00	WS1	407	y	47:03	56:12	slack water	93	26WS101	20:00	8	3	changed DV tape
	WS2	408	y				94	26WS102		8	3	
7:00	WS1	409	y	0:00	7:55	current increasing; camera repositioned several times	95	26WS103	21:00	9	3	
	WS2	410	y				96	26WS104		9	3	
8:00	WS1	411	y	8:05	16:08	moderate current; some bedload transport	97	26WS105	0:00	9	3	started tape too early,
	WS2	412	y				98	26WS106		9	3	restarted
9:00	WS1	413	y	16:08	24:03	strong current	99	26WS107	1:00	9	3	at correct time
	WS2	414	y				100	26WS108		9	3	batt. 2 put in camera
10:00	WS1	415	y	24:03	31:59	moderate current; not much bedload transport	101	26WS109	2:00	9	3	
	WS2	417	y			observed	102	26WS110		9	3	
11:00	WS1	418	y	31:59	39:55	moderate current; not much bedload transport	103	26WS111	3:00	9	3	
	WS2	419	y				104	26WS112		9	3	

NB: VHS tape did not record on to tape during entire station. Copied DV tape to VHS tape using camera and ship's video recorder.

**Area A: 24-hr Station 21-22/10/2004**

**Station 37**

Notes: Stations taken every hour on the hour. Camera = 00-08 mins past the hour. WS1 = 02 mins past the hour. WS2 = 06 mins past the hour.

Table 10.6. Station 37 log sheet.

Time (GMT)	Water Sample	Filter Paper Number	Camera (y/n)	DV Tape Time (Start)	DV Tape Time (End)	Comments	Filter Paper Seq. No.	Water Sample No.	DV Tape No.	VHS Tape No.	Notes
11:02	WS1	471	Y	0:07:00	8:03:00	Algae and sessile forms dense cover hard substrate	163	37WS163	16		
11:06	WS2	472					164	37WS164	16		
12:02	WS1	473	Y	8:03:00	16:18:08	Algae Halimeda(?) thick cover	165	37WS165	16		
12:06	WS2	474					166	37WS166	16		
13:02	WS1	475	y	16:18:08	24:20:00	thick algae	167	37WS167	16		
13:06	WS2	476					168	37WS168	16		
14:02	WS1	477	y	24:20:00	31:56:17	algae - lots and lots	169	37WS169	16		
14:06	WS2	478					170	37WS170	16		
15:02	WS1	479	y	31:56:17	59:09:00	algae - lots. Fish and seagrass ?? problem with remote. Surfaced to replace battery/tape	171	37WS171	16		
15:06	WS2	480					172	37WS172	16		
16:02	WS1	481	y	0:34:05	8:36:21	algae - lots.	173	37WS173	17		
16:06	WS2	482					174	37WS174	17		
17:02	WS1	483	y	8:36:21	16:48:01	algae, seagrass (??)	175	37WS175	17		
17:06	WS2	484					176	37WS176	17		
18:02	WS1	485	y	16:48:01	24:42:04	algae, seagrass (??)	177	37WS177	17		
18:06	WS2	486					178	37WS178	17		
19:02	WS1	487	y	24:42:04	33:47:22	algae - lots. Nutrient sample 37NR4 taken	179	37WS179	17		
19:06	WS2	488				Camera pulled. Battery/tape change.	180	37WS180	17		
20:02	WS1	489	y	00:31:02	08:52:04	algae - lots of.	181	37WS181	18		
20:06	WS2	490					182	37WS182	18		

*Post-cruise Report Survey 273: Torres Strait*

21:02	WS1	491	y	08:52:04	17:19:08	algae	183	37WS183	18
21:06	WS2	492					184	37WS184	18
22:02	WS1	493	y	17:19:08	25:13:02	algae	185	37WS185	18
22:06	WS2	494					186	37WS186	18
23:02	WS1	495	y	25:13:02	33:19:24	algae, some seagrass	187	37WS187	18
23:06	WS2	496					188	37WS188	18
0:02	WS1	497	y	33:19:24	41:19:22	algae	189	37WS189	18
0:06	WS2	498				Camera pulled. Battery/tape change.	190	37WS190	18
1:02	WS1	499	y	0:08:00	10:47:00		191	37WS191	19
1:06	WS2	500					192	37WS192	19
2:02	WS1	501	y	10:47:00	19:55:20	algae	193	37WS193	19
2:06	WS2	502					194	37WS194	19
3:02	WS1	503	y	19:55:20	28:55:02	algae	195	37WS195	19
3:06	WS2	505					196	37WS196	19
4:02	WS1	506	y	28:55:02	37:05:01	camera flying continuously - moving too much to hold steady.	197	37WS197	19
4:06	WS2	508				little yellow fish.	198	37WS198	19
5:02	WS1	510	y	37:05:01	45:34:07	camera flying continuously - moving too much to hold steady.	199	37WS199	19
5:06	WS2	509				algae, sea-whips, soft coral	200	37WS200	19
6:02	WS1	511	y	45:34:07	53:34:15	camera flying continuously - moving too much to hold steady.	201	37WS201	19
6:06	WS2	512				algae, sea-whips, soft coral. Camera pulled - new battery/tape.	202	37WS202	19
7:02	WS1	513	y	0.00	0:03:00	camera frame broken. End of camera deployments	203	37WS203	20
7:06	WS2	514					204	37WS204	20
8:02	WS1	515	N				205	37WS205	
8:06	WS2	516					206	37WS206	
9:02	WS1	517	N				207	37WS207	
9:06	WS2	518					208	37WS208	
10:02	WS1	519	N				209	37WS209	
10:06	WS2	520					210	37WS210	
11:02	WS1	521	N				211	37WS211	
11:06	WS2	522					212	37WS212	

**Area B: 24-hr Station 20-21/10/2004**

**Station 36**

Notes: Stations taken every hour on the hour. Camera = 00-08 mins past the hour. WS1 = 02 mins past the hour. WS2 = 06 mins past the hour.

Table 10.7. Station 36 log sheet

Time (GMT)	Station 36 Water Sample	Filter Paper Number	Camera (y/n)	DV Tape Time (Start)	DV Tape Time (End)	Comments	Filter Paper Seq. No.	Water Sample Seq. No.	Time (UTC)	DV Tape No.	VHS Tape No.	Notes
8:02	WS1	420	Y		14:16	First nutrient sample taken 36NS01	113	36WS113		12		
8:06	WS2	421				rippled bed minor bedload bursts	114	36WS114		12		
9:02	WS1	422	Y	14:16	22:16		115	36WS115		12		
9:06	WS2	423					116	36WS116		12		
10:02	WS1	424	Y	22:16	31:49:00		117	36WS117		12		
10:07	WS2	425				WS2 1 minute late (bottle leaked)	118	36WS118		12		
11:02	WS1	426	Y	31:49:00	40:05:00		119	36WS119		12		
11:06	WS2	427				Pulled camera to change battery/tape	120	36WS120		12		
12:02	WS1	428	Y	0:00:00	9:16	2 fish	121	36WS121		12		
12:09	WS2	429				WS2 3 minutes late (bottle leaked)	122	36WS122		12		
13:02	WS1	430	Y	9:16	17:01		123	36WS123		12		
13:06	WS2	431					124	36WS124		12		
14:02	WS1	432	y	17:01	25:01:00	Dragging a lot - brought to sfc after to fix light	125	36WS125		12		
14:06	WS2	433					126	36WS126		12		
15:02	WS1	434	Y	25:33:00	33:56:00	BOUNCING DUE TO BOAT ROLLING	127	36WS127		12		
15:07	WS2	435				Nutrient sample 36NR2 taken at 15:20	128	36WS128		12		
16:02	WS1	436	y	33:56:21	42:24:05	dragging too much - camera let fly.	129	36WS129		12		
16:11	WS2	437				2nd niskin not firing properly.	130	36WS130		12		
17:02	WS1	438	Y	42:24:05	51:04:17	SOME FISH, ANCHOR CHAIN, DRAGGING A LOT.	131	36WS131		12		
17:06	WS2	439				after - brought to sfc. Change battery/DV tape.	132	36WS132		12		
						DV TAPE 13. dragging a lot. Moved camera during						
18:02	WS1	440	Y	0:13:24	8:25:16	record.	133	36WS133		13		
18:06	WS2	441					134	36WS134		13		
19:02	WS1	442	y	8:25:16	16:27:14	Small fish - still	135	36WS135		13		
19:06	WS2	443					136	36WS136		13		

*Post-cruise Report Survey 273: Torres Strait*

20:02	WS1	444	y	16:27:14	24:49:18	some bedload transport	137	36WS137	13
20:06	WS2	445					138	36WS138	13
21:02	WS1	446	y	24:49:18	32:48:15	bursts and sweeps	139	36WS139	13
21:06	WS2	447					140	36WS140	13
22:02	WS1	448	y	32:48:15	40:49:15	bursts and sweeps	141	36WS141	13
22:06	WS2	449					142	36WS142	13
23:02	WS1	450	y	40:49:15	48:54:12	advancing ripple/bedload	143	36WS143	13
23:06	WS2	451				Pulled camera to change battery/tape	144	36WS144	13
0:02	WS1	452	y	0:00:00	8:02:00		145	36WS145	14
0:06	WS2	453					146	36WS146	14
1:02	WS1	454	y	8:02:00	15:53:02	No motion, still	147	36WS147	14
1:06	WS2	455					148	36WS148	14
2:02	WS1	456	y	15:53:02	24:02:03	On edge of sandwave	149	36WS149	14
2:06	WS2	457					150	36WS150	14
3:02	WS1	458	y	24:02:03	32:08:05	still. Algae swaying.	151	36WS151	14
3:06	WS2	459					152	36WS152	14
4:02	WS1	460	y	32:08:05	40:46:11	some bedload transport, dragging camera a lot.	153	36WS153	14
4:06	WS2	461				Pulled camera to change battery/tape	154	36WS154	14
5:02	WS1	462	y	0:00:00	8:12:13	in trough of sandwaves. Dragging a lot.	155	36WS155	15
5:06	WS2	464					156	36WS156	15
6:02	WS1	465	y	8:12:13	16:41:22	dragged a lot. Some bedload.	157	36WS157	15
6:06	WS2	466					158	36WS158	15
7:02	WS1	467	y	16:41:22	26:59:22	dragging a lot. Moved continuously during deployment	159	36WS159	15
7:06	WS2	468					160	36WS160	15
8:02	WS1	469	y	26:59:22	37:48:18	Nutrient sample 36NR3 taken at 08:06	161	36WS161	15
8:06	WS2	470					162	36WS162	15